NASA CR-134726

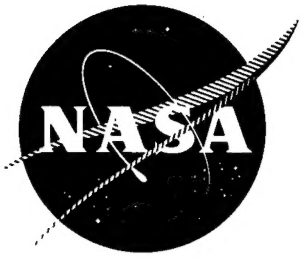

Composite-Reinforced Propellant Tanks (Final Report)

by

L. D. Brown, M. J. Martin, B. J. Aleck and R. Landes

GRUMMAN AEROSPACE CORPORATION

prepared for

NATIONAL AERONAUTICS AND SPACE ADMINISTRATION

NASA Lewis Research Center

Contract NAS 3-14368

James R. Faddoul, Project Manager

DISCLAIMER NOTICE

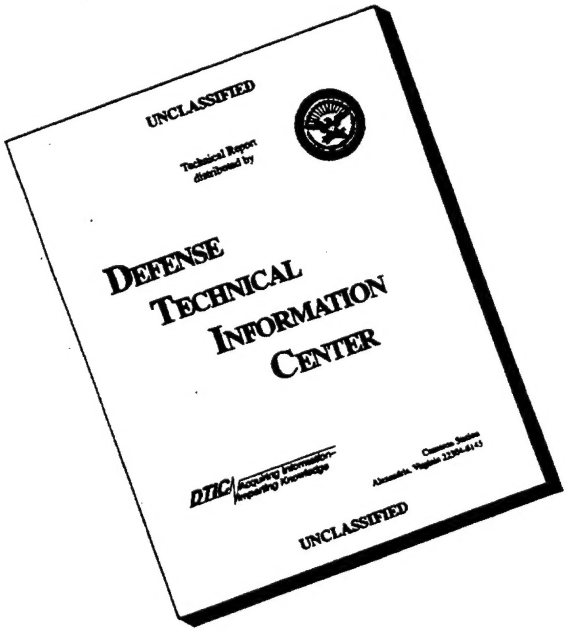

THIS DOCUMENT IS BEST QUALITY AVAILABLE. THE COPY FURNISHED TO DTIC CONTAINED A SIGNIFICANT NUMBER OF PAGES WHICH DO NOT REPRODUCE LEGIBLY.

1. Report No. NASA-CR-134726	2. Government Accession No.	3. Recipient's Catalog No.
4. Title and Subtitle COMPOSITE-REINFORCED PROPELLANT TANKS (FINAL REPORT)		5. Report Date February 1975 6. Performing Organization Code
7. Author(s) Lawrence D. Brown, Michael J. Martin and Benjamin J. Aleck (Grumman Aerospace Corp.) and Robert Landes (Structural Composites Industries)		8. Performing Organization Report No. 10. Work Unit No.
9. Performing Organization Name and Address Grumman Aerospace Corporation Bethpage, New York 11714		11. Contract or Grant No. NAS 3-14368
12. Sponsoring Agency Name and Address National Aeronautics and Space Administration 21000 Brookpark Rd. Lewis Research Center, Cleveland, Ohio 44135		13. Type of Report and Period Covered Contractor Report 14. Sponsoring Agency Code

15. Supplementary Notes
Project Manager, James R. Faddoul
Materials and Structures Division
NASA Lewis Research Center
Cleveland, Ohio 44135

16. Abstract

Design studies involving weight and cost were carried out for several structural concepts applicable to Space Shuttle disposable tankage. An effective design, a honeycomb stabilized pressure vessel, was chosen for test, and a test model was designed and fabricated.

17. Key Words (Suggested by Author(s))			18. Distribution Statement
Bonded	Low-cost	Tankage	Unclassified, Unlimited
Composite	Optimization	2219 Al Alloy	
Constrictive-stiffened	Overwrap		
Cryogenic	Sandwich		
Integral	S-Glass		
Kevlar	Space Shuttle		

19. Security Classif. (of this report)	20. Security Classif. (of this page)	21. No. of Pages	22. Price*
Unclassified	Unclassified		$3.00

* For sale by the National Technical Information Service, Springfield, Virginia 22151

FOREWORD

The work described herein was performed by the Grumman Aerospace Corporation with Structural Composites Industries as an associate under NASA Contract NAS 3-14368. Mr. James R. Faddoul, Materials and Structures Division, NASA Lewis Research Center, was Program Manager. The contract was initiated in June 1971 and redirected December 1971.

CONTENTS

CONTENTS (CONT)

SUMMARY

The Space Shuttle Orbiter employs a large disposable LH_2 and LOX tank on each flight. The objective of this program was to determine if costs could be reduced by using composite tank construction. The total cost was considered, tooling, material, repeated fabrication costs and the cost of transporting each extra kilogram from fabrication through launch, to separation. Although weight reduction could be achieved by overwrapping the monocoque LOX tank with prestressed glass fiber, the complexity of the fabrication led to costs exceeding the savings in transportation. The baseline for the LH_2 tank was an integrally-stiffened 2219 aluminum alloy shell, required to sustain large bending moments and hence longitudinal compression loads. Composite construction offered a substantial cost savings in fabrication options here, and overcame a slight increase in transportation cost. Two composite designs were found attractive: 1) a sandwich design consisting of a 2219 aluminum alloy inner cylinder with a paper honeycomb core, overwrapped with two layers of glass cloth; 2) a design involving bonding and mechanically attaching (without through-penetrations) "Z" stiffeners and frames to the aluminum shell in order to construct a vessel which had very much the appearance of the baseline design. A test program was devised to test the sandwich design and two vessels simulating a 1/6 scale LH_2 tank were constructed, thereby also checking the projected ease of fabrication. The testing of the hardware was beyond the scope of this project, but is planned by NASA LeRC. The conclusions drawn are that composites will not save cost on the Shuttle LOX tank but would be a substantial cost saver on the LH_2 tank.

INTRODUCTION

A. OBJECTIVE

The objective of this program is the determination of the value of composite materials in the fabrication of structurally efficient, minimum cost, large scale, disposable propellant tanks for use with the Space Shuttle system.

B. BACKGROUND

At the time this program was initiated, the Space Shuttle system under consideration was the Grumman C2F configuration. Very large integral tankage was a common feature of the recoverable Booster and the Orbiter. In this initial effort, weight saving was the primary consideration with cost secondary. In executing the program, six design concepts were evaluated that employed composite materials to achieve weight reductions. The results of this initial effort are described and discussed in Appendices A and B. The continued effort would have resulted in the design, fabrication, and test of the selected designs, one set for the Booster tanks and one set for the Orbiter tanks.

Gross changes in the Space Shuttle concept occurred, such as the series-burn ballistic recoverable booster and the non-integral external drop-tanks for the Orbiter, because of drastic reductions in anticipated Shuttle annual budgets. In order to assure the relevance of the continuing program, a redirection was issued which reflected the urgent emphsais on reduced cost and in which the importance of weight was reflected by its impact on costs. Because the booster situation was still fluid, attention was concentrated on the cylindrical portions of external HO tankage of the Grumman 040S Shuttle configuration.

C. SCOPE

The contract scope consisted of analytical evaluations of several concepts of composite-reinforced 2219 aluminum alloy tank designs and the selection of an effective design for construction as a scale test model. The program effort consisted of two main tasks. In Task I - Design Evaluation, the materials, designs and costs of large-scale, disposable propellant tanks were evaluated. Cost was the primary selection criteria; weight was of secondary importance. In the development of the composite-reinforced tanks designs, composite properties were examined, analytical methods were determined, and parametric weight and cost studies were carried out. Component and materials evaluation in support of the analytical study consisted of material property and material-structural interaction investigations. In Task II - Experimental Evaluation, subscale models typical of low-cost disposable tankage were designed and fabricated to verify the low cost construction features and the structural adequacy. Test conditions typical of the Space Shuttle service environment were determined. Material evaluation in support of the design was also carried out.

COMPOSITE-REINFORCED PROPELLANT TANKS

A. TASK I - DESIGN EVALUATION

In this task, materials, designs, and costs of large-scale disposable propellant tanks were evaluated.

1. Configuration and Geometry

The Grumman 040S Shuttle configuration, consisting of a ballistic recoverable booster, disposable LH_2 and LO_2 tank, and Orbiter vehicle, is depicted in Figure 1. The disposable tank is cylindrical, with a conical taper in the LO_2 portion at the forward end. The end domes are elliptical. Welded 2219-T87 aluminum alloy is used for the pressure shell. Insulation is applied to the external surface, and any rings or stringers are on the internal surface. The aft interstage attachment to the Orbiter penetrates the LH_2 pressure shell, all other attachments are to skirt structure. The geometry of the disposable tank is given in Figure 2.

2. Environment and Loading Conditions

The critical loading conditions at the tank stations studied in the program are given in Tables 1 and 2. These load conditions and stations for analysis have been selected to show representative sections of the tank and to explore the full range of tank environment. The critical flight conditions correspond to the end of first stage boost and to post-orbit insertion. The LH_2 tank ultimate load intensity envelope for the end boost condition is given in Figure 3. The two other conditions included in the tables occur during the overwrap and cure processes. The temperatures of the tank wall structure were determined as follows:

a. Flight: End boost - the structural temperature equals the propellant temperature for an externally insulated tank

   Post-orbit insertion - the structural temperature is due to the combined effort of (external) ascent heating and (internal) autogeneous gas pressurization.

b. Manufacturer: Cure and post-cure - the temperature is determined by the manufacturing requirements of the resin system.

3. Structural Concepts

The structural concepts considered in this redirected contract effort were derived from the most promising of those considered in the original contract effort. These are discussed below and are illustrated in Figure 4. Because the tanks under consideration have most of their weight in the cylindrical sections, the design effort has been directed to these regions.

The baseline LH_2 tank consists of a 2219-T87 aluminum alloy pressure shell internally stiffened against axial compression by integral axial stiffeners and mechanically fastened rings. The "Integral Stringer" concept, Concept A (integrally stiffened design), also has internal integral axial stiffeners as in the baseline tank but is circumferentially overwrapped with S-glass or PRD fibers in order to reduce structural weight. The "Z-Stiffened" concept, Concept B, differs from Concept A in that the stiffeners are zee sections and that they and the rings are bonded to the shell. The "Sandwich" concept, Concept C, consists of an aluminum pressure shell stiffened as a honeycomb sandwich with a thin, glass fabric outer face.

The LO_2 baseline tank consists of a monocoque aluminum pressure shell. The "Membrane" concept, Concept D, utilizes circumferential overwrap of S-glass or PRD on the pressure shell.

4. Materials

a. ALUMINUM ALLOY 2219 Aluminum alloy 2219 was selected as the metal shell component of the composite reinforced propellant tanks. Handbook properties for the -T62 and -T87 conditions from 450°K to 78°K were used in the parametric study of tank configurations. The results are presented in Tables 3 and 4 (compiled from References 1, 2 and 3).

Although solution treatment and aging after welding provides optimum weld-joint strength, joint efficiency and joint ductility with 2219 aluminum for composite reinforced shells, this heat treatment cycle is not feasible for the tanks of interest. Instead, it was assumed that the metal shells will be fabricated in the -T37/-T87 temper, and have thickened weld lands which will be artifically aged/as-welded after welding.

b. COMPOSITE REINFORCEMENT FOR FILAMENT OVERWRAPPING Design properties at 450°K to 78°K were established for candidate filament-overwrapped composites which circumferentially reinforce the 2219 aluminum alloy propellant tanks. Initially, S-glass/epoxy, *PRD-49-III/epoxy, boron/epoxy, and graphite/epoxy were evaluated. Glass and PRD were selected as the most promising candidates based on strength, density, raw material cost, and fabricated composite cost. Resultant unidirectional filament-wound composite material properties for use in parametric design studies are presented in Table 5 and discussed below.

(1) S-901 Glass Filament/Epoxy This material has a very high demonstrated tensile strength-to-weight ratio in large filament wound tank structures. The composite tensile modulus increases by 10% from the room temperature value (RT) at 78°K (Ref. 1, 5). No change in modulus occurs from RT to 450°K. The composite strength increases 25% to 40% in going from ambient to cryogenic temperatures, but at 450°K a 20% reduction from the room temperature strength is observed (Refs. 1, 5 through 9). Glass filament/epoxy composites are subject to strength degradation due to cyclic loads and sustained loads, especially when the load level is high compared with the single-cycle strength. A significant amount of glass filament-wound

---

*Kelvar-49 is the current trade name.

vessel cyclic and sustained loading data is available to permit selection of reliable factors for glass/epoxy reinforcement of metal tankage structures.

Sustained Load Effects: Prestressing of filaments in order to reduce LOX tank weight would subject these fibers to long-term loading at room-temperature. The two design values studied were 82.8 kN/cm^2 and 55.2 kN/cm^2. The single-cycle strength is 152 kN/cm^2. The lower prestress, which is 36.5% of ultimate, could be sustained indefinitely at room temperature*. If the higher prestress, which is 54.4% of single-cycle strength, were used, the vessel would fail in less than one year,* if stored at room temperature. Storage at lower temperature would reduce the stress level. At cryogenic storage conditions, the sustained load capability would be very high. For example, vessels have been held for 70 days at 90% of single cycle ultimate at 78^{o}K (Ref. 9).

Coefficient of Thermal Expansion: Extensive data are available for 450^{o}K to 78^{o}K thermal coefficients of expansion for S-901 glass/epoxy filament-wound composites (Ref. 1, 5, 9).

Overview Glass/epoxy wound composite is by far the most mature of the candidate composite material systems in terms of state-of-the-art and successful application to operational systems. Techniques required to obtain composites of high quality, with consistently reproducible properties (raw material uniformity, resin content, void content, prestress, composite curing parameters, strength, and elastic properties) are known and understood to a greater degree than with the other candidate composite material systems. Quality-assurance systems exist for S-901 glass composite and include raw material specifications and fabrication process specifications. Current raw material costs ($11-$13/kg)** are much lower than for PRD fibers. High levels of prestress are practical. Fabrication of very thin individual layers is practical and significant in achieving minimum-weight tank designs.

(2) PRD-49-III Epoxy This composite system is relatively new, and evaluations of it indicate a strength-to-weight ratio advantage over S-901 glass/epoxy. In addition, PRD-49-III/epoxy composites have greater than twice the Youngs Modulus/density ratio of glass composites. Filament strength translation into composite strength is excellent. Accordingly, the PRD-49-III/epoxy wound composite is a leading candidate for tension loaded tank elements. Because of high strength of PDR-49-III, with higher modulus than glass, higher levels of stress can be developed in the filaments at lower strains in the metal shell substrate. Offsetting these advantages is a negative coefficient of expansion for PRD-49-III/epoxy composites, which works against thermal strain compatibility between the windings and metal shell during changes in operating temperatures. As a result, higher levels of filament pretension in the as-fabricated tank at room temperature are required to achieve design conditions at cryogenic temperatures. In addition, the negative thermal expansion

---

*Based on SCI proprietary data.

**The $11-13/kg is for highest quality S-901 glass; a commercial grade of the material is available which has 10% lower strength and the same modulus as S-901 glass.

coefficient increases the rate of filament stress increase (compared to glass/epoxy composites) when the tank is used at elevated temperatures. Current low compressive strength properties do not make the material an outstanding candidate for axial compression applications.

The data in Table 5 for PRD-49 composites are based on information derived from DuPont (the filament manufacturer) and from NASA-LeRC which is sponsoring work to evaluate PRD-49 in cryogenic filament-wound pressure vessels. Comments on the data follow.

Strength. The limited 4 in.-diameter by 6 in.-long pressure vessel tests conducted to date have yielded somewhat lower effective strength levels than have been attained with NOL rings. It is not known if strength levels obtained in the simple rings and small vessels will be achieved in the large tanks of interest. In the absence of other information, and with the assumption that PRD-49-III strength levels will increase somewhat as filament and composite fabrication parameters are optimized, the NOL ring strength data have been adopted.

At 78°K, the NASA-LeRC sponsored work shows the composite strength to be essentially the same as at 297°K.

Data are not available for the 450°K design condition. A strength of 80% of the room temperature value was adopted as a reasonable estimate.

Room temperature test results on the small filament-wound vessels and on simple laminates have shown dramatically that PRD-49 composites are insensitive to cyclic and sustained loadings. For example, in the pressure vessels, 1000 cycles to 60% of single cycle strength produced no strength degradation and 1000 cycles were sustained at the 90% load level prior to failure. Under static loading conditions, PRD-49 composites can sustain loading at 90% of ultimate without failure for 1000 hours. Thus, the indication is that cyclic and sustained loading will not seriously degrade the composite strength levels at room temperature for the tank service loadings anticipated. PRD-49 composites may be expected to display these same characteristics at 78°K and 450°K.

Overview. PRD-49/epoxy composite is a relatively new material; however, much work is in progress and is being initiated to provide evaluations and performance demonstrations of the material. Its properties are quite attractive as a filament reinforcement of metal tankage. The fiber currently costs much more than S-901 glass fibers, and substantially less than boron or high-strength graphite fibers. However, current raw material costs of $44/kg are projected to drop as material sales volume increases.

(c.) MATERIALS USED FOR HONEYCOMB REINFORCEMENT. Mechanical properties of the materials used in the analysis of Concept C, the honeycomb reinforced tank, were obtained from various specifications and commerical sources. These properties are given in Table 6. Part I of Table 6 describes cloth properties, Part II gives core properties and Part III gives the adhesive properties.

5. Analysis

a. CRITERIA Criteria and groundrules which reflect Grumman Shuttle analysis procedures were defined for composite reinforced tanks. The following criteria were utilized:

(1) When flight loads and internal pressure act together, ultimate load consists of ultimate flight loads coupled with limit pressure loads. This is shown schematically in the figure below. When internal pressure relieves axial compressive flight loads,

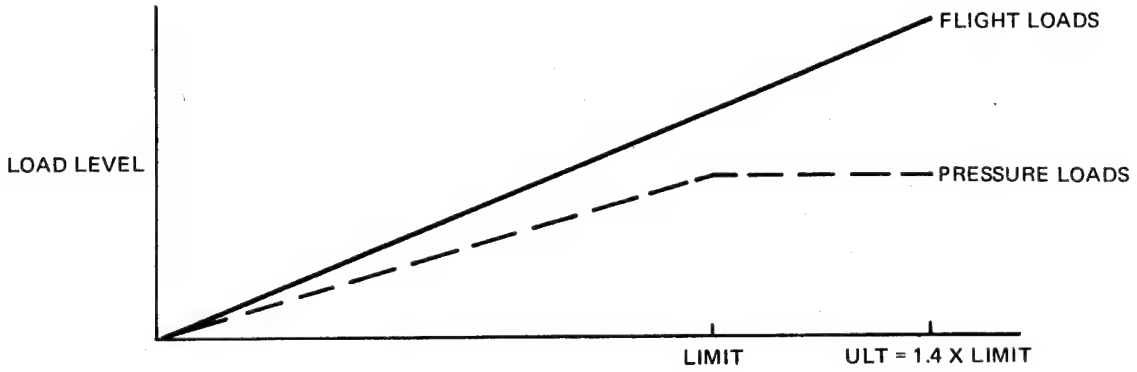

1.4 x flight load is combined with the axial load corresponding to minimum system pressure to determine ultimate axial load. Where internal pressure adds to tensile flight loads, 1.4 x flight load is combined with the axial load corresponding to maximum system pressure. Pressure vessels will be designed for a pressure of 1.4 times maximum limit pressure as a separate design condition.

(2) Stresses for biaxial load cases will be computed using the octahedral shear stress theory: $\sqrt{f_x^2 + f_y^2 - f_x f_y} \leq F$. For stresses combined with axial compression, F is set equal to F_{cy}. For biaxial tension cases, F is set to $F_{allow} \approx .92\ F_{tu}$ where F_{allow} is determined by plasticity calculations.

(3) In overwrapped designs, the maximum overwrap tensile stress is $F_{tu}/1.4$ at limit load and the maximum compressive liner stress is $F_{cy}/1.15$.

The following groundrules were assumed:

(1) Two stations on the LO_2 tank, Sta 1240 and 1550, will be studied.

(2) Two points at Stations 3050 and 4065 on the upper surface of the LH_2 tank will be studied.

(3) Frame spacing has been fixed at 76.2 cm.

(4) External pressure will not be a design condition.

b. COMPRESSION PANEL OPTIMIZATION Automated procedures exist at Grumman for obtaining minimum-weight configurations for axially compressed, stiffened panels. A computer program for integrally stiffened panels is based on the analysis procedure of Ref 11 and incorporates the random search synthesis procedure of Ref 12. A second program for zee-stiffened panels uses the analysis of Ref 13 in conjunction with a minimization method based on Refs 14 and 15. For specified materials and loads, these computer programs develop minimum-weight sections and give as results the stiffener dimensions, spacing, and sheet thickness. Also included in the output are the critical stresses of the panel elements in the various buckling and failing modes. A slight modification to the zee-stiffened panel program was necessary in order to account for bonding of the stiffeners to the sheet instead of riveted attachments. A triangular distribution of reactive forces between the sheet and attached flange of the stiffener was assumed. The "equivalent" rivet offset distance from the stiffener web is therefore one-third of the attached flange width.

c. MEMBRANE OVERWRAP A computer program for circumferentially overwrapped cylindrical pressure vessels was also developed (Ref. 16) to aid in the investigation of the various fiber overwrap materials. Wrap and liner thickness and stresses are calculated for various loading conditions and temperature when a wrap prestress and a design condition liner hoop stress are specified.

d. GENERAL INSTABILITY General instability strength of the stiffened shells was determined using a computer program based on the results of Ref 17. Additional cross checks were made using the program of Ref 18.

e. HONEYCOMB Honeycomb analysis was based on the methods of Ref 19. Initial calculations included the effects of face-sheet stiffness (Ref. 20) but these were found to be negligible for the configurations considered.

f. PROCEDURE The analysis tools discussed above were incorporated into a design procedure. Many configurations were analyzed, thereby leading to more efficient designs. The design criteria were coupled with the analysis, and minimum-weight designs consistent with the criteria and groundrules were determined. Since the procedures differ somewhat for the various structural concepts, they are discussed separately below, and followed by some sample calculations.

(1) Integrally-Stiffened and Z-Stiffened Designs, Concepts A and B

If it is assumed that the net ultimate axial load (Condition 1 - end boost) acts alone (i.e., tank pressure is neglected), a compression-only minimum weight design can be determined for each specified tank wall thickness by using the computer optimization programs for integrally-stiffened or zee-stiffened panels. Each of these designs is able to sustain the applied ultimate axial load, but are of different weights and are working at different stress levels. The maximum stiffener stress (as well as local and overall instability stresses, geometry, etc.) is given in the results. These are included in Tables 7 and 8. The panel weight (or "smeared" thickness) is also obtained for each specified skin thickness and is shown in Figure 5.

Each of these results is then checked for combined stresses using the (maximum compressive) sheet edge stress and the hoop stress due to the internal limit tank pressure of Condition 1.

The designs are also checked as pressure vessels (1.4 x limit tank pressure)

The lightest weight designs which satisfy all the load conditions and criteria are designated as "baseline" (all aluminum) panels. (The integral stiffened panel, Concept A, was designated as the Shuttle LH_2 tank baseline structure.)

For each candidate panel, the (maximum compressive) sheet edge stress from (a) is used to determine an allowable hoop stress which satisfies the combined stress criteria. These are listed in the last column of Tables 7 and 8.

The composite overwrap computer program for pressurized cylindrical tanks is used to determine overwrapped designs and to calculate wrap and metal liner stresses for all load conditions. A typical set of results is given in Table 9. The wrap prestress and design condition allowable liner hoop stress are specified for each set of calculations.

These designs are checked for the combined stress and overwrapped design criteria.

The lightest of these which meet all the criteria are selected as overwrapped designs. Weight comparisons of the various designs are given in Tables 10 and 11.

The required ring size to provide general instability strength was determined by varying the ring size until the general instability load exceeded the net ultimate applied load. A knockdown factor of .75 was used with the calculated critical load.

The dimensions and unit weights of the minimum weight sections are summarized in Tables 12 and 13.

(2) Sandwich Design, Concept C

The required thickness of equal aluminum face-sheets for biaxial strength is determined using the combined stress criteria and the applied axial and hoop loads for the loading conditions.

For the aluminum honeycomb core, the core depth required to satisfy general instability for the applied ultimate axial load is determined using the honeycomb cylinder analysis and design charts.

Local instability (wrinkling and intercell buckling) of the face sheets is checked.

This design is classified as a "baseline".

For the composite sandwich, the inner aluminum face sheet thickness is assumed equal to the sum of the face sheet thickness obtained in (a).

For a range of fiberglass outer face sheet thicknesses and a given honeycomb core, core depths required to satisfy general instability are determined. These calculations are carried out in Table 14 for the paper core sandwich.

Local instability of the face sheets is again checked.

The lightest of the designs which meet all the criteria are selected as composite reinforced designs. The results are summarized in Table 15.

Rings are not required since general instability was satisfied without them. A summary of unit weights for the LH_2 tank is given in Table 16.

(3) Membrane Design, Concept D (LO_2 Tank)

A baseline aluminum thickness is determined for the pressure loading conditions and design criteria.

The composite overwrap computer program for pressurized cylinders is used to determine overwrapped designs. For specified values of overwrap prestress and design condition liner hoop stress, wrap and liner thicknesses which satisfy the load conditions and criteria are determined. By systematically varying the prestress and hoop stress, panels of different local weights are obtained. A plot of local weight ("equivalent" aluminum thickness) as a function of prestress and hoop stress is presented in Figures 6 and 7. The minimum weight designs were selected and are presented in Table 17.

g. SAMPLE CALCULATIONS Some sample calculations which illustrate the procedures discussed in the previous subsection are given here. The cross-sections chosen for illustration were selected from the results of the optimization studies. The material properties are those quoted in Tables 3, 4, 5, and 6.

(1) LH_2 Tank - Baseline Structure - Integrally Stiffened at Sta 3050, Condition 1

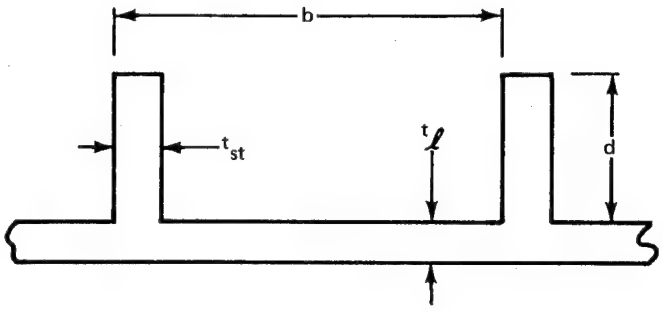

$b = 18.1$ cm $\quad t_\ell = .343$ cm
$d = 4.44$ cm $\quad t_{st} = .335$ cm
$\bar{t}_\ell = t_\ell + dt_{st}/b = .426$
$h = d + t/2 = 4.61$ cm
$N_{appd} = -6130$ N/cm (ult)
$L = 76.2$ cm (frame spacing)

Following the analysis method of Reference 11,

$r_b = h/b = .255$

$r_t = t_{st}/t_\ell = .977$

$r_b V_t = .249$

$K_c = 4.24$ (Fig 1 of Ref 1)

Local Buckling

$$f_{cr} = .094\, K_c E \left(\frac{t_\ell}{b}\right)^2$$

$E = 8.75 \times 10^6$ N/cm^2 (2219-T87 @ 20°K)

$f_{cr} = 12100$ N/cm^2

Required stiffener rigidity:

$$\nu_{req'd} = \left(\frac{EI_{st}}{bD}\right)_{req'd} = \text{antilog}\left(m \log \frac{L}{b} + C\right)$$

Where: $m = 2.325 - .0905\, K_c + .0625\, r_b\, r_t = 1.956$

$C = -.175 + .187\, K_c + .325\, r_b r_t = .701$

$\nu_{req'd} = 83.8$ for buckling

Applied stress:

$$f_c = N_{appd}/t_\ell = 14400 \text{ N/cm}^2 > f_{cr}$$

For post buckling: $\gamma_{req'd} = \gamma_{req'd}\, f_c/f_{cr} \approx 100$

$$\gamma_{actual} = (1 - \nu^2)\, r_b r_t \left(\frac{h^2}{t_\ell}\right) \frac{4(b'_e/b) + r_b r_t}{(b'_e/b) + r_b r_t}$$

using $b'_e/b = .5$, $\gamma_{actual} = 123 > \gamma'_{req'd}$

Buckling of outstanding flange:

$$f_{st} = .384\, E \left(\frac{t_{st}}{d}\right)^2 = 18600 \text{ N/cm}^2 > f_c$$

Panel flexural instability: For the skin edge stress equal to $f_e = 18600$ N/cm^2:

$$f_{cr}/f_e = .65$$

Effective widths for load and stiffness:

$$b_e/b = 1.20(f_{cr}/f_e)^{2/5} - .65(f_{cr}/f_e)^{4/5} + .45\,(f_{cr}/f_e)^{6/5} = .818$$

$$b'_e/b = .72\,(f_{cr}/f_e)^{2/5} - .13\,(f_{cr}/f_e)^{4/5} - .09\,(f_{cr}/f_e)^{6/5} = .460$$

Radius of gyration:

$$\rho_R = \frac{h}{\sqrt{12}} \sqrt{\frac{r_b r_t (4b'_e/b + r_b r_t)}{(b_e/b + r_b r_t)(b'_e/b + r_b r_t)}} = 1.105 \text{ cm}$$

$$L/\rho_R = 69$$

$$f_{col} = \frac{\pi^2 E}{(L/\rho_R)2} = 18100 \text{ N/cm}^2 \approx f_e < f_{st}$$

Panel failing stress:

$$f_{all} = f_e \frac{r_b r_t + b_e/b}{1 + r_b r_t} = 15600 \text{ N/cm}^2 > f_c$$

Combined stresses:

$$f_{hoop} = pR/t_{\ell} = 26.9 \times 378.46/.343 = 29700 \text{ N/cm}^2 \text{ at limit load}$$

$$f_{axial} = f_e = -18300 \text{ N/cm}^2 \text{ at ultimate load}$$

$$F = \sqrt{f_{axial}^2 + f_{hoop}^2 - f_{axial} f_{hoop}} = 42000 \text{ N/cm}^2$$

$$F_{ty} = 45800 \text{ N/cm}^2 > F$$

For Condition 2 at limit pressure at T=367°K, $f_{hoop} = pR/t = 24.8 \times 378.5/.343 = 27400 \text{ N/cm}^2$

$$F_{tu}/1.4 = 27600 \text{ N/cm}^2 > f_{hoop}$$

(2) LH_2 Tank - Concept A - Integrally Stiffened and Overwrapped at Sta 3050, Condition 1

b = 22.1 cm	$t_{\ell} = .208$ cm	$r_b = .222$	$r_b r_t = .471$
d = 4.80 cm	$t_{st} = .442$ cm	$r_t = 2.12$	
h = 4.90 cm	$\bar{t}_{\ell} = .305$ cm	L = 76.2 cm	$N_{appd} = -6130$ N/cm (ult)

Local buckling:

$$K_c = 6.13 \text{ (Fig. 1 or Ref. 1)}$$

$$f_{cr} = .904 K_c E \left(\frac{t_{\ell}}{b}\right)^2 = 4300 \text{ N/cm}^2$$

Required stiffener rigidity.

$$m = 1.794 \qquad c = 1.123$$

$$\gamma_{req'd} = 122.5 \text{ for buckling}$$

Applied stress:

$$f_c = N_{appd}/\bar{t}_{\ell} = 20100 \text{ N/cm}^2$$

For post buckling.

$$\gamma'_{req'd} = 576$$

$$\gamma_{actual} = 607 \text{ for } b'_e/b = .5$$

Buckling of the outstanding flange:

$$f_{st} = 31200 \text{ N/cm}^2 \quad > f_c$$

Panel flexural instability for the skin edge stress equal to $f_e = 31200 \text{ N/cm}^2$:

$$f_{cr}/f_e = .138$$

$$b_e/b = .452$$

$$b'_e/b = .290$$

Radius of gyration:

$$\rho_R = 1.479$$

$$L/\rho_R = 51.6$$

$$f_{col} = 32200 \text{ N/cm}^2 \approx f_e$$

No plastic correction is required since the proportional limit stress is approximately:

$$f_{pl} = .7 F_{cy} = 32000 \text{ N/cm}^2$$

Panel failing stress:

$$f_{pl} = 2000 \text{ N/cm}^2 \approx f_c$$

Combined stresses:

$$F = \sqrt{f_{axial}^2 + f_{hoop}^2 - f_{axial} f_{hoop}} = F_{cy}$$

$$f_{axial} = f_e = -31200 \text{ N/cm}^2 \text{ at ultimate load}$$

Therefore, the maximum allowable hoop stress is:

$$f_{hoop} = 22300 \text{ N/cm}^2 \text{ at limit pressure (see criteria)}$$

Overwrap Design

From Reference 16, the liner hoop stress is:

$$f_{hoop} = \frac{pR}{t_\ell} - \frac{1}{t_\ell} \left[E_\ell t_\ell \epsilon_i + pR \left(1 - \frac{\nu}{2} \frac{p_x}{p}\right)\right] \frac{E_w t_w}{E_\ell t_\ell + E_w t_w}$$

and the liner axial stress is:

$$f_{axial} = \frac{p_x R}{2 t_\ell}$$

where the subscript "w" refers to the wrap, p_x is the pressure causing axial stresses, and:

$$\epsilon_i = \frac{f_{prestress}}{E_w} + (\alpha - \alpha_w)(T - T_{initial})$$

where $T_{initial} = 367^{\circ}K$, the cure temperature

Hoop stress in the wrap:

$$f_w = \frac{1}{t_w}\left[E_\ell t_\ell \epsilon_i + pR\left(1 - \frac{\nu}{2}\frac{p_x}{p}\right)\right]\frac{E_w t_w}{E_\ell t_\ell + E_w t_w}$$

Material properties obtained from Tables 3, 4, and 5 for the overwrap analysis:

	2219-T87		S-GLASS	
	-20° K	367° K	20° K	-367° K
E, N/cm²	8.75×10^6	7.14×10^6	6.28×10^6	5.72×10^6
F_{tu}, N/cm²	64000	38600	190000	138000
F_{cy}, N/cm²	45800	31200	–	–
α, cm/cm°C	16.0×10^{-6}	–	2.88×10^{-6}	–

Wrap prestress for S-Glass is:

$$f_{prestress} = 82800 \text{ N/cm}^2$$

For Condition 1, at limit pressure p = 26.9 N/cm² and T = 20°K.

$$f_{hoop} = 22300 \text{ N/cm}^2 \text{ (allowable liner hoop stress)}$$

$$f_w = 87100 \text{ N/cm}^2$$

For Condition 2, at limit pressure p = 24.8 N/cm² and T = 367°K:

$$f_{hoop} = 15500 \text{ N/cm}^2$$

$$f_w = 97600 \text{ N/cm}^2$$

$$F_w/1.4 = 98600 \text{ N/cm}^2 > f_w \text{ (see criteria)}$$

For Condition 4 - post-cure, at T = 367°K:

$$f_{hoop} = -21900 \text{ N/cm}^2$$

$$F_{cy}/1.15 = 27100 \text{ N/cm}^2 > f_{hoop} \text{ (see criteria)}$$

These results are included in Tables 7 through 12 along with the results of calculations carried out for other configurations and concepts.

(3) LH_2 Tank - Concept C - Sandwich Design at Sta 3050

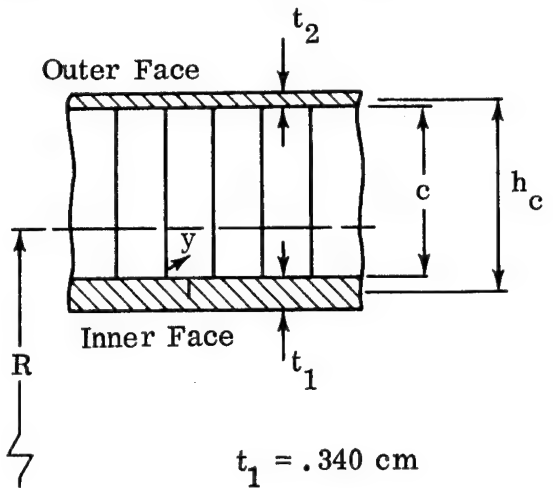

$t_1 = .340$ cm

$t_2 = .051$ cm

$c = 4.60$ cm

$h_c = 4.80$ cm

Outer Face: 1581 Glass Cloth

$F_{tu} = 88200$ N/cm^2

$F_{cy} = 72200$ N/cm^2

$E = 2.91 \times 10^6$ N/cm^2 at 20°K

Paper Core: HNC-3/8-60(20)E-2.0

$G_{cw} = 2620$ N/cm^2

$E_c = 20400$ N/cm^2 at 20°K

Inner Face: 2219-T87 Aluminum Alloy

See previous pages for mechanical properties

Inner face thickness:

For Condition 2 at limit pressure and T = 367°K

$f_{hoop} = pr/t_1 = 24.8 \times 378.5/.340 = 27600$ N/cm^2

$F_{tu}/1.4 = 27600$ N/cm$^2 \approx f_{hoop}$ (see criteria)

Condition 1 is less critical

Outer face thickness:

A minimum of two layers of fiberglass is recommended for manufacturing and quality assurance reasons by GAC's materials and manufacturing groups.

General Instability, for Condition 1 at ultimate load: Following the analysis method of Reference 19;

Face sheet stiffness at T = 20°K:

$E_1 t_1 = 8.75 \times 10^6 \times .340 = 2.98 \times 10^6$

$E_2 t_2 = 2.91 \times 10^6 \times .051 = .15 \times 10^6$

$\Sigma = 3.13 \times 10^6$, and $\frac{E_2 t_2}{E_1 t_1} = .0504$

$t_{eff} = t_1 \times \Sigma Et/E_1 t_1 = .340 \times 3.13 \times 10^6/2.98 \times 10^6 = .357$ cm

$\bar{y} = \Sigma yEt/\Sigma Et = 4.63 \times .15 \times 10^6/3.13 \times 10^6 = .222$ cm

$R_{cg} = 378.46 + .17 + .22 = 378.85$ (negligible correction)

Radius of gyration:

$$\rho = h_c \sqrt{E_2 t_2 / E_1 t_1} \div \left[1 + E_2 t_2 / E_1 t_1\right]$$

$$\rho = 4.82 \sqrt{.0504}/1.0504 = 1.029 \text{ cm}$$

$$R/\rho = 378.85/1.029 = 368$$

from which the knockdown factor γ_c is obtained from Figure 4.2-8 of Reference 19.

$$\gamma_c = .43$$

Uncorrected shell buckling stress:

$$f_{01} = 2.1\ E_1\ \rho/R = 2.1 \times 8.75 \times 10^6/368 = 49900 \text{ N/cm}^2$$

Shear crimping stress:

$$f_{crimp} = h_c G_{xz}/t_{eff} = 4.82 \times 2620/.357 = 35400 \text{ N/cm}^2$$

Buckling coefficient:

$$K_c = 1 - \gamma_c f_{o1}/4\ f_{crimp} = .85$$

Critical elastic buckling stress:

$$f_{cr_{el}} = \gamma_c K_c f_o = .43 \times .85 \times 49900 = 18100 \text{ N/cm}^2$$

Applied axial compressive stress, Condition 1:

$$f_{appd} = 6130/.357 = 17200 \text{ N/cm}^2$$

Plasticity correction:

$$f_{axial} = -17200 \text{ N/cm}^2$$

$$f_{hoop} = 27600 \text{ N/cm}^2$$

$$F = \sqrt{f_a^2 + f_h^2 - f_a f_h} \leq F_{cy} \text{ (yield criteria)}$$

from which:

$$f_{axial_{yield}} = F_{cy}/\sqrt{1 + R^2 - R} \quad \text{where } R = f_{hoop}/f_{axial}$$

$$R = 27600/(-17200) = -1.61$$

$$f_{axial_{yield}} = .439\ F_{cy} = 31700 \text{ N/cm}^2$$

Using the plasticity reduction curve of Figure 8:

$$\frac{f_{cr_{el}}}{f_{axial_{yield}}} = .571$$

from which:

$$\frac{f_{cr}}{f_{axial_{yield}}} = .570 \text{ (no plastic correction)}$$

and

$$f_{cr} = 18100 \text{ N/cm}^2$$

Face wrinkling:

$$f_{wr_{el}} = 0.33E \left(\frac{E_c t}{E_c}\right)^{1/2}$$

for the aluminum face:

$$f_{wr_{el}} = 0.33 \times 8.75 \times 10^6 \left(\frac{20400 \times .340}{8.75 \times 10^6 \times 4.60}\right)^{1/2} = 38000 \text{ N/cm}^2$$

Using Figure 8 in the same manner as above:

$$f_{wr} = 26900 \text{ N/cm}^2 > f_{cr}$$

For the fiberglass face:

$$f_{wr_{el}} = 0.33 \times 2.91 \times 10^6 \left(\frac{20400 \times .051}{2.91 \times 10^6 \times 4.60}\right)^{1/2} = 8400 \text{ N/cm}^2$$

Applied fiberglass face stress:

$$f = \frac{6130 - 17200 \times .340}{.051} = 5500 \text{ N/cm}^2 < f_{wr}$$

These results and those for other honeycomb configurations are given in Tables 14 and 15.

6. Design Results

Unit weights at two points on the upper surface of the LH_2 tank have been determined for the different concepts. These weights are summarized in Table 16. The results shown are for the minimum weight cross-sections derived using the analysis of Section 5. Integrally stiffened Concepts A (Integral Stringer) and B (Z-Stiffened), result in significant unit weight reductions relative to the all aluminum design when prestressed circumferential overwrap is applied. The weight reduction is greater for the panels with the lower axial load. The overwrap prestresses listed in the tables are the maximum values which can be used while also satisfying the design criteria. In general, a higher value of the wrap prestress will result in a greater weight reduction. The sandwich, Concept C, results in a slightly higher unit weight relative to the baseline.

Unit weights at two stations on the LO_2 tank have been determined for the baseline and overwrapped concepts. These are presented in Table 17. Again, the overwrap prestresses listed in the tables are the maximum values which can be used.

It should be noted that the unit weights given in the tables are idealized weights and that the unit weights of the actual structure would be somewaht higher.

7. Manufacturing Options and Estimated Cost

As part of the evaluation of the various concepts, alternative methods of fabrication were reviewed by the Grumman Product Manufacturing Department. The alternatives were appraised on the basis of cost, manufacturing complexity and the requirements for successful development technology. A system of baseline values was established for each of these parameters. This permitted the evaluation of each alternative in terms of dollars per kilo or dollars per square meter. Welding and X-rays were estimated in dollars per linear meter. Precision of the dollar value assigned each process or operation was not as critical as the level of manufacturing difficulty, as reflected in the cost of the various designs.

Estimates were based on industry-wide manufacturing facilities. Limitations of the existing capacities for machining, rolling, brake-forming, chem-milling etc. were considered. Costs of tooling and cost of test facilities that were required because they were not commercially available were amortized over the full tank production as non-recurring costs.

The approximate dimensions of the Orbiter tank cylindrical portions are given below.

TANK	DIAMETER, CM	LENGTH, CM	CIRCUMFERENCE, CM
LO_2	757	233	2376
LH_2	757	2037	2376

The conical region of the LOX tank has an axial length of about 368 cm, a small diameter of about 590 cm and large diameter of about 757 cm. The developed cone requires differently shaped rectangular envelopes, depending on the number of equal-size central angles of the developed cone selected. The envelope dimensions are illustrated in Fig. 9 for a single- and a seven-segment option. They are tabulated below for a number of options.

NUMBER OF EQUAL CENTRAL ANGLES	CENTRAL ANGLE	(HEIGHT)	(WIDTH)
1	79.4 deg	2193 cm	686 cm
2	39.7	1165	458
3	26.5	786	414
4	19.85	592	397
7	11.35 deg	339 cm	385 cm

The available sheet sizes depend on the thickness required. For comparison with the area (circumference x length) of the cylinder and (height x width) of the conical segment envelopes, the sizes are:

THICKNESS	TRANSVERSE DIM	LONGITUDINAL DIM
6.35 cm	295 cm	856 cm
5.10	290	808
2.54	366	1880
0.95 cm	366 cm	2500 cm

The schedule of thicknesses for the stations and designs for which costs were established are listed below. Only the baseline and its variants required thick sheet; all the other designs required less than the 0.95 cm minimum gage.

a. MANUFACUTRING OPTIONS. Prior to discussing estimated costs, a description of the alternative designs and methods of fabrication is presented. Since the LOX tank is thin and monocoque in all variants, no thickness alternatives exist. For the LH_2 tank baseline configuration, the thicknesses designated A, B and C offer alternative manufacturing approaches.

(1) Stock size: 6.35 cm x 295 cm x 856 cm. The stiffeners on one side of the plate are integrally machined to the desired height. The ring frame flanges on the opposite side of the plate are also integrally machined. After the tank has been overwrapped, the frames are riveted to the flanges. The design implications of this concept are designated Ⓐ on Fig. 10 through 14.

(2) Stock size: 5.1 x 290 x 808 cm. The stiffeners on one side of the plate are integrally machined to their designed height. After the metal is welded and overwrapped, the frames are bonded to the tank's external surface. The design implications of this concept are designated Ⓑ on Fig. 10 through 14.

(3) Stock size: 2.54 x 366 x 1880 cm. Flanges to be used as stiffener attachments are integrally machined on one side of the plate. Extrusions are riveted to the flanges in order to achieve the stiffener's designed height. Frames are applied as in (2). The design implications of this concept are designated Ⓒ on Fig. 10 through 14.

Two methods of fabrication for the above design may be used to construct the LH_2 tank's cylindrieal portion:

(1) The cylinder may be constructed from four 1880 cm-long x 283 cm cylindrical-arc segments which are welded together. Each segment is composed of a plate (or plates) machined while flat and then formed into arcs of a circular cylinder. These segments are machine welded in a fixture (See Figures 11 and 12.) Material stock sizes impose constraints on this procedure. The maximum length available for the 5.1 cm stock is 808 cm, for 6.35 cm stock, it is 856 cm. Since the tank length is 2037 cm, the segments fabricated from 5.1 (B) and 6.35 (A) cm stock must be spliced twice and the 2.54 cm thickness plate must be spliced once, as indicated in Fig. 11.

(2) The cylinder may be fabricated from plate (or plates) machined in the flat and formed to a longitudinally split cylinder with a 378.5 cm radius. Each longitudinal split line and each junction of adjacent cylinders is machine-welded after the mating parts have been butted and held in a fixture. Because of the variations in sheet width with thickness the Ⓐ design requires 8 cylinders, the Ⓑ designs 7 cylinders, and the Ⓒ designs 6 cylinders to achieve a cylinder length of 2037 cm. See Fig. 13 and 14.

The overwrapped baseline and the baseline designs are closely similar, so no additional discussion of the integrally stiffened fabrication is required.

The design alternatives for the zee-stiffened design are confined to the ability of forming a tank from rolled plate approximately .95 cm thick. Available stock material in .95 cm thickness is 366 cm wide and up to 2500 cm long. For the Orbiter LH_2 tank cylinder, (circumference = 476 cm, length = 2037 cm), two alternative fabrication methods are feasible.

(1) Taking advantage of the material stock length, the sheet is rolled and welded along the longitudinal axis using 6.5 or 7 sheets. Each of the sheets is chem-milled leaving thickened lands at the edges and pads for blind fastener and frame connections. Frames and stiffeners are bonded to the tank external surface after overwrapping (See Figure 15).

(2) The cylinder is fabricated by rolling the sheets into cylindrical segments 757 cm in diameter. The ends, butted and held in a fixture, are machine welded. Segments of 366 cm maximum arc length are formed and, by butt welding six together, the 2037 cm length can be achieved. Frames and stiffeners will be attached after overwrapping. Chem-milling operations will be identical with Method 1 (See Figure 16). It should be noted that the total weld length for both methods is approximately equal.

Method 1): 2037 x 7 = 14,260 cm
Method 2): 2376 x 5 + 2037 = 13920 cm

For the honeycomb design, three alternative methods of construction are available (see Figures 17, 18 and 19) based primarily on the size of existing autoclaves.

(1) The largest autoclave required would accommodate a full-length vessel 2037 cm long x 757 cm in diameter. The vessel's metal parts could be assembled either as girth welded circular cylinders 366 cm long and 757 cm in diameter, or from seven formed circular segments of 378.5 cm radius of 2037 cm axial length and 338 cm arc length. The vessel shown in Fig. 17 would be pressurized (with sealing closures retained mechanically by longitudinal struts to avoid applying axial load on the cylinder) to round and stabilize its shape. The honeycomb core would be adhesively bonded and then the glass cloth face sheet would be tautly wrapped and bonded.

(2) Suppose an autoclave to be available which can accommodate a 757 cm-diameter vessel but a shorter length than 2037 cm. The tanks would then

be made of right circular cylinders whose axial length equals the sheet width of 366 cm. Since the circumference of these cylinders, 2037 cm, is smaller than the 2500 cm sheet length, a single longitudinal joint will be required. The number of cylinders girth welded together before autoclaving on the honeycomb core and glass cloth will be determined by available autoclave dimensions. The minimum diameter is 757 cm and length 366 cm. In all other respects the fabrication proceed as in Method 1.

(3) Suppose a long but shallow autoclave were available. Since the cylinder is only 2037 cm long, it is possible to use seven circular-arc segments of 338 cm arc length. The chord length would be 329 cm and the height 38 cm. The 2037 cm x 329 cm x 38 cm envelope of these segments defines the autoclave required. The honeycomb core would be adhesively bonded and then the two layers of glass cloth superposed and bonded. The weld details and the splice between these segments is indicated in Fig. 18 and 19.

b. COSTS. The objective of this task is to select, on the basis of cost savings, the best of the designs studied in the previous sections of the report. In order to accomplish this goal, total program costs for each of the concepts were estimated and compared to the baseline tank. Total program costs are made up of the transportation and manufacturing costs discussed below.

The concepts for which program costs were evaluated are those listed in Table 18. PRD was eliminated from use as an overwrap material because there were no weight savings for it relative to the S-glass overwrapped concepts while its manufacturing costs were higher than those for S-glass. The use of glass or aluminum core in the honeycomb concept was eliminated for similar reasons.

1. Transportation Costs. - Unit transportation cost, expressed in dollars per kilogram, is the value of an increment of weight added to any component in the Shuttle stack (orbiter, HO tank, or Booster) while at the same time maintaining a constant mission performance. This cost was determined by the Grumman Shuttle program to provide a basis for cost effectiveness tradeoffs during the Shuttle systems evaluation and selection study. A unit transportation cost of $22,000 per kilogram was specified for the HO tank, and is used in this evaluation. The unit weights of the concepts, summarized in Table 18, were used to estimate weights of the cylindrical portion of the LH_2 tank and the cone-cylinder portion of the LO_2 tank. These results are shown in Table 19. For the LH_2 tank, the area was reduced by 33.4 m^2 (7%) to allow for non-typical structure in the region of the Orbiter aft interstage fitting. The unit weights, multiplied by their respective areas, give the theoretical cylinder weights shown. These weights, multiplied by the non-optimum factors (NOF) described below, result in the estimated cylinder weights. The product of the cylinder delta weights and the unit transportation cost is the delta transportation cost also listed in Table 19.

The NOF is the ratio between likely actual and theoretically possible minimum weights. One should expect that the NOF's will exist. They account for the effect of drawing tolerances (permitting larger than minimum dimensions for manufacture and

inspection), fillets, weld lands, extra plastic at joints in honeycomb and other weight raisers which were not considered in obtaining an ideal weight. The weights departments of aerospace companies must include these effects in order to derive useable, reliable weight estimates in preliminary design. They have accumulated statistical data on different types of structures in order to make their predictions. The GAC Weights Department considers its factors accurate to within 5 to 10 percent.

2. Manufacturing Costs. Manufacturing costs are the costs of producing the flight articles and include the following:

- Material
- Tool material
- Production labor
- Quality control labor
- Tool design labor
- Tool manufacturing labor
- Manufacturing management

A breakdown of manufacturing costs is given in Table 20.

3. Program Costs. - The unit recurring and non-recurring manufacturing costs are converted to total program manufacturing costs for each concept in Table 21. Delta manufacturing costs for the program are also determined. Total program delta costs are listed in Table 22. These combine the transportation delta costs for Table 19 and the manufacturing delta costs from Table 21.

8. Results

For the LH_2 tank, Concept C, the honeycomb stiffened aluminum pressure vessel, has the potential for the greatest cost savings. Concept B, bonded-on Z stiffeners, also has potential for significant cost savings. It can be seen in the table of total program costs (Table 22) that the LH_2 tank cost savings are due primarily to the manufacturing delta costs rather than the transportation costs. In the table of manufacturing cost breakdown, it can also be observed that the controlling items are the recurring material and manufacturing costs. For Concept A, these items total $157 million, while for Concepts B and C these items total $66 million and $62 million respectively. The cost difference of approximately $93 million is primarily a consequence of machining integrally stiffened planks from thick billets for Concept A. The use of thinner gage sheet and plate in Concepts B and C therefore accounts for the cost savings while the structure remains competitive from a weight viewpoint.

No cost savings were obtained for the LO_2 tank.

B. TASK II - EXPERIMENTAL EVALUATION

The major cost saving shown in Task I was achieved on the LH_2 tankage. Therefore, experimental verification of the ease of fabrication and of the structural adequacy of the novel sandwich construction was undertaken. For this purpose, a subscale cylindrical model was designed to represent the full-scale Shuttle tankage. Two test articles and a set of end-dome assemblies were fabricated for subsequent structural testing.

1. Modeling and Design

The configuration of the honeycomb reinforced pressure vessel is such that direct scaling down of the full sized tank is not possible; e.g., the honeycomb cell size and the number of plies in the composite outer face cannot be scaled. The table below gives the critical dimensions of the full-scale and 1/6-scale models.

	Full Scale	Ideal Model	Actual Model
Outer Facing Glass Cloth, t, cm	.0584	.0083	.0584
Honeycomb Cell Depth, cm	4.60	.651	.673
Honeycomb Cell Size, cm	.956	.160	.48
Inner 2219 Al. Alloy t, cm	.340	.0572	.0762
Cylinder radius, cm	378.5	63.67	63.67

The design procedure for the model was based on the following considerations, which reflected practical material limitations while assuring a valuable structural model.

First, the inner face thickness was determined such that the ratio of longitudinal stress to hoop stress in the model would be the same as in the full sized tank, while at the same time approximately maintaining the full scale margin of safety. This stress ratio is shown on the failure criteria curve in Fig. 20. Then the outer face thickness was set at the minimum of two layers recommended by Grumman's Materials and Manufacturing Groups. The core selected for the model was the only commercially available paper honeycomb with a small cell size. The core depth required to provide strength for general instability was then determined for this configuration.

The test sections are approximately 203 cm. in length, not including transitions to the non-representative 6061 aluminum alloy test structure. This test structure consists of end domes, Y-rings, and tank skirts, and provides for internal pressurization, external load application, and support. The overall configuration of the model is illustrated in Figure 21.

2. Materials

Typical mechanical properties of the model materials were used in all sizing calculations and are given in Table 23. Materials evaluation was carried out at Structural Composites Industries (SCI) in order to determine mechanical properties for use in predicting the strength of the test model.

a. COMPOSITE FACING MATERIAL. The criteria for selection of facing materials included: adequate strength from 21°K to 367°K in service; a vendor limitation on the paper honeycomb cure temperature to 394°K max; insensitivity to likely variations in temperature within a large autoclave; and sufficient bench life with good handling characteristics. Based on vendor data, the candidate prepregs were Cordopreg E-293/7581-I550 and Reliapreg R-I500/7581. Initially, Cordopreg was the first choice because of its high room temperature strength, but its high safe lower cure temperature was outside acceptable limits. Tensile and flexural tests were conducted on laminates of these materials. Two- and eight-ply vacuum-bagged laminates, cured at 394°K, were tested at room temperature and at 367°K as ASTM D638 tensile coupons. The results, shown in Table 24, revealed that Cordopreg exhibited significant strength reduction at 367°K, suggesting that the cure temperature was too low. Two- and four-hour cures at ≈ 14°K increments between 367°K and 421°K were applied to a series of vacuum-bagged twelve-ply laminates. Triplicate flexural room-temperature tests, reported in Table 25, showed that the Reliapreg material had a safe lower limit cure temperature of 367°K compared with 408°K for the Cordopreg.

b. HONEYCOMB CORE. The honeycomb core material selected for use in the sandwich construction is TUF-COMB 200 paper honeycomb in .48 cm cell size, .064 specific gravity. The height is .673 cm. The paper core can be bonded with basic sandwich adhesive and bonding techniques. However, an upper temperature limit of 394°K is recommended by the manufacturer since the paper may become brittle. As discussed previously, this maximum bonding temperature imposes some limitation in the processing and selection of candidate adhesive and skin-facing materials.

Shear strengths and moduli of TUF-COMB 200 honeycomb were determined on compressive plate shear specimens. Test samples 5.08 x 17.8 x 1.27 cm thick were laid up on steel plates using FM-123-2 adhesive film and cured in an oven at 393°K for 4 hours. Tests were conducted in accordance with MIL-STD-401B. In the L-direction, the tests were run at room temperature, 393°K and 88°K; in the W-direction, the tests were done at room temperature only. Testing was accomplished

on a Baldwin test machine at a .063 cm/min loading rate. All specimens exhibited core shear failure at the ultimate loads. The test results are given in Table 26.

Flatwise compressive properties of TUF-COMB 200 honeycomb were developed from sandwich panels fabricated using both the primary and alternate composite facing materials selected for the sandwich tank construction. The sandwich panels had a chemically milled 2219-T62 aluminum sheet for facing on one side and 2-ply glass-laminate facing on the other side to simulate the cylindrical tank wall cross-section. The honeycomb thickness was 1.27 cm. Testing was in accordance with MIL-STD-401B. The compressive loads were applied to the specimens which were 5.08 cm square through a spherical loading block of the self-aligning type. The tests were conducted at RT and 367°K. Test data are presented in Table 27.

Flatwise tensile specimens were prepared from the same sandwich panels used in the compression test. The test specimens were subjected to additional thermal soak at 393°K for four hours during the bonding of the aluminum loading blocks to the facings. The specimens were placed in a self-aligning loading fixture and the loads were applied at a constant rate of .127 cm/min cross-head speed until failure occurred. Tests were conducted at RT and at 367°K.

The results of the flatwise tension (Table 28) show a considerable difference in the strengths and mode of failure between two sandwich panels fabricated from the primary and alternate composite facing materials. The honeycomb core used was Hexcell TUF-COMB 200-3/16-4.0. As noted previously with the 2- and 8-ply laminate tensile strength test, higher strengths were obtained from the sandwich specimens utilizing Reliapreg R-1500 facing material. The failure occurred in the adhesive at the core/aluminum interface for the Reliapreg facing panel tested at 367°K. The failure of the Cordopreg facing panel at 367°K occurred in the glass facing, which verified the relatively poor strength of the Cordopreg material cured at 393°K.

c. ADHESIVE. A literature search and contacts with various material suppliers were made to select candidate adhesive for bonding honeycomb core. A processed adhesive in a film form was preferred and selected over a paste type for convenience and ease of application, uniformity in thickness, and generally longer bench life at ambient condition. FM-123-2, a modified epoxy adhesive manufactured by Bloomingdale Department of American Cyanamid Company, was selected as a primary candidate material. A recommended 380°K cure temperature of the adhesive is compatible with the maximum temperature established by the paper honeycomb. Test data available from NASA-MSC suggested that FM-123-2 is a good candidate material for cryogenic application. An alternate candidate adhesive was selected. This was Reliabond 391-1, a modified epoxy film, similar to FM-123-2 in processing characteristics, but with higher reported strength properties. FM-123-2 was selected.

d. ALUMINUM ALLOY WELD STRENGTH. The results of quality assurance tests of welds between 2219-T81 components are reported in Table 32 and are consistent with that expected. The strength of the unusual girth welds between the 2219 aluminum transition ring and the 6061 aluminum end domes and skirt assembly is established by the data shown in Table 33. These data establish that the weld is stronger than the 6061 base metal.

3. Testing

Test conditions which are representative of the full sized LH_2 tank environment have been formulated for the scale models. These conditions correspond to the flight loads discussed in Section II. A. 2.

Since there does not appear to be the structural necessity of performing the more complicated and expensive testing to the exact environment of the full sized tank, some simplifications have been made. LN_2 will be substituted for LH_2 as the cold load test pressurization medium, and hot air is to be used for pressurization in the hot load test. The external loading will also be simplified to be a pure bending load rather than a combined axial and bending load. The primary purpose of the tank testing, which is to verify the method of structural analysis used in sizing the full sized tank, will still be satisfied if these simplifications are made. The simplified test will demonstrate whether the buckling strength of the composite reinforced pressure shell can be predicted within reasonable limits when the complications of property corrections at cryogenic temperatures, internal pressure stabilization, biaxial stresses, etc. are taken into account.

a. TEST SEQUENCE. An outline of the test plan is presented in Table 29 for the two test articles. Rather than test each article to ultimate load and failure in one of the two critical conditions as would be the usual test procedure, it is planned to perform ultimate and failure loading for the end boost (axial compression in shell wall) condition only. Test data on structural instability (with its large scatter) is felt to be more useful than the burst test data which would be obtained from a post-orbit-insertion condition test. Therefore, only one article will be tested in the post-orbit-insertion condition and in addition, it will only be tested to the limit (maximum operating) load level in order to keep the stresses in the shell wall in the elastic range. With this test procedure, the test models will be tested to an equivalent full sized tank environment and a maximum of useful data will be obtained.

An additional alternate test condition is proposed because of the honeycomb structure of the tank wall. It consists of filling the tank with LH_2, and maintaining the tank in the full condition for a time period before emptying. The purpose of the test is to determine the susceptibility of the honeycomb to "cryobombing". The phenomenon can be explained in simple terms as follows: The temperature of LH_2 at one atmosphere pressure is 20°K while the melting point of air is approximately 55°K. Therefore, any air contained within a cell of the honeycomb core will solidify when the tank is filled with LH_2 and the wall temperature reaches the fluid temperature. If in addition a minute hole or porosity exists in the fiberglass outer face, additional air will be drawn in because of the reduced pressure within the cell. This additional air will also solidify. Under these circumstances, a tank standing full of LH_2 could, over a period of time, accumulate solid and some liquid air within a cell (or cells). When the tank is emptied of LH_2 and the temperature of the air within the cell subsequently rises above its boiling point, a sudden pressure increase will result from the change of state. The smallness of the hole or porosity would prevent the pressure from immediately equalizing itself with the external atmosphere and failure of the core could occur. The pressure of the gas can be determined approximately using the gas law, $P = wRT$. The density, w, of liquid air is 880 kg/m^3. If the cell were one-quarter full of air, the density after change of state would be approximately 220 kg/m^3. The temperature of air somewhat above its boiling point is 90°K and the gas constant, R, of air is 287 Nm/kg°K. The pressure of the constrained gaseous air would then be:

$$P = wRT = 220 \times 287 \times 90 \times 10^{-4} \approx 570 \text{ N/cm}^2$$

which is greater than the strength of some of the honeycomb cores considered in this report. If testing shows that a "cryobombing" problem exists, the core and fiberglass faces will be required to have built in vent holes distributed over the tank surface and will result in increased costs for this concept. The LH_2 tank fill test would be scheduled to occur after limit (maximum operating) strength for the flight loads has been demonstrated.

b. CALCULATION OF TEST LOADS. The size of the sub-scale model of the LH_2 tank was established so that the aluminum alloy inner face would be working at approximately the same stress level as the full sized tank.

In the full sized tank for Condition 1 (end boost, on the compression side), the stress ratios, R, for a positive margin of safety (see Figure 20) are:

$$R_{axial} = f_{axial}/F_{cy} = -.39$$

$$R_{hoop} = f_{hoop}/F_{cy} = +.66$$

Therefore, in the test tank at $T = 78^{o}K$, the axial and hoop stresses on the compression side are:

$$f_{axial} = -.39 \times 41900 = -16300 \text{ N/cm}^2$$

$$f_{hoop} = +.66 \times 41900 = +27700 \text{ N/cm}^2$$

From the test results for two layers of R-1500 fiberglass at room temperature:

$$E\ (0^{o} \text{ direction}) = 2.20 \times 10^{6} \text{ N/cm}^2$$

$$E\ (90^{o} \text{ direction}) = 2.06 \times 10^{6} \text{ N/cm}^2$$

and

$$E_{fg} = \sqrt{E(0) \times E\ (90)} = 2.12 \times 10^{6} \text{ N/cm}^2$$

Therefore, for elastic properties at room temperature:

$$(Et)_{fg} = 2.12 \times 10^{6} \times .0584 = .124 \times 10^{6}$$

$$(Et)_{al} = 7.24 \times 10^{6} \times .0762 = .551 \times 10^{6}$$

$$\Sigma (Et) = .675 \times 10^{6}$$

$$(Et)_{fg}/(Et)_{al} = .225$$

The configuration of scale model wall cross-section is:

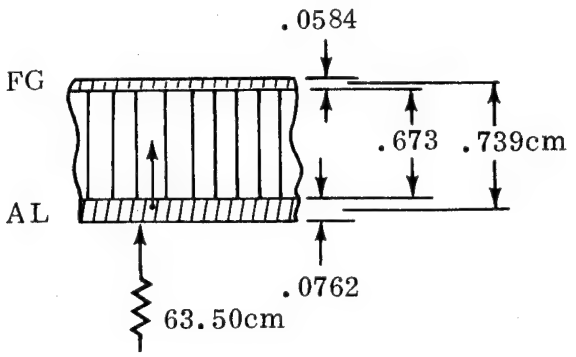

$$t_{eff} = t_{al} \frac{\Sigma (Et)}{(Et)_{al}} = .0762 \ \frac{.675 \times 10^6}{.551 \times 10^6}$$

$$t_{eff} = .0934 \text{ cm}$$

$$\overline{y} = \frac{\Sigma (yEt)}{\Sigma (Et)} = \frac{.739 \times .124 \times 10^6}{.675 \times 10^6}$$

$$\overline{y} = .136 \text{ cm}$$

$$R_{cg} = 63.50 + .038 + .136 = 63.67 \text{ cm}$$

$$f_{hoop} = pR_{cg}/t_{eff} = 63.67\ p/.0934 = 27700 \text{ N/cm}^2$$

$$p = 40.6 \text{ N/cm}^2$$

The LN_2 head pressure is approximately:

$$\Delta p = 810 \text{ kg/m}^3 \times 2.67\text{m} \times 9.807 \text{ N/kg} \approx 2.1 \text{ N/cm}^2$$

The system pressure is therefore:

$$p_{sys} = p - \Delta p = 40.6 - 2.1 = 38.5 \text{ N/cm}^2$$

The axial stress on the compression side of the model must be:

$$f_{axial} = -16300 \text{ N/cm}^2$$

and

$$N_{axial} = f_{axial}\, t_{eff} = M/\pi R^2 + p_{sys}\, R/2$$

Therefore: $-16300 \times .0934 = -1522 = M/\pi\ (63.67)^2 + 38.5 \times 63.67/2$

and $M = -(1522 + 1226) \times 12740 = -35.0 \times 10^6$ cm N at ultimate load.

At limit load:

$$M = -35.0 \times 10^6/1.4 = -25.0 \times 10^6 \text{ cm N}$$

For Condition 1 - end boost;

$$p_{sys} = 38.5 \text{ N/cm}^2$$

$$p = p_{sys} + \Delta p = 40.6 \text{ N/cm}^2$$

$$M_{ult} = 35.0 \times 10^6 \text{ cm N}$$

$$M_{lim} = -25.0 \times 10^6 \text{ cm N}$$

N_{axial} = -1522 N/cm (ultimate, compression side)

$T = 78^{o}K$

Following the procedure of the design criteria, the system pressure for Condition 2, post orbit insertion at T = 367oK, can be determined.

$$F_{tu}/1.4 = 40900/1.4 = p_{sys}\ R/t_{al} = p_{sys} \times 63.5/.0762$$

from which: $p_{sys} = 35.1\ N/cm^2$

The test loads are summarized in Table 30.

c. PREDICTED FAILING STRESSES. The shell instability stresses for the scale model are calculated here using the methods of Reference 19.

The radius of gyration of the composite honeycomb sandwich is:

$$\rho = h_c \sqrt{(Et)_{fg}/(Et)_{al}} \div \left[1 + (ET)_{fg}/(Et)_{al} \right]$$

$$\rho = .739 \times \sqrt{.225}/1.225 = .285\ cm$$

and, $R/\rho = 63.67/.285 = 224$

The "knockdown" factor which relates the average experimental results to the predications of classical, small-deflection shell buckling theory is obtained from the correction curve in the above reference.

For $R/\rho = 224$, $\gamma_c = .47$

The uncorrected shell buckling stress can be calculated at the LN_2 temperature of 77oK as:

$$f_o = 2.1\ E_{al}\ \rho/R = 2.1 \times 8.07 \times 10^6/224 = 75,600\ N/cm^2$$

The shear crimping stress can be calculated as approximately:

$$f_{crimp} = h_c\ G_{cw}/t_{eff} = .739 \times 13900/.0934 = 110,000\ N/cm^2$$

where the core transverse shear modulus has been approximated as:

$$G_{cw}\ (78^{o}K) = G_{cw}\ (RT) \times G_{cl}\ (78^{o}K)/G_{cl}\ (RT)$$

$$G_{cw} = 7800 \times 19000/10700 = 13900\ N/cm^2$$

using the test data of Table 23. The buckling coefficient is:

$$K_c = 1 - f_o/4\ f_{crimp} = .828$$

The critical elastic buckling stress of the shell is:

$$f_{cr_{el}} = \gamma_c K_c f_o = .47 \times .828 \times 75600 = 29400 \text{ N/cm}^2$$

The plastic buckling stress can be obtained from the elastic buckling stress as follows, using the octahedral shear stress criteria for combined stresses.

$$\overline{f} = \sqrt{f_{axial}^2 + f_{hoop}^2 - f_{axial} f_{hoop}} \leq F_{cy}$$

Using the above expression, an axial stress at which yielding occurs can be determined for the test tank.

$$f_{axial,'yield'} = F_{cy} \div \sqrt{1 + R^2 - R}$$

where

$$R = f_{hoop}/f_{axial}$$

The applied axial and hoop stresses in the aluminum pressure shell were determined in the previous section, from which:

$$f_{hoop}/f_{axial} = 27700/(-16300) = -1.69$$

and

$$f_{axial,'yield'} = .424 \, F_{cy}$$

$$f_{axial,'yield'} = .424 \times 41900 = 17,800 \text{ N/cm}^2$$

The critical plastic buckling stress for the shell can now be obtained by using a standard plasticity reduction curve (Figure 8) for uniaxial compression and taking combined stresses into account by substituting the axial 'yield' stress for F_{cy}.

$$f_{cr_{el}}/f_{axial,'yield'} = 29400/17800 = 1.65$$

and from the figure:

$$f_{cr}/f_{axial,'yield'} = .92$$

Therefore:

$$f_{cr} = .92 \times 17800 = 16,400 \text{ N/cm}^2$$

which is approximately equal to the applied compressive stress in the aluminum alloy inner face.

The stabilizing effect of internal pressurization can be estimated using the data presented in Reference 21 for monocoque cylinders. An equivalent monocoque cylinder thickness, t_{eq}, can be determined for the sandwich shell. For a rectangular section, the radius of gyration is:

$$\rho = \sqrt{I/A} = \sqrt{(bt^3/12)\ (1/bt)} = t/3.46$$

Therefore, the equivalent thickness is:

$$t_{eq} = 3.46\ \rho$$

and

$$R/t_{eq} = R/3.46\rho = 224/3.46 = 64.8$$

for the scale model. The increase in buckling stress due to internal pressurization is plotted in the above reference as a function of the parameter $(p/E)\ (R/t)^2$. Using the above value of R/t_{eq}, the parameter is evaluated as

$$(40.6/8.07 \times 10^6)\ (64.8)^2 = .0211$$

from which

$$\Delta F_{cr_p} = .030\ E(t_{eq}/R)$$

Again using the curves of the reference, the buckling stress of an unpressurized cylinder with the same R/t_{eq} can be determined as follows.

The buckling stress of an axially compressed cylinder is given by the expression

$$F_{cr} = .905\ K_c E\ (t_{eq}/L)^2$$

where $K_c = K_c\ (Z)$ and $Z = .95\ L^2/Rt_{eq}$. Rewriting these expressions,

$$(t_{eq}/L)^2 = .95\ t_{eq}/ZR$$

$$F_{cr} = .86\ (K_c/Z)\ E\ (t_{eq}/R)$$

For the scale model, $L/R = 3.2$:

$$Z = .95\ (L/R)^2\ R/t_{eq} = .95 \times 3.2^2 \times 64.8 = 630$$

from which $K_c = 210$ for average data.

Therefore:

$$F_{cr} = .86 \times (210/630)\ E\ (t_{eq}/R)$$

or

$$F_{cr} = .287\ E\ (t_{eq}/R)$$

The increase in elastic buckling stress due to internal pressurization is:

$$\Delta F_{cr_p}/F_{cr} = .030/.287 = .104$$

or approximately a 10% increase. With plasticity correction, the difference will be even smaller. The stabilizing effect of internal pressure can therefore be neglected because the increase in buckling in small compared to the scatter in shell buckling data.

Local instability of the face sheets can also be determined using the methods contained in Reference 19. Only the wrinkling instability of each face will be checked since the intracell instability mode of local buckling is less critical than the face wrinkling mode for the scale model honeycomb configuration.

The critical stress for face wrinkling instability f_{wr} is given by the expression

$$f_{wr}/E_f = 0.33\ (E_c t_f/E_f t_c)^{1/2},$$

where the subscript f refers to the face and subscript c refers to the core.

The following calculations are carried out using the values of material properties at 77°K. For the honeycomb core, the compressive modulus can be estimated using the data of Table 23.

$$E_c\ (77^{\circ}K) = E_c\ (RT) \times G_{cl}\ (77^{\circ}K)/G_{cl}\ (RT)$$

$$E_c = 48400 \times 19000/10700 = 85,900\ N/cm^2$$

and

$$E_c/t_c = 85900/.739 = 116200\ N/cm^3$$

For the aluminum face:

$$E_f/t_f = 8.07 \times 10^6/.0762 = 105.9 \times 10^6\ N/cm^3$$

For the fiberglass face:

$$E_f/t_f = 2.58 \times 10^6/.0584 = 45.9 \times 10^6\ N/cm^3$$

The wrinkling stress of the aluminum face is:

$$f_{wr_{el}} = 0.33 \times 8.07 \times 10^6 \times (.1162 \times 10^6/105.9 \times 10^6)^{1/2}$$

$$f_{wr_{el}} = 88200\ N/cm^2$$

which is greater than the proportional limit stress. The result will be corrected for plasticity effects using Figure 8. (There is no interaction with transverse tension for wrinkling instability).

$$F_{cy} = 41900 \text{ N/cm}^2$$

$$f_{wr_{el}}/F_{cy} = 88200/41900 = 2.10$$

Therefore:

$$f_{wr}/F_{cy} = .92$$

$$f_{wr} = .92 \times 41900 = 38500 \text{ N/cm}^2$$

The wrinkling stress of the fiberglass face is:

$$f_{wr_{el}} = 0.33 \times 2.58 \times 10^6 \times (.1162 \times 10^6/45.9 \times 10^6)^{1/2}$$

$$f_{wr_{el}} = 42800 \text{ N/cm}^2$$

The strength limit for fiberglass is:

$$F = 49100 \text{ N/cm}^2$$

Since fiberglass behaves almost elastically,

$$f_{wr} = f_{wr_{el}} = 42800 \text{ N/cm}^2$$

The stress in the tank wall can be determined from the applied loads, stress-strain relations, and strain compatibility. These are given below. Primed quantities refer to the fiberglass face and unprimed quantities refer to the aluminum face. An "x" subscript refers to the axial direction and a "y" subscript refers to the hoop direction.

$$N_x = (f_x t) + (f_x t)'$$

$$N_y = (f_y t) + (f_y t)'$$

$$\epsilon_x = \frac{1}{E}(f_x - \nu f_y) + \alpha \Delta T$$

$$\epsilon_y = \frac{1}{E}(f_y - \nu f_x) + \alpha \Delta T$$

$$\epsilon'_x = \frac{1}{E'}(f'_x - \nu' f'_y) + \alpha' \Delta T = \epsilon_x$$

$$\epsilon'_y = \frac{1}{E'}(f'_y - \nu' f'_x) + \alpha' \Delta T = \epsilon_y$$

Combining the above by eliminating the fiberglass stresses results in:

$$(f_x t)\left[1+\frac{(Et)}{(Et)'}\right]-(f_y t)\,\nu\left[1+\frac{\nu'(Et)}{\nu(Et)'}\right]=\frac{(Et)}{(Et)'}\left[N_x-\nu' N_y\right]+(Et)(\alpha'-\alpha)\Delta T$$

$$(f_y t)\left[1+\frac{(Et)}{(Et)'}\right]-(f_x t)\,\nu\left[1+\frac{\nu'(Et)}{\nu(Et)'}\right]=\frac{(Et)}{(Et)'}\left[N_y-\nu' N_x\right]+(Et)(\alpha'-\alpha)\Delta T$$

The values of the material properties at $77^{\circ}K$ are:

$E = 8.07 \times 10^6$ N/cm^2 $\qquad$ $E' = 2.58 \times 10^6$ N/cm^2

$\nu = .3$ $\qquad$ $\nu' = .04$

$\alpha = 16.02 \times 10^{-6}$ cm/cm$^{\circ}$C $\qquad$ $\alpha' = 5.04 \times 10^{-6}$ cm/cm$^{\circ}$C

$t = .0762$ cm $\qquad$ $t' = .0584$ cm

$\Delta T = T_{final} - T_{initial} = 77^{\circ}K - 392^{\circ}K = -315^{\circ}K,$

$(\alpha'-\alpha)\Delta T = 3460 \times 10^{-6}$ cm/cm

Substituting these values into the equations:

$$(f_x t) \times 5.13 - (f_y t) \times 0.464 = 4.13\left[N_x - 0.04\, N_y\right] + 2130$$

$$(f_y t) \times 5.13 - (f_x t) \times 0.464 = 4.13\left[N_y - 0.04\, N_x\right] + 2130$$

which are valid for Condition 1 - End boost, or:

$$(f_x t) - (f_y t) \times 0.0905 = 0.806\left[N_x - 0.04\, N_y\right] + 415$$

$$(f_y t) - (f_x t) \times 0.0905 = 0.806\left[N_y - 0.04\, N_x\right] + 415$$

from which:

$$(f_x t) = 0.810\, N_x + 0.041\, N_y + 456$$

$$(f_y t) = 0.810\, N_y + 0.041\, N_x + 456$$

and:

$$(f_x t)' = N_x - (f_x t)$$

$$(f_y t)' = N_y - (f_y t)$$

The values of N_x and N_y, the distributed axial and hoop shell load, respectively, can be obtained from the section of applied loads. The constant term corresponds to the thermal stress developed in cooling to cryogenic temperatures from the zero-stress (cure) temperature.

In the absence of the external applied loads N_x and N_y, the stresses due to temperature change only are

$$f_x = f_y = \frac{456}{.0762} = 5980 \text{ N/cm}^2, \text{ in the aluminum face}$$

and

$$f'_x = f'_y = -\frac{.0762}{.0584} \times 5980 = -7790 \text{ N/cm}^2, \text{ in the fiberglass face.}$$

It should be noted that these are membrane (average) stresses in the faces and that the extreme fiber stresses will be higher. This difference is important for the aluminum face since the neutral axis is close to that face. For the case where the thermal stress in the axial and hoop directions is the same and the applied external loads are zero, the stress-strain relations can be written as:

$$\epsilon = \frac{1-\nu}{E} f + \alpha \Delta T$$

$$\epsilon' = \frac{1-\nu'}{E'} f' + \alpha' \Delta T$$

Substituting:

$$\epsilon = \frac{.7}{8.07 \times 10^6} 5980 - 16.02 \times 10^{-6} \times 315$$

$$\epsilon' = \frac{.96}{2.58 \times 10^6} \times 7790 - 5.04 \times 10^{-6} \times 315$$

$$\epsilon = 520 \times 10^{-6} - 5050 \times 10^{-6} = -4530 \times 10^{-6}$$

$$\epsilon' = 2920 \times 10^{-6} - 1590 \times 10^{-6} = -4510 \times 10^{-6} = \epsilon$$

The total strains are equal for both faces but the mechanical and free thermal strains are different for each. The thermal stress at the extreme fiber of the aluminum face can be obtained from the mechanical strain as

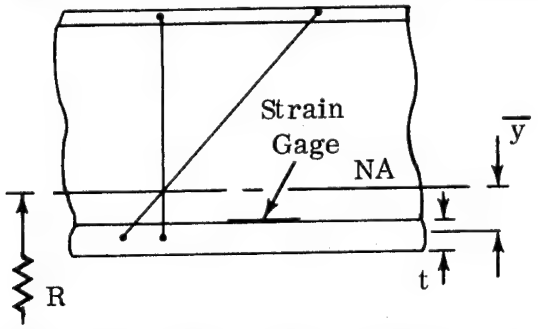

$$\epsilon_{max} = \frac{y + t/2}{\bar{y}} \epsilon$$

or equivalently:

$$f_{max} = \frac{\bar{y} + t/2}{\bar{y}} f$$

$$f_{max} = \frac{.136 + .038}{.136} 5980 = 7650 \text{ N/cm}^2$$

Similarly, the thermal stress on the outer face of the aluminum skin is:

$$f_{min} = \frac{.136 - .038}{.136} 5980 = 4300 \text{ N/cm}^2$$

This effect can be important in interpreting the strain measurements made in the tests because the strain gages are mounted on the outer face of the aluminum skin. (See sketch).

The external applied loads for Condition 1, end boost at ultimate load, are:

$N_x = M/\pi R^2 + p_{xyx} R/2 = -1522$ N/cm and

$N_y = pR = 2580$ N/cm on the compression side

and

$N_x = 3974$ N/cm and

$N_y = 2580$ N/cm on the tension side.

The load distribution and stresses in the face sheets are shown in Table 31 for the above loads as determined using the expressions:

$$(f_x t) = 0.810\ N_x + 0.041\ N_y$$

$$(f_y t) = 0.810\ N_y + 0.041\ N_x$$

A discrepancy exists between these calculated stresses and those predicted in the section on the calculation of test loads. In the analysis method for honeycomb shell instability of Ref. 19, uniaxial rather than biaxial stress-strain relations are used. That is, ν and ν equal zero. For that case, the equations for the aluminum face sheet stresses in the model due to the distributed shell loads only reduce to:

$$(f_x t) = 0.806\ N_x$$

$$(f_y t) = 0.806\ N_y$$

For the biaxial case, these equations are:

$$(f_x t) = \left[0.806 + 0.041\ N_y/N_x\right] N_x$$

$$(f_y t) = \left[0.806 + 0.041\ N_x/N_y\right] N_y$$

which, for the Condition 1 load ratio of $N_y/N_x = -1.69$, result in:

$$(f_x t) = 0.741\ N_x$$

$$(f_y t) = 0.782\ N_y$$

An error of approximately 8% is therefore involved in using uniaxial stress-strain relations to determine the face sheet stresses, or equivalently, a 7% increase in applied bending moment would be required to produce the desired stress level in the aluminum face sheet. The analytical approach used in Ref. 19 is to use a "knock-down" factor based on test data to correct predicted instability stresses based on a simplified theory. Since the knockdown factor and the theory cannot be separated

from each other, the simplified theory is used to predict the shell instability stresses and the biaxial stress-strain relations will be used to evaluate the tank tests.

The strains in the aluminum face can be determined from the above stresses using the stress-strain relations:

$$\epsilon_x = \frac{1}{E}(f_x - \nu f_y) + \alpha \Delta T$$

$$\epsilon_y = \frac{1}{E}(f_y - \nu f_x) + \alpha \Delta T$$

In these expressions, the stresses are due to the combined effects of external applied loads and stresses developed in cooling from the stress-free temperature. Since the thermal stress and strain are constant over the shell surface, their effect can be separated from the strains due to applied loads:

$$\epsilon_{ttl} = \epsilon + \epsilon_T + \alpha \Delta T$$

where ϵ is the strain due to the external applied loads, $\epsilon_T = (1 - \nu) f_T/E$ is the strain due to thermal stresses, and $\alpha \Delta T$ is the free thermal expansion. From previous calculations for the aluminum face:

$$\epsilon_T + \alpha \Delta T = 520 \times 10^{-6} - 5050 \times 10^{-6} = -4530 \times 10^{-6}$$

The strains due to the external applied loads only and the total strains are also included in Table 31.

In the tests, the mechanical and thermal strains will be measured separately. First, the change in strain will be measured as the tank is filled with the cryogen and the wall temperature cools to the temperature of the fluid. (Transient effects are included in these measurements). The strain gages will then be rebalanced to a zero output, and the change in strain due to the application of the external loads will be a separate measurement. This procedure should simplify the comparison of experimental results with theory since temperature-induced strains which are constant over the tank surface will be measured as separate quantities and the strains due to external loads will have been obtained directly. It should also simplify the calibration of the strain recording instrumentation.

d. INSTRUMENTATION. During the tests, instrumentation must be provided for the measurement of the applied loads, pressure, temperature, overall cylinder deflections, and local biaxial strains over a temperature range of 78°C to 367°K.

As part of the provision for data acquisition, strain gages and temperature sensors were applied to the external surface of the aluminum pressure shell during the tank fabrication process. These were installed at the locations shown in Figure 21 using the procedure described in Appendix D. The gage selected for strain measurement was the Micro-Measurements WK-13-250TM-350 encapsulated two-leg "T" rosette with a strain range of ± 1.5% over a temperature range of 4°K to 560°K. The gages are aligned with legs in the axial and hoop directions. Two of the total of eleven rosettes per test article have a uniaxial gage oriented at 45° to the rosette axis, added to form a three-leg rectangular rosette. The surface temperature transducer selected was the Trans-Sonics Type 1371 precision resistance thermometer with an accuracy of ±0.8° K over a range 20°K to 367°K. Four of these are applied to each

test article. M-Bond 600 epoxy adhesive was used to bond both the strain gages and temperature sensors to the aluminum pressure shell. This adhesive has an elongation capability of 1% at cryogenic temperatures and 3% at room and elevated temperatures.

Additional instrumentation for load, pressure, and deflection measurements, which should be provided at the test facility, is also indicated in Figure 21. If hydraulic jacks are used to apply loads, it is anticipated that calibrated 200 kN load-cells will be used in series to monitor the actual loads applied instead of relying on low-friction jacks and pressure measurements. The pressure, approximately 40 N/cm^2 in the cryogenic fluids, would be monitored by near-ambient pneumatic gages with long low-heat/leak tubes joined to the tankage. The large hoop and longitudinal displacements are readily measured with differential transformers with critical elements shielded from the cryogenic environment.

4. Specimen Fabrication

Two cylindrical test sections and a set of common end closure assemblies were manufactured at Structural Composites Industries (SCI). Each cylindrical test section consisted of four chem-milled 2219 aluminum alloy panels joined by longitudinal welds to form a cylinder which in turn was joined by girth welds to tapered 2219 alloy rings at each end. After the application of strain gages and temperature sensors, the metal shell was reinforced with a paper honeycomb core and a two layer woven fiberglass outer face. The transition rings provide an increased metal thickness in order to reduce the stress level in the low strength weld which will join the 2219 alloy shell of the test sections to the 6061 aluminum alloy end closure assemblies. Each of the non-representative end closure assemblies consisted of an end dome, Y-ring, skirt, and attachment ring joined together by welding. These assemblies were fabricated from 6061 aluminum alloy because of the unavailability of 2219 material to manufacture these parts. Drawings of the test section and end closure assemblies are given in Appendix C.

The tooling concepts and fabrication processes used in the manufacture of the two full length test articles were verified by the prior construction of a full-diameter, short-length prototype unit.

a. TOOLING A preliminary review of the entire process for fabrication of the full-length test specimens was conducted to select specific processes which should be verified during fabrication of a prototype test specimen. Special attention was given to a rubber-bladder concept which had been initially selected as the method for supporting the cylindrical metal shell during application of the composite structure. After careful examination of the possible effects each composite application process might have on a metal shell supported by a non-rigid mandrel (e.g., sag, local buckling/flattening, ovality, etc.) it was decided use of this mandrel concept was too risky.

The rubber-bladder concept was replaced by a rigid-mandrel design which consisted of a segmented, sponge-rubber coated, rigid glass fabric/epoxy cylinder, supported and located with rounding rings, and capable of contracting to a smaller diameter to allow insertion and removal of the test specimen during fabrication.

Usefulness of this type of tool for the full length test specimen fabrication was verified by the construction of a full-diameter, short-length prototype unit discussed in the following paragraphs.

b. PROTOTYPE SPECIMEN A 61 cm long by 127 cm diameter 2219 aluminum cylindrical shell was fabricated from four chem-milled flat panels which were machine tungsten-inert gas (TIG) -welded together (duplicating the full length metal model specimen fabrication process). This full-diameter, short-length aluminum shell was assembled to the previously discussed mandrel support fixture, and the resultant unit was used to fabricate a composite reinforced prototype specimen.

Several stages of the processing are depicted in Figure 22 through 26. Figure 22 shows the 2219 aluminum cylinder assembled to the mandrel support fixture. At this point in the processing, the impression of the honeycomb core was recorded on vinyl film to allow for adjustments in adhesive pattern layout in the weld land areas.

Based on the results of the core impression tests, the aluminum cylinder was cleaned, primed and the FM 123-2 adhesive film applied to the surface as shown in Figure 23. Also shown in Figure 23 is a portion of the strain gage/wire layout used to evaluate wire encapsulation and radial versus axial exit of wires.

Figure 24 shows the honeycomb core applied to the test cylinder. Following vacuum bagging and cure of the honeycomb/adhesive system, the prepreg outer skin was applied over the honeycomb material and the unit was again vacuum bagged and cured. At this stage the processing was complete and the test cylinder was removed from the mandrel support fixture. The completed prototype test cylinder is shown in Figure 25. A typical cross section of the prototype tank wall is shown in Figure 26. Close inspection of Figure 26 indicates the excellent adhesive fill in the weld land areas (aluminum decreases in thickness from right to left in the photograph).

Examination of the prototype specimen and analysis of the process operations used to fabricate the specimen allowed the following decisions to be made regarding full scale test specimen fabrication:

- Delete the core impression test - the vinyl film acts as an adhesive for paper honeycomb.
- Fully encapsulate all strain gage wires with adhesive and exit wires axially along specimen - minimizes discontinuities and potential for electrical "shorts".
- Core sanding over weld lands is not required since the discontinuity is negligible.
- A differential vacuum probe will be used (and monitored regularly) during core curing to insure proper bonding.

c. FULL-LENGTH TANK MODEL Two 1/6-scale model composite reinforced aluminum test cylinders (SCI Dwg. No. 126931 and 126932) and the top and bottom end closure assemblies (SCI Dwg. No. 126930) were fabricated. See Appendix C, Fig. 89 through 91. The final assembly, Fig. 92, was never made.

(1) Cylindrical Aluminum Test Section Each 2219 aluminum shell test section P/N 1269331, was fabricated from four .154 cm thick flat panels which were chem-milled to obtain the required .076 cm thick membrane sections. The four panels were subsequently roll-formed and joined longitudinally by automatic TIG welding. Radiobraphic inspection of the welds indicated some linear porosity, which was considered acceptable and two defects (gas holes) not acceptable according to the specifications. These two defects were ground out and manually welded, re-X-rayed and accepted. A completed cylindrical test section is shown in Figure 27.

Manual girth welding of the transition rings to the cylindrical test section proved to be inadequate. The many variants which SCI's subcontractor tried were based on his successful results for SCI with smaller vessels. The unsuccessful variants included:

a. Tack weld fixturing with TIG welding from the inside. Local buckling occurred.

b. Tack weld fixturing with TIG welds from outside. Local buckles occurred at repairs of regions of lack of fusion.

c. Internal copper chill and junction preheated to 360^{o}K prior to TIG welding from outside. Repair at regions of lack fusion caused local buckling.

d. External copper chill and juncture preheated to 360^{o}K prior to internal TIG welding. Locally concave welds occurred. Repair from inside or outside caused local buckles. Figure 28 shows typical examples of the buckles.

SCI changed welding subcontractors to procure automated continuous girth welds. The subcontractor elected to use internal copper chills. The transition rings were removed from each test cylinder. The weld zones of all components were machined, as shown in Figure 29, which details the resulting geometry. The welding fixture shown in Figure 30, consisted of a massive expandable "wagon wheel" for internal support, fit-up, and weld bead control, plus two external locating rings. Weld schedules were developed using short cylinders of 2219 aluminum sheet material fixtured with the new tools on automatic TIG welding equipment. Visual and radiographic inspection of the sample welds indicated clear, well penetrated, cosmetically good welds.

The developed weld process was subsequently used to TIG fusion-butt weld two transition rings to each of the two aluminum test cylinder sections. Visual examination of each of the four welds indicated minor and very isolated elastic buckling ("oil-canning"). One weld had a small area of mismatch which should have a negligible effect on load transfer. Generally, the welds were cosmetically good with

only minor variations in bead width/height. Subsequent radiographic inspection of the four welds revealed many indications. These consisted of: cracks, lack of fusion, tailed porosity, chained porosity and isolated round porosity. Cylinder S/N P1 exhibited approximately 20% more defects per weld than those observed in cylinder S/N P2; it was decided to repair the better welds of cylinder S/N P2 first.

Cylinder S/N P2 - In preparation for repair welding the defects in the girth welds of cylinder P2, the (internal) weld bead was ground flush with the mating surfaces. Both welds on cylinder P2 were again radiographically inspected; results of the inspection indicated only two defect areas remained (one per each weld). The first defect area, in one girth weld (G2), consisted of two 0.102-cm diameter pores approximately 0.6 cm apart; the second defect area, occurred in the other girth weld (G1), of 2.0 cm chained porosity.

The defects in weld G2 of cylinder S/N P2 were ground out and repaired; examination of the repair indicated a crack. Similarly, repair of the chained porosity in weld G1 caused three cracks. Again, the defects were ground out and repaired; two new cracks appeared in weld G2 and one new crack appeared in weld G1. This process was continued two more times until radiographic inspection indicated clear welds, and the unit was subsequently accepted for use.

The membrane thickness profile for each of the four chem-milled aluminum panels forming cylinder S/N P2 was obtained using Vidi gage equipment. Results indicated the range in thickness was from 0.0714 to 0.084 cm with 90% of the area measuring 0.076 cm thick.

After completion of the thickness measurements, cylinder S/N P2 was cleaned with MEK and aged for 18 hours at 450°K to place the 2219 aluminum into the required T81 condition. Samples simulating both the longitudinal seam welds and the girth welds accompanied the cylinder through the aging process. The weld samples were subsequently machined and tested per Federal Test Method 151A, Configuration F2. Results of the tensile tests are included as Table 32. Also included in Table 32 are preproduction tensile test results for transverse oriented longitudinal seam welds.

Cylinder S/N P1 - The underbead on both girth welds of cylinder S/N P1 was ground flush with the mating surfaces and the resultant weld bead subjected to radiographic inspection. Results of the inspection indicated the dressing eliminated 80% of the indications. Repair welding of the remaining defects in the girth welds of S/N P1 was initiated, and cracks developed in a manner similar to that which occurred in S/N P2. The task of grinding/repair welding and repair of subsequent cracking of welds in S/N 2 caused considerable oil-canning in the weld region before radiographic inspection indicated the welds were clear.

The type of oil-canning (buckles) which was experienced was similar to that of Figure 28. In order to eliminate the oil-canning, cylinder S/N P1 was placed over an expansion tool and locally stretched approximately 0.3%. Because of the geometric discontinuities located at the transition ring/cylinder juncture, the expansion was not uniform and most of the buckles remained in the metal. A multilayer glass fabric shim was constructed to conform to the internal shape of the

cylinder (refer to Figure 29) in the buckled area (weld zone) which allowed the expansion to be applied to a uniform manner. With the shim attached, the cylinder was again locally expanded 0.6%. This time about 90% of the oil canning was eliminated; the total permanent set in the area of the girth weld was approximately 0.1% of the original weld diameter. Just prior to this operation, the subcontractor inadvertantly dropped a tool on the thin membrane, making a cruciform shaped tear. It was possible to push the surfaces to their original contour and weld the edges because the tear surfaces, each about 8 cm long happened to be substantially hoop and longitudinal. Existing tooling (with grooved weld chills in the required girth and longitudinal directions) was used to make this repair and the distortion at this location was negligible.

Since the welds in the thin membrane region degraded the strength of the 2219-T87 thin membrane, that region was patched externally with two layers of woven fiberglass cloth about 16 cm in diameter, attached by bonding, during subsequent application of composites.

After completion of the stretching process, cylinder P2 was cleaned with MEK and aged for 18 hours at 450°K, to place the 2219 aluminum in the T81 condition. The cylindrical aluminum test section, ready for application of the composite sandwich material, is shown in Figure 31.

(2) End-Closure Assemblies Fabrication details for the non-representative 6061 aluminum end-closure assemblies (P/N 1269330-1, 2) are contained in Appendix C. No special problems were encountered during the fabrication or assembly of the components. Several stages of end-closure fabrication are depicted in Figures 32 through 36. Figures 32 and 33 show the as-formed top and bottom end domes respectively.

Figure 34 shows the extension/support ring subassembly ready for welding to the "Y-ring". Internal and external views of the completed bottom end-closure assembly are shown in Figures 35 and 36 respectively.

Welding the 6061 aluminum end-closures to the composite reinforced 2219 aluminum test cylinders was beyond the scope of this program. In order to demonstrate feasibility of this operation, flat samples simulating the dissimilar alloy joint were prepared and tested. The samples were fabricated from 0.25-inch thick plates of 2219-T47 and 6061-T42 aluminum alloys, welded together, machined into uniaxial specimens and the specimens tested to failure in tension.

Results of these tests were recorded in Table 33. Two types of weld beads were evaluated: (1) weld bead "as is", and (2) weld bead ground flush. Test results are relatively consistant (independent of weld bead) and acceptable in value for this application. It should be noted that all failures were in the parent 6061-T42 material.

(3) Cylindrical Sandwich Structure Fabrication of the honeycomb sandwich portion of the cylindrical test section was, generally, accomplished according to SCI specifications. Specific deviations from the specifications, and photographic coverage of major processes, are described in the paragraphs that follow.

All composite process operations were performed on a full-length mandrel support fixture fabricated according to the previously developed procedures. The mandrel assembly, shown in Figure 37, consisted of a neoprene sponge-padded glass-fabric/epoxy (split) cylinder supported by cam-centered rounding rings and joined by a metal tie-bar.

Because of the long time span required to fabricate the aluminum cylinders, the Reliapreg R-1500/7851 facing material and the FM-123-2 adhesive (required for the sandwich structure) had exceeded their respective shelf lives. In order to verify the suitability of these materials for use in fabricating the sandwich portion of the shell, the two materials were submitted to requalification testing. Results of the tests were contained in Tables 34 through 36. Prior (as received) test values are contained in the tables for reference. All values were within design limits and the materials were accepted for use in fabrication.

Cylinder S/N P2 - Several stages in the processing of cylinder S/N P2 are shown in Figures 38 through 43. Figure 38 shows the 2219 aluminum cylinder assembled to the mandrel support fixture. At this initial stage in the processing the aluminum shell had been chemically cleaned with paste cleaner, rinsed with water, and was awaiting the application of FM123B primer.

Figure 39 shows the local strips of FM-123-2 adhesive film, which were being applied to each weld land (axially and circumferentially) of the primed cylinder. Also shown in the figure are several of the strain gages which had been bonded to the aluminum prior to adhesive film application. Figure 40 shows a typical biaxial strain gage and one of the surface temperature transducers.

Adhesive film was then applied to the entire surface of the cylinder, windows cut in the film to bare the gages, gage wires applied and encapsulated with adhesive film, and the preassembled honeycomb core fitted to the adhesive lined cylinder. The unit was then vacuumed bagged, cured, and locally, in the transition ring region, filled with Corefil 615. Figure 41 shows the cylinder at this stage of the process.

The next operations consisted of: trimming (tapering) the core at each end; application of the R-1500 prepreg skin material; vacuum bagging; and cure. At this point in the process cylinder P2 was de-bagged and visually inspected. The inspection revealed several axially oriented wrinkles in the skin material which were judged unacceptable. Removal of skin material in the wrinkle regions was initiated so that a standard "step joint overlay" repair technique could be employed. Figure 42 shows the cylinder at this stage of the process. Close inspection of the photo indicates one of the skin wrinkles in addition to the partially completed removal of another wrinkle.

The "patchwork quilt" effect depicted in Figure 42 and the apparent ease of skin material removal without damage to the core resulted in the decision to completely strip the skin material from the core and repeat the operation. The following conclusion/recommendations resulted from an analysis of the skin material process operation:

- Skin material (prepreg) was not stretched tight enough during its application.
- Normal resin flow caused additional relaxation during the initial cure stage.
- Heat and mechanical work (teflon paddle) should be used locally as the prepreg is applied.
- All wrinkles should be removed from the bag material during application of the vacuum.

All strain gages were checked and were functioning properly at this stage of the processing. R-1500 prepreg was again applied to the cylinder using the recommended changes in procedure. Visual inspection of the cylinder after cure indicated an excellent sandwich structure free of all skin wrinkles. The cylinder was then hoop wrapped with 20-end S-Glass roving in the transition ring regions, cured, and removed from the mandrel assembly. Figure 43 shows the completed honeycomb sandwich reinforced aluminum test cylinder.

The unit was subjected to final inspection; results of the dimensional inspection are shown in Figure 44. All strain gages and temperature sensors, shown schematically in Figure 45 were given a final continuity check. Results, shown in Figure 46, were disappointing; two-thirds of the gages had been lost during the final processing operations. No explanation for the shorted gages were determined.

Cylinder S/N P1 - The same sequence of process operations discussed for cylinder S/N P2 was used to fabricate the sandwich portion of cylinder S/N P1; modification of specific procedures developed during the fabrication of cylinder S/N P2 were incorporated into the processing of cylinder S/N P1. Only one new problem was encountered during the fabrication of this unit.

The normal procedure used for each vacuum bagging operation required the bundle of strain gage leads, which terminated at the end of the cylinder, to be individually identified with tags, wrapped with vinyl film, and sealed with zinc chromate putty. During the final bagging operation for cylinder S/N P1, the vinyl film covering of the strain gage lead bundle was omitted and the zinc chromate was allowed to be in direct contact with the lead wire bundle. Inspection of the lead wire bundle after cure and debagging of the unit indicated the zinc chromate had softened, flowed between wires and identification tags, and completely obliterated the identification of individual strain gage leads. This created the problem of (1) establishing which two wires, from the entire bundle, lead to specific gage; (2) where that specific gage was located on the part and (3) whether that gage was oriented axially or circumferentially.

Resistance checks of all lead combinations established the number of functional gages and their corresponding parts of lead wires. Local heating (heat gun) of the cylinder inside surface was used to establish the location of each functional gage on the unit. Whether the gage was oriented axially or circumferentially could not be established. Gage direction will be evident upon internal pressurization or axial loading of the unit. Figure 47 contains the information obtained during this operation; locations of gages by number are shown on Figure 45.

Figure 48 indicates the values of selected final dimensions for cylinder S/N P1. Comparison of these values to those obtained for cylinder S/M P2 (Figure 44) indicates the amount of local transition ring permanent set experienced by cylinder S/N P1 during expansion to relieve buckles.

d. FINAL INSPECTION The vessels sent to Lewis Lab by SCI were unpacked and inspected. On the basis of visual inspection, the NASA program manager and the Grumman project engineer consider the quality of all the girth welds to the transition region of questionable reliability because of substantial numbers of regions of apparent lack of complete penetration. PSM, a Fansteel subsidiary, has certified to SCI that these welds passed Grumman's rigid specifications. Subsequent reinspection of the X-rays by Grumman QC personnel confirms the visual observation that these welds are barely within specification.

(1) S/N P1: There were a few additional surprises. There seemed to be an unwelded plug on S/N P1, about 1/4" diameter of aluminum alloy, near the reported and repaired tear in the thin shell. (Subsequent X-ray inspection did not reveal any weld or lack of fusion at this location.) Neither PSM or SCI has any recollection of this flaw. The inside of this vessel is discolored. SCI states that this occurred when the paste cleaner used to prepare the outer surface for bonding of composite was unwittingly applied to the inner surface and not removed. The resulting scale was not removable without damage to the shell and was therefore not removed.

The round-up mandrel was apparently not strong enough to maintain the designed cylindrical shape of the vessel during the curing of the glass cloth overwrap. Hence "flats" are distributed over the surface of the vessel. In addition, the curing vessel seems to have rested on a meridian during cure. As a result, there are a series of shallow .06" depressions about 1/4" wide and 1" long along this meridian.

(2) S/N P2: This vessel is somewhat rounder than S/N P1 but there is a region about one square foot at one end which is rather deeply (about 1'') buckled. The fiberglass is blackened in this area and the core is not visible through it. SCI states that the darkened area is corefill.

(3) Suggestions on Testing The vessels cannot be tested in the projected manner without reinforcing the areas noted in the section Final Inspection above. These can be reinforced without interfering with the principal test region.

The girth welds on both vessels should be reinforced axially with strong stiff fibers bonded to the inner surface.

The vessels should be rounded by internal pressurization with end plates closing off the vessel. The end plates should be supported by a central strut.

If pressurization removes the buckles the ends should be welded on and the vessels tested as planned.

For S/N P_2, the buckle will probably not be removed by pressurization. Since the expected loading is by an axial force and moment and importantly, no shear, the buckle can be tolerated if located at the neutral axis during test.

Alternatively, this region can be removed from significant testing by internally encapsulating the 1 1/2 feet from the end of the vessel containing the buckle, prior to welding of the end closures to the cylinder.

DISCUSSION OF RESULTS

The design effort has led to two interesting options using composites to reduce cost on the Shuttle hydrogen drop tank. This tank must sustain high axial compressive loads due to longitudinal bending. For the baseline tank, integral aluminum stiffeners and rings are contemplated. The bonded stiffener concept avoids the complex machining and forming operations required to produce a similar-appearing structure. One major advantage of this system is that, because it has the appearance of the baseline design, it is more readily acceptable. Misgivings about peeling of the bond are circumvented by using mechanical hold-down attachments at the ends and also distributed along the length to act as debond arrestors.

A still-lower cost option avoids local stiffeners by means of a thin monocoque aluminum shell stabilized with external epoxy-inpregnated paper honeycomb covered with glass epoxy composite cloth. The fit-up problem, difficult with concentric metallic shells joined by a honeycomb, is readily solved with laid-up cloth. There is an acceptance problem with this configuration because of NASA's unfavorable experience with some large honeycomb vessels. Moderately large subscale vessels had worked well but expensive full-scale ones were made with inadequate quality assurance. The resulting premature failures have led to skepticism about scaling to full size; only a successful full-scale demonstration model can dispel this skepticism.

There is a second consideration with honeycomb which we termed "cryobombing". One can postulate that air would condense in the cells of the honeycomb when the vessel is filled with liquid hydrogen. On emptying, or the accompanying rise in wall temperature due to an abort, the liquid air could gasify quickly. Pressures within the cells, high enough to rip off the glass cloth, could be generated. One objective of the proposed test program is to determine if this possibility can be realized.

Even if the tests show a high degree of probability of "cryoboming", the proposed honeycomb design is viable. A perforated honeycomb and a frequently-perforated glass cover can be fabricated inside the aluminum vessel to stabilize it. Cryobombing could thus be avoided at a moderate cost. Although the same idea might seem practical on the outside, the foam insulation normally applied would inhibit external perforations from working properly.

From a fabrication viewpoint, the program has shown the need for adequate welding and wrapping tooling, to protect the unstabilized tank structure.

Although the tooling used on this program was not adequate to maintain the desired roundness or straightness of the cylinder, the tooling for full-scale need not be complex. The difficulties experienced were related to the need for atypical end-connections, required for testing of the model. At the ends of the full-scale cylinders, similar local problems would be solved taking advantage of the experience gained during this development effort. Simpler tooling can be assured if the vessel's internal diameter is held constant while the thickness of the metallic end rigs increase. In those regions, automated welding on well-fitted parts, use of a substantiated weld schedule designed to minimize required weld repairs, and the use of

an expanding ring to eliminate shrinkage buckles due to weld repairs, will assure cylinder roundness. In the full-scale fabrication, it would be impractical to rest the vessel on its side before the external glass cloth was bonded to the honeycomb core and cured. This apparently happened to one of the subscale models during its curing operation.

On this basis, the projected ease of fabrication can be justified.

CONCLUSIONS

The use of composites was studied as a means of cost saving on the Space Shuttle Orbiter disposable tankage. It was concluded that the weight saving due to constrictive overwrap on the monocoque LOX tank was not cost-effective. For the LH_2 tank, the increased weight over the integrally-stiffened tank baseline was justified by substantial fabrication cost-savings resulting from the use of the composites. Two attractive options were established: 1) a sandwich of glass-cloth outer face, paper honeycomb core, and 2219 aluminum alloy inner shell, and 2) a stiffened shell with bonded and mechanically attached stiffeners and ring frames.

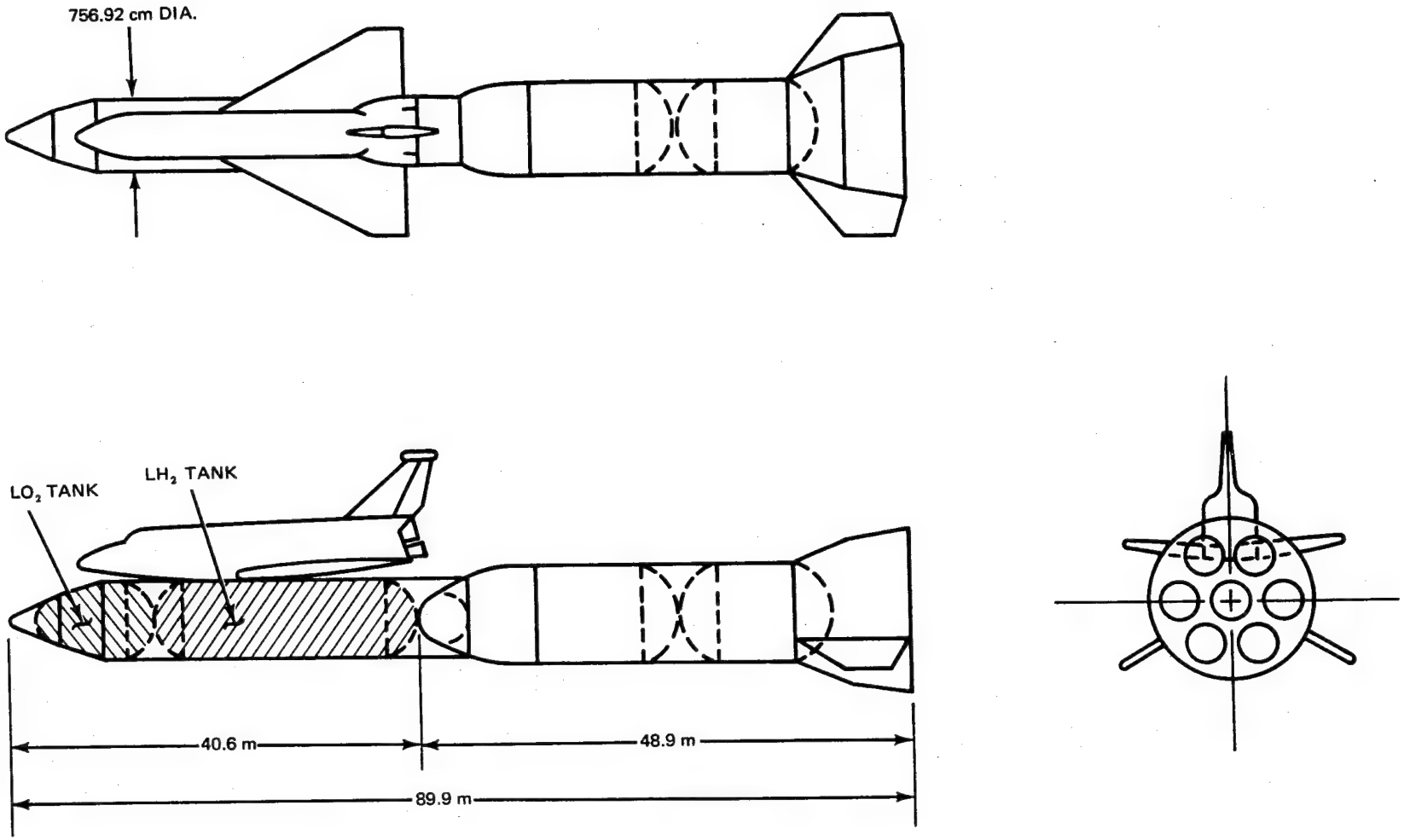

Fig. 1 Series Ballistic Recoverable Configuration External Tanks

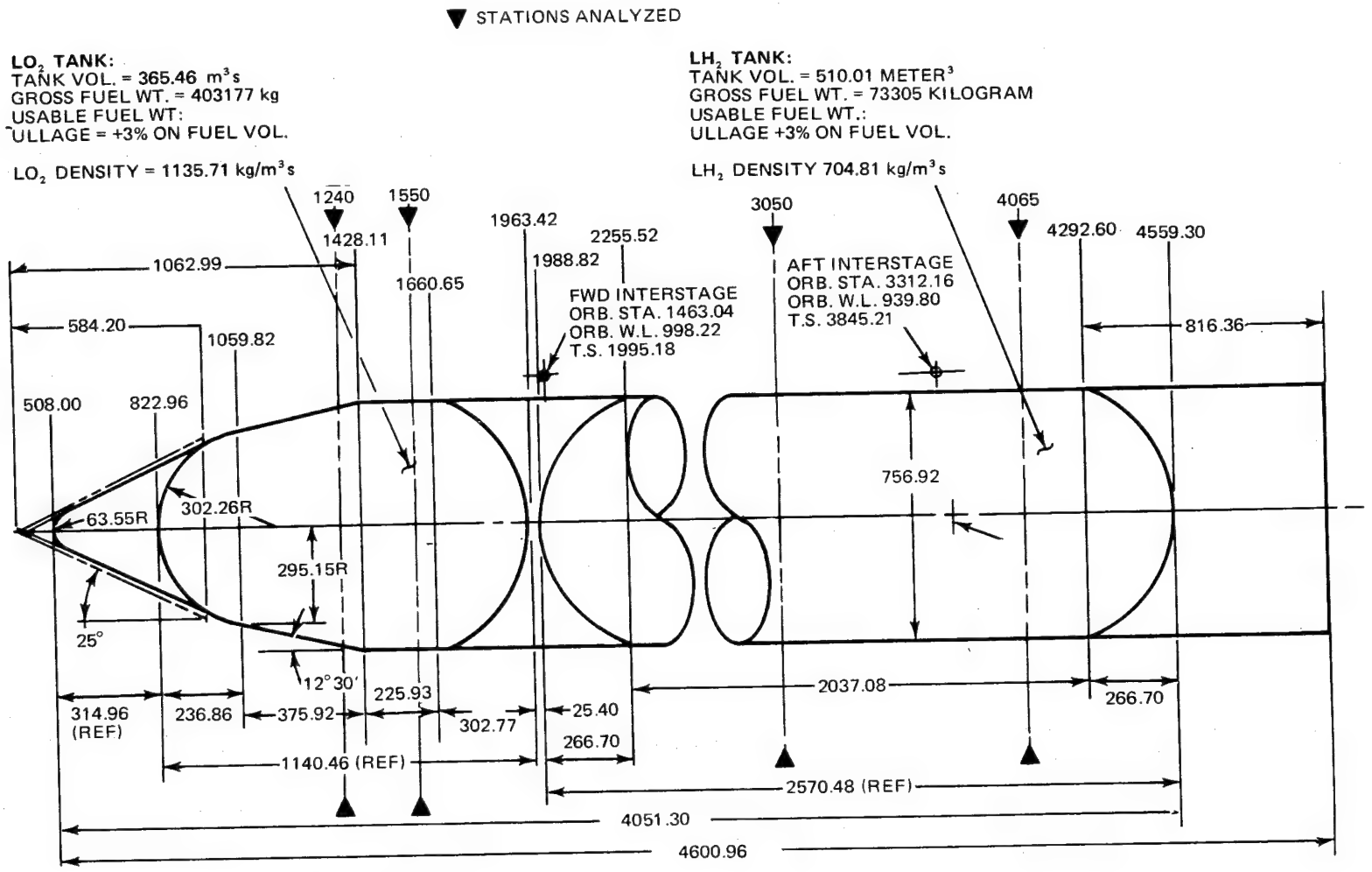

NOTE: ALL DIMENSIONS ARE FOR WET SURFACES
STATIONS AND LINEAR DIMENSIONS ARE IN CENTIMETERS

Fig. 2 HO Tank Geometry 040A Vehicle

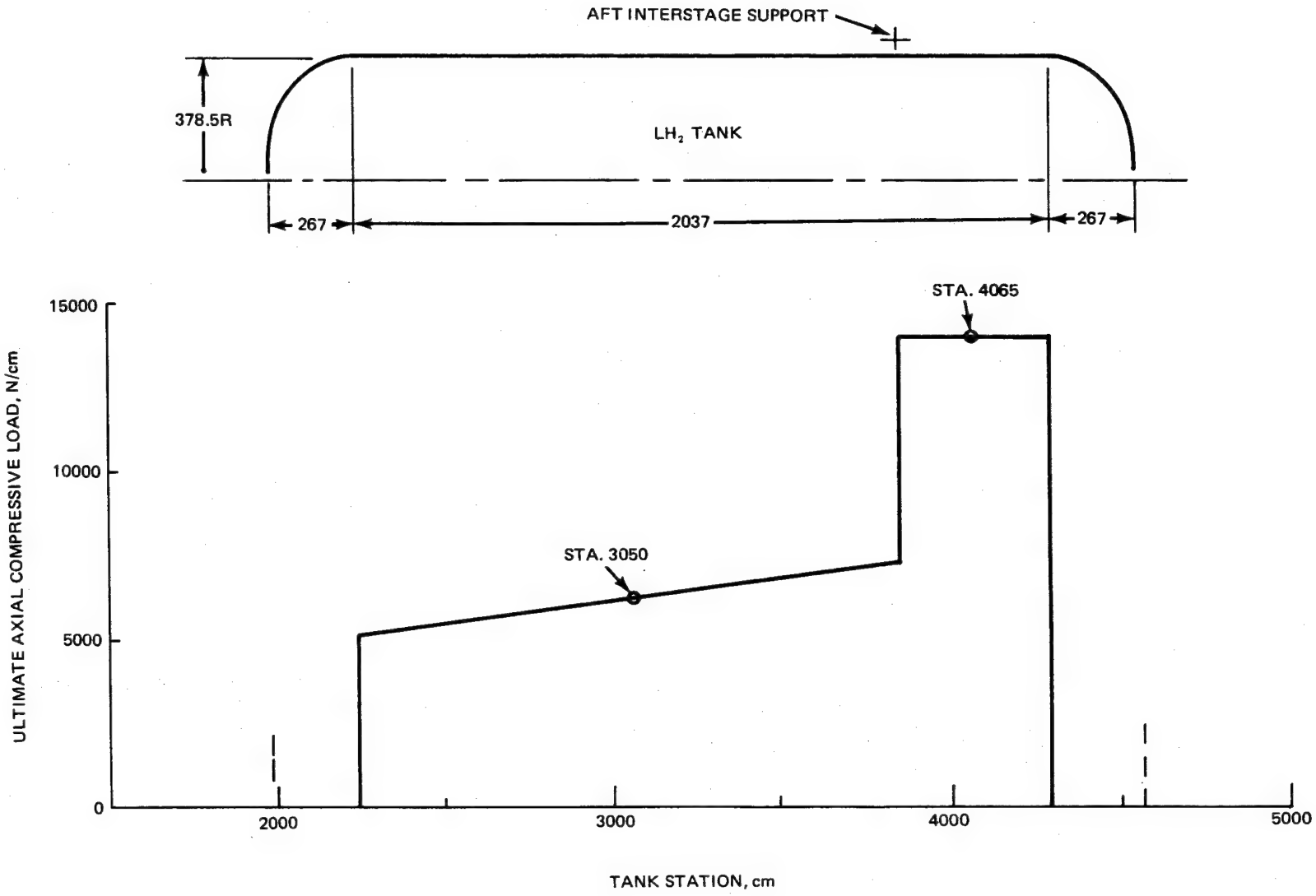

Fig. 3 LH_2 Tank Ultimate Load Intensity at End Boost

CONCEPT A – INTEGRALLY STIFFENED OVER-WRAPPED TANK – (LH_2)

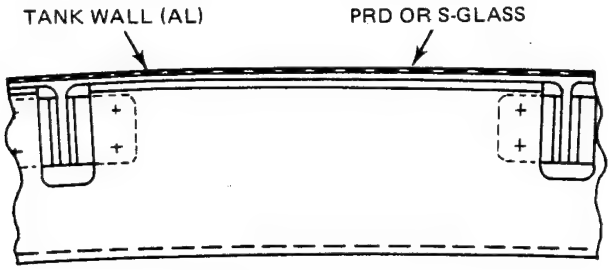

VIEW LOOKING FWD

CONCEPT C – SANDWICH CONSTRUCTION TANK (LH_2)

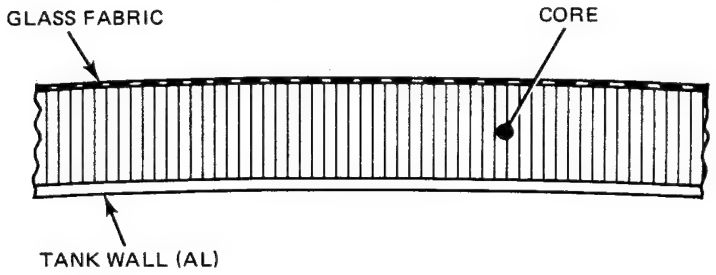

VIEW LOOKING FWD

CONCEPT B – BONDED STIFFENERS OVER-WRAPPED TANK (LH_2)

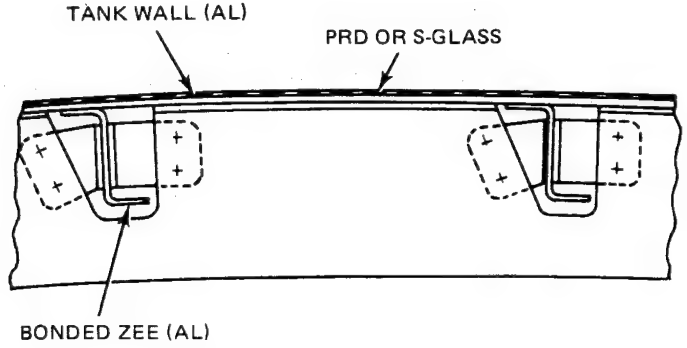

VIEW LOOKING FWD

CONCEPT D – UNSTIFFENED OVERWRAPPED TANK (LO_2)

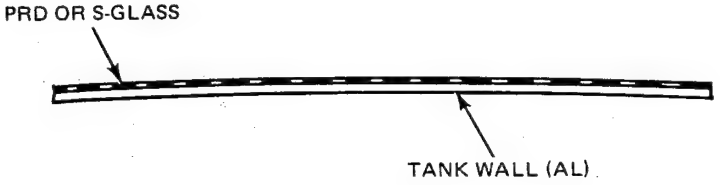

VIEW LOOKING FWD

Fig. 4 Design Concepts

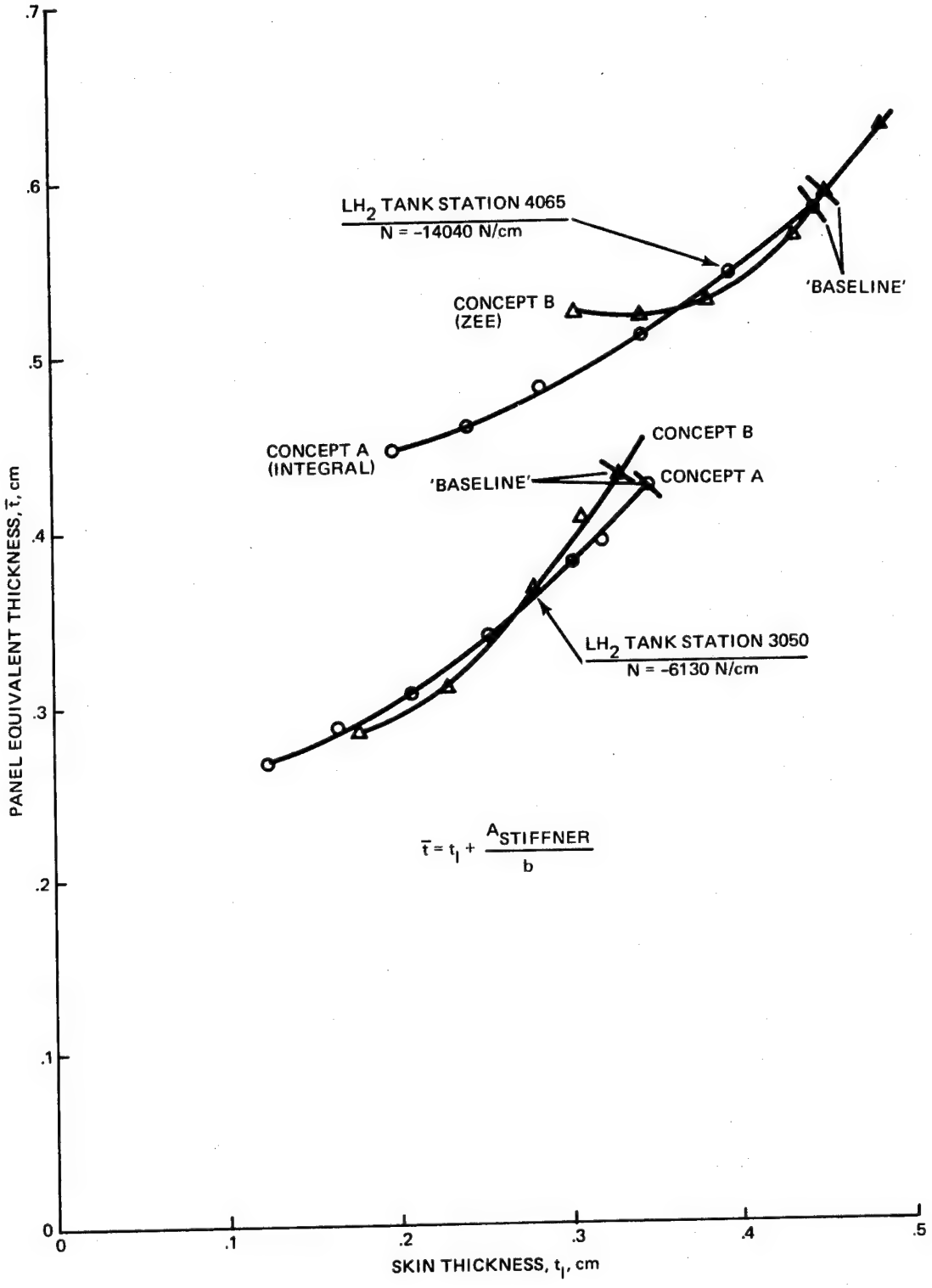

Fig. 5 Results of Compression Optimization Programs

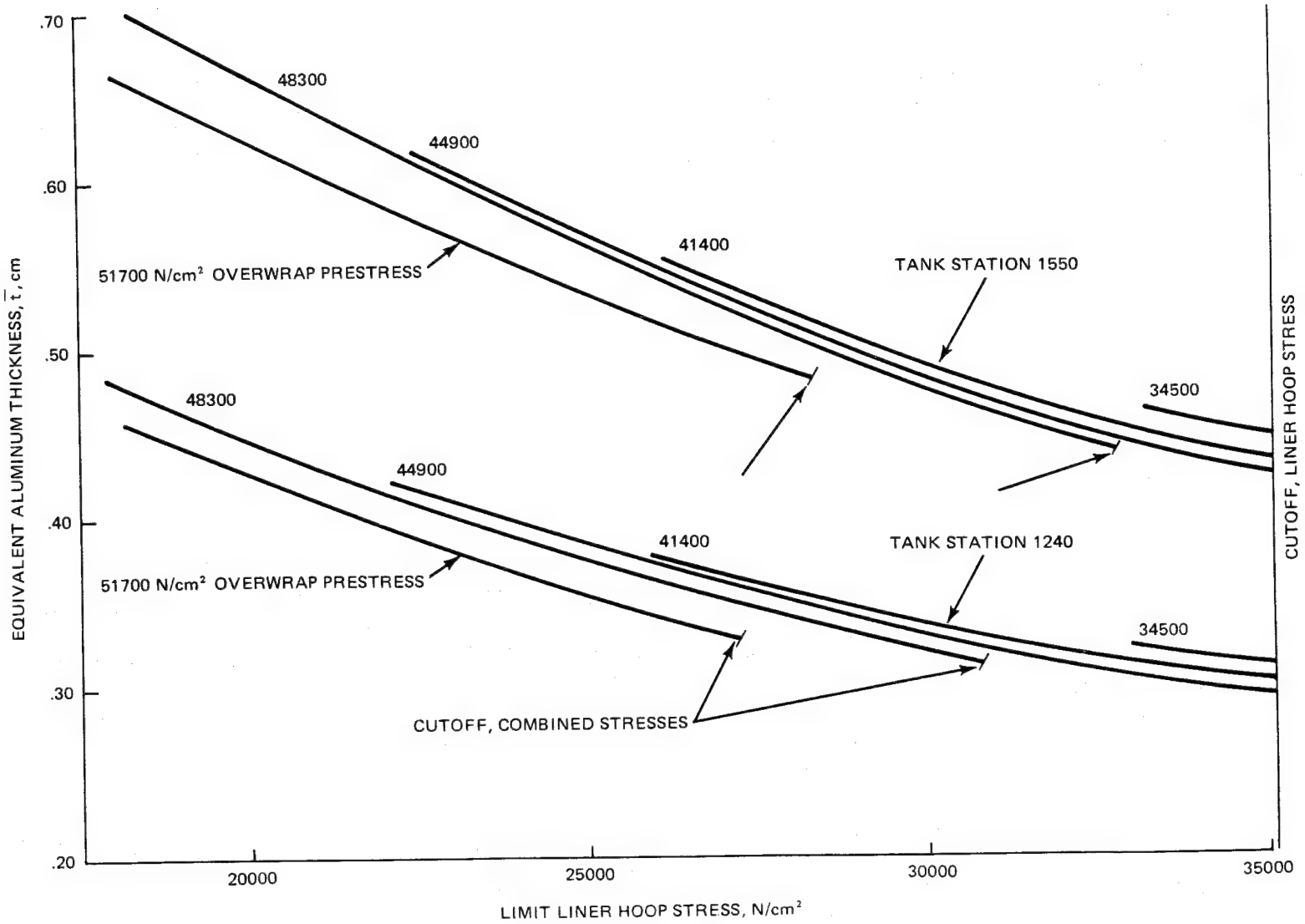

Fig. 6 LO_2 Tank, S-Glass Overwrap at T = 260°C, Cond. 1

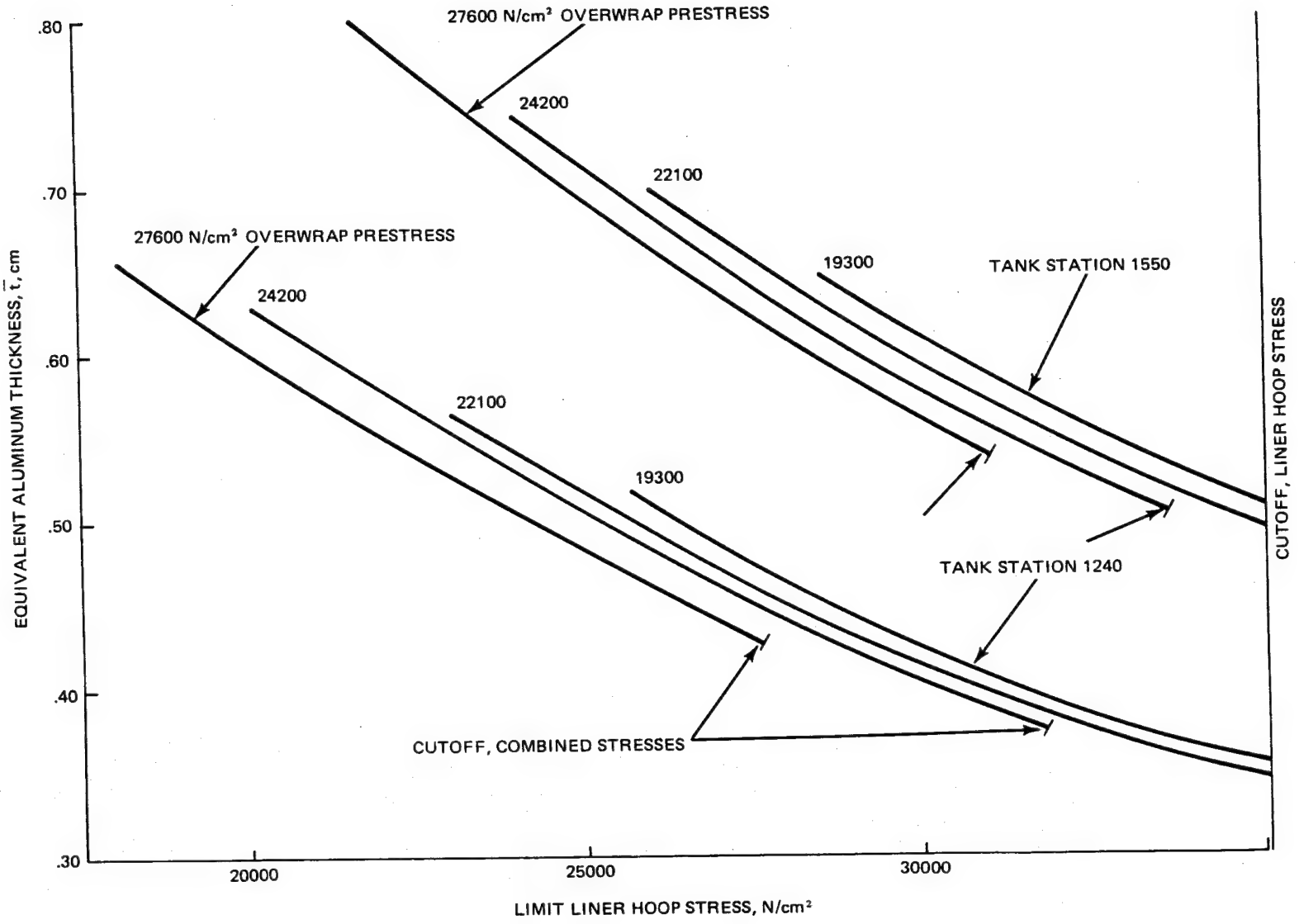

Fig. 7 LO_2 Tank, PRD Overwrap at T = 260°C, Cond. 1

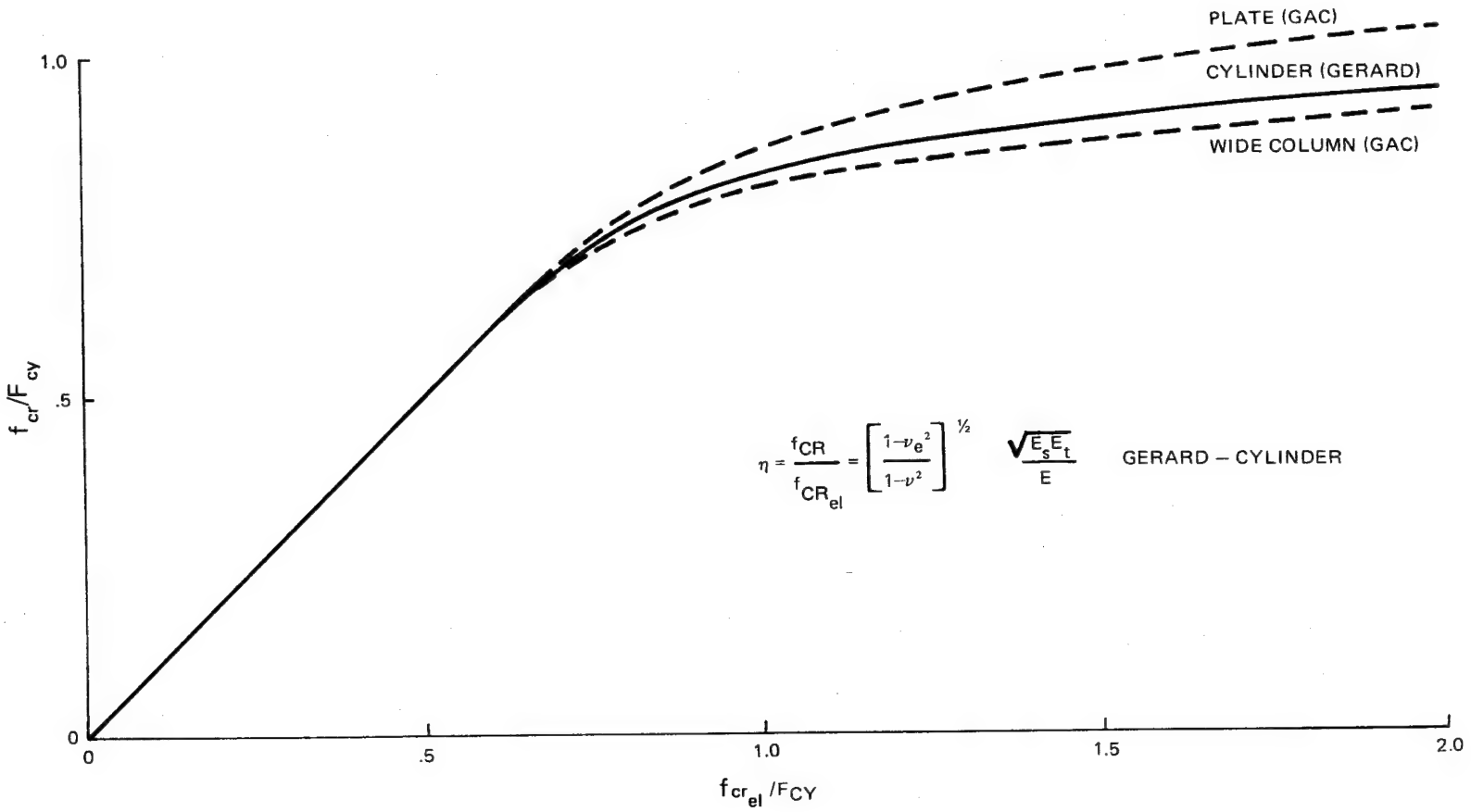

Fig. 8 2219 Aluminum Alloy Plastic Buckling Curves

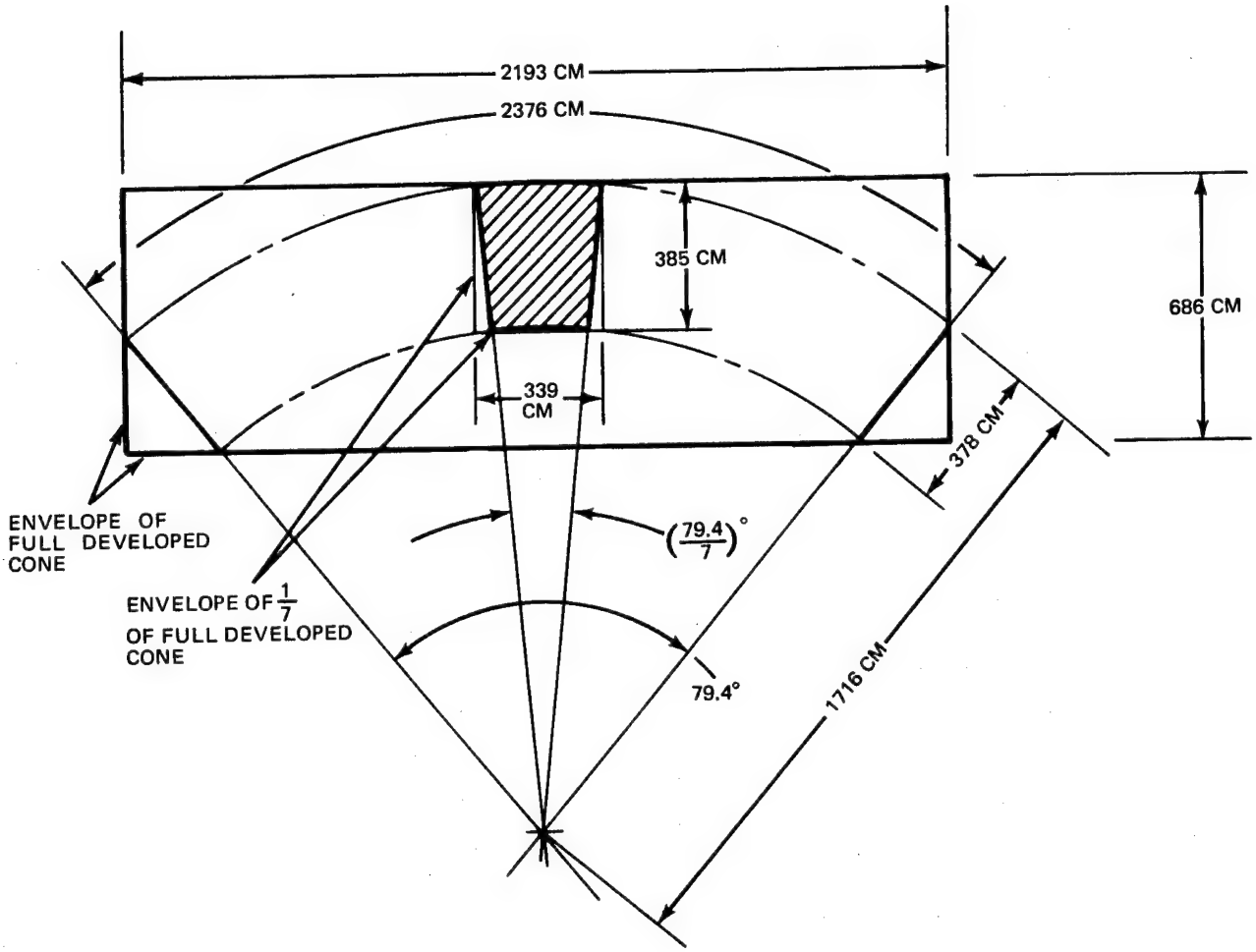

Fig. 9 Developed Cone Surface of Orbiter Lox Tank

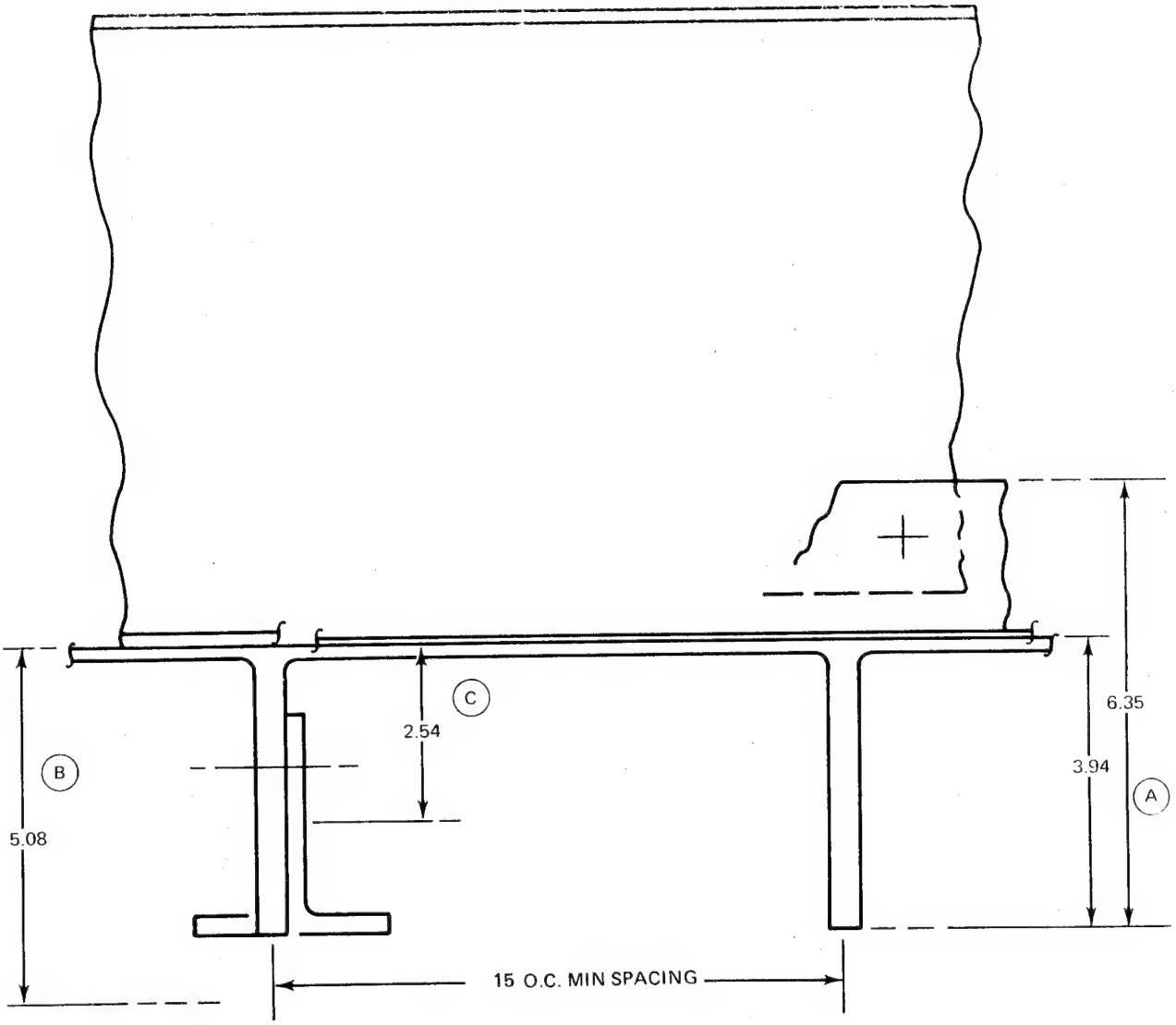

NOTE: ALL DIMENSIONS IN CENTIMETERS.

Fig. 10 Alternative Machining Methods for Orbiter LH_2 Tank

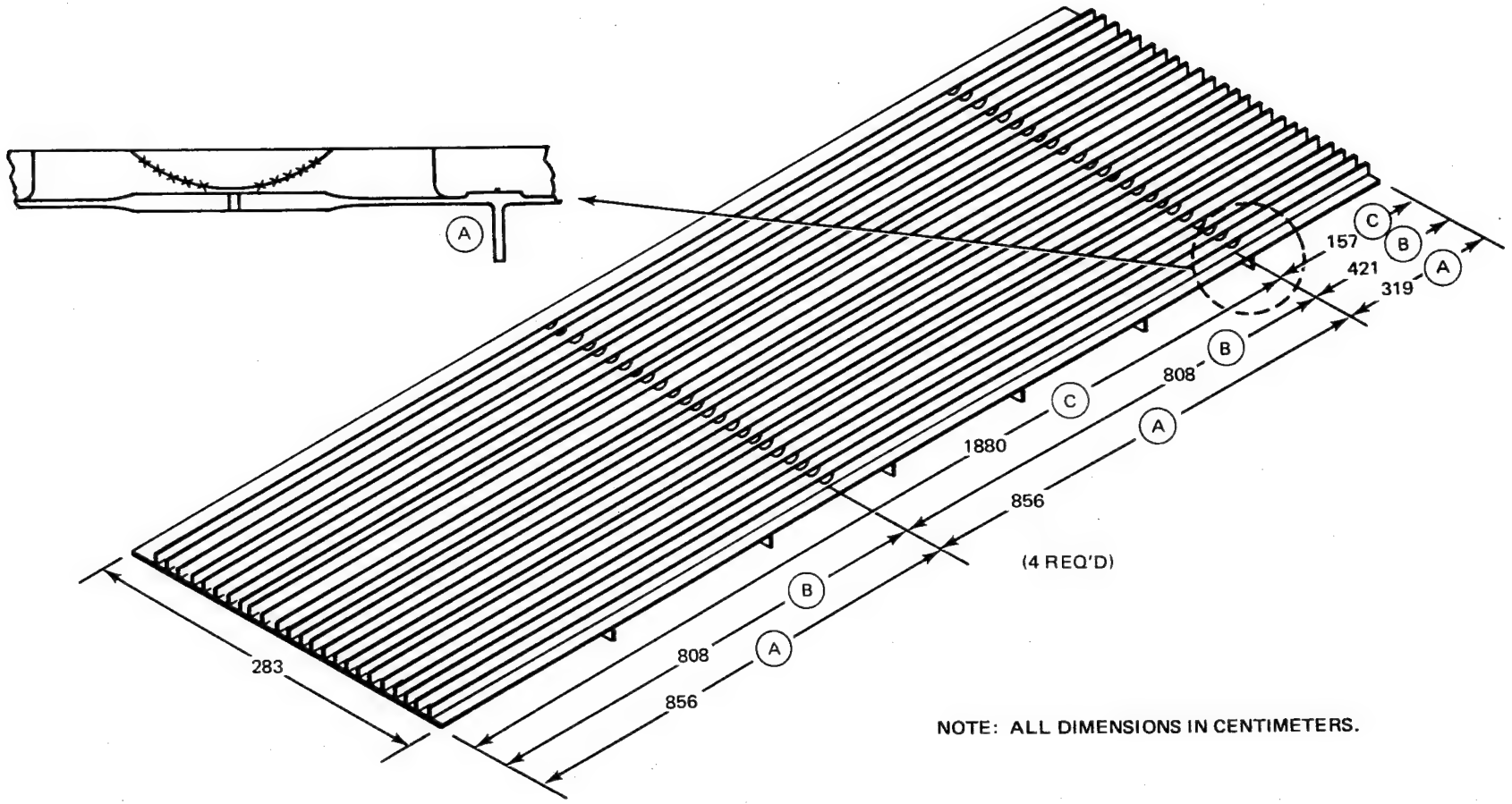

Fig. 11 Longitudinally Machined Flat Plate for Orbiter LH_2 Tank

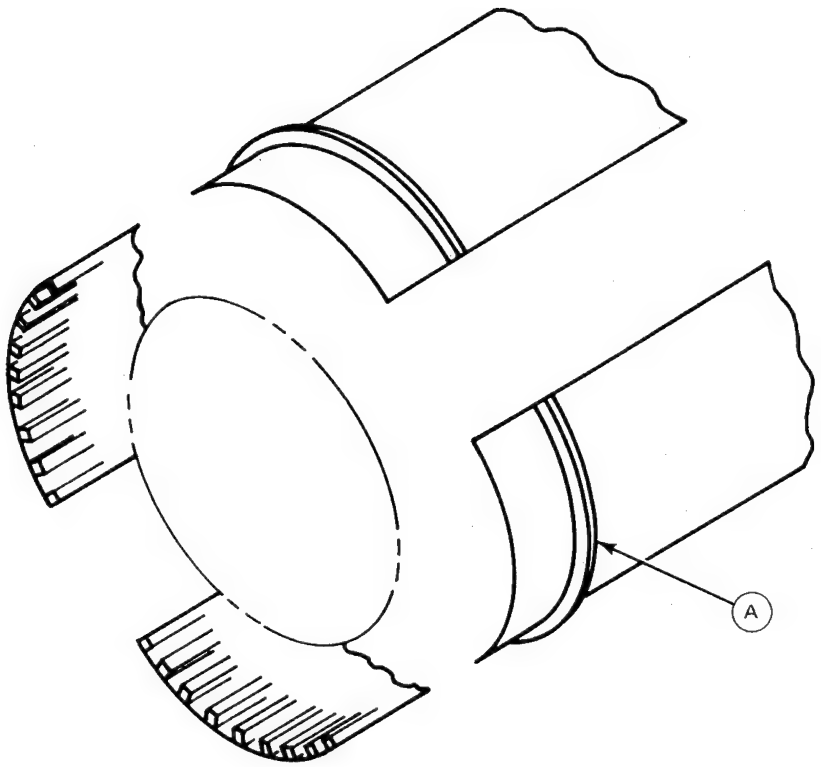

Fig. 12 Plates Rolled and Longitudinally Welded for Orbiter LH_2 Tank

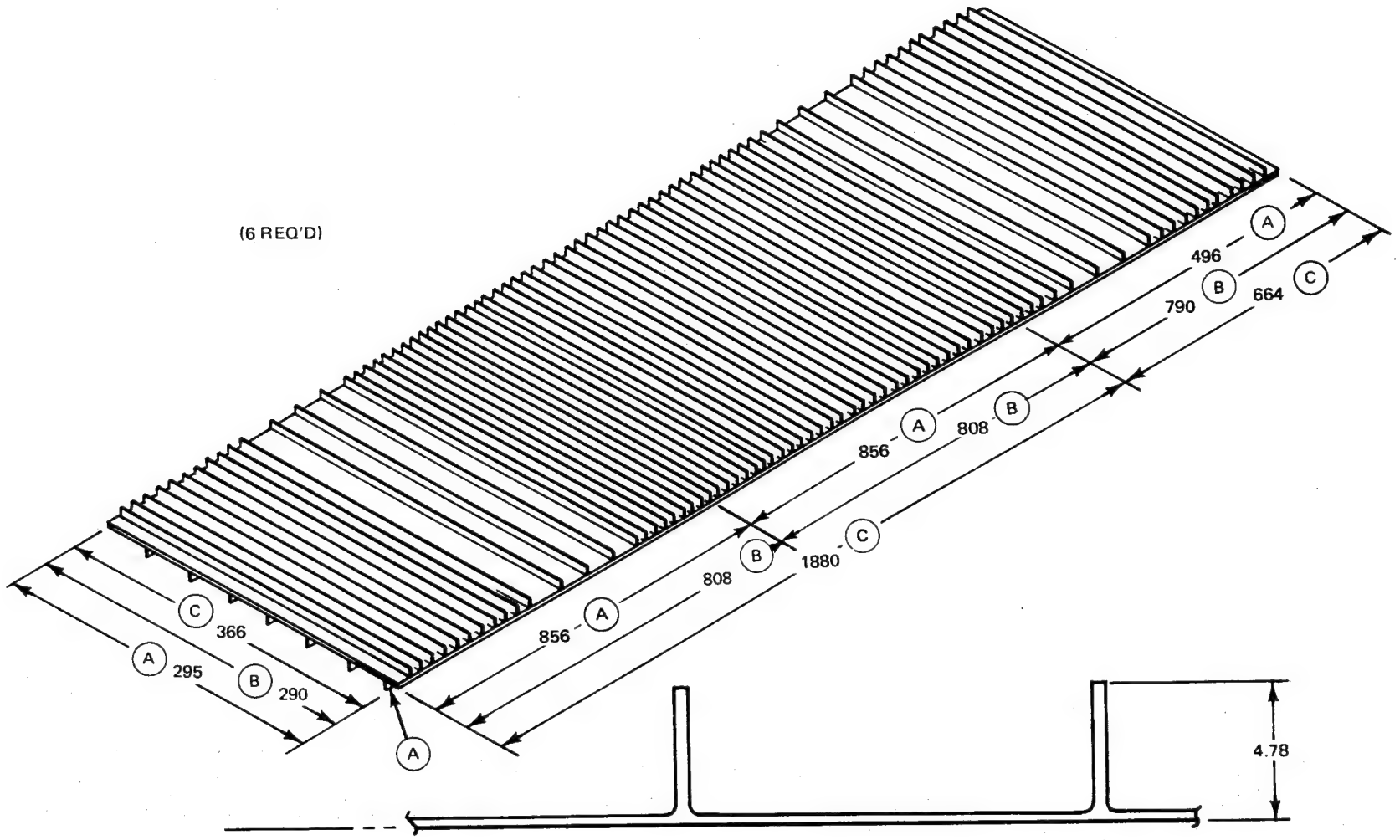

NOTE: ALL DIMENSIONS IN CENTIMETERS.

Fig. 13 Transveresly Machined Flat Plate for Orbiter LH_2 Tank

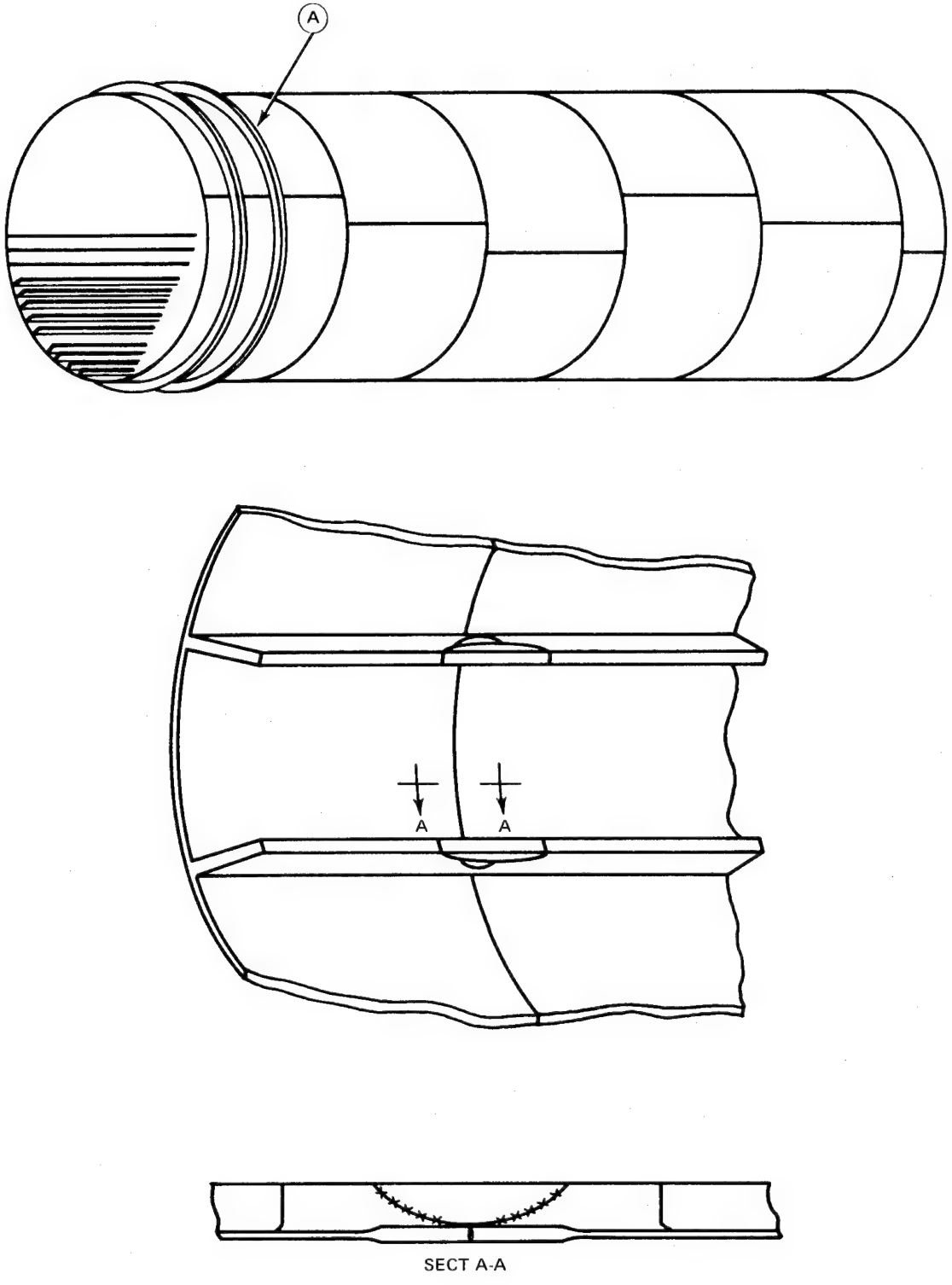

Fig. 14 Plates Rolled into Cylinders, Girth-Welded for Orbiter LH_2 Tank

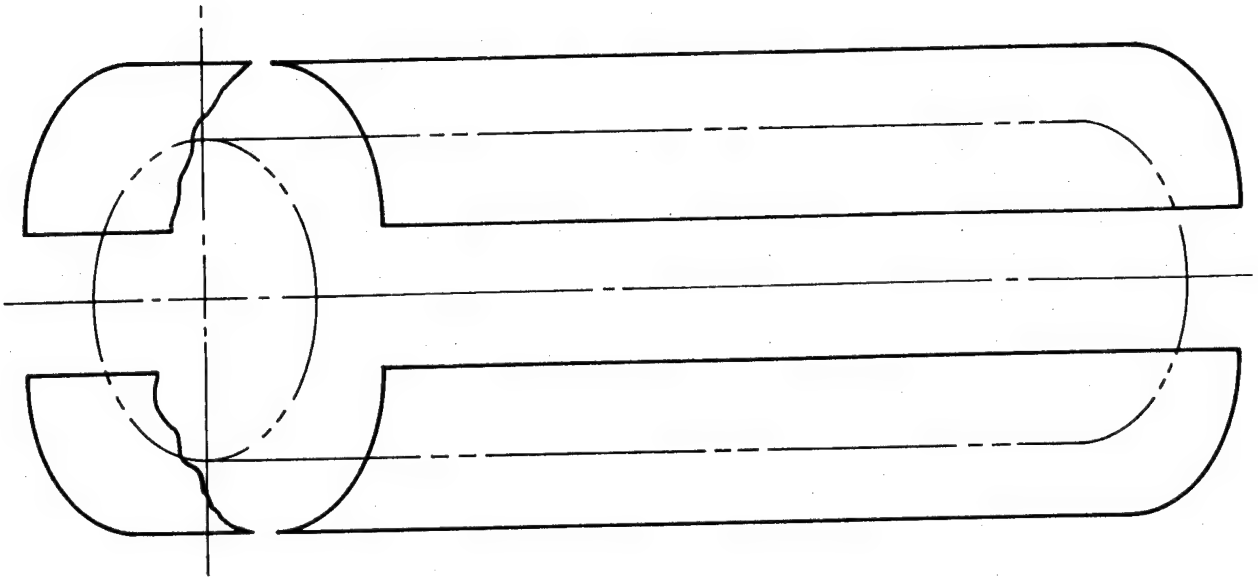

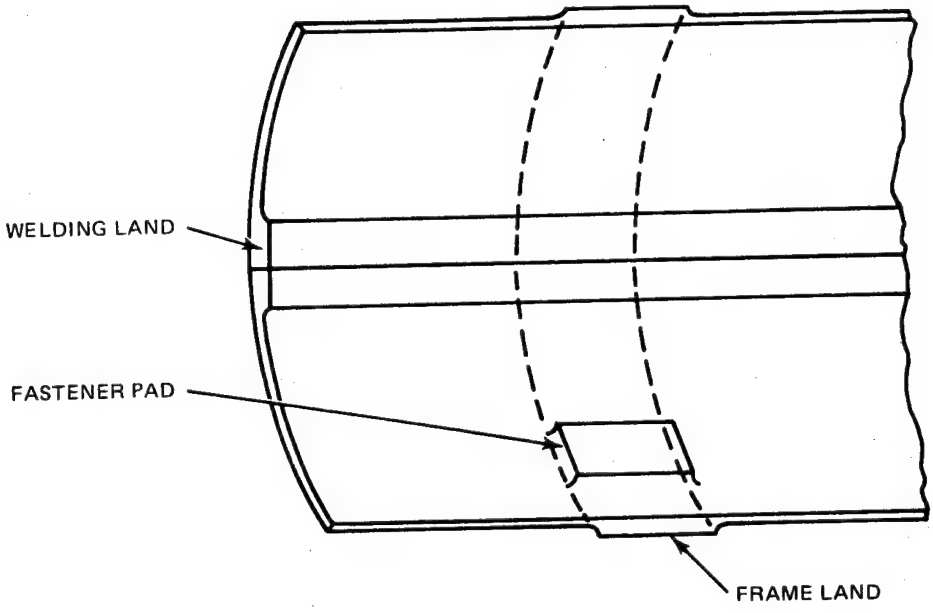

CHEM-MILLING DETAIL

Fig. 15 Plates Rolled and Welded Longitudinally for Bonded "Z" Concept Orbiter LH_2 Tank

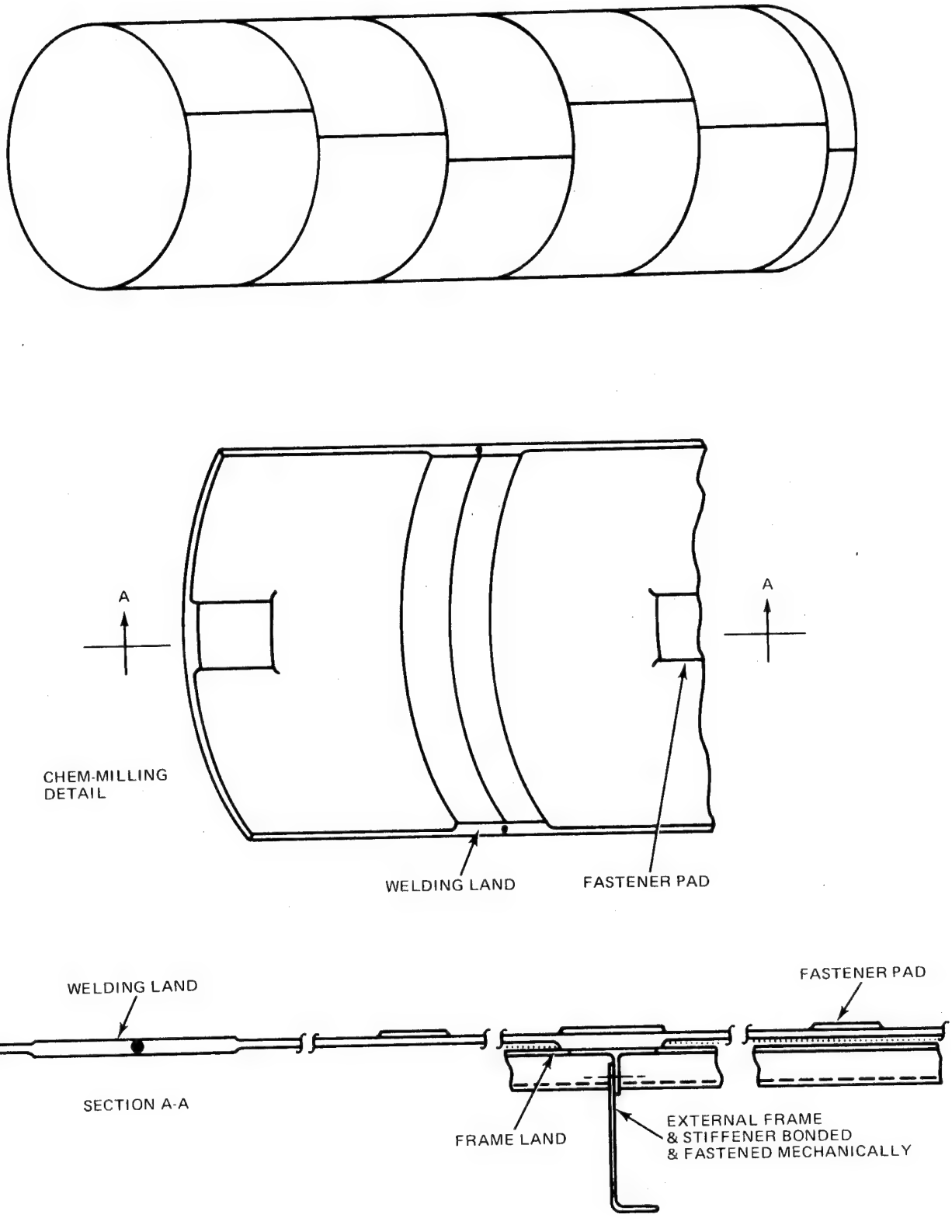

Fig. 16 Plates Rolled, Chem-Milled and Welded for Bonded "Z" Concept Orbiter LH_2 Tank

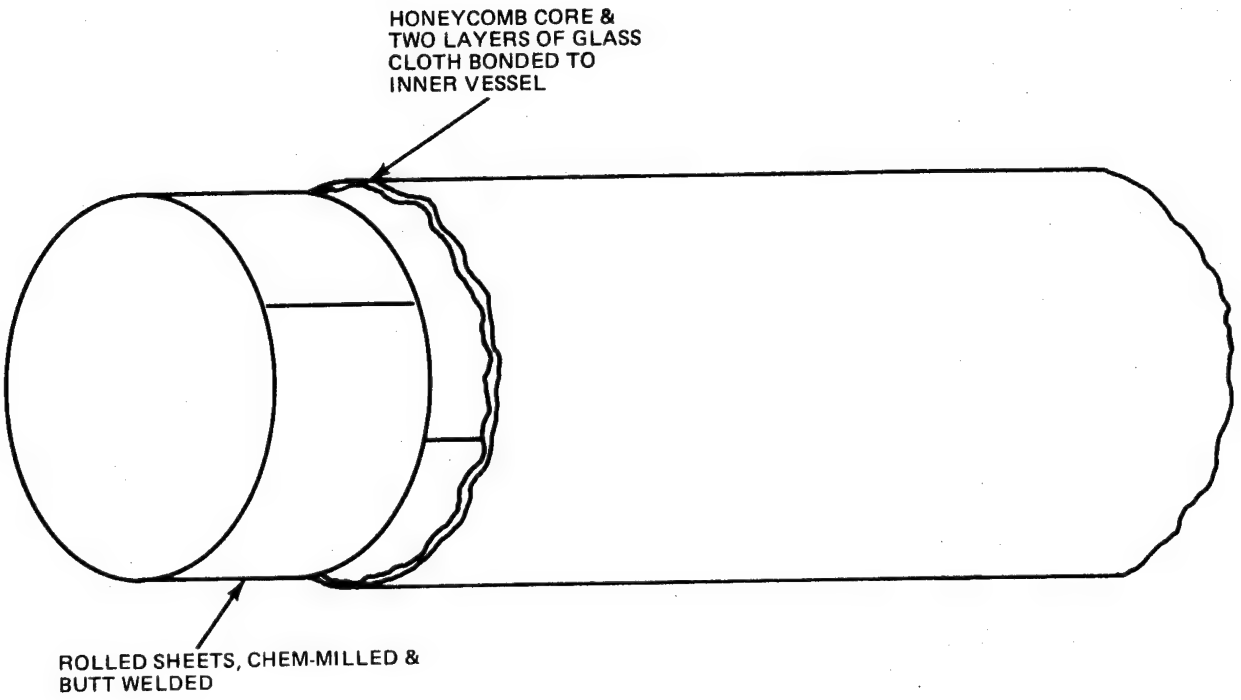

Fig. 17 Sandwich Construction, Method #1, Orbiter LH_2 Tank

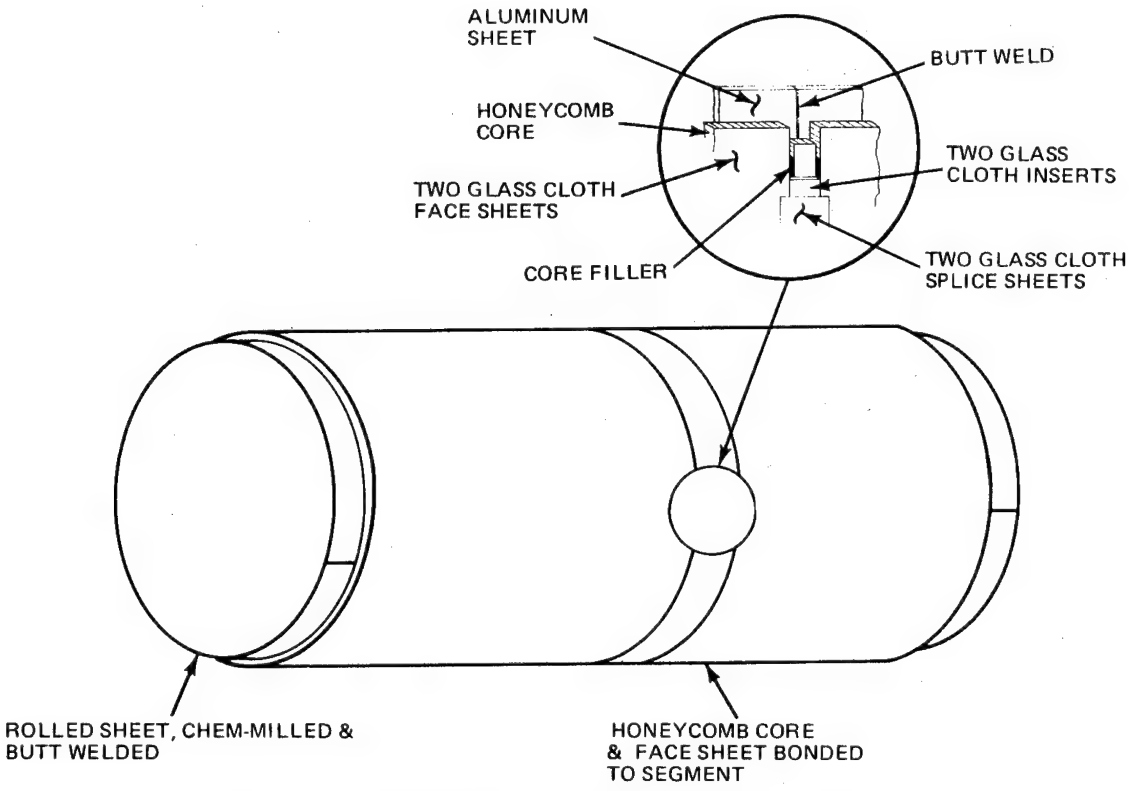

Fig. 18 Sandwich Construction, Method #2, Orbiter LH_2 Tank

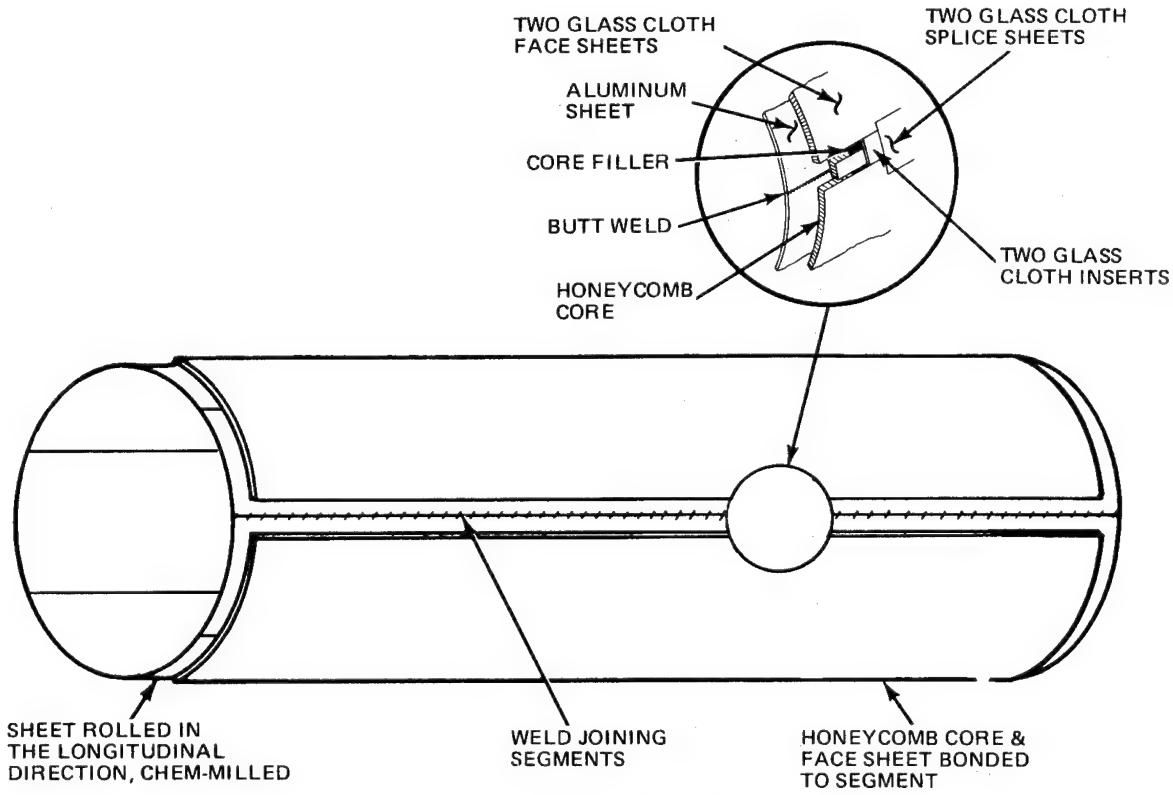

Fig. 19 Sandwich Construction, Method #3, Orbiter LH_2 Tank

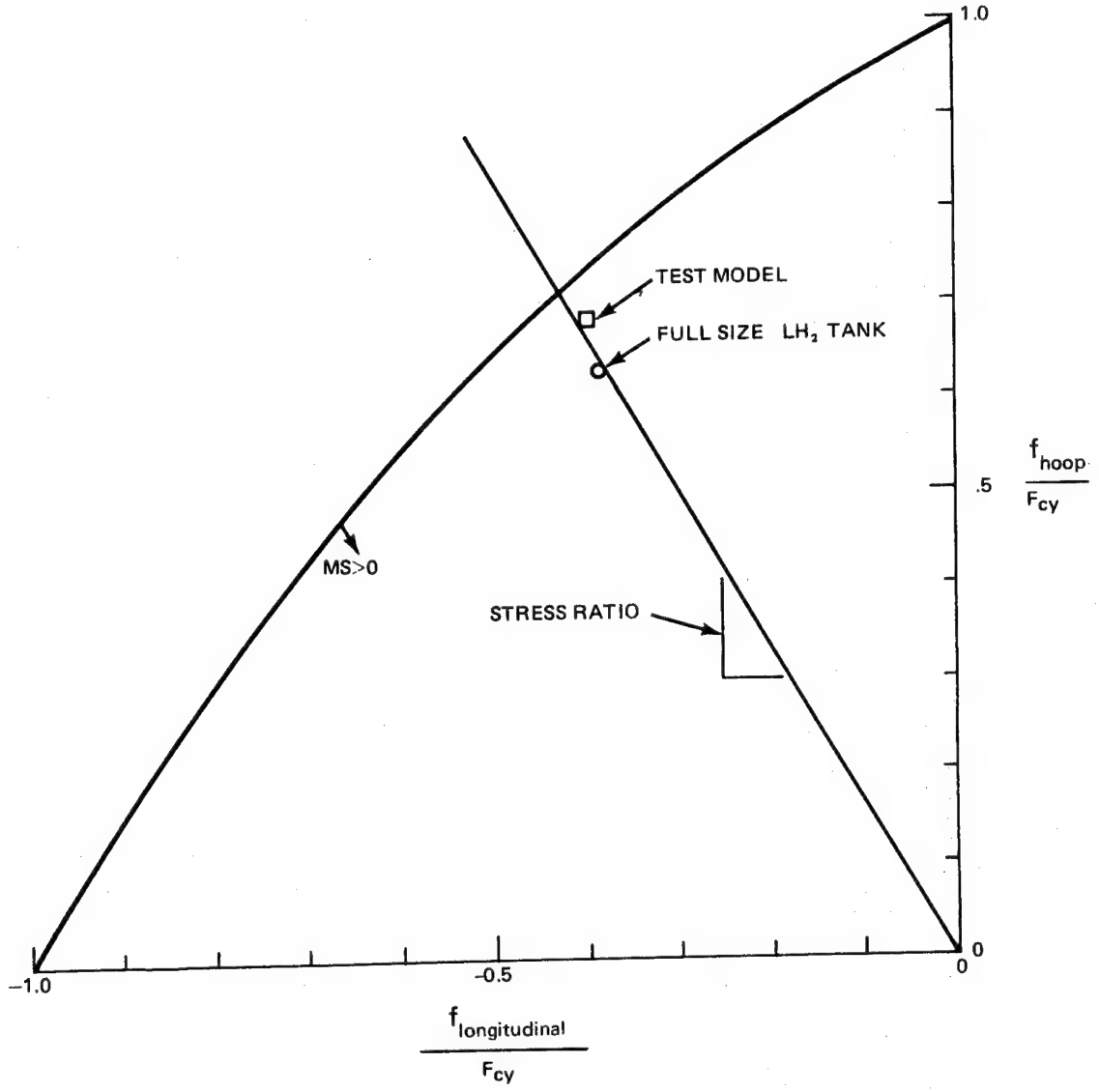

Fig. 20 Failure Criteria

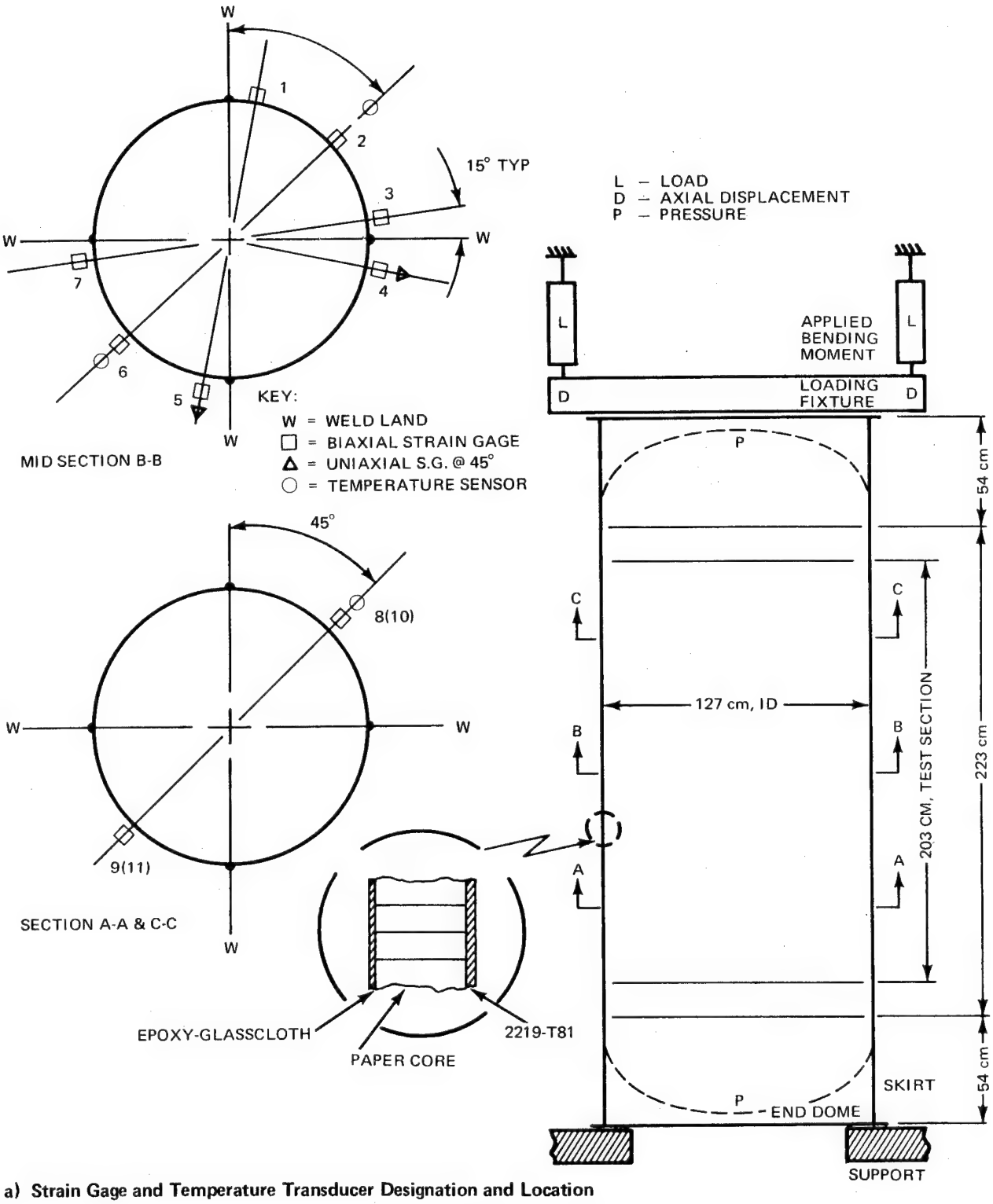

a) Strain Gage and Temperature Transducer Designation and Location

Fig. 21 Schematic of Test Article

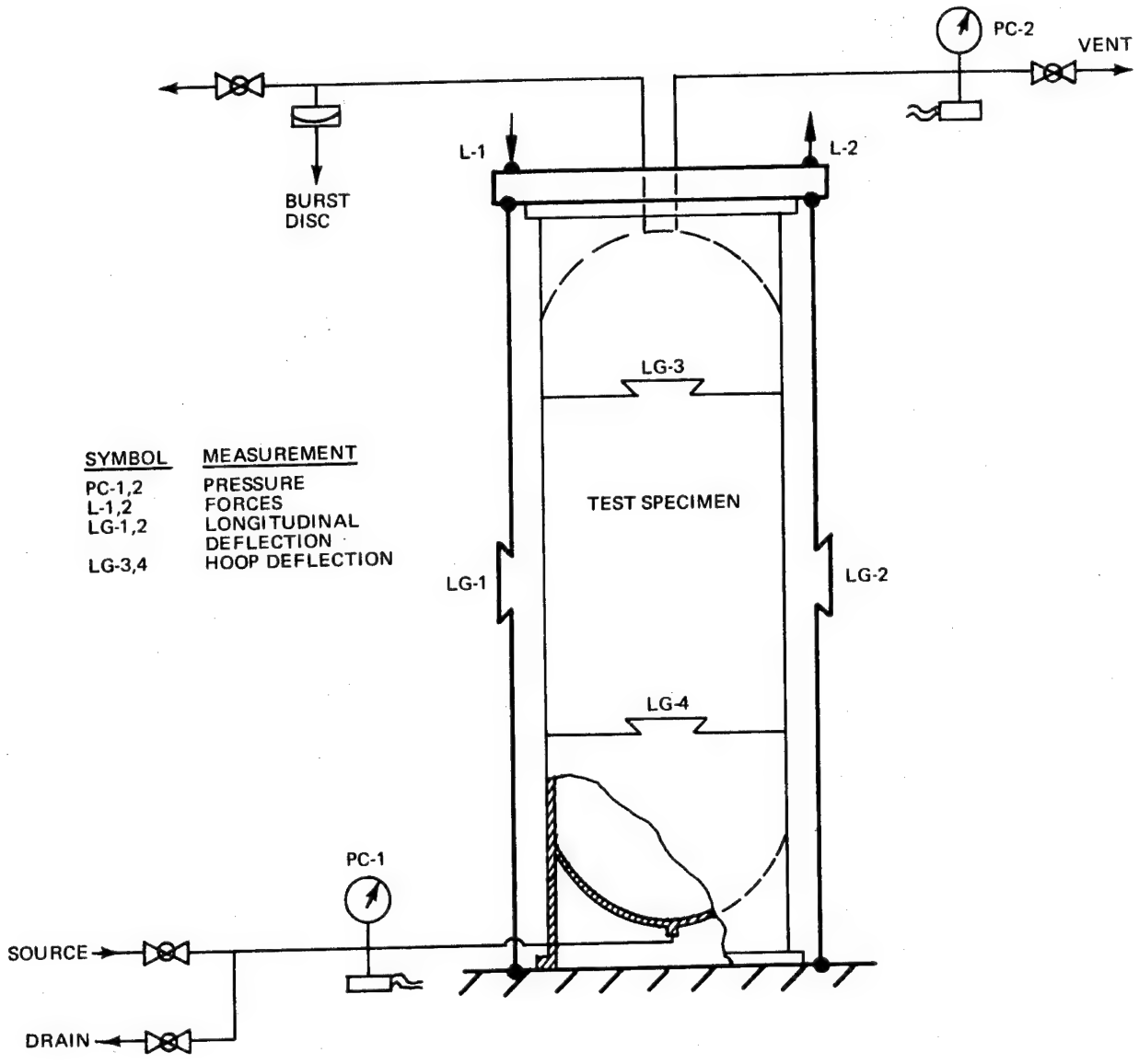

b) Test-Site Instrumentation Designation and Location

Fig. 21 Schematic of Test Article (Cont'd)

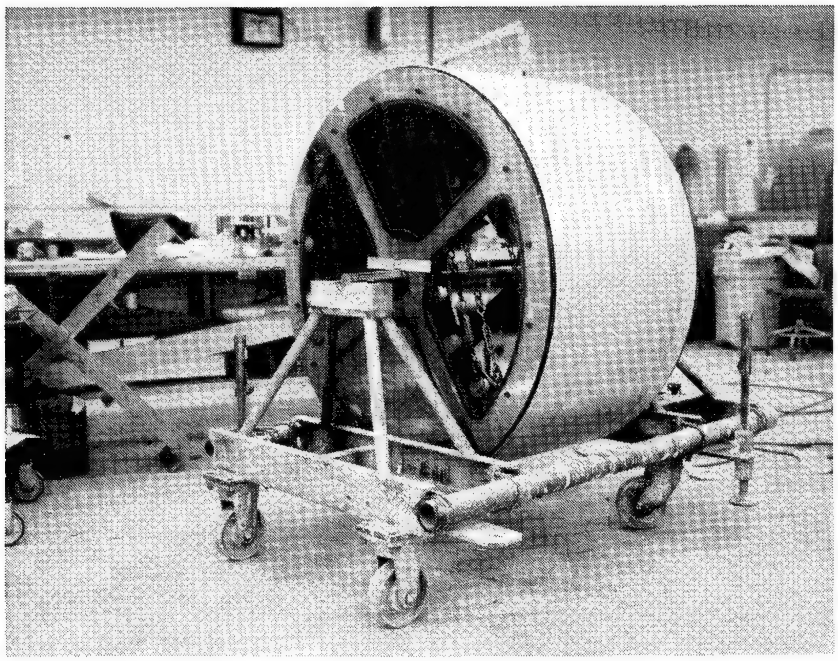

Fig. 22 Prototype Shell of 2219 Aluminum Assembled to Mandrel Support Fixture

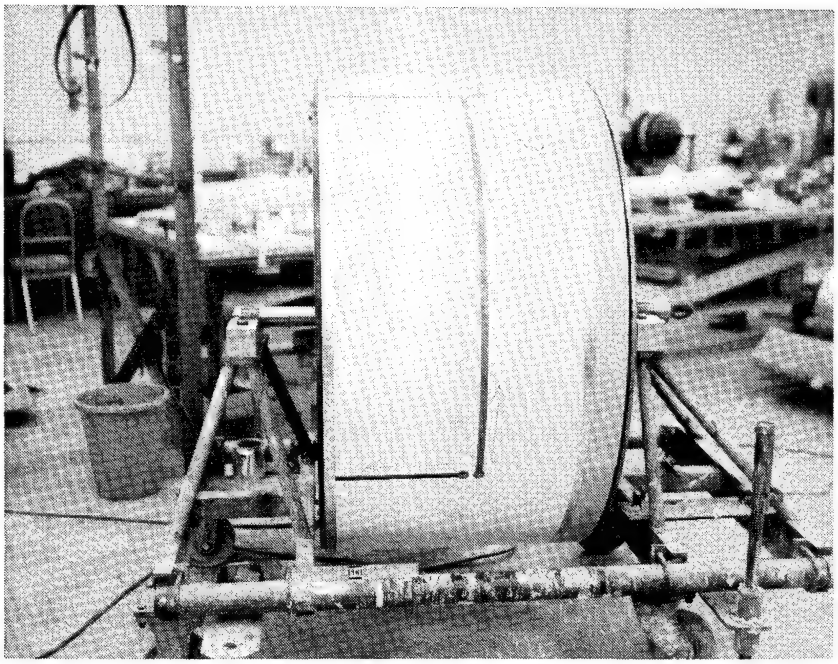

Fig. 23 Adhesive Layer Showing Strain Gage Wire Location on Prototype

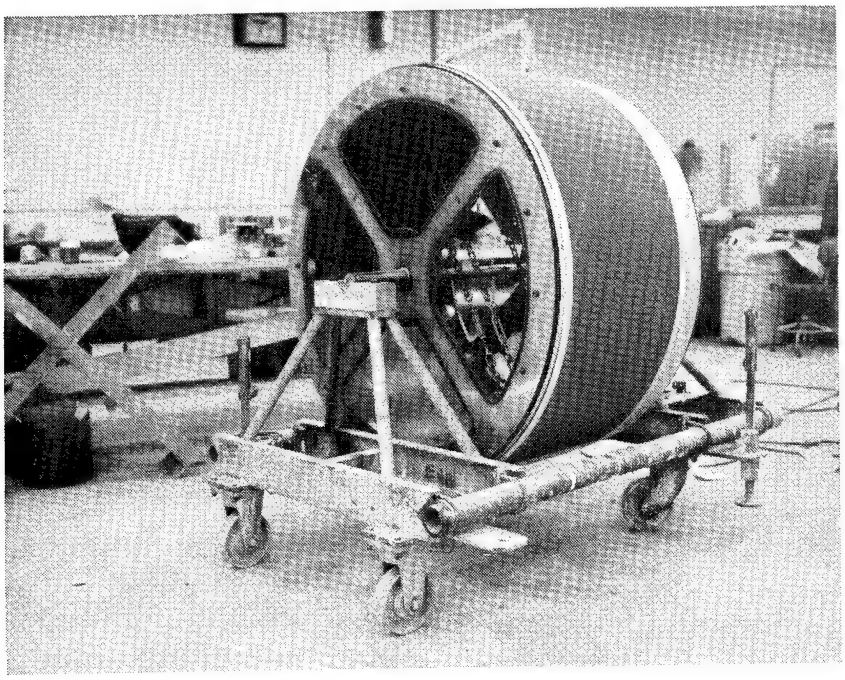

Fig. 24 Honeycomb Core Applied to Prototype Test Cylinder

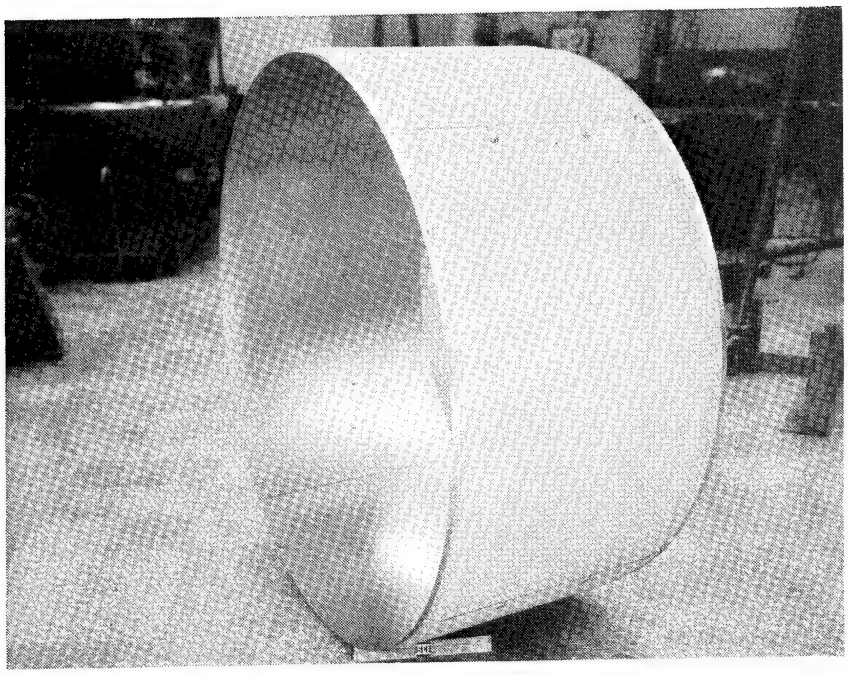

Fig. 25 Completed Prototype Test Cylinder

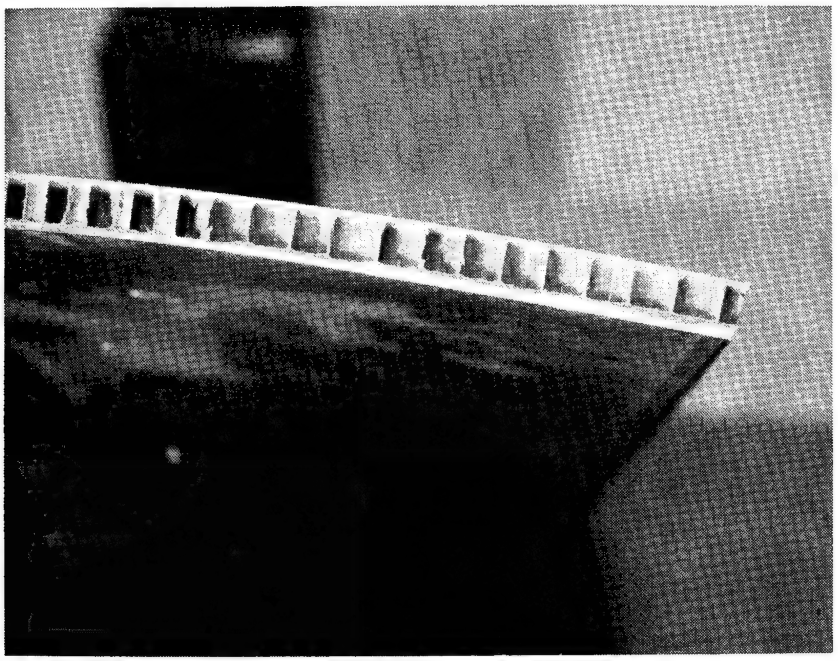

Fig. 26 Cross Section of Wall from Completed Prototype Test Cylinder

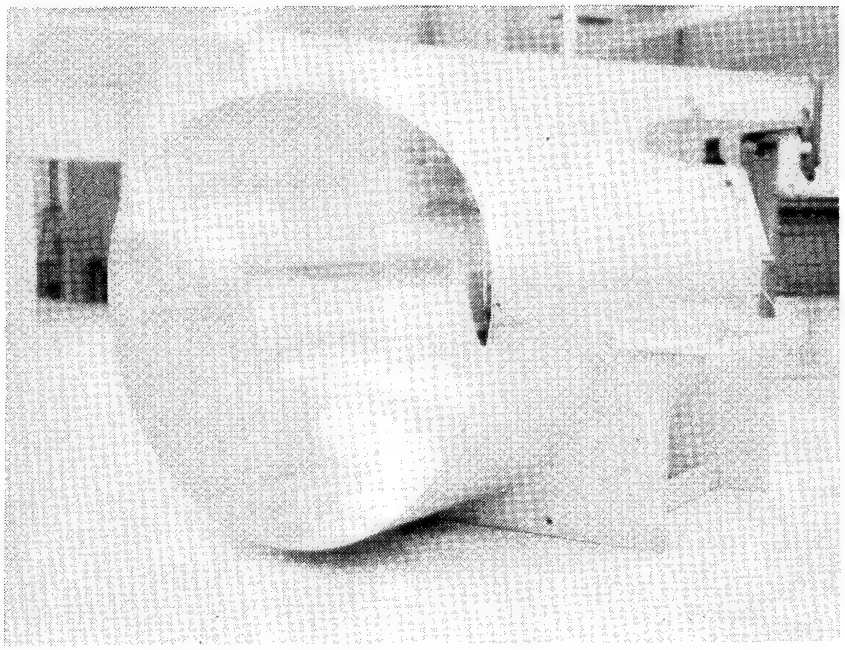

Fig. 27 Full-Size Cylindrical Test Section, Metal Shell

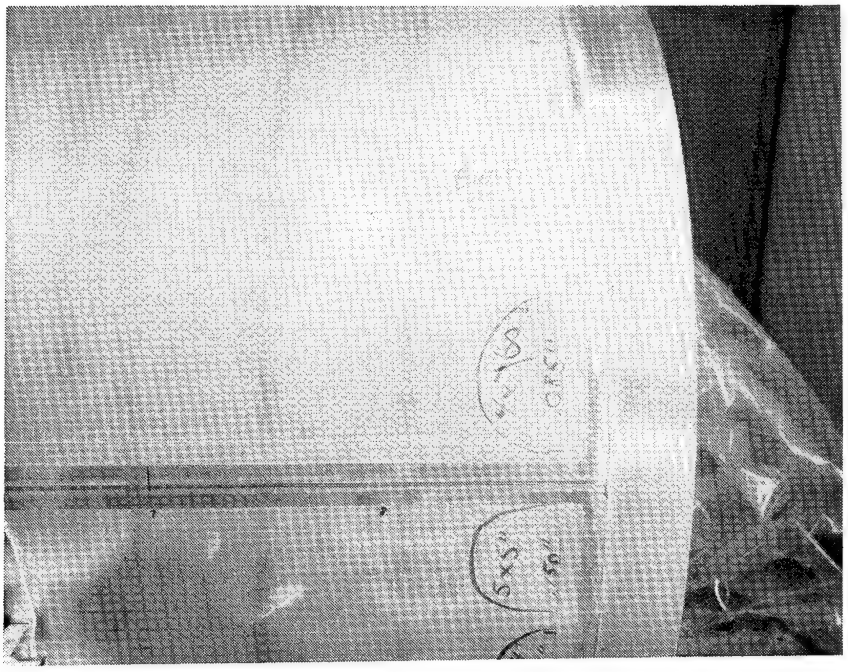

A) CIRCLED AREAS SHOW APPROXIMATE SIZE OF LOCAL BUCKLES.

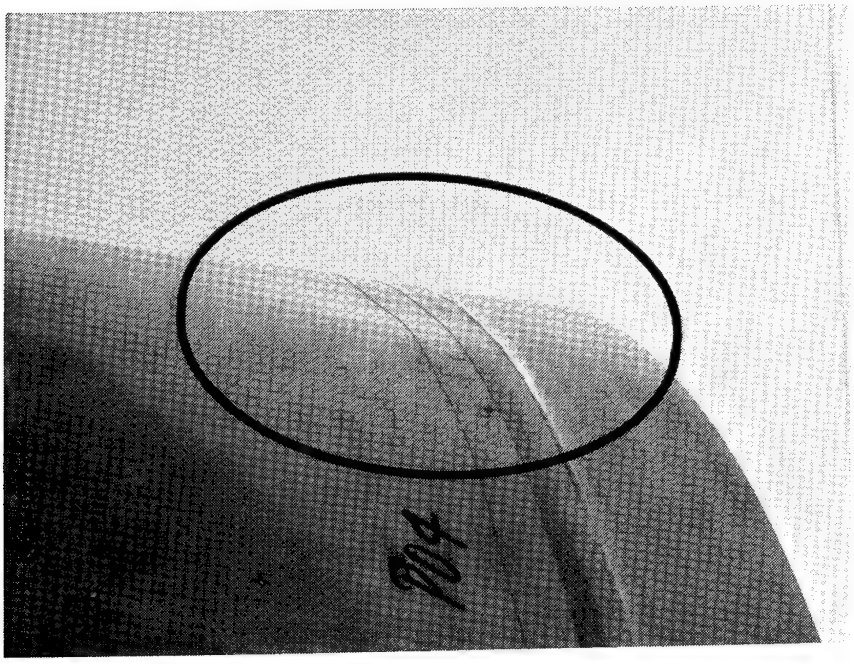

B) DETAIL OF BUCKLED REGION.

Fig. 28 Typical Full-Scale 2219 Aluminum Test Cylinder-to-Transition Ring Weld Region

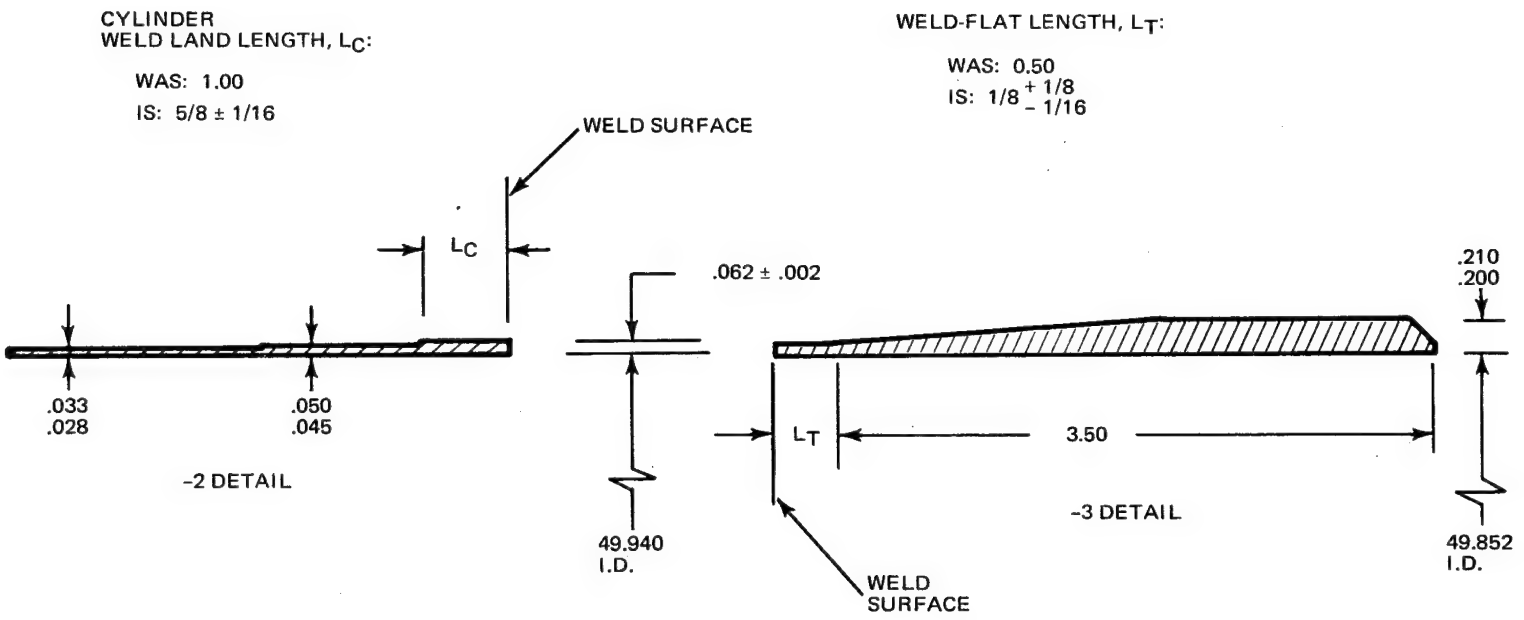

REF: P/N 1269331
2219 ALUMINUM SHELL–
TANK TEST SECTION

NOTE: DIMENSIONS ON THIS SHOP DRAWING ARE IN INCHES.

Fig. 29 Transition Ring, Weld Details

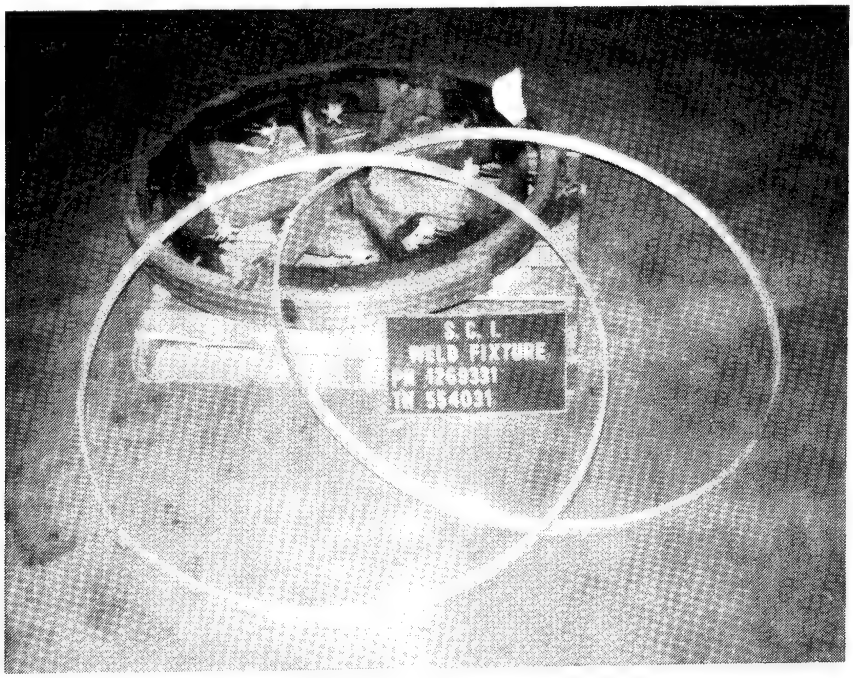

Fig. 30 Girth Weld Tooling

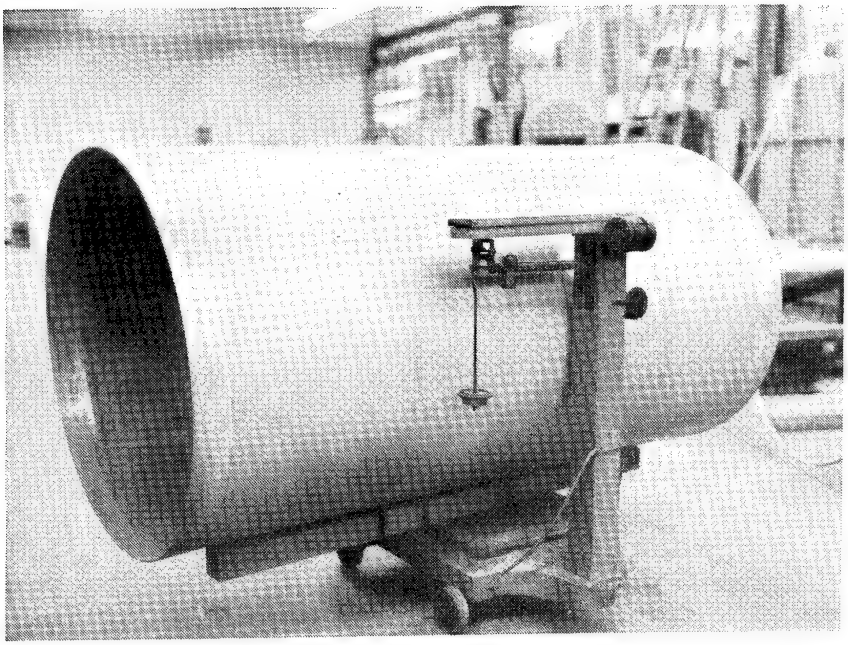

Fig. 31 Tank Test Section, 2219 Aluminum Shell, P/N 1269331

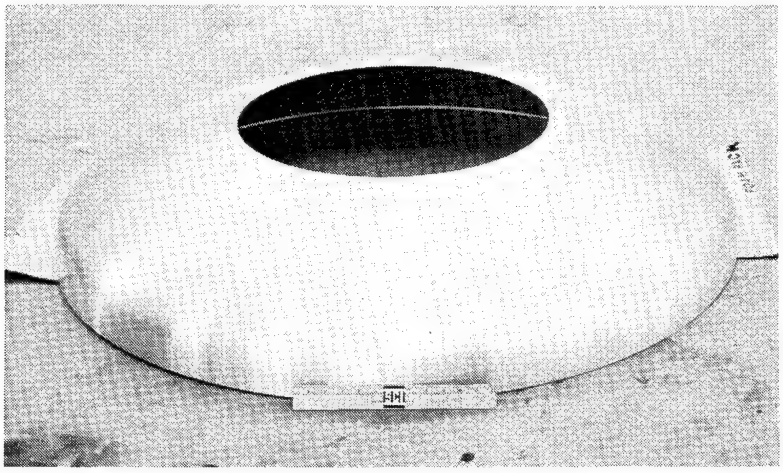

Fig. 32 Top End Closure Assembly 6061 Aluminum Head

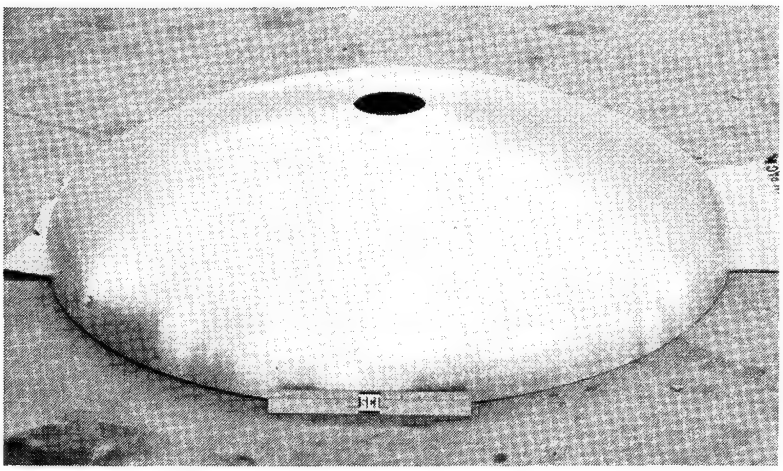

Fig. 33 Bottom End Closure Assembly 6061 Aluminum Head

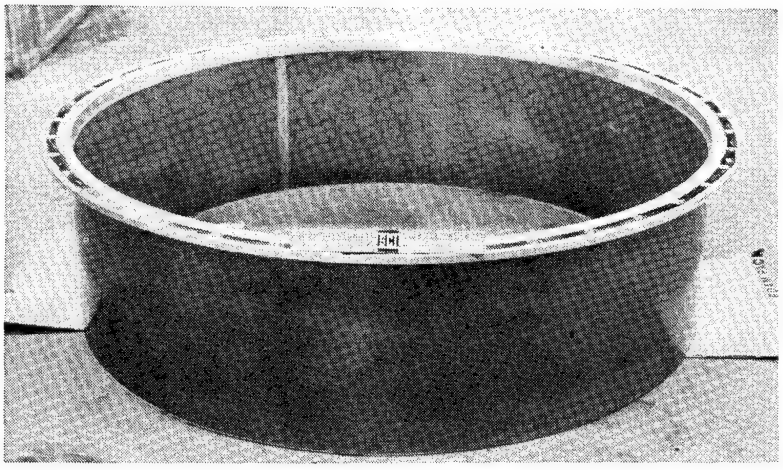

Fig. 34 Extension/Support Ring Subassembly, 6061 Aluminum

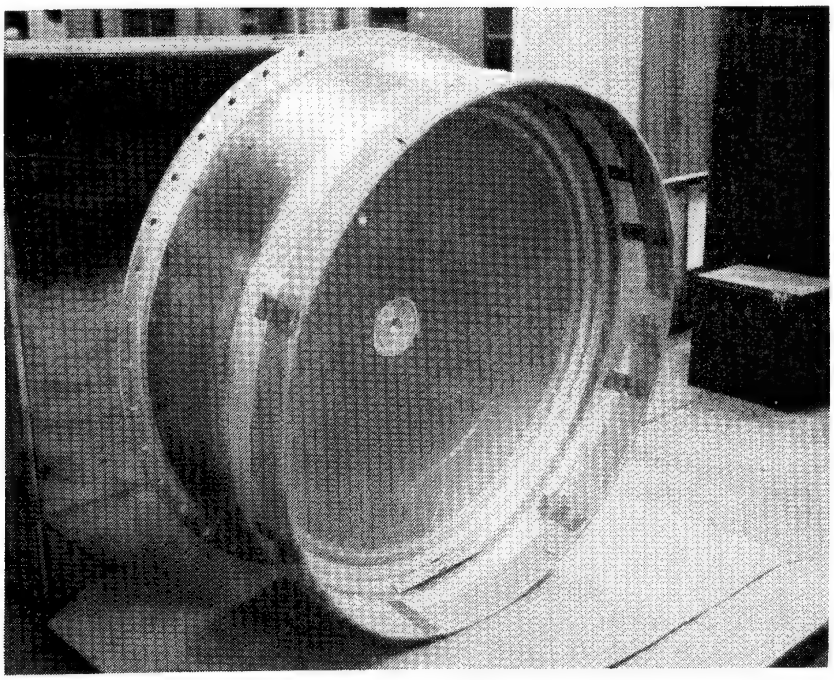

Fig. 35 Internal View of End Closure Assembly

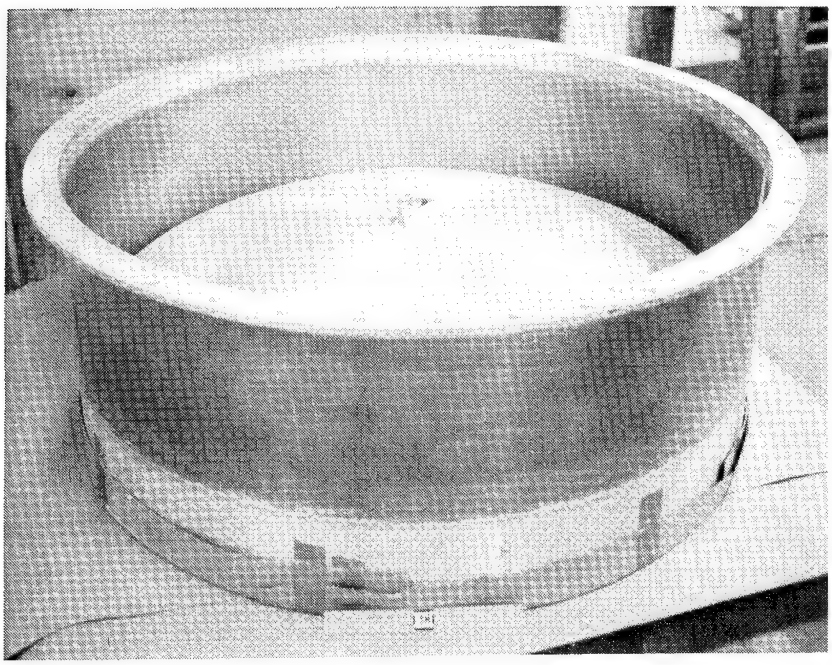

Fig. 36 External View of End Closure Assembly

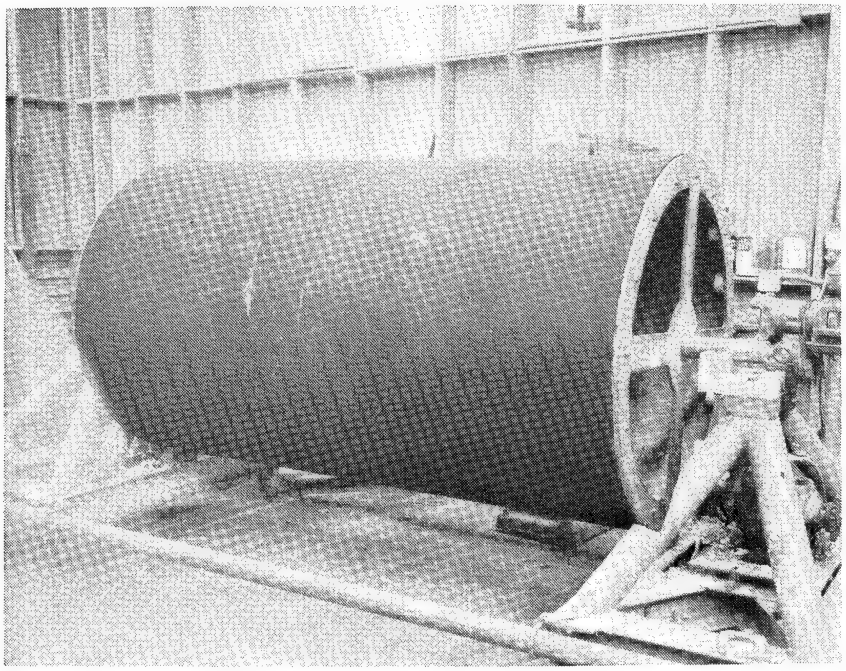

Fig. 37 Completed Full-Scale Mandrel Support Fixture

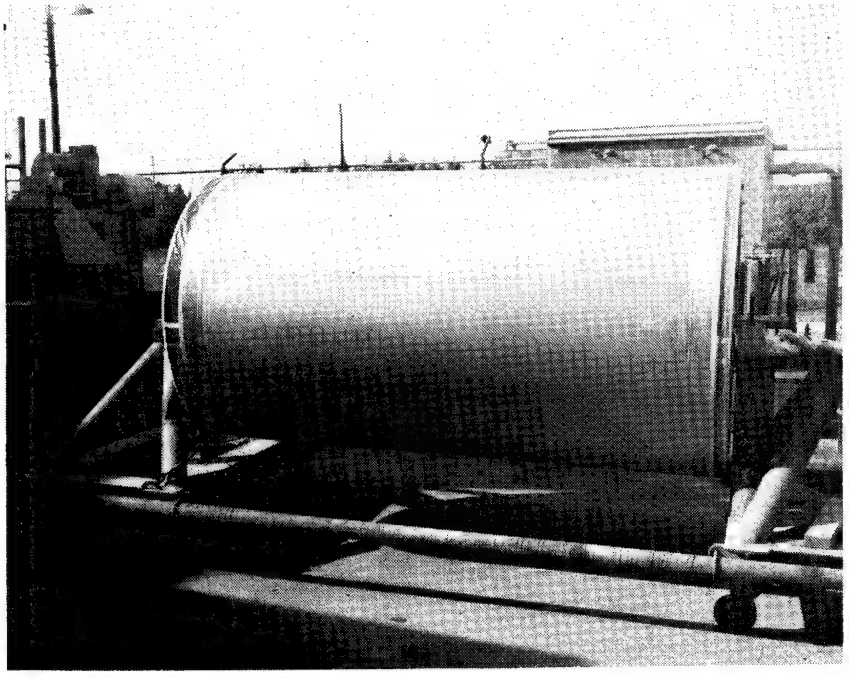

Fig. 38 Aluminum Shell Assembled to Mandrel Support Fixture

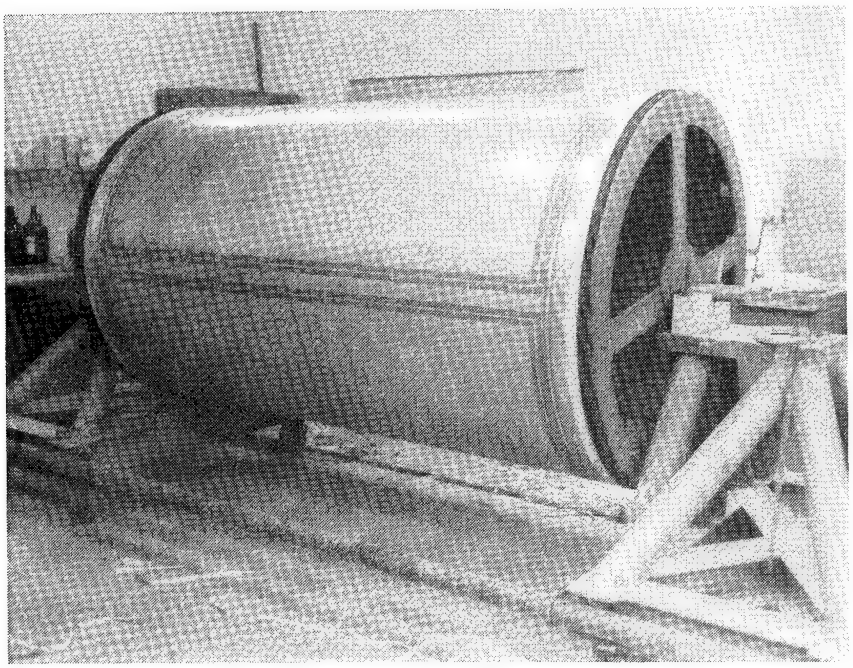

Fig. 39 Adhesive-Filled Weld Lands

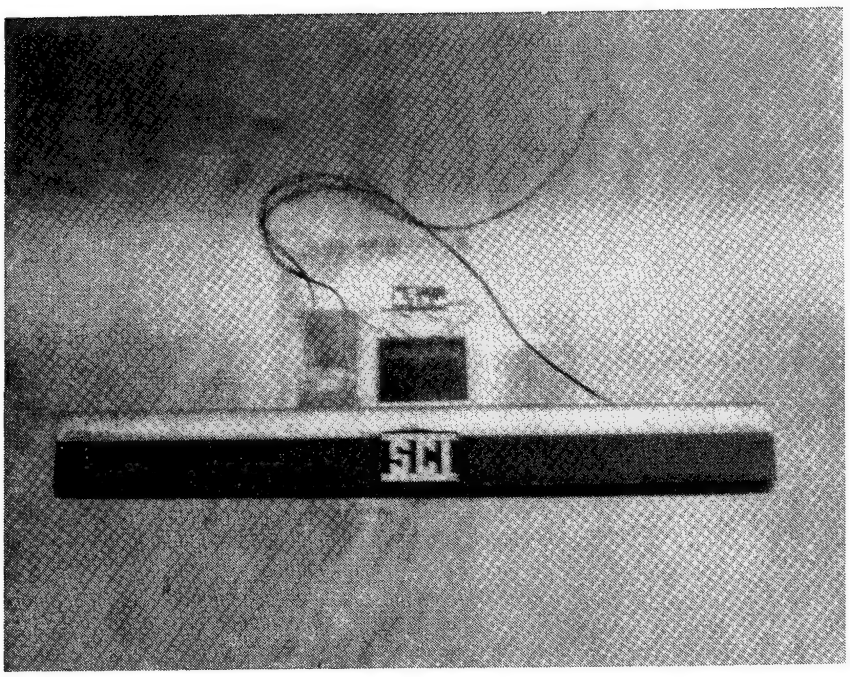

Fig. 40 Bonded Biaxial Strain Gage & Temperature Transducer

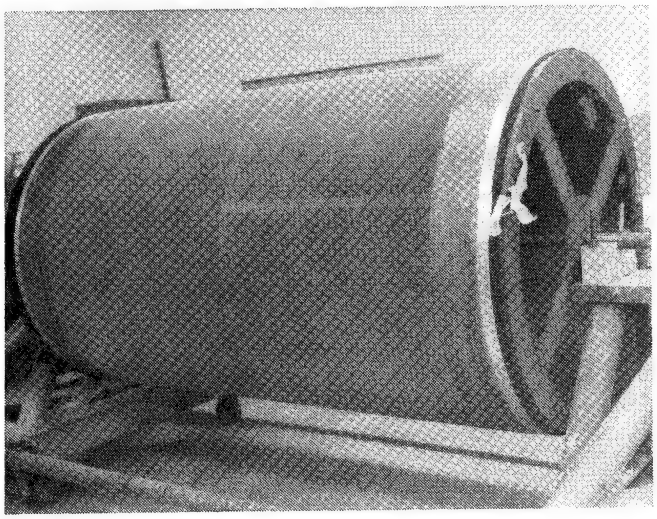

Fig. 41 Honeycomb Core Applied to Test Cylinder

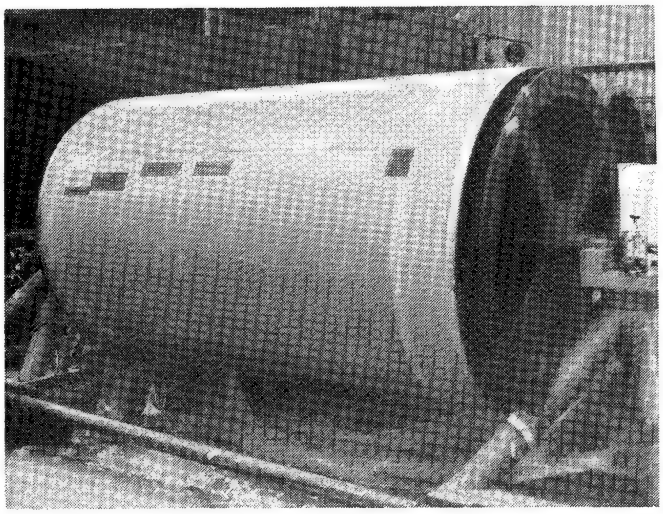

Fig. 42 Repair of Skin Wrinkles

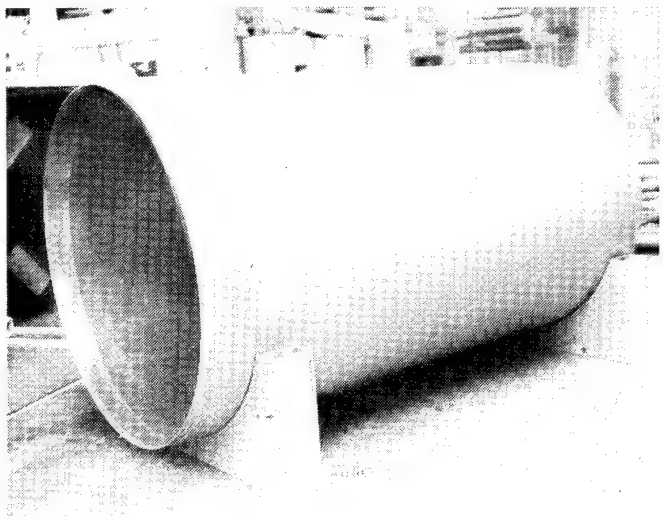

Fig. 43 Completed Composite-Reinforced Aluminum Test Cylinder, P/N 1269332-1

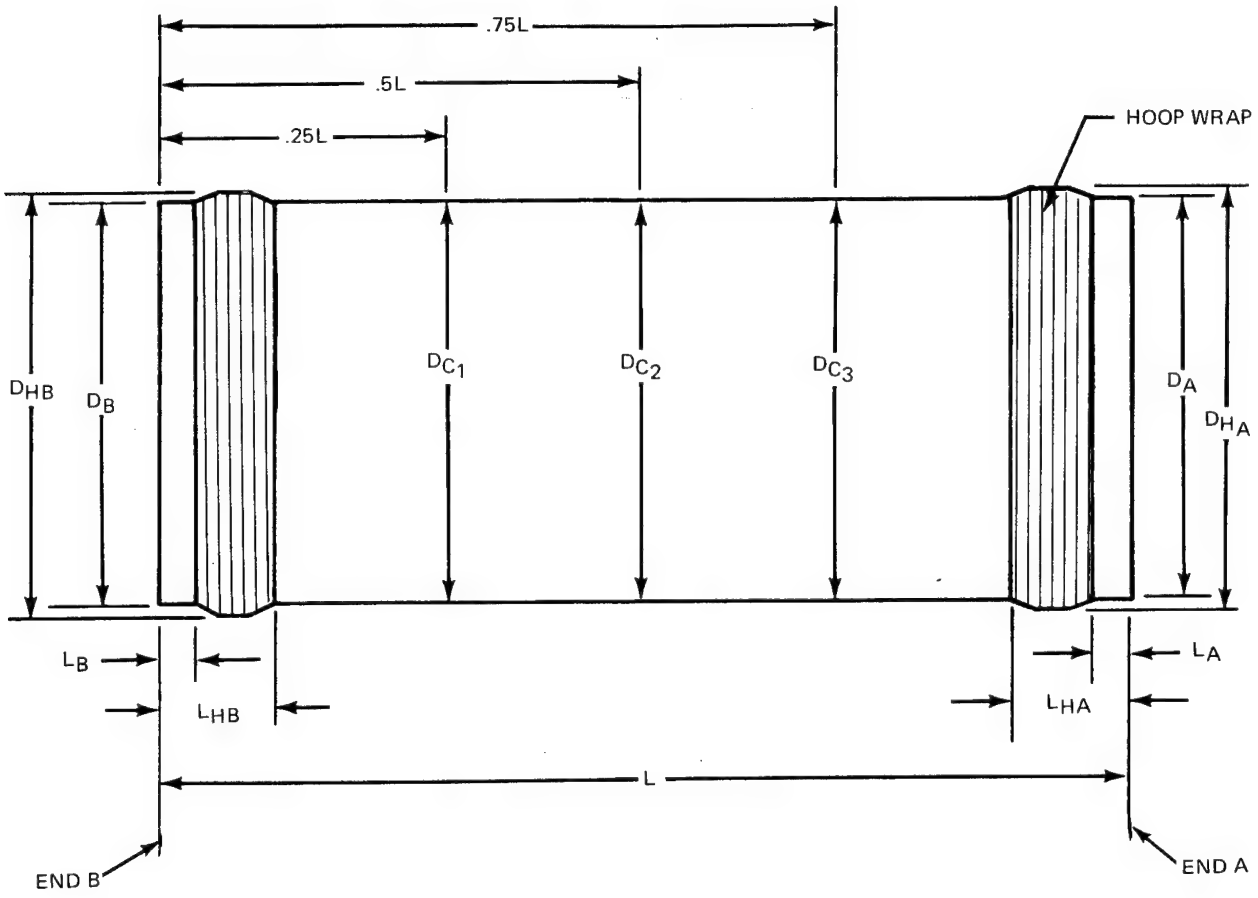

DIAMETERS (IN.)		LENGTHS (IN)		CYLINDER WEIGHT = 116.5 LBS
D_B	50.296"	L_B	1.75"	
D_A	50.292"	L_A	1.75"	
D_{HB}	50.784"	L_{HB}	7.75"	
D_{HA}	50.765"	L_{HA}	7"	
D_{C1}	50.655"	L	86¾"	
D_{C2}	50.657"			
D_{C3}	50.675"			

Fig. 44 Shop Dimensional Inspection Record, Ser No. P-2

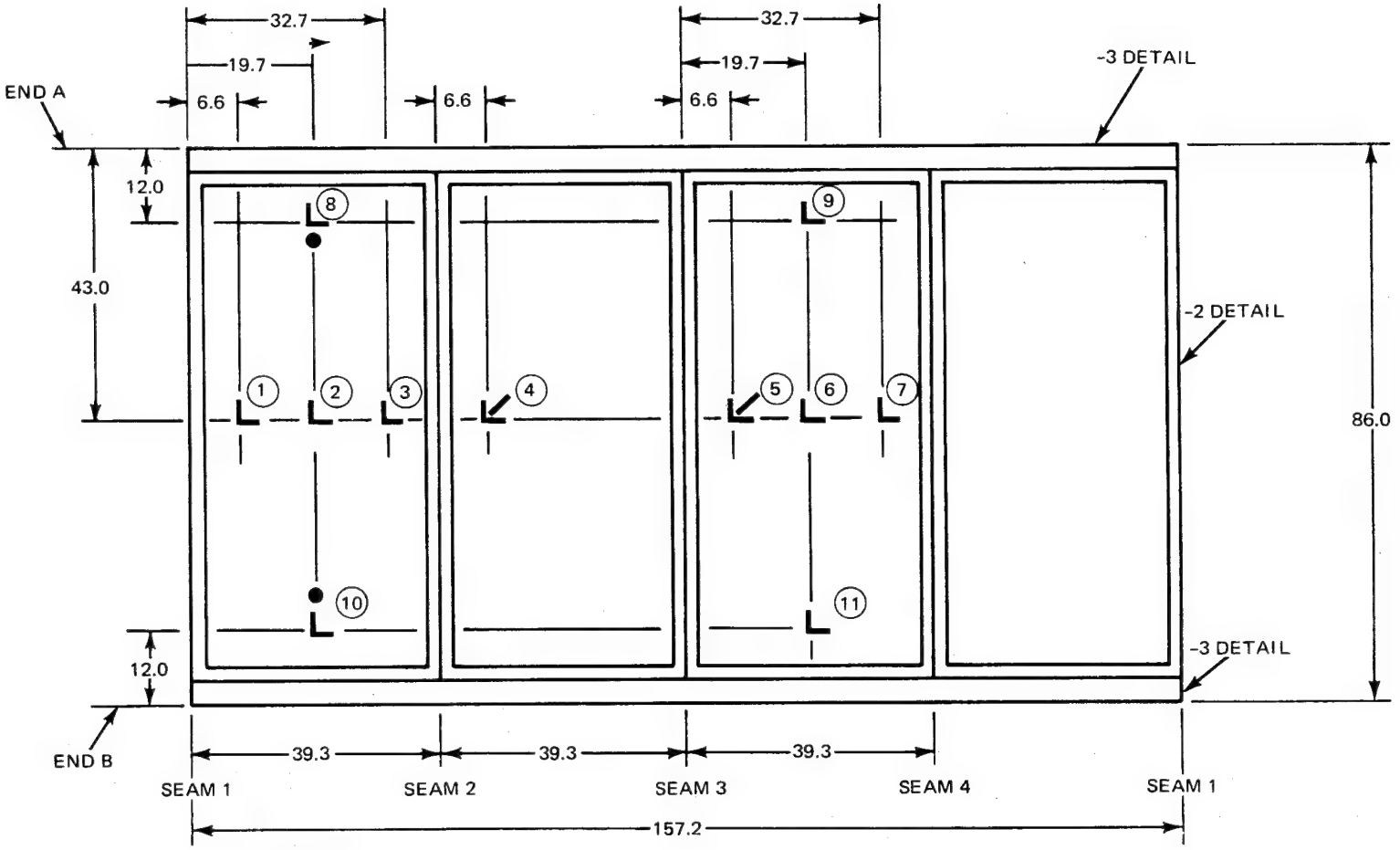

NOTES:

1. ALL DIMENSIONS IN INCHES
2. DRAWING NOT TO SCALE
3. KEY:
   - BIAXIAL STRAIN GAGE
   - ROSETTE STRAIN GAGE
   - TEMPERATURE SENSOR
   - (N) GAGE NUMBER

Strain Gage and Temperature Transducer Designation and Location, Ser No. P-1

GAUGE DESIGNATION (L = LONGITUDINAL H = HOOP)	CONDITION
1L	SHORTED
1H	SHORTED
2L	SHORTED
2H	SHORTED
3L	SHORTED
3H	SHORTED
4L	SHORTED
4H	SHORTED
5L	OK @ 194° K
5H	SHORTED
6L	SHORTED
6H	SHORTED
7L	OK @ 194° K
7H	SHORTED
8L	SHORTED
8H	SHORTED
9L	OK @ 194° K
9H	SHORTED
10L	OK @ 194° K
10H	SHORTED
11L	SHORTED
11H	OK @ 194° K
TEMP SENSOR 2	SHORTED
TEMP SENSOR 6	OK @ 304° K
TEMP SENSOR 8	OK @ 304° K
TEMP SENSOR 10	OK @ 304° K
4 - 45°	SHORTED
5 - 45°	OK @ 194° K

Fig. 46 Strain Gage and Temperature Transducer Condition, Ser No. P-2

GAUGE DESIGNATION (L = LONGITUDINAL H = HOOP)	CONDITION
1L	OPEN
1H	OPEN
2L	ONE GAUGE OPEN
2H	
3L	ONE GAUGE ONLY
3H	
4L	ONE GAUGE ONLY
4H	
5L	TWO GAUGES OK
5H	* ONE GAUGE OPEN
6L	ONE GAUGE OPEN
6H	ONE GAUGE OPEN
7L	OK
7H	OK
8L	OPEN
8H	OPEN
9L	ONE GAUGE OPEN
9H	
10L	OK
10H	OK
11L	OK
11H	OK
TEMP SENSOR 2	OK
TEMP SENSOR 6	OK
TEMP SENSOR 8	OK
TEMP SENSOR 10	OK
4 - 45°	OPEN
5 - 45°	*

Fig. 47 Strain Gage and Temperature Transducer Condition, Ser No. P-1

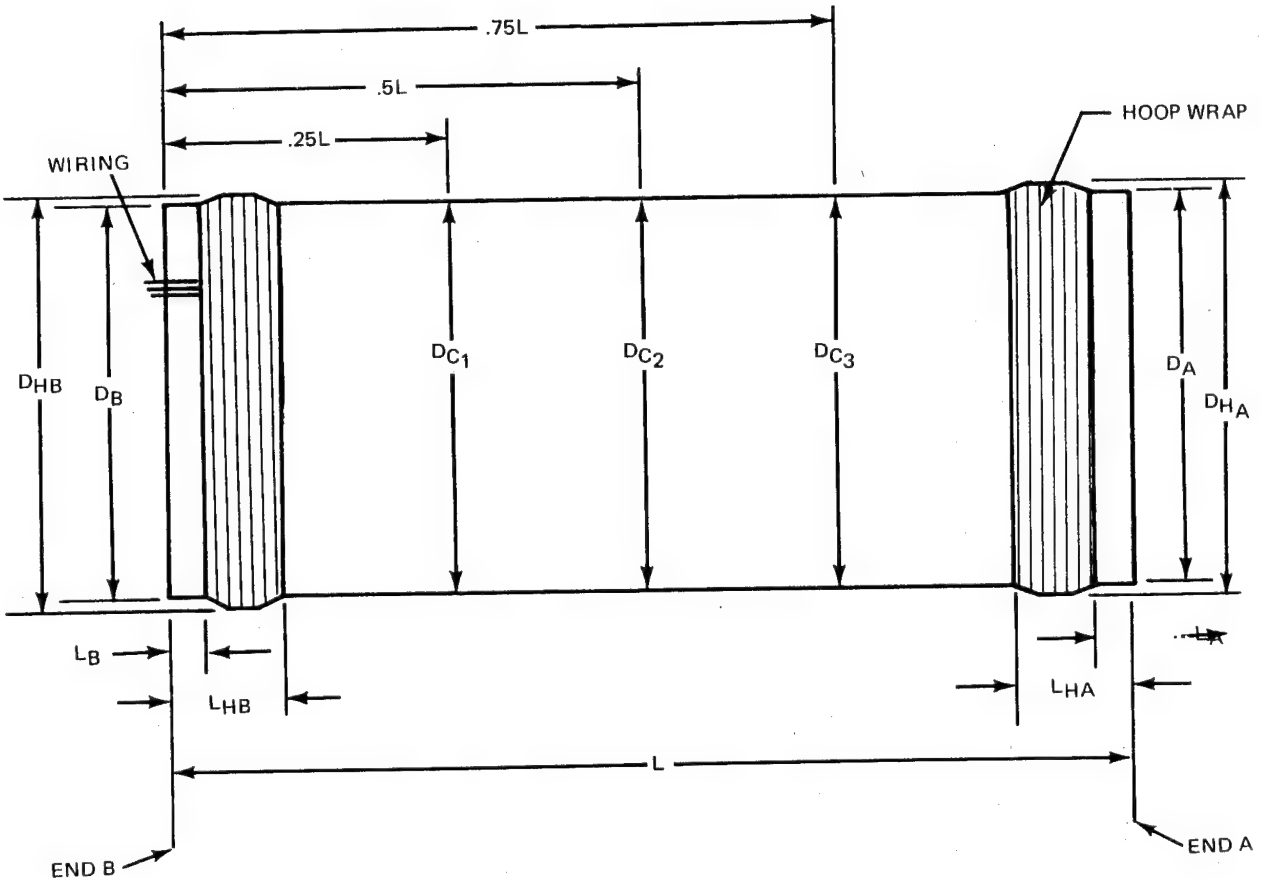

DIAMETERS (IN.)		LENGTHS (IN)	
D_B	50.420"	L_B	1.5"
D_A	50.558"	L_A	1.5"
D_{HB}	50.843"	L_{HB}	7.687"
D_{HA}	51.011"	L_{HA}	7.687"
D_{C1}	50.655"	L	86.5"
D_{C2}	50.674"		
D_{C3}	50.672"		

CYLINDER WEIGHT = 107.5 LBS

Fig. 48 Shop Dimensional Inspection Record, Ser. No. P-1

Table 1 Loading Conditions – LH_2 Tank

A) CONDITION 1 – END OF FIRST STAGE BOOST (TANK FULL)

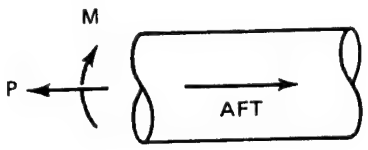

$$N_F = \frac{1}{2\pi R}\left[P \pm \frac{2M}{R}\right]$$

$$N_{UM} = N_F + \frac{P_{SYS}\,R}{2}$$

$$N_{ULT} = 1.4N_F + \frac{P_{SYS}R}{2}$$

UPPER SURFACE OF TANK R = 378.46 cm		STA 3050	STA 4065
P, TANK AXIAL LOAD, LIMIT,	(N)	-13.3×10^6	-16.7×10^6
M, TANK BENDING MOMENT, LIMIT,	(cmN)	700×10^6	2620×10^6
N_F, DISTRIBUTED FLIGHT LOAD, LIMIT,	(N/cm)	−7180	−12930
P, TANK PRESSURE, LIMIT, (INCL HYDROSTATIC)	(N/cm^2)	26.9 MAX	29.2 MAX
P_{SYS}, SYSTEM PRESSURE,	(N/cm^2)	24.8 MAX 20.7 MIN	24.8 MAX 20.7 MIN
P_{SYS} R/2,	(N/cm)	3920	3920
N_{LIM}, NET AXIAL LOAD, LIMIT,	(N/cm)	−3260	−8910
N_{ULT}, NET AXIAL LOAD, ULTIMATE,	(N/cm)	−6130	−14040
TANK WALL TEMPERATURE (°k)	(° K)	20.4	20.4

B) CONDITION 2 – POST ORBIT INSERTION (TANK EMPTY)

P_{SYS}, SYSTEM PRESSURE, (NEWTON/cm^2) 24.8 MAX

TANK WALL TEMPERATURE (° K) 367

C) CONDITION 3 – CURE

RIGID MANDREL, ZERO STRESS IN LINER

TANK WALL TEMPERATURE (° K) 367

D) CONDITION 4 – POST-CURE

NET PRESSURE IS ZERO

TANK WALL TEMPERATURE (° K) 367

Table 2 Loading Conditions, LO_2 Tank

A) CONDITION 1 – END OF FIRST STAGE BOOST (TANK FULL)

		STA 1240 R = 336.80 cm	STA 1550 R = 378.46 cm
P, TANK PRESSURE, LIMIT, (INCL HYDROSTATIC)	(N/cm^2)	37.4 MAX	48.3 MAX
P_{SYS}, SYSTEM PRESSURE,	(N/cm^2)	26.2 MAX	26.2 MAX
TANK WALL TEMPERATURE (°K)		88.6	88.6

B) CONDITION 2 – POST ORBIT INSERTION (TANK EMPTY)

P_{SYS}, SYSTEM PRESSURE, (N/cm^2)	17.2 MAX
TANK WALL TEMPERATURE (°K)	533

C) CONDITION 3 – CURE

RIGID MANDREL, ZERO STRESS IN LINER

TANK WALL TEMPERATURE (°K)	367

D)CONDITION 4 – POST-CURE

NET PRESSURE IS ZERO

TANK WALL TEMPERATURE (°K)	367

Table 3. Typical Properties of 2219 Aluminum for Use in Parametric Study

	SPECIMEN DIRECTION	2219 – T62				2219 – T87			
		450°K	260°K	77°K	20°K	450°K	260°K	77°K	20°K
PROPORTIONAL LIMIT, kN/cm²									
TENSION	L	18.1	36.8	34.4	35.8	21.7	35.8	42.6	46.9
	T	18.6	37.5	33.7	36.5	21.7	36.5	43.4	46.1
COMPRESSION	L	18.1	36.8	34.4	35.8	21.7	35.8	42.6	46.9
	T	18.6	37.5	33.7	36.8	21.7	36.5	43.4	46.1
YIELD STRENGTH, kN/cm²									
TENSION	L	20.1	29.6	38.6	40.0	24.1	40.0	47.5	52.4
	T	20.6	30.6	37.8	40.6	24.1	40.6	48.1	51.6
COMPRESSION	L	20.1	29.6	38.6	40.0	24.1	40.0	47.5	52.4
	T	20.6	30.6	37.8	40.6	24.1	40.6	48.1	51.6
TENSILE STRENGTH, kN/cm²									
TENSION	L	29.2	40.6	53.8	63.4	29.6	47.5	57.9	68.9
	T	31.0	43.4	54.4	63.4	28.9	46.7	58.1	67.5
ELONGATION, % IN 5.1 cm									
TENSION	L		10.5	12	14		10	12	13
	T		10	14.5	14		10	12	14
MODULUS OF ELASTICITY, MN/cm²									
TENSION	L	6.7	7.1	7.9	8.0	6.7	7.1	6.9	8.0
	T	6.7	7.1	7.7	8.3	6.7	7.1	7.7	8.3
COMPRESSION	L	6.7	7.1	7.9	8.0	6.7	7.1	7.9	8.0
	T	6.7	7.1	7.7	8.3	6.7	7.1	7.7	8.3
WELD JOINT PROPERTIES		HEAT TREATED AFTER WELDING				AS-WELDED			
JOINT EFFICIENCY, %	L		114	96	87.5		73	69	68
	T		103.5	98	87.5		76	69	69
ELONGATION, % IN 5.1 cm	L		9.0	7.0	4.0		4	4.5	2.5
POISSON'S RATIO			0.325	0.335	0.335		0.325	0.335	0.335

Table 4 2219 Aluminum Characterization Analysis

PROPERTY	2219 – T62	2219 – T87
SPECIFIC GRAVITY	2.83	2.83
COEFFICIENT OF THERMAL EXPANSION, μCM/CM°K		
78°K TO 297°K	17.3	17.3
293°K TO 374°K	22.4	22.4
297°K TO 450°K	22.5	22.5
POISSON'S RATIO	0.325	0.325

Table 5 Uniaxial Filament-Wound Composite Material Properties for use in Parametric Study of Filament Overwrapped Tanks

PROPERTY	COMPOSITE SYSTEM	
	S-901 GLASS/EPOXY	PRD-49-III/EPOXY
FILAMENT		
ULTIMATE STRENGTH, kN/cm²	459.0	268.0
ELASTIC MODULUS, MN/cm²	8.55	12.8
SPECIFIC GRAVITY	2.4	1.4
COMPOSITE		
FILAMENT FRACTION IN COMPOSITE, VOL %	67	65
SPECIFIC GRAVITY	2.0	1.4
LONGITUDINAL MODULUS, MN/cm²		
450°K	5.7	7.3
297°K	5.7	8.4
78°K	6.3	9.6
LONGITUDINAL TENSILE ULTIMATE STRENGTH, kN/cm²		
450°K	120.0	99.1(3)
297°K	152.0	124.0
78°K	190.0	124.0
LONGITUDINAL TENSILE OPERATING STRESS, (2)kN/cm²		
450°K	71.6	66.1(1)
297°K	91.0	82.6(1)
78°K	113.7	82.6(1)
COEFFICIENT OF THERMAL EXPANSION, μcm/cm°K		
78°K to 297°K	2.9	–3.59
297°K to 450°K	2.5	–5.55

NOTES:

(1) ASSUMED VALUE BASED ON 1.5 SAFETY FACTOR.

(2) ALL OPERATING STRESSES ARE BASED ON ZERO-STRESS TO FULL-OPERATING-STRESS CYCLIC LOADING, WHICH IS CONSERVATIVE.

(3) ESTIMATED VALUE.

Table 6. Mechanical Properties of Materials Used in Concept C (Honeycomb) Analysis

I. 1581 Fiberglass Cloth Laminate (37.6% Resin, t = .026 cm/layer)

PARALLEL / NORMAL	TENSILE STRENGTH	COMPRESSIVE STRENGTH	TENSILE MODULUS
TEMPERATURE	N/cm^2	N/cm^2	N/cm^2
295° K	63800 / 58200	43100 / 40800	2.27×10^6 / 2.19×10^6
20° K	95000 / 81300	75200 / 69000	2.94×10^6 / 2.88×10^6

ASSUME 92% OF RT PROPERTIES AT 94° C

II Honeycomb Core – RT Properties

	BASIS	STRENGTH			MODULUS		
		F_C N/cm^2	F_{SL} N/cm^2	F_{SW} N/cm^2	E_C N/cm^2	G_{CL} N/cm^2	G_{CW} N/cm^2
ALUMINUM 1/4-2024-.0015-2.8	MIN	145	134	69	2900	19300	9600
FIBERGLASS (1) HRH327-3/8-2.5	TYP	131	114	31	13100	8970	4140
PAPER (2) HNC-3/8-60(20)E-2.0	TYP	96	48	26	22800	6210	2760

(1) GLASS
1.13 x RT @ 20° K
.99 x RT @ 367° K

(2) PAPER
1.18 x RT @ 20° K
.32 x RT @ 367° K

ASSUME, MIN = .80 x TYP

III Adhesives

TYPE	TEST	CONDITION	RESULT
RELIABOND 393-1	FLATWISE TENSION	RT	18.9 N/cm^2
		355° K	16.0
		218° K	16.0
	SANDWICH PEEL	RT	4.5 cm N/cm
		355° K	3.4
		218° K	2.2
FM123-2	FLATWISE TENSION	RT	16.0 N/cm^2
		355° K	7.4
		218° K	20.0
	SANDWICH PEEL	RT	5.3 cm N/cm
		3.55° K	5.2
		218° K	5.5

REF MIL-A-25463

Table 7 — Concept A (Integral Stiffening), Results of Compression Optimization Program

LH_2 TANK STATION cm	SKIN THICKNESS t_ℓ, cm	STIFFENER SPACING b, cm	STIFFENER WIDTH t_{st}, cm	STIFFENER DEPTH d, cm	(3) $\bar{t}_\ell$, cm	SKIN BUCKLING STRESS f_{cr}, kN/cm²	AXIAL COMPRESSIVE STRESS AT ULTIMATE LOAD, COND.1		ALLOWABLE HOOP STRESS(4) f_{hoop}, kN/cm²
							SKIN EDGE STRESS f_e, kN/cm²	PANEL FAIL. STRESS f_{all}, kN/cm²	
3050	.343 (1)	18.1	.335	4.44	.426	12.1	18.3	15.6	–
	.318	21.2	.343	4.60	.391	7.7	19.2	15.7	31.8
	.300	18.5	.348	4.44	.381	9.3	19.8	16.2	31.4
	.254	20.8	.391	4.65	.340	6.1	24.2	18.1	31.0
	.208 (2)	22.1	.442	4.80	.305	4.3	31.2	20.1	22.3
	.163	17.8	.470	4.75	.287	4.3	32.7	22.5	18.0
	.122	19.7	.551	5.18	.267	2.1	36.0	25.0	14.4
4065	.444 (1)	18.3	.490	5.15	.581	20.6	27.2	24.3	–
	.394	17.1	.495	5.15	.544	20.5	30.4	25.9	21.0
	.343	16.4	.534	5.18	.510	18.1	33.9	27.7	16.6
	.292 (2)	16.9	.582	5.44	.480	14.5	37.6	29.4	11.9
	.242	17.6	.650	5.94	.459	9.7	39.6	30.5	9.0
	.198	15.9	.660	6.02	.447	8.1	40.2	31.5	8.8

NOTES: (1) "BASELINE", ALL-ALUMINUM

(2) OVERWRAPPED DESIGN

(3) "SMEARED" THICKNESS, SKIN + STIFFENER (NO WRAP)

(4) COMBINED STRESS CRITERIA, COND. 1, AXIAL COMPRESSION + PRESSURIZATION

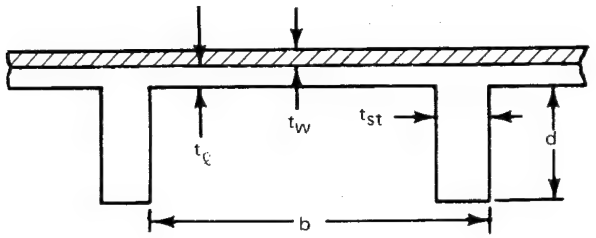

Table 8 — Concept B (Z-Stiffening), Results of Compression Optimization Program

LH_2 TANK STATION cm	SKIN THICKNESS t_l, cm	STIFFNER SPACING b, cm	STIFFENER AREA A_{st}, cm^2	(3) $\bar{t}_{\ell}$cm	SKIN BUCKLING STRESS f_{cr}, kN/cm^2	AXIAL COMPRESSIVE STRESS AT ULTIMATE LOAD		ALLOWABLE HOOP STRESS (4) f_{hoop}, kN/cm^2
						SKIN EDGE STRESS f_e, kN/cm^2	PANEL FAIL. STRESS f_{all}, kN/cm^2	
3050	.331 (1)	15.4	1.58	.432	14.1	18.6	16.6	—
	.307	16.2	1.57	.404	11.0	22.1	17.1	29.1
	.279	19.5	1.65	.363	7.2	24.4	19.4	27.3
	.228 (2)	19.5	1.57	.310	5.3	32.1	19.4	19.3
	.178	19.6	2.11	.284	3.7	33.7	21.9	17.9
4065	.482	19.4	2.84	.627	20.2	33.8	27.7	—
	.447 (1)	16.0	2.25	.589	24.0	26.4	24.8	—
	.432	19.3	2.59	.566	17.1	31.3	26.7	20.1
	.381	19.3	2.84	.529	14.5	35.7	26.9	14.4
	.343 (2)	16.8	2.96	.521	14.7	35.1	27.1	15.2
	.305	20.6	4.50	.523	9.9	35.4	27.0	14.8

NOTES: (1) "BASELINE", ALL-ALUMINUM

(2) OVERWRAPPED DESIGN

(3) "SMEARED" THICKNESS, SKIN + STIFFENER (NO WRAP)

(4) COMBINED STRESS CRITERIA, COND. 1, AXIAL COMPRESSION + PRESSURIZATION

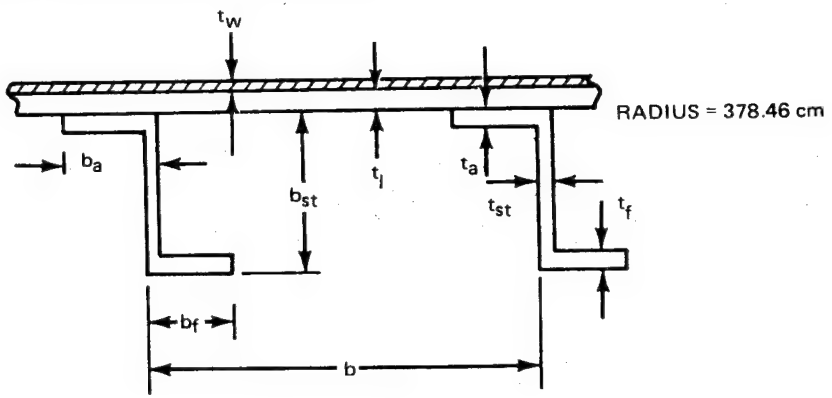

Table 9. LH_2 Tank Concepts A & B, Results of Composite Overwrap Program*

LH_2 TANK STATION cm	CONCEPT	COND.	TEMP °K	WRAP MATERIAL	WRAP PRESTRESS kN/cm²	t_ℓ cm	t_w cm	LIMIT HOOP STRESS	
								LINER f_ℓ kN/cm²	WRAP f_w kN/cm²
3050	A (INTEGRAL)	1	20.4	S-GLASS	82.8	.211	.064	22.3	87.1
		2	364					15.5	97.6
		4	364					-21.9	73.0
	A	1	20.4	PRD	69.0	.208	.099	22.3	56.8
		2	364					7.5	81.1
		4	364					-24.6	52.9
	B (ZEE)	1	20.4	S-GLASS	82.8	.229	.066	19.3	84.6
		2	364					12.6	95.7
		4	364					-21.9	73.0
	B	1	20.4	PRD	69.0	.229	.109	19.3	52.9
		2	364					4.9	77.9
		4	364					-24.5	52.5
4065	A	1	20.4	S-GLASS	82.8	.305	.092	11.9	81.4
		2	364					3.9	90.4
		4	364					-21.9	73.0
	A	1	20.4	PRD	69.0	.292	.155	11.9	48.3
		2	364					4.9	69.0
		4	364					-26.8	51.1
	B	1	20.4	S-GLASS	82.8	.348	.069	15.2	83.1
		2	364					8.3	94.0
		4	364					-15.6	78.1
	B	1	20.4	PRD	69.0	.338	.122	15.2	50.9
		2	364					1.3	76.9
		4	364					-20.1	57.7

* THESE RESULTS ARE THE TABULAR LISTING IN THE PROGRAM PRINTOUT CLOSEST TO THE ACTUAL GEOMETRY; THEY ARE WITHIN A FEW PERCENT OF THE THEORETICAL VALUES.

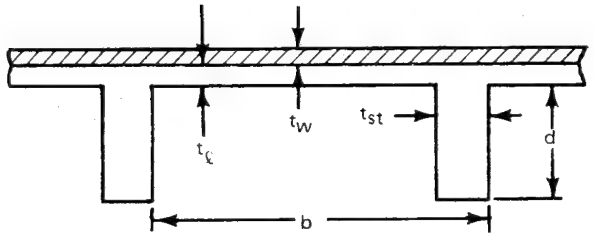

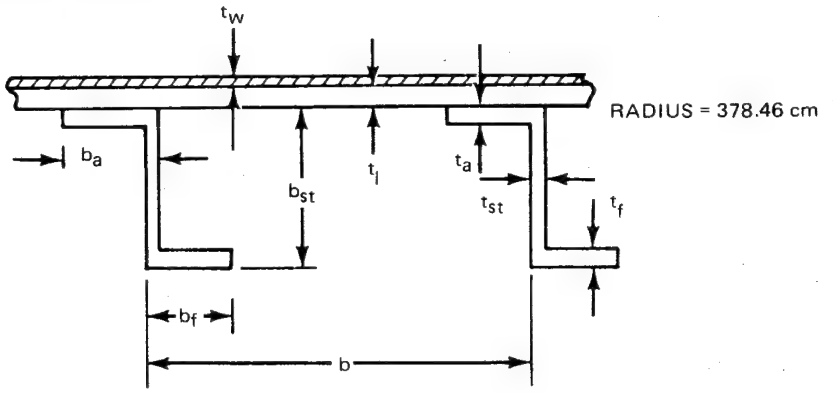

Table 10 Unit Weight Comparisons of Overwrapped Design Concepts, LH_2 Tank Sta. 3050

CONCEPT	WRAP MATERIAL	WRAP PRESTRESS kN/cm²	ALLOWABLE HOOP STRESS IN LINER kN/cm²	LINER THICKNESS t_ℓ, cm	EQUIV.(1) PANEL THICKNESS $\bar{t}_\ell$, cm	WRAP THICKNESS t_w, cm	EQUIV.(2) WRAP THICKNESS $\bar{t}_w$, cm	TOTAL(3) EQUIV. THICKNESS $\bar{t}$, cm
A	S-GLASS	82.8	22.3	.208	.305	.063	.046	.351
			27.6	.254	.341	— (4)	—	—
		55.2	22.3	.208	.305	.079	.058	.363
			27.6	.254	.341	.043	.032	.373
	PRD	69.0	22.3	.208	.305	.096	.048	.353
			27.6	.254	.341	—	—	—
		55.2	22.3	.208	.305	.138	.069	.374
			27.6	.254	.341	.074	.037	.378
B	S-GLASS	82.8	17.9	.178	.285	—	—	—
			19.3	.228	.310	.068	.050	.360
		55.2	17.9	.178	.285	—	—	—
			19.3	.228	.310	.085	.062	.372
	PRD	69.0	17.9	.178	.285	—	—	—
			19.3	.228	.310	.106	.053	.363
		55.2	17.9	.178	.285	—	—	—
			19.3	.228	.310	.158	.079	.389

(1) $\bar{t}_\ell = t_\ell + A_{stiff}/b$

(2) $\bar{t}_w = t_w \rho_w / \rho_{AL}$

(3) $\bar{t} = \bar{t}_\ell + \bar{t}_w$

(4) NO DESIGN; ALL OF CRITERIA CANNOT BE SATISFIED

Table 11 Unit Weight Comparisons of Overwrapped Design Concepts, LH_2 Tank Sta. 4065

CONCEPT	WRAP MATERIAL	WRAP PRESTRESS kN/cm²	ALLOWABLE HOOP STRESS IN LINER kN/cm²	LINER THICKNESS t_ℓ, cm	EQUIV. (1) PANEL THICKNESS $\bar{t}_\ell$, cm	WRAP THICKNESS t_w, cm	EQUIV. (2) WRAP THICKNESS $\bar{t}_w$, cm	TOTAL (3) EQUIV. THICKNESS $\bar{t}$, cm
A	S-GLASS	82.8	11.9	.292	.480	.093	.068	.548
			16.6	.343	.510	.063	.046	.556
		55.2	11.9	.292	.480	.117	.085	.565
			16.6	.343	.510	.078	.057	.567
	PRD	69.0	11.9	.292	.480	.154	.077	.557
			16.6	.343	.510	.102	.051	.561
		55.2	11.9	.292	.480	— (4)	—	—
			16.6	.343	.510	.154	.077	.587
B	S-GLASS	82.8	14.8	.305	.523	.079	.058	.581
			15.3	.343	.520	.070	.051	.571
		55.2	14.8	.305	.523	.097	.071	.594
			15.3	.343	.520	.085	.062	.582
	PRD	69.0	14.8	.305	.523	.124	.062	.585
			15.3	.343	.520	.114	.057	.577
		55.2	14.8	.305	.523	.190	.095	.618
			15.3	.343	.520	.170	.085	.605

NOTES: (1) "BASELINE", ALL-ALUMINUM

(2) OVERWRAPPED DESIGN

(3) "SMEARED" THICKNESS, SKIN + STIFFENER (NO WRAP)

(4) COMBINED STRESS CRITERIA, COND. 1, AXIAL COMPRESSION + PRESSURIZATION

Table 12 Concept A, Integral Stiffener Plus Overwrap

LH_2 TANK STATION cm	CRITICAL COND (1)	OVERWRAP MATERIAL	OVERWRAP PRESTRESS kN/cm^2	b cm	t_{st} cm	d cm	t_w cm	t_ℓ cm	(2) t_{eq} cm	(3) WEIGHT kg/m^2
3050	1,2	ALL ALUMINUM	–	18.1	.335	4.44	–	.343	.455	12.6
3050	1,2,4	PRD	69.0	22.1	.442	4.80	.097	.208	.381	10.5
3050	1,2,4	S-GLASS	82.8	22.1	.442	4.80	.064	.208	.378	10.5
4065	1.2	ALL ALUMINUM	–	18.3	.490	5.15	–	.444	.622	17.2
4065	1,2,4	PRD	69.0	16.85	.582	5.44	.155	.292	.600	16.6
4065	1,2,4	S-GLASS	82.8	16.85	.582	5.44	.094	.292	.589	16.3

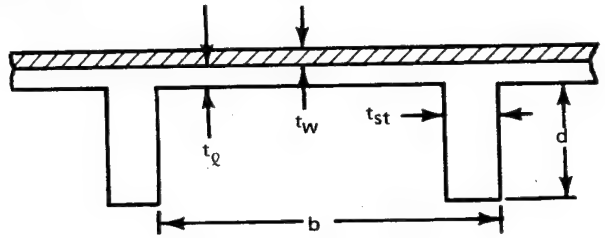

(1) COND 1 – END BOOST
COND 2 – POST ORBIT INSERTION
COND 4 – POST CURE

(2) EQUIVALENT THICKNESS OF ALUMINUM, INCLUDING WRAP AND RINGS

(3) INCLUDING WRAP AND RINGS
RING SIZE FOR GENERAL INSTABILITY (.75 KNOCK DOWN FACTOR) BASED ON 76.2 cm RING SPACING
STA. 3050; $I = 17.04\ cm^4$, $A = 2.19\ cm^2$
STA. 4065; $I = 24.75\ cm^4$, $A = 3.10\ cm^2$

Table 13 – Concept B, Bonded Zee Stiffener plus Overwrap

LH_2 TANK STATION cm	CRITICAL COND[1] COND	OVERWRAP MATERIAL	OVERWRAP PRESTRESS kN/cm²	b cm	t_a cm	t_{st} cm	t_f cm	b_a cm	b_{st} cm	b_f cm	t_w cm	t_l cm	t_{eq}[2] cm	WEIGHT[3] kg/m²
3050	1,2	ALL ALUMINUM	–	15.4	.170	.154	.281	2.900	3.82	1.482	–	.331	.460	12.7
3050	1,2,4	PRD	69.0	19.5	.191	.168	.295	1.945	4.46	1.826	.107	.228	.391	10.8
3050	1,2,4	S-GLASS	82.8	19.5	.191	.168	.295	1.945	4.46	1.826	.069	.228	.389	10.8
4065	1,2	ALL ALUMINUM	–	16.0	.295	.203	.444	2.760	4.64	1.458	–	.447	.630	17.4
4065	1,2,4	PRD	69.0	16.8	.371	.221	.432	2.315	5.75	2.330	.114	.343	.617	17.1
4065	1,2,4	S-GLASS	82.8	16.8	.371	.221	.432	2.315	5.75	2.330	.053	.343	.615	17.0

(1) COND 1 – END BOOST
COND 2 – POST ORBIT INSERTION
COND 4 – POST CURE

(2) EQUIVALENT THICKNESS OF ALUMINUM, INCLUDING WRAP AND RINGS.

(3) INCLUDING WRAP AND RINGS.
FOR RING SIZE AND SPACING, SEE TABLE 1.

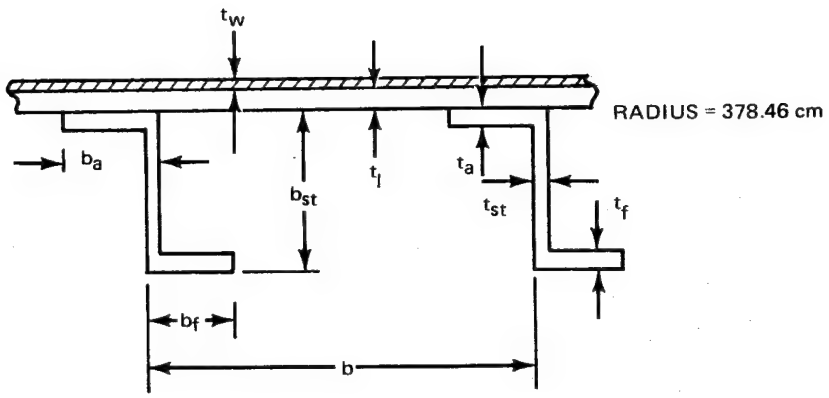

Table 14. LH_2 Tank Concept C (Honeycomb Stiffening), Weight Determination

T = 20° K	UNITS	STATION 3050			STATION 4065		
FIBERGLASS; E_2	N/cm^2	2.91×10^6	2.91×10^6	2.91×10^6	2.91×10^6	2.91×10^6	2.91×10^6
t_2	cm	.051	.102	.153	.051	.102	.153
ALUMINUM; E_1	N/cm^2	8.75×10^6	8.75×10^6	8.75×10^6	8.75×10^6	8.75×10^6	8.75×10^6
t_1	cm	.340	.340	.340	.488	.488	.488
$E_1 = t_1 (1 + E_2 t_2 / E_1 t_1)$	cm	.357	.374	.391	.505	.521	.539
$C_1 = E_2 t_2 / E_1 t_1 / (1 + E_2 t_2 / E_1 t_1)$		.213	.289	.339	.181	.247	.292
CORE [1] G_{cw}	N/cm^2	2620	2620	2620	2620	2620	2620
R	cm	378.5	378.5	378.5	378.5	378.5	378.5
$f_{o1} = 2.1 C_1 E_1 h/R$	N/cm^2	10350h	14030h	16440h	8780h	11970h	14160h
$f_{crimp\ 1} = HG_{cw}/t_1$	N/cm^2	7130h	7020h	6690h	5190h	5040h	4860h
$f_{o1}/f_{crimp\ 1}$		1.45	2.00	2.46	1.69	2.37	2.91
$R/\rho = R/C_1 h$		1776/h	1310/h	1117/h	2090/h	1533/h	1296/h
$K_c = 1-(\gamma_c/4)\ (f_{o1}/f_{cimp\ 1})$		$1-.36\gamma_c$	$1-.50\gamma_c$	$1-.61\gamma_c$	$1-.42\gamma_c$	$1-.59\gamma_c$	$1-.73\gamma_c$
$N_{CR} = \gamma_c K_c f_{o1} t_1$	N/cm	$3800\gamma_c Kch$	$5240\gamma_c Kch$	$6430\gamma_c K_c h$	$4430\gamma_c K_c h$	$6240\gamma_c K_c h$	$7630\gamma_c K_c h$
N_{CR} REQUIRED ÷ .95 [2]	N/cm	6450	6450	6450	14800	14800	14800
$N_{crimp\ 1} = f_{crimp\ 1} t_1 = G_{cwh}$	N/cm	2620h	2620h	2620h	2620h	2620h	2620h
γ_c		.43	.43	.43	.47	.48	.49
Ncr	N/cm	1380h	1770h	2020h	1665h	2160h	2390h
h	cm	4.80	3.70	3.20	8.70	6.90	6.20
c	cm	4.60	3.48	2.96	8.43	6.60	5.88
WEIGHTS							
ALUMINUM (.00276 kg/cm^3)	kg/m^2	9.38	9.38	9.38	13.47	13.47	13.47
FIBERGLASS (.00202 kg/cm^3)	kg/m^2	1.03	2.06	3.09	1.03	2.06	3.09
BOND	kg/m^2	.97	.97	.97	.97	.97	.97
CORE (32 kg/cm^3)	kg/m^2	1.47	1.11	.95	2.69	2.11	1.88
Σ WEIGHTS	kg/m^2	12.75	13.52	14.39	18.15	18.61	19.41

(1) PAPER CORE HNC - 3/8 - 60 (20) E - 2.0

(2) TO ACCOUNT FOR PLASTICITY CORRECTION

Table 15. Concept C, Honeycomb Stiffening

LH_2 TANK STATION cm	CRITICAL COND. (1)	CORE MATERIAL (2)	OUTER FACE MATERIAL (3)	t_i cm	t_o cm	h cm	WEIGHT (4) $\frac{kg}{m^2}$
3050	1,2	ALUMINUM	ALUMINUM	.170	.170	1.69	11.2
3050	1,2	ALUMINUM	GLASS	.340	.051	4.18	13.3
3050	1,2	GLASS	GLASS	.340	.051	4.81	13.1
3050	1,2	PAPER	GLASS	.340	.051	4.80	12.8
4065	1	ALUMINUM	ALUMINUM	.244	.244	2.43	15.5
4065	1	ALUMINUM	GLASS	.488	.102	5.02	18.7
4065	1	GLASS	GLASS	.488	.102	6.82	19.1
4065	1	PAPER	GLASS	.488	.102	8.70	18.2

(1) SEE TABLE 1

(2) ALUMINUM CORE, 1/4-2024-0015-2.3; GLASS REINFORCED PLASTIC CORE, HRH-3/8-2.5; PAPER CORE, HNC-3/8-60(20)E-2.0

(3) INNER FACE MATERIAL IS 2219-T87; OUTER FACING: 2219-T87 ALUMINUM OR 1581 EPOXY/GLASS CLOTH

(4) WEIGHT INCLUDES FACING, CORE, AND WEIGHT OF TWO BOND LINES AT .97 kg/m^2

(5) SUBSCRIPTS c, o AND i REPRESENT CORE, INNER AND OUTER FACES, RESPECTIVELY

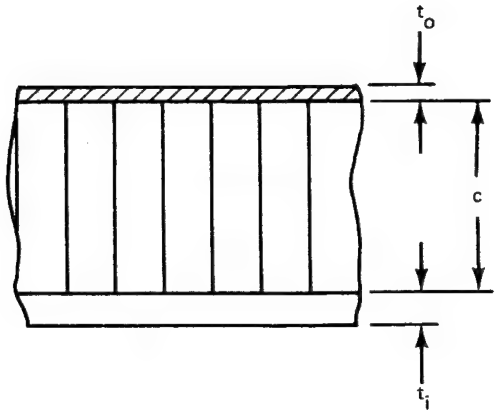

RADIUS = 378.45cm

$$h = c + \frac{t_i + t_o}{2}$$

TANK CYLINDER LENGTHS
STA. 3050, 1600 cm
STA. 4065, 457 cm

Table 16 Summary of Unit Weights, LH_2 Tank

LH_2 TANK STATION; cm	CONFIGURATION	WEIGHT (1) kg/m²	REL. WT. (2)
3050	INTEGRAL STIFFENED, ALL ALUMINUM (BASE LINE)	12.6	1.000
	ZEE STIFFENED, ALL ALUMINUM	12.7	1.010
	HONEYCOMB, ALL ALUMINUM	11.2	.888
	INTEGRAL, S-GLASS OVERWRAP	10.5	.834
	INTEGRAL, PRD OVERWRAP	10.5	.838
	ZEE, S-GLASS OVERWRAP	10.8	.856
	ZEE, PRD OVERWRAP	10.8	.861
	HONEYCOMB, ALUMINUM CORE, COMPOSITE OUTER FACE	13.3	1.055
	HONEYCOMB, GLASS CORE, COMPOSITE OUTER FACE	13.1	1.045
	HONEYCOMB, PAPER CORE, COMPOSITE OUTER FACE	12.9	1.015
4065	INTEGRAL STIFFENED, ALL ALUMINUM (BASE LINE)	17.2	1.000
	ZEE STIFFENED, ALL ALUMINUM	17.4	1.012
	HONEYCOMB, ALL ALUMINUM	15.5	.901
	INTEGRAL, S-GLASS OVERWRAP	16.3	.946
	INTEGRAL, PRD OVERWRAP	16.6	.963
	ZEE, S-GLASS OVERWRAP	17.0	.986
	ZEE, PRD OVERWRAP	17.1	.992
	HONEYCOMB, ALUMINUM CORE, COMPOSITE OUTER FACE	18.7	1.085
	HONEYCOMB, GLASS CORE, COMPOSITE OUTER FACE	19.1	1.110
	HONEYCOMB, PAPER CORE, COMPOSITE OUTER FACE	18.9	1.100

NOTE:

IDEALIZED PANEL WEIGHT, DOES NOT INCLUDE NON-OPTIMUM FACTOR (NOF)

(1) WEIGHT OF INTEGRAL-STIFFENED AND ZEE-STIFFENED DESIGNS INCLUDES RINGS AND WRAP' HONEYCOMB DESIGNS INCLUDE CORE AND BOND'

(2) RELATION WEIGHT = WEIGHT OF DESIGN/WEIGHT OF THE INTEGRAL STIFFENED BASELINE DESIGN

Table 17 Summary of Unit Weights, LO_2 TANK

LO_2 TANK STATION cm	RADIUS cm	OVERWRAP MATERIAL	OVERWRAP PRESTRESS kN/cm²	t_w cm	t_l cm	t_{eq} cm	WEIGHT kg/m²	REL. WT.
1240	336.80	BASE LINE ALL ALUMINUM	—	—	.488	13.5	13.5	1.000
		PRD	22.1	.120	.284	.346	9.6	0.71
		S-GLASS	44.9	.079	.094	.295	8.82	.61
1550	378.46	BASE LINE ALL ALUMINUM	—	—	.534	—	14.8	1.000
		PRD	22.1	.155	.419	.498	13.8	.93
		S-GLASS	44.9	.112	.343	.424	11.8	.80

CASE 1 — END BOOST

CASE 2 — POST ORBIT INSERTION

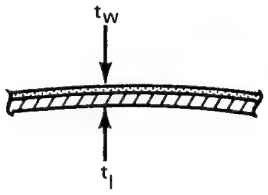

Table 18 - Concepts Selected for Cost Evaluation

TANK STATION cm	CONFIGURATION	UNIT WEIGHT[1] kg/m²	MAX Al THICKNESS REQD, [2] cm	SHEET STOCK DESIGNATION
	LH_2 TANK			
3050	BASELINE, INTEGRAL STIFFENED, ALL ALUMINUM	12.6	4.78	B
	ZEE STIFFENED, ALL ALUMINUM	13.2	.331	D
	INTEGRAL STIFFENED + S-GLASS OVERWRAP	10.5	5.01	B
	ZEE STIFFENED + S-GLASS OVERWRAP	10.8	.228	D
	HONEYCOMB, PAPER CORE, COMPOSITE OUTER FACE	12.9	.340	D
4065	BASELINE, INTEGRAL STIFFENED, ALL ALUMINUM	17.2	5.59	A
	ZEE STIFFENED, ALL ALUMINUM	17.4	.447	D
	INTEGRAL STIFFENED + S-GLASS OVERWRAP	16.3	5.74	A
	ZEE STIFFENED + S-GLASS OVERWRAP	17.0	.343	D
	HONEYCOMB; PAPER CORE; COMPOSITE OUTER FACE	18.9	.488	D
	LO_2 TANK			
1240	BASELINE, ALUMINUM MONOCOQUE	13.5	.488	D
	ALUMINUM MONOCOQUE + S-GLASS OVERWRAP	8.2	.094	D
1550	BASELINE, ALUMINUM MONOCOQUE	14.8	.534	D
	ALUMINUM MONOCOQUE + S-GLASS OVERWRAP	11.8	.343	D

(1) IDEALIZED PANEL WEIGHT, DOES NOT INCLUDE NON-OPTIMUM FACTOR (NOF)
(2) STIFFENER PLUS SKIN THICKNESS; RING FRAME ATTACHMENT NOT INCLUDED

Table 19 - Transportation Costs

CONCEPT	TANK STATION cm	UNIT WEIGHT kg/m²	AREA m²	INCREMENTAL WEIGHT kg	THEORETICAL CYLINDER kg	NOF (1)	ESTIMATED (2) CYLINDER kg	DELTA WEIGHT kg	TRANSPORTATION DELTA COSTS $ x 10⁶
LH_2 TANK									
BASELINE (INTEGRAL)	3050 4065	12.6 17.2	357.5 92.9	4510 1600	6110	1.25	7630	—	—
BONDED Z	3050 4065	13.2 17.4	357.5 92.9	4730 1620	6350	1.25	7940	+ 310	+ 6.8
INTEGRAL + OVERWRAP	3050 4065	10.5 16.3	357.5 92.9	3750 1520	5270	1.25	6590	- 1040	- 22.9
BONDED Z + OVERWRAP	3050 4065	10.8 17.0	357.5 92.5	3860 1580	5440	1.25	6800	- 830	- 18.3
HONEYCOMB STABILIZED	3050 4065	12.9 18.9	357.5 92.5	4560 1750	6310	1.10	6920	- 710	- 15.6
LO_2 TANK									
BASELINE	1240 1550	13.5 14.8	85.0 53.5	1150 795	1945	1.05	2040	—	—
OVERWRAPPED	1240 1550	8.2 11.8	85.0 53.5	694 626	1320	1.05	1385	- 665	- 14.4

(1) NON-OPTIMUM FACTOR.

(2) NOT INCLUDING THE REGION OF THE AFT INTERSTAGE ATTACHMENT.

Table 20 - Manufacturing Cost Breakdown

COSTS NOT INCLUDING OVERWRAP

	CONCEPT A INTEG. STIFFENERS LH_2 Cyl				CONCEPT B BONDED STIFFENERS & RINGS LH_2 Cyl			
	NON- RECURRING (5)		RECURRING (445)		NON- RECURRING (5)		RECURRING (445)	
	HOURS	AMOUNT	HOURS	AMOUNT	HOURS	AMOUNT	HOURS	AMOUNT
MATERIAL DOLLARS		$1,081,794		$ 96,279,710		$ 318,314		$28,329,934
TOOL MATERIAL DOLLARS		350,619		345,753		128,433		241,119
RC 20 MANUFACTURING	260,933	2,794,592	5,699,310	61,039,610	177,794	1,904,174	3,586,674	38,413,279
RC 30 QUALITY CONTROL	44,340	555,137	583,581	7,306,434	30,855	386,305	367,464	4,600,649
RC 74 TOOL FABR.	103,985	1,149,034	272,951	3,016,109	83,735	921,272	190,985	2,110,384
RC 40 TOOL DESIGN	43,855	593,797	54,638	739,799	24,355	329,767	38,809	525,474
RC 52 MFG. MANAGEMENT	39,140	488,858	854,897	$ 10,677,663	26,669	333,096	538,001	6,719,632
TOTAL		$7,013,831		$179,405,078		$4,325,361		$80,940,471
UNIT COST		$1,402,766		$ 403,157		$ 865,072		$ 181,889
NUMBER OF METERS		488		488		488		488
DOLLARS PER SQ. METER		$ 2,875		$ 826		$ 1,770		$ 372

	CONCEPT C PAPER CORE SANDWICH - LH_2 Cyl				MONOCOQUE- LO_2 Cyl			
	NON- RECURRING (5)		RECURRING (445)		NON- RECURRING (5)		RECURRING (445)	
	HOURS	AMOUNT	HOURS	AMOUNT	HOURS	AMOUNT	HOURS	AMOUNT
MATERIAL DOLLARS		$ 394,898		$35,145,945		$ 54,018		$4,807,581
TOOL MATERIAL DOLLARS		247,303		120,740		110,701		53,562
RC 20 MANUFACTURING	131,129	1,404,392	2,558,877	27,405,687	13,950	149,405	301,715	3,231,368
RC 30 QUALITY CONTROL	27,936	349,759	260,638	3,263,188	3,670	45,948	32,955	412,597
RC 74 TOOL FABR.	34,210	378,020	95,025	1,050,026	31,560	348,738	44,790	494,930
RC 40 TOOL DESIGN	15,075	204,115	18,843	255,134	11,217	151,878	10,860	147,044
RC 52 MFG. MANAGEMENT	19,669	245,666	383,832	4,794,062	2,090	26,104	45,260	565,297
TOTAL		$3,224,153		$72,034,782		$886,792		$9,712,379
UNIT COST		$ 644,831		$ 161,876		$177,358		$ 21,826
NUMBER OF SQ. METERS		488		488		66.6		66.6
DOLLARS PER SQ. METER		$ 1,320		$ 332		$ 2,660		$ 328

OVERWRAP COSTS (S - GLASS)

	DOLLARS PER SQUARE METER	
	NON - RECURRING	RECURRING
LH_2 TANK	439	108
LO_2 TANK	861	286

Table 21 Manufacturing Cost Comparison

CONCEPT	UNIT COSTS, $/m²		PROGRAM COSTS, $ x 10⁶			
	NON–RECURRING	RECURRING	NON–RECURRING	RECURRING	TOTAL	DELTA COST $ X 10⁶
LH_2 TANK			(1)	(2)		
BASELINE (INTEGRAL)	2875	826	6.4	166	172.4	–
BONDED Z	1770	372	4.0	74.6	78.6	–93.8
INTEGRAL + OVERWRAP	3314	934	7.4	188	195.4	+23.0
BONDED Z + OVERWRAP	2209	480	5.0	96.2	101.2	–71.2
HONEYCOMB STABILIZED	1320	332	3.0	66.5	69.5	–102.9
LO_2 TANK			(3)	(4)		
BASELINE	2660	328	1.84	20.10	21.94	–
OVERWRAPPED	3520	614	2.43	37.90	40.33	+18.4

(1) UNIT COSTS x 5 TANKS x 450.4m²

(2) UNIT COSTS x 445 TANKS x 450.4m²

(3) UNIT COSTS x 5 TANKS x 138.5m²

(4) UNIT COSTS x 445 TANKS x 138.5m²

Table 22 Total Program Cost Increments

CONCEPT	TRANSPORTATION DELTA COST $ x 10⁶	MANUFACTURING DELTA COST $ x 10⁶	TOTAL PROGRAM DELTA COST $ x 10⁶
LH_2 TANK			
BASELINE (INTEGRAL)	–	–	–
BONDED Z	+ 6.8	– 93.8	– 87.0
INTEGRAL + OVERWRAP	–22.9	+ 23.0	+ 0.1
BONDED Z + OVERWRAP	–18.3	– 71.2	– 89.5
HONEYCOMB STABILIZED	–15.6	–102.9	–118.5
LO_2 TANK			
BASELINE	–	–	–
OVERWRAPPED	–14.4	+ 18.4	+ 4.0

Table 23 Typical Mechanical Properties for Model Design

	TEMPERATURE °K	F_{tu} kN/cm²	F_{ty} kN/cm²	F_{cy} kN/cm²	E x 10^6 N/cm²
2219-T81 (INNER FACE)	367	41.0	31.7	32.3	6.97
	294	45.6	35.2	35.9	7.24
	78	53.2	41.0	41.9	8.07
	TEMPERATURE °C	**F 0° DIRECT. kN/cm²**	**F 90° DIRECT. kN/cm²**	**E 0° DIRECT. 10^6 N/cm²**	**E 90° DIRECT. 10^6 N/cm²**
GLASS CLOTH[1] (OUTER FACE)	367	28.5	23.9	1.90	1.68
	294	37.3	29.1	2.20	2.06
	78	55.6[3]	43.4[3]	2.66[3]	2.50[3]
	TEMPERATURE	**F_c N/cm²**	**E_c N/cm²**	**G_{cl} N/cm²**	**G_{cw} N/cm²**
HONEYCOMB[2] CORE	367	182	–	3240	–
	294	576	48400	10700	7800
	78	–	–	19000	–

NOTES:

(1) RELIAPREG R-1500/7581, 2 PLIES

(2) TUF 200 – 3/16 – 4.0

(3) ESTIMATED: F(RT) x 1.49; E(RT) x 1.21

Table 24 Tensile Properties of Glass-Fabric Facing Materials

FABRIC WEAVE DIRECTION	NO. OF PLIES	TENSILE PROPERTIES			
		STRENGTH, kN/cm²		MODULUS, 10^6 x N/cm²	
		294° K	367° K	294° K	367° K
CORDOPREG E - 295/7581 - 1550					
0°	8	34.5	19.9	2.26	1.31
	2	35.0	17.9	2.42	1.37
90°	8	33.6	15.0	1.94	0.92
	2	31.2	16.2	2.18	0.92
0°	14	38.3[1]		2.66[1]	
RELIAPREG R - 1500/7581					
0°	8	39.6	33.0	2.21	2.02
	2	37.3	28.5	2.20	1.90
90°	8	32.0	26.6	1.97	1.63
	2	29.1	23.9	2.06	1.68
0°		38.6[2]		2.48[2]	2.42[3]

(1) REPORTED VALUE FROM FERRO CORPORATION; LAMINATE MOLDED IN PRESS AT 55N/cm², CURED AT 436°K FOR 1 HOUR AND POSTCURED IN AN OVEN FOR 311°K FOR 4 HOURS.

(2) REPORTED VALUE FROM RELIABLE MANUFACTURING COMPANY; LAMINATE VACUUM-BAG CURED FOR 1 HOUR AT 393°K

(3) TESTED AT 344°K

Table 25 Cure Evaluation Data of Glass-Fabric Facing Materials

CURE		COMPOSITE PROPERTIES			
		CORDOPREG E - 293/7581		RELIAPREG R - 1500/7581	
TEMPERATURE °K	TIME HOUR	THICKNESS cm	FLEXURAL STRENGTH N/cm²	THICKNESS cm	FLEXURAL STRENGTH N/cm²
367	2	(1)	(1)	0.335	49200
	4	0.338	14300	0.335	57600
380°	2	0.335	8600	0.328	58500
	4	0.333	47600	0.338	56200
394	2	0.345	51100	0.333	57800
	4	0.356	43400	0.328	56700
409	2	0.351	56400	0.328	60500
	4	0.345	54000	0.315	61600
421	2	0.351	52900	0.328	60200
	4	0.335	55800	0.322	61800

(1) LAMINATE WAS NOT SUFFICIENTLY CURED TO PREPARE FLEXURAL BEAM SPECIMENS.

Table 26 Core Shear Properties of TUF-COMB 200 Honeycomb

TEST TEMP °K	CORE-SHEAR PROPERTIES (1)							
	L-DIRECTION				W-DIRECTION			
	STRENGTH		MODULUS		STRENGTH		MODULUS	
	N/cm²	AVG	N/cm²	AVG	N/cm²	AVG	N/cm²	AVG
294	150	182	(7450) (2)	10700	106	109	7450	7800
	172		9930		110		8140	
	220		11400		111		7860	
367	54	54	3380	3240				
	54		3380		—	—	—	—
	54		3040					
88	198	206	16700	19000				
	215		21900		—	—	—	—
	220 (3)		18400(3)					

NOTES:

(1) ALL TEST SPECIMENS EXHIBITED CORE SHEAR FAILURE.

(2) OMIT FROM AVERAGE.

(3) TESTED AT −130°C WHILE THE SPECIMEN WAS AT A TRANSIENT TEMPERATURE CONDITION DUE TO INCOMPLETE EXPOSURE TO COLD ENVIRONMENT.

Table 27 Compressive Properties of TUF-COMB 200 Honeycomb Sandwich Panel

	CORE COMPRESSIVE PROPERTIES							
	PANEL 1 (1)				PANEL 2 (2)			
TEST TEMP. °C	STRENGTH		MODULUS		STRENGTH		MODULUS	
	N/cm²	AVG	N/cm²	AVG	N/cm²	AVG	N/cm²	AVG
294	546	576	42600	48400	574	617	47400	51300
	595		43300		683		56600	
	586		59400		593		49300	
367	168	182			199	185		
	195		–	–	183		–	–
	184				168			
294 (3)	366			65600	–	–	–	–

NOTES:

(1) THE PANEL WAS CONSTRUCTED WITH CORDOPREG E-293 FACING ON ONE SIDE AND 2219-T62 ALUMINUM SHEET BONDED TO THE CORE WITH FM-123-2 ADHESIVE FILM FOR THE OTHER FACING.

(2) SAME BASIC CONSTRUCTION AS PANEL 1, EXCEPT RELIAPREG R-1500 AND RELIABOND E-393-1 ADHESIVE FILM WERE USED.

(3) DATA REPORTED BY HEXCEL FOR TUF-COMB 200-3/16-4.0 HONEYCOMB.

Table 28 Flatwise Tensile Strength of TUF-COMB 200 Honeycomb Sandwich Panel

	FLATWISE TENSILE STRENGTH					
	PANEL 1 (1)			PANEL 2 (2)		
TEST TEMP °K	STRENGTH		FAILURE MODE	STRENGTH		FAILURE MODE
	N/cm²	AVG		N/cm²	AVG	
294	375	354	50% CORE SHEAR	448	452	80% CORE SHEAR
	306		20% CORE SHEAR	475		100% CORE SHEAR
	379		90% CORE SHEAR	434		100% CORE SHEAR
367	90	85	100% GLASS FACING	119	96	ADHESIVE, CORE TO AL
	76		100% GLASS FACING	89		ADHESIVE, CORE TO AL
	89		100% GLASS FACING	80		ADHESIVE, CORE TO AL

NOTES:

(1) THE PANEL WAS CONSTRUCTED WITH CORDOPREG E-293 FACING ON ONE SIDE AND 2219-T62 ALUMINUM SHEET BONDED TO THE CORE WITH FM-123-2 ADHESIVE FILM FOR THE OTHER FACING.

(2) SAME BASIC CONSTRUCTION AS PANEL 1, EXCEPT RELIAPREG R-1500 AND RELIABOND E-393-1 ADHESIVE FILM WERE USED.

Table 29 Test Plan Outline

TEST		ARTICLE	
		#1	#2
1.	LIMIT COLD LOAD TEST (COND 1, END BOOST)		
	A. FILL WITH LN_2, INSPECT.	X	X
	B. APPLY LIMIT PRESSURE, HOLD, RELIEVE, & INSPECT.	X	X
	C. APPLY LIMIT PRESSURE + BENDING MOMENT (BM), HOLD, EMPTY TANK, & INSPECT	X	X
2.	LIMIT HOT LOAD TEST (COND 2, POST ORBIT INSERTION)		
	A. FILL TANK, HEAT TO +200° F, & INSPECT.		X
	B. APPLY LIMIT PRESSURE AT TEMPERATURE, HOLD, EMPTY TANK, & INSPECT		X
2a.	LH_2 TANK FILL (ALTERNATE TEST CONDITION POSSIBLE BETWEEN LIMIT HOT LOAD AND ULTIMATE COLD LOAD TESTS)		
	A. FILL WITH LH_2, MAINTAIN FULL TANK, EMPTY TANK, & INSPECT	X	X
3.	ULTIMATE COLD LOAD TEST (COND 1, END BOOST) CONT'D		
	A. FILL WITH LN_2, APPLY LIMIT PRESSURE + LIMIT BM, HOLD, RELIEVE, & INSPECT	X	X
	B. APPLY LIMIT PRESSURE + ULTIMATE BM, HOLD, & RELIEVE	X	X
	C. APPLY LIMIT PRESSURE + ULTIMATE BM, INCREASE BM TO TANK FAILURE	X	X

Table 30 Loading Conditions

CONDITION	TEMP. °C	SYSTEM INTERNAL PRESSURE N/cm^2	APPLIED BENDING MOMENT cmN
1. END BOOST (LIMIT)	78	38.5	25.0×10^6
1. END BOOST (ULTIMATE)	78	38.5	35.0×10^6
2. POST ORBIT INSERTION	367	35.1	—
2a. LH_2 TANK FILL	20	—	—

Table 31 Cond. 1 — Model Stresses and Strains at Ultimate Load

	TENSION SIDE (SEE NOTE)	COMPRESSION SIDE (SEE NOTE)
N_X, APPLIED, N/cm	3974	−1522
N_Y, APPLIED, N/cm	2580	2580
$(f_X t) = 0.810\ N_X + 0.041\ N_Y$, N/cm	3326	−1128
$(f_Y t) = 0.810\ N_Y + 0.041\ N_X$, N/cm	2253	2028
$(f_X t)' = N_X - (f_X t)$, N/cm	648	−398
$(f_Y t)' = N_Y - (f_Y t)$, N/cm	327	552
f_X, N/cm^2	43600	−14800
f_Y, N/cm^2	29600	26600
f'_X, N/cm^2	11100	−6800
f'_Y, N/cm^2	5600	9440
$\epsilon_X = \frac{1}{E}(f_X - \nu f_Y)$	4250×10^{-6}	-2800×10^{-6}
$\epsilon_Y = \frac{1}{E}(f_Y - \nu f_X)$	2060×10^{-6}	3840×10^{-6}
$\epsilon_T = +\alpha\Delta T$ (THERMAL)	-4530×10^{-6}	-4530×10^{-6}
$\epsilon_{X_{TTL}}$ (INCLUDING THERMAL)	-280×10^{-6}	-7330×10^{-6}
$\epsilon_{Y_{TTL}}$ (INCLUDING THERMAL)	-2470×10^{-6}	-690×10^{-6}

NOTE:

STRESS AND STRAIN DUE TO EXTERNAL APPLIED LOADS ONLY, NO THERMAL EFFECTS EXCEPT FOR TOTAL STRAIN.

Table 32 Tensile Properties of Weld Specimens of 2219-T81 Aluminum (1)

WELD SIMULATION	SPECIMEN DESCRIPTION	SERIAL NUMBER	THICKNESS cm	0.2% YIELD STRENGTH MN/m²	ULTIMATE TENSILE STRENGTH MN/m²	ELONGATION IN 5.08 CM %	FAILURE LOCATION
TRANSITION RING TO CYLINDER GIRTH WELD, 2319 ALUMINUM ROD ADDED	TRANSVERSE WELD BEAD-AS RECEIVED	1	0.160	273	321	1.5	HEAT AFFECTED ZONE
		2		292	332	1.5	
		3		288	330	1.0	
	TRANSVERSE WELD BEAD GROUND FLUSH – BOTH SIDES	4	0.155	234	281	2.5	WELD AREA
		5		241	294	2.5	
		6		239	285	2.0	
CYLINDER LONGITUDINAL SEAM WELD, NO ROD ADDED(2)	AXIALLY ORIENTED WELD	7	0.160	330	425	8.5	GAGE AREA
		8		337	428	8.5	
		9		339	432	10.0	
		10		330	423	8.5	
	TRANSVERSE ORIENTED WELD	11	0.160	310	332	1.0	WELD AREA
		12		321	335	1.5	
		13		314	332	1.5	
		14		321	342	1.5	
	PREPRODUCTION TRANSVERSE ORIENTED WELD	1P	0.157		328	N.R.	WELD AREA
		2P			329		
		3P		N.R.	330		
		4P			335		

NOTES:

(1) ALL SAMPLES WELDED IN THE T31 CONDITION AND AGED WITH THE CYLINDER SECTION TO THE T81 CONDITION AFTER WELDING

(2) WELDS SEAM LEVELED AFTER WELDING AND BEFORE AGING

Table 33 Tensile Test of Transverse Welds of 6061-T42 to 2219 T42 Aluminum Alloy Using 4043 Weld Wire

WELD CONDITION	DIMENSIONS cm/cm	AREA cm^2	ULT. TENSILE LOAD N	ULT. TENSILE STRESS N/cm^2	FAILURE LOCATION
FLUSH	1.284/.590	.758	13,360	17,600	PARENT METAL 6061
FLUSH	1.290/.600	.773	13,750	17,800	PARENT METAL 6061
FLUSH	1.292/.621	.801	14,160	17,600	PARENT METAL 6061
FLUSH	1.287/.580	.746	13,250	17,800	PARENT METAL 6061
INTACT	1.275/.611	.776	13,800	17,800	PARENT METAL 6061
INTACT	1.280/.609	.776	14,550	18,700	PARENT METAL 6061
INTACT	1.290/.613	.792	14,150	17,900	PARENT METAL 6061

Table 34 Tensile Properties of 2-Ply Laminates of Reliapreg R-1500/7851(1)

TEST TEMPERATURE	SAMPLE NUMBER (2)	THICKNESS cm	STRENGTH MN/m^2	MODULUS 10^3 MN/m^2
ROOM TEMPERATURE	1	0.0612	363	20.2
	2	0.0620	352	20.1
	3	0.0615	348	19.9
PRIOR TEST RESULTS			372	22.0

(1) SPECIMEN CONFIGURATION AND TEST PROCEDURES WERE PER ASTM D638; ORIENTATION WAS IN WARP (0°) DIRECTION.

(2) SPECIMENS WERE CUT FROM A LAMINATE CURED FOR 3.5 HOURS AT 394° K.

Table 35 Flexural Strength of 12-Ply Laminates of Reliapreg R-1500/7581(1)

TEST TEMPERATURE	SAMPLE NUMBER (2)	FABRIC WEAVE DIRECTION	THICKNESS cm	FLEXURAL STRENGTH MN/m²
ROOM TEMPERATURE	1	0°	0.284	644
	2	0°	0.290	672
	3	0°	0.292	656
	4	90°	0.282	541
	5	90°	0.290	527
PRIOR TEST RESULTS		0°	0.328	567

NOTES:

(1) TESTS WERE PERFORMED PER ASTM D790

(2) THE 1.27 cm WIDE BY 5.08 cm LONG SPECIMENS WERE CUT FROM A LAMINATE WHICH WAS CURED FOR 3.5 HOURS AT 394° K

Table 36 Flatwise Tensile Strength of Tuf-Comb 200 Honeycomb Sandwich Panel

TEST TEMPERATURE	SAMPLE NUMBER (1)	STRENGTH N/cm²	FAILURE MODE
ROOM TEMPERATURE	1	526	ADHESIVE, CORE TO SKIN
	2	558	
	3	534	
PRIOR TEST RESULTS (2)		452	CORE SHEAR

NOTES:

(1) THE TWO INCH SQUARE PANELS WERE CONSTRUCTED FROM TUF-COMB 200 CORE BONDED TO 2-PLY R-1500/7581 FACINGS (AND ALUMINUM LOAD BLOCKS) USING FM-123-2 ADHESIVE.

(2) THE PANEL WAS CONSTRUCTED WITH RELIAPREG R-1500 FACING ON ONE SIDE AND 2219-T62 ALUMINUM SHEET BONDED TO THE CORE WITH RELIABOND E-393-I ADHESIVE.

APPENDIX A

DESIGN STUDIES - ORIGINAL PROGRAM EFFORT

OBJECTIVE

The objective of the original program was the evaluation of the effectiveness of composite materials in providing increased structural efficiency in large-scale propellant tanks.

DESIGN EVALUATION

Analytical evaluations were performed for several concepts of composite reinforced tanks applicable to the integral Orbiter and Booster tanks of the Grumman C2F Space Shuttle configuration (see Figures 49 and 50). Composite properties were determined, analytical methods were developed, parametric weight optimization studies were carried out, and cost analyses were performed.

The baseline metal tank designs submitted in the technical proposal were used for comparison in the study; their unit weights are included in Table 50. Six design concepts which apply composite reinforcement to large-scale propellant tanks were studied. These are depicted in Figure 51. They are: Concept 1, Integrally Stiffened/External Ring Design; Concept 2, Stiffened Z Design; Concept 3, Integrally Stiffened/Internal Ring Design; Concept 4, Reinforced-Stiffener Design; Concept 5, Honeycomb Design; and Concept 6, Corrugated Stiffened Design. The concepts were investigated at two stations on the Orbiter and Booster LO_2 tanks and at three stations on the Orbiter and Booster LH_2 tanks. The locations were chosen to represent the range of loading over a tank length.

Critical design loads for the tank locations are given in Tables 37 through 40. The design criteria and methods of analysis developed in the original contract effort are equivalent to those given in the main text except that a safety factor (FS) of 1.5 for ultimate load was used instead of a factor of 1.4.

Concept 1, Integrally Stiffened/External Ring Design

For Concept 1, the aluminum tank is reinforced with internal integral stringers and external rings. Vehicle flight loads produce stresses in the axial direction while internal pressure and constrictive overwrap produce stresses in the circumferential direction. Maximum hoop tension stress in the liner occurs during the cold conditions with internal pressurization. Maximum compression stress in the liner occurs in the elevated-temperature condition.

Five fibers were considered in the original study and all were analyzed for this concept. The composites, and the arbitrarily-chosen pre-tensions on a rigid mandrel are:

S-901 glass/epoxy	51700 and 69000 N/cm^2
PRD-49-I/epoxy	69000 and 103400/Ncm^2
Boron/epoxy	41400 and 62100 N/cm^2
HTS graphite/epoxy	51700 and 69000 N/cm^2
Boron/aluminum	41400 and 55200 N/cm^2

At the time the design studies were initiated, experimental values of achievable pretensions were lacking. The values analyzed represented a range then thought reasonable. The use of two values was desirable in order to establish the design implications of various prestress magnitudes. Physical and mechanical properties for the composites are discussed under material properties.

For design of Concept 1, use was made of the methods and automated procedures discussed in the analysis section of the main text. After determining the optimum compression panel and its longitudinal working stress, the required amount of overwrap is determined and general instability checks are made. The results of the analysis for this concept are presented in Tables 41a through 41d. Overall, S-glass and PRD-49-I fiber composites result in lower weight designs and, in general, a higher overwrap prestress will result in a lower unit weight. Boron and graphite epoxy composites are also effective, but these and boron/aluminum exhibit significant compressive stresses in the wrap at low temperature (-185°C) and zero internal pressure (See Table 42). This condition would exist during filling of the propellant tanks. Because of the above trends, only S-glass and PRD overwrap were considered in the remaining concepts that require overwrap reinforcement.

Concept 2*, Zee-Stiffened Design

This concept differs from Concept 1 in the stringer type and placement, using external bonded and attached zees. Table 43 contains summaries of the results for this concept.

Concept 3*, Integral Stiffened/Internal Ring Design

This concept is similar to Concept 1 but with internal instead of external rings. The results are given in Table 44.

Concept 4, Reinforced-Stiffener Design

This concept studies the advantages of composite reinforcement of tank stiffening members (rings and stringers). Figures 52 and 53 show typical examples. The hydrogen tanks with their long cylindrical lengths and higher load intensities will provide better opportunities for reducing stiffener weight. On the basis of their size alone, rings also present a high potential for reducing weight.

In a parallel study not related to this contract, (Ref. 22), the use of boron-aluminum to replace stiffness-designed all-aluminum tank frames resulted in a 27%

---

*The designs and methods of analysis for Concepts 1, 2, and 3 are similar because axial and ring stiffening is used in conjunction with circumferential overwrap. The stiffening differs in type, location, and method of attachment.

weight saving. Boron-epoxy reinforced stiffened panel tests (Ref. 23) show weight savings of 15% to 25% for load intensities of interest in this study.

Because of the large difference in coefficients of thermal expansion between aluminum and boron-epoxy, bond strengths and cure temperatures become critical for reinforcement of aluminum members. Since the basic tank is aluminum, reinforcement of integral stiffening would encounter this problem. An alternate design, which lessens the thermal incompatibility, uses a small integral tang with the basic shell and mechanically fastens a titanium stiffener to the panel. The boron-epoxy is then used to reinforce the titanium ring or stringer. Then titanium provides a buffer of intermediate thermal coefficient of expansion between the composite and the aluminum.

Boron-aluminum also has a much lower thermal coefficient of expansion than aluminum. Three methods of attaching boron-aluminum to aluminum are proposed: bonding, brazing and mechanical fastening. Bonding would be susceptible to the same problems that occur with boron-epoxy. Brazing requires high temperatures which would degrade the properties of the adjacent structure. Mechanical fastening (through solid aluminum sections of the boron-aluminum composite reinforcement) would be preferred. Analysis of ring designs such as those shown in Fig. 52 resulted in a 37% weight saving by means of the boron-aluminum reinforcement.

Boron-aluminum, because of its high internal peel, bond and shear strength, is used more flexibly than boron-epoxy. The boron-epoxy is more readily used as a solid bar acting as a flange on a stiffener. Such designs independently investigated in Boeing's stiffened panel tests and analyses of Ref. 23 are relevant to tank design since the stiffeners are bonded to the basic panel and do not require penetrations of the pressure shell. Design load intensity of the panels was approximately 14000 N/cm. Stiffeners of aluminum and titanium were considered in the Boeing study. Effects of the bonding of the boron-epoxy to the metal stiffeners were reflected in the test values. The designs of the stiffened panels are shown in Fig. 53. In the above reference, analyses of test results indicate that "panel failure was in part caused by the high peel loads developed in skin-stiffener bonds" due to buckling of the intermediate skins. This caused the designs to fall somewhat short of their design strength. However, significant weight savings were indicated in comparison with all-metal stiffened panels.

In the present study, the design features boron-epoxy-reinforced, external zee-stiffening. Part of the stringer outside flange is a unidirectional boron/epoxy composite. The computer program that was used for Concept 2 was also used for this design, the one notable difference being that the minimum skin gage was greater in this case, since the benefit of hoop overwrap is not present. After all-metal designs were obtained, outside flange material in excess of the web thickness was replaced by an equivalent amount of boron-epoxy composite. (Note that an all-metal zee-stiffened design is heavier than an all-metal integrally stiffened design, so that the resulting weight savings due to boron reinforcement are not sufficient to reduce the weight below that of the baseline.) Since the composite is unidirectional, the extent of reduction of stiffener torsional rigidity would have to be assessed through testing.

Weights for Concept 4 designs are shown in Table 45.

Concept 5, Honeycomb Design

This concept consists of a honeycomb sandwich made up of 2219-T87 aluminum alloy face sheets in combination with a 2024-T81 aluminum alloy core.

In the original program effort, the general and panel instability for honeycomb sandwich construction was determined through use of the automated procedure of Ref. 24. Utilization of this program requires that the sandwich cross-section be converted to an equivalent isotropic sheet. General instability allowables were determined at each design station as if the corresponding section were constant along the entire cylinder length. For panel instability, a cylinder length of one ring spacing was used and the ring area and inertia were set equal to zero. "Knockdown" factors of .75 and .90 were used with the general and panel instability allowables, respectively.

The results for this concept are given in Table 46. For the Orbiter LO_2 tank, the minimum required face sheet thickness alone satisfied both the general and panel instability allowables. Therefore, a monocoque construction is adequate for this tank.

Concept 6, Corrugation-Stiffened Design

In this concept, internal pressure loads are beamed to the tank rings by means of longitudinal corrugations which also carry tank axial and bending loads. The corrugations between rings are analyzed as stiffened panels. Hoop loads are reacted only by the rings since corrugations have minimal transverse external stiffness. Composite overwrap is applied circumferentially to the rings which are then analyzed for hoop loads in a manner analogous to an unstiffened, circumferentially overwrapped tank but with areas substituted for thicknesses. The rings should also be sized to sustain vehicle flight loads. In Ref. 24, it is observed that the ring stiffness criteria of Shanley (Ref. 25), is unconservative for corrugation-stiffened cylinders. Overall tank strength is determined by the general instability load obtained using the work of Ref. 24. For the cases where the ring stiffness, based on hoop load or flight load requirements, is insufficient from the general instability standpoint, the ring size is increased until the general instability load equals the applied load. All strength and stability criteria are then satisfied.

A method was evolved for the structural analysis of corrugation-stiffened panels composed of flat elements and subjected to axial compression and lateral pressure (beam column). A digital computer program was written in order to systematize the calculations for a large number of loading conditions. For a given ring spacing (column length) and angle of corrugation (see sketch), the corrugation thickness and element length were determined for a minimum positive margin of safety. The ring spacings considered were limited to the existing vehicle ring spacing or half this value.

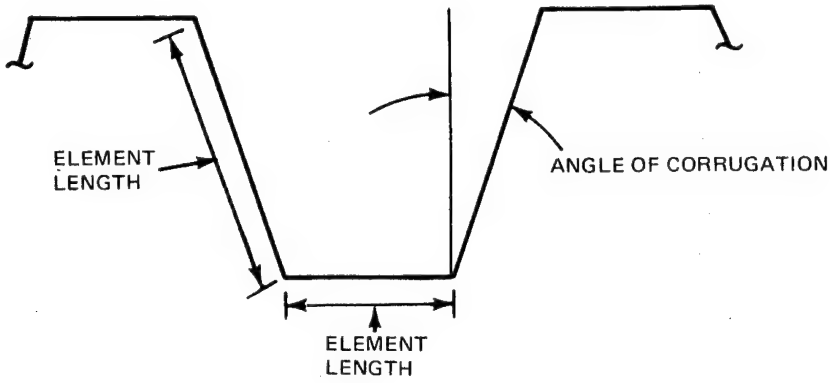

Calculated shell weights for the corrugated wall concept are shown in Table 47. They include the weights of intermediate rings required to support the hoop pressure load and also to reduce the column length of the wall section.

MATERIAL PROPERTIES USED IN DESIGN

In addition to the material properties data given in the main text, additional data was required in the initial effort for boron-epoxy and graphite-epoxy filament wound composites. They appear in Table 48. The boron-epoxy room temperature data was developed in Ref. 26 and the cyclic life and sustained load data are derived from Ref. 27. The coefficient of expansion of boron-epoxy was obtained from Ref. 28. For the graphite-epoxy (Courtalds or Hercules ATS), the references were as follows: modules of elasticity, Ref. 29 and 30; strength, Ref. 31 and 32; cyclic fatigue, Ref. 32; thermal coefficient of expansion, Ref. 33.

MANUFACTURING OPTIONS AND ESTIMATED COSTS

As part of the evaluation of the six concepts, alternative designs and methods of fabrication were reviewed by the Grumman Product Manufacturing Department. The alternatives were appraised on the basis of cost, manufacturing complexity and the requirement for successful technology development, and a system of baseline values established for each of these parameters. This made it possible to evaluate each of the alternatives in terms of dollars per kilogram or dollars per square meter. Welding and X-rays were estimated in dollars per linear meter. Precision of the dollar value assigned to each process or operation was not as critical as the level of manufacturing difficulty, as reflected by the relative cost of the various designs. Also, since relative cost of the various designs was the consideration, only the Orbiter tank costs were estimated.

Estimates were based on industry-wide manufacturing facilities. Limitations of the existing capacities for machining, rolling, brake-forming, welding, sonic testing, chem-milling etc. were considered. Costs of tooling and costs of test facilities that were required because they were not commercially available were amortized over the entire tank production as nonrecurring costs.

The approximate dimensions of the cylindrical portions of the Shuttle tankage are given below.

Tank	Length, cm	Diameter, cm
Orbiter LO_2	610	366
Orbiter LH_2	1880	366
Booster LH_2	2920	1000
Booster LO_2	690	1000

MANUFACTURING OPTIONS

Prior to discussing the estimated costs, a description of the alternative designs and methods of fabrication is presented. For the integrally stiffened/external ring design, Concept 1, three alternative designs (Figure 54) are possible, depending upon available material stock size. For the Orbiter LH_2 tanks, they are:

(a) Stock size: 6.35 cm x 295 cm x 856 cm
The stiffeners on one side of the plate are integrally machined to their designed height. The ring frame flanges on the opposite side of the plate are also integrally machined. After the tank has been overwrapped, the frames are riveted to the flanges. The design implications of this concept are designated Ⓐ on Fig. 54 through 58.

(b) Stock size: 5.1 cm x 290 cm x 808 cm
The stiffeners on one side of the plate are integrally machined to their designed height. After the metal is welded and overwrapped, the frames are bonded to the tank's external surface. The design implications of this concept are designated Ⓑ on Fig. 54 through 58.

(c) Stock size: 2.54 cm x 366 cm x 1880 cm
Flanges to be used as stiffener attachments are integrally machined on one side of the plate. Extrusions are riveted to the flanges in order to achieve the stiffeners' designed height. Frames are applied as in (b). The design implications of this concept are designated Ⓒ on Fig. 54 through 58.

In the discussion of estimated costs at the end of this section, these alternatives are denoted as 1a, 1b, and 1c. This notation is also used for the Orbiter LO_2 tanks.

Two methods of fabrication for the above design may be used to construct the LH_2 tank's cylindrical portion.

Method 1: The cylinder is constructed from four 1880 cm-long x 283 cm cylindrical-arc segments which are welded together. Each segment is composed of a plate (or plates) machined while flat and then formed into arcs of a circular cylinder. These segments are machine welded in a fixture (See Figures 55 and 56). Material stock sizes impose constraints on this procedure. The maximum length available for the 5.1 cm stock is 808 cm, for 6.35 cm stock, it is 856 cm. Since the tank length is 1880 cm, the segments fabricated from 5.1 to 6.35 cm stock must be spliced (Figure 55). Segments fabricated from 2.54 cm stock, which has a length of 1880 cm, need not be spliced.

Method 2: The cylinder is fabricated from plate (or plates) machined in the flat and formed to a longitudinally split cylinder with a 180 cm radius. Each longitudinal split line and junction of adjacent cylindrical segments, butted and held in a fixture, is machine welded. Because of the material stock size available, six of these cylindrical segments must be used to achieve the 1880 cm length (Figures 57 and 58).

The three Orbiter LO_2 designs, based on material stock sizes (Ⓐ , Ⓑ and Ⓒ respectively in Fig. 59) are:

(a) Stock size: 7.62 x 244 x 845 cm
The stiffeners on one side of the plate are integrally machined to their designed height. The frame flanges on the opposite side of the plate are also integrally machined. After the tank has been welded and overwrapped, frames are riveted to the flanges.

(b) Stock size: 6.35 x 295 x 856 cm
The stiffeners on one side of the plate are integrally machined to their designed height. After the tank has been welded and overwrapped, the frames are bonded to the external surface.

(c) Stock size: 5.1 x 290 x 808 cm
Flanges to be used as stiffener attachment are integrally machined on one side of the plate. Flanges to be used as frame attachments are integrally machined on the opposite side of the plate. After welding and overwrapping, stiffeners and frames are riveted to their respective flanges.

Two methods of fabrication for the above designs may be employed to construct the LO_2 tank's cylindrical portion.

Method 1: Both the cylinder and cone are constructed from four full axial-length quadrants which are welded together. It is convenient to machine the quadrants from flat plate and then to form the developed shape with single curvature, as part of a cone or cylinder as required. These segments are machine welded in a fixture (See Figure 60). Material stock size has no effect on this method.

Method 2: The cylinder or cone is fabricated from a plate (or plates) machined in the flat and formed to the required radius. The ends, butted and held in a fixture, are machine welded. Conical and cylindrical segments are butted, trim fitted and welded together in the weld fixture (See Figure 61). Material stock thickness determines the number of segments required. Since 7.62 cm-thick plates are 244 cm wide, two segments are required for both the cylinder and the cone. The 6.35 cm-thick plate is 295 cm wide. The cone must therefore be made in two pieces. The lengths of the alternatives are less than the cylinder's circumference of 1130 cm; hence, the plates must be spliced to form the cylinder and the cone.

The design alternatives for the zee-stiffened design, Concept 2, are confined to the ability of forming a tank from rolled plate approximately .95 cm thick. Available stock material in .95 cm thickness is 366 cm wide and up to 2500 cm long. For the Orbiter LH_2 tank cylinder, (circumference = 1130 cm, length = 1880 cm), two alternative fabrication methods are feasible.

Method 1: Taking advantage of the material stock length, the sheet is rolled and welded along the longitudinal axis using four sheets. Each of the sheets is chem-milled leaving thickened lands at the edges and pads for blind fastener and frame connections. Frames and stiffeners are bonded to the tank external surface after overwrapping (See Figure 62).

Method 2: The cylinder is fabricated by rolling the sheets into cylindrical segments 360 cm in diameter. The ends, butted and held in a fixture, are machine welded. Segments of 366 cm maximum are formed and, by butt welding six together, the 1880 cm length is achieved. Frames and stiffeners are attached after overwrapping. Chem-milling operations are identical with Method 1 (See Figure 63). It should be noted that the total weld length for both methods is approximately equal.

Method 1): $1880 \times 4 = 7520$ cm
Method 2): $1130 \times 5 + 1880 = 7530$ cm

For the LO_2 Orbiter tank the second alternative would be the most logical to use. Both the cylinder and the cone length are less than 366 cm, and the circumferences are within the 2500 cm stock length (See Figure 64).

For Concept 3, integrally stiffened/internal ring design, uninterrupted wrapping of the outside is possible. Clips used for TPS attachment are bonded and mechanically fastened at the ring location on the outside and contained by the overwrap. Two alternative designs are available for the LH_2 and LO_2 Orbiter tank cylinders. They are identical with alternatives 1b and 1c. (See Figure 54 Ⓑ and Ⓒ , 59 Ⓑ and Ⓒ .) Two alternative methods of construction are identical with Concept 1. (External rings, (See Figures 55-58, 60, 61).

For the reinforced stiffener design, Concept 4, the cylindrical portion of the LH_2 orbiter tank is made by machining stock material 2.54 x 366 x 1880 cm in the flat (see Figure 55) and rolling and welding four pieces as shown in Figure 56. An alternative method is to machine in the flat and roll the plates into complete but split cylindrical segments (see Figure 57). Six complete cylindrical segments are welded to make up the 1880 cm length (see Figure 58). In both methods, the flanges for rings and stiffeners are machined on one side of the plate and, when rolled, they appear on the outside of the tank. Boron-reinforced aluminum sheet sections are then riveted to these flanges. The method of machining and rolling the plates in the transverse direction is most advantageous for the cylinder and cone of the Orbiter LO_2 tank. Both cylinder and cone length are less than the 366 cm stock width.

For the honeycomb design, Concept 5, three alternative methods of construction are available (see Figures 65, 66 and 67) based primarily on the size of existing autoclaves.

Method 1: The largest autoclave required would accommodate a full vessel 2300 cm long x 380 cm in diameter for the Orbiter LH_2 tank or 3650 cm long and 1000 cm in diameter for the booster LH_2 tank. The vessel's metal parts could be assembled either as girth welded circular cylinders 366 cm long and 380 or 1000 cm in diameter, or from formed circular segments of appropriate corresponding radius and full axial length, their arc length being equal to or

less than 366 cm. The resulting vessel, shown in Fig. 65, would be pressurized (with sealing closures retained mechanically by longitudinal struts to avoid applying axial load on the cylinder) to round and stabilize its shape. The honeycomb core would be adhesively bonded and then external metal skin bonded to the core.

Method 2: Suppose an autoclave to be available which can accommodate a 366 cm long by 380 cm diameter Orbiter tank (or 1000 cm diameter Booster tank). A convenient cylinder length would be seven times the ring frame spacing of 50.8 cm, or 350.6 cm. Such a cylinder would be converted to a sandwich construction exactly as in Method 1. However, girth joints would be required between cylinders, as shown in Fig. 66.

Method 3: Suppose the use of a long shallow autoclave, 3600 cm long for the Booster and 2300 cm long for the Orbiter. To make the Orbiter, the vessel would be made from quadrants whose envelope is 2300 cm x 270 cm x 56 cm. For the Booster, the envelope would be 3600 cm x 342 cm x 30 cm. Nine such segments would be required per tank. The unspliced 2500 cm length of sheet (366 cm wide) would suffice for the Orbiter tanks; a longitudinal splice would be required to achieve the 3600 cm length of the Booster. The honeycomb core would be adhesively bonded and then the outer metal face would be bonded. The splice details are shown in Fig. 67.

The corrugation-stiffened tank design, Concept 6, with ring frames spaced at ten inch intervals along the cylinder, is shown in Figure 68. For the LH_2 orbiter tank (1880 cm long) cylinder, sheets of .127 cm 2219-T87 material must be corrugated in the longitudinal direction. Assuming a sheet to be 366 cm wide and 1880 cm long, and that facilities for brake-forming a sheet this long exist, an efficient use of the material is achieved with a corrugated circumference of 178 cm. Efficient material use can be shown with the help of the figure below.

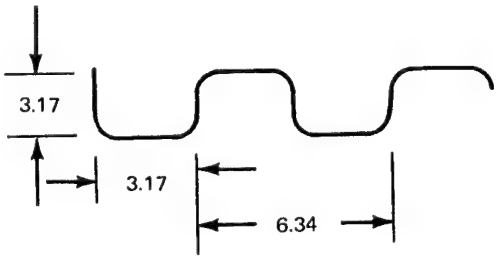

Thus, each 6.34 cm-long corrugation requires 12.68 cm of sheet. A sheet width of 366 cm provides 366/12.68 = 28 corrugations and the circumferential length provided is therefore 6.34 x 28 = 178 cm. Seven sections 178 cm long are required to provide a 1130 cm circumference. The sheets are held in a fixture and welded longitudinally. At the ends of the sheet, the corrugations must have a transition down to a monocoque cylinder, in order to facilitate welding. To keep this region from buckling, a sandwich stiffening system is desirable. The end domes, also of sandwich construction, are welded to the transition region. Should the capacity of the brake-forming facilities be less than 1880 cm, additional sandwich-stiffened transitions will be required at each weld. (See Figure 68, Section A-A). At 25.4 cm frame intervals, the external corrugations are filled with densified honeycomb core, with each segment having a bonded Delron-type fastener. Segmented frames

are assembled on the cylinder over the core and counter-sunk screws are installed. A mandrel is installed inside the tank either for the full tank length or locally at each frame location. The contacting flange of the frame is overwrapped, using S-glass filament. After overwrapping, the entire tank with the honeycomb transitions is cured.

As an alternative method of forming the corrugation transition to a cylinder, the ends of the corrugations may be cut and welded as shown in Figure 69. Additional ring frames may be added at the weld and transition area to provide the required structural properties formerly obtained with a honeycomb splice.

Estimated Costs

Costs for the baseline design and the study concepts for the Orbiter are given in terms of dollars per square meter. These costs are based on fabricating seven tanks, one qualification test item and six production tanks, with delivery dates ranging over an eight-year period.

Recurring and non-recurring costs for the baseline design and Concepts 1 through 4 are shown in Table 49. Costs for Concept 5 are not shown due to the much higher fabrication costs for the sandwich construction. Compared to ring stringer tank construction, sandwich construction tooling is 2-1/2 time more costly, recurring labor costs are 60% higher and material costs (for an equal weight per square meter) are 50% higher. Concept 6 weights are consistently among the highest weights and construction costs are high compared to ring-stringer construction. Aluminum sheets could be formed into the required corrugated pattern by brake-forming; however, forming sheets 1880 cm long repeately with tolerable accuracy is beyond the present capability of manufacturing facilities. Transitions from corrugations to a cylinder must be made to provide welding lands for cylinder segment and end dome joining. Difficulties encountered in forming the transition by simply deforming the material led to the consideration of the cutting, forming and welding alternative shown in Figure A-21. However, the cost of tooling to support the welding process was such to make the concept incapable of competing with the other contenders. Hence, costs for Concept 6 are now shown in Table 49.

RESULTS

Table 50 is a summary of unit weights for the baseline and six study concepts. Values shown for the overwrapped concepts are minimum weight PRD and S-glass designs from Tables 41 through 44, with prestresses limited to the recommended maximum values given in the tables. At stations 3000 and 3560, the longitudinal loadings predominate. Hence, the analyses indicate that overwrapping is not efficient. For Concept 4, analyses were not performed at stations 1333 and 1650, since the low longitudinal loadings render the concept inapplicable.

Table 51 is a summary of average tank unit weights and costs. Tank unit weights were determined by averaging station weights of Table 50. Tank unit costs are average values for different fabrication alternatives shown in Table 49. As noted, only Orbiter tankage costs were computed. In addition, detailed costs for Concepts 5 and 6 were not computed since they were estimated, at the outset, to be significantly higher than the baseline cost. Table 51 indicates that for three out of four tanks, weight savings from 5 - 30% can be achieved with filament overwrapped designs. The total weight saving due to filament wrapping could be 1320 kg for the Booster and 430 kg for the Orbiter. Sandwich construction is the lightest design for the orbiter LH_2 tank, due to the high longitudinal loadings. Concepts 2 and 4 show significant cost savings (15 - 30%) over the baseline.

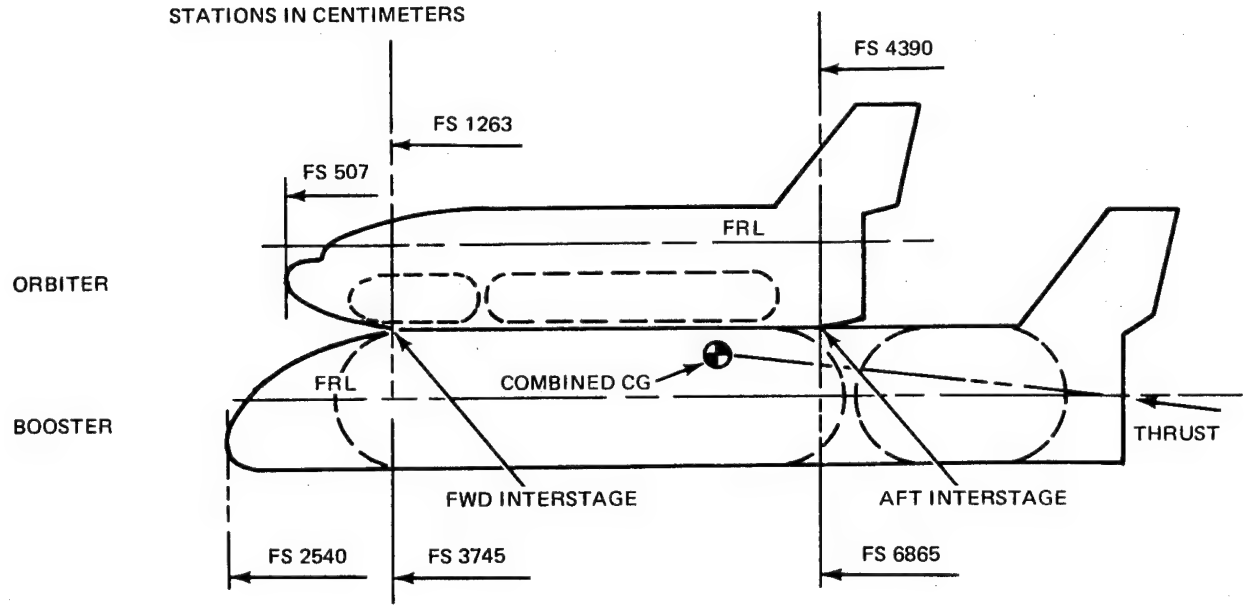

Fig. 49 Combined Orbiter/Booster Design C2F

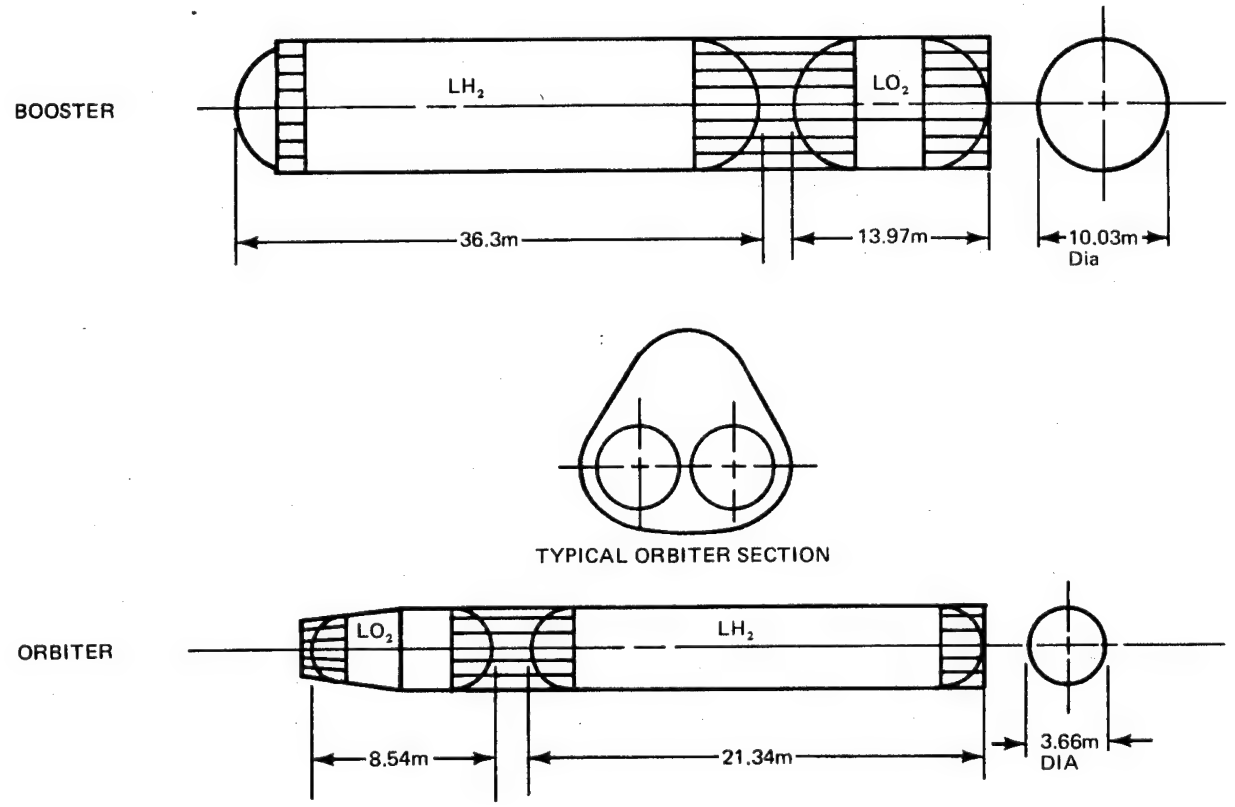

Fig. 50 Orbiter and Booster Propellant Tanks

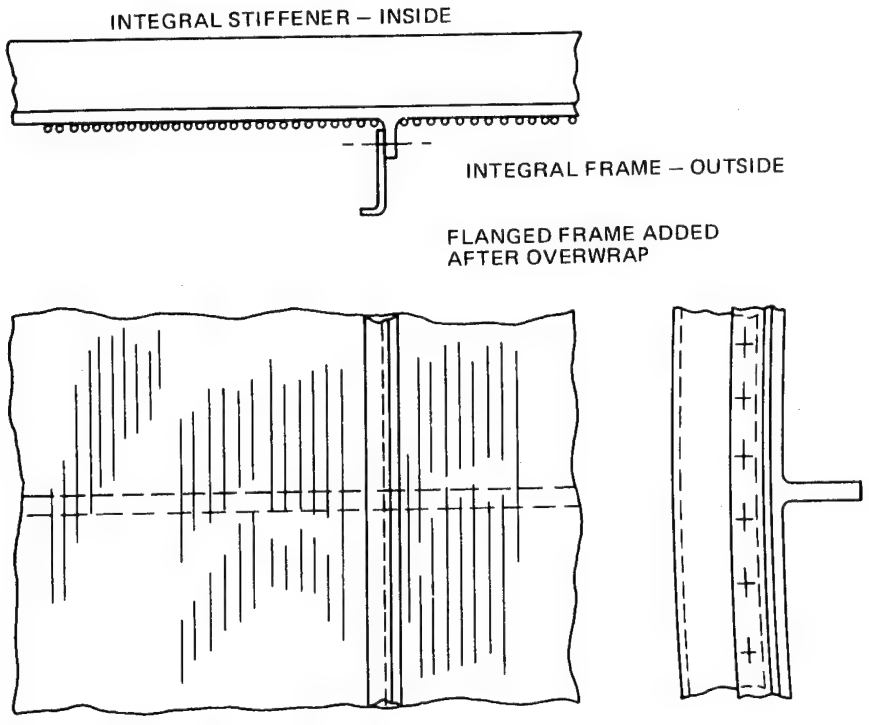

CONCEPT 1 – OVERWRAP BETWEEN FRAMES

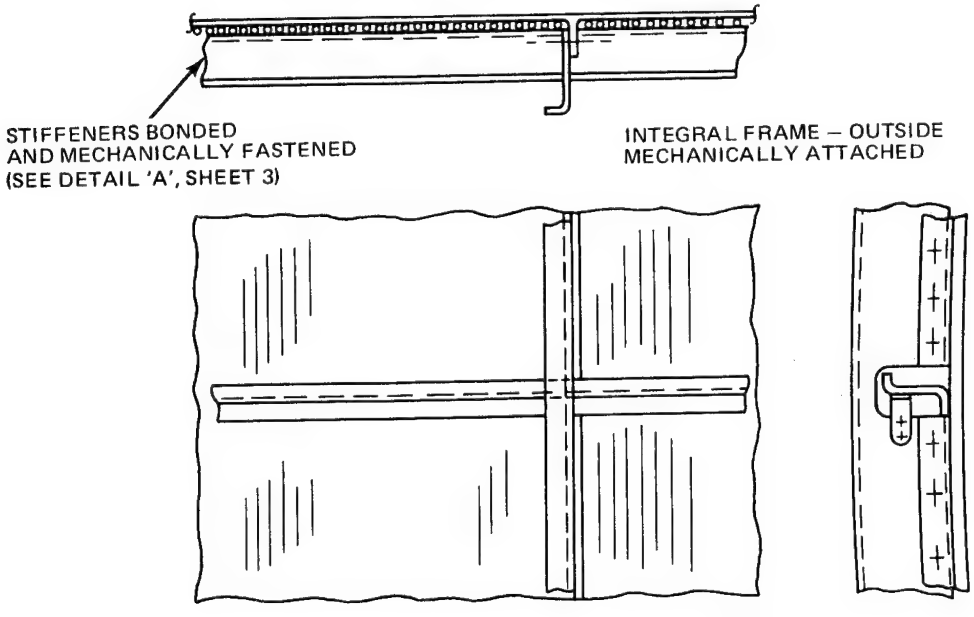

CONCEPT 2 – OVERWRAP BETWEEN FRAMES

Fig. 51 Six Design Concepts (Sheet 1 of 3)

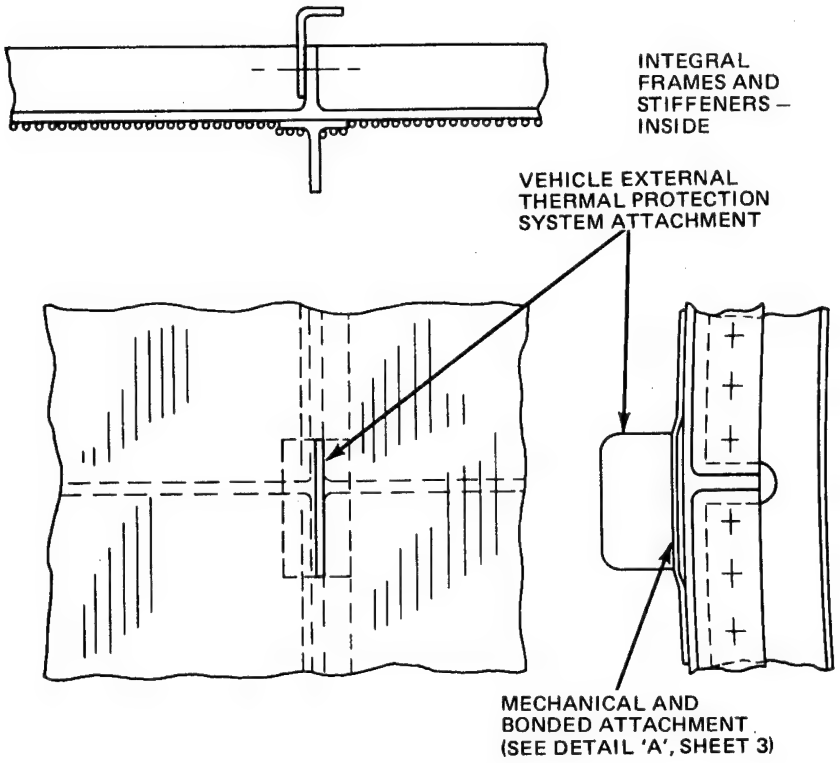

CONCEPT 3 – COMPLETE OVERWRAP

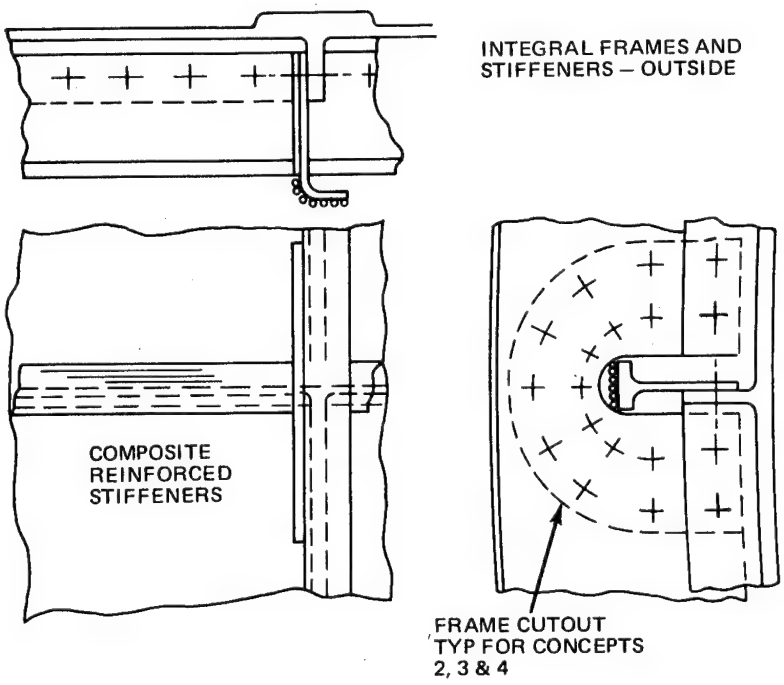

CONCEPT 4 – NO OVERWRAP

Fig. 51 Six Design Concepts (Sheet 2 of 3)

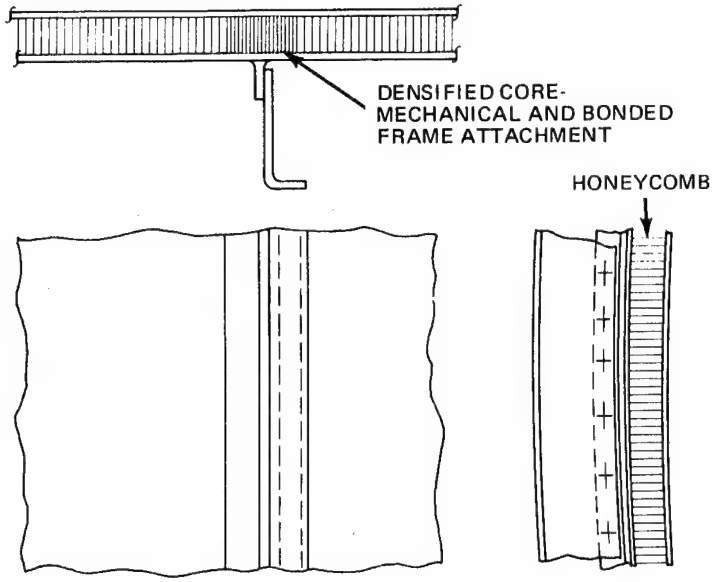

CONCEPT 5 – NO OVERWRAP

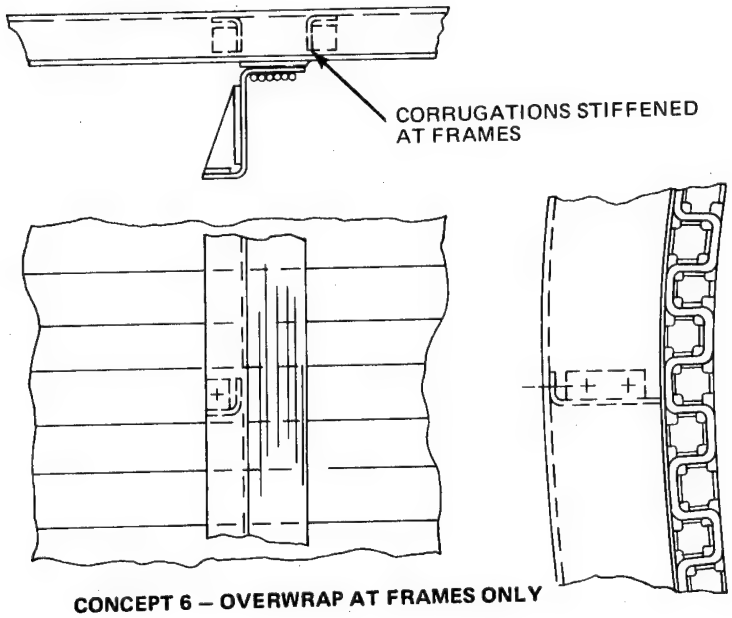

CONCEPT 6 – OVERWRAP AT FRAMES ONLY

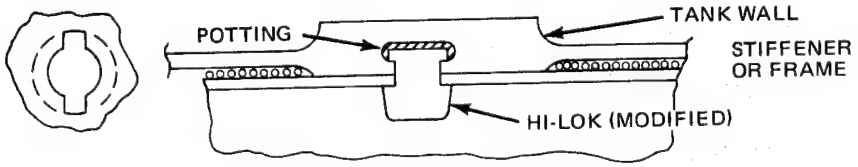

DETAIL 'A' – MECHANICAL ATTACHMENT

Fig. 51 Six Design Concepts (Sheet 3 of 3)

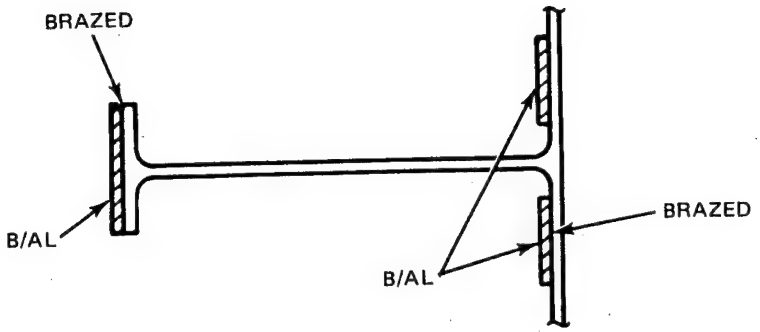

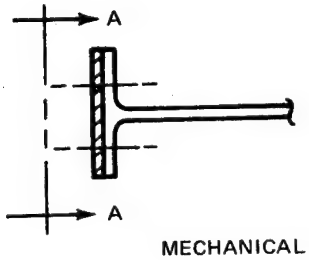

MECHANICAL FASTENERS

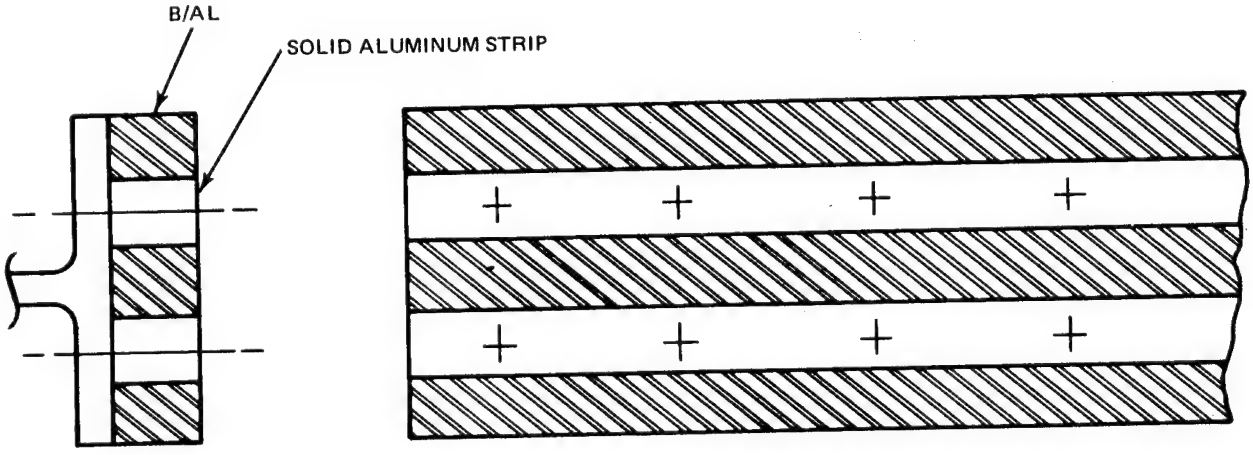

VIEW A-A

Fig. 52 Boron-Aluminum Applications

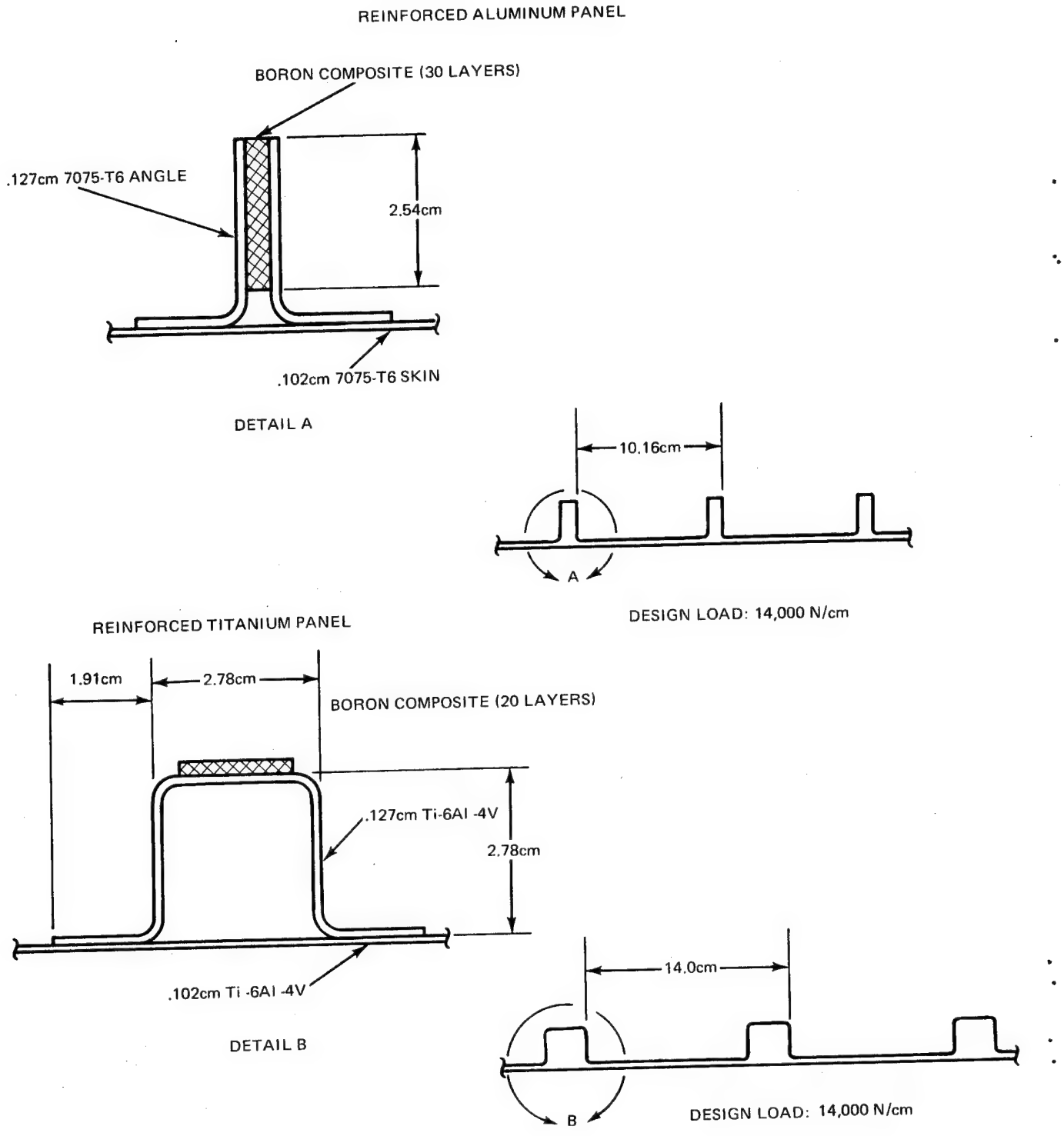

Fig. 53 Composite Reinforced Test Panels

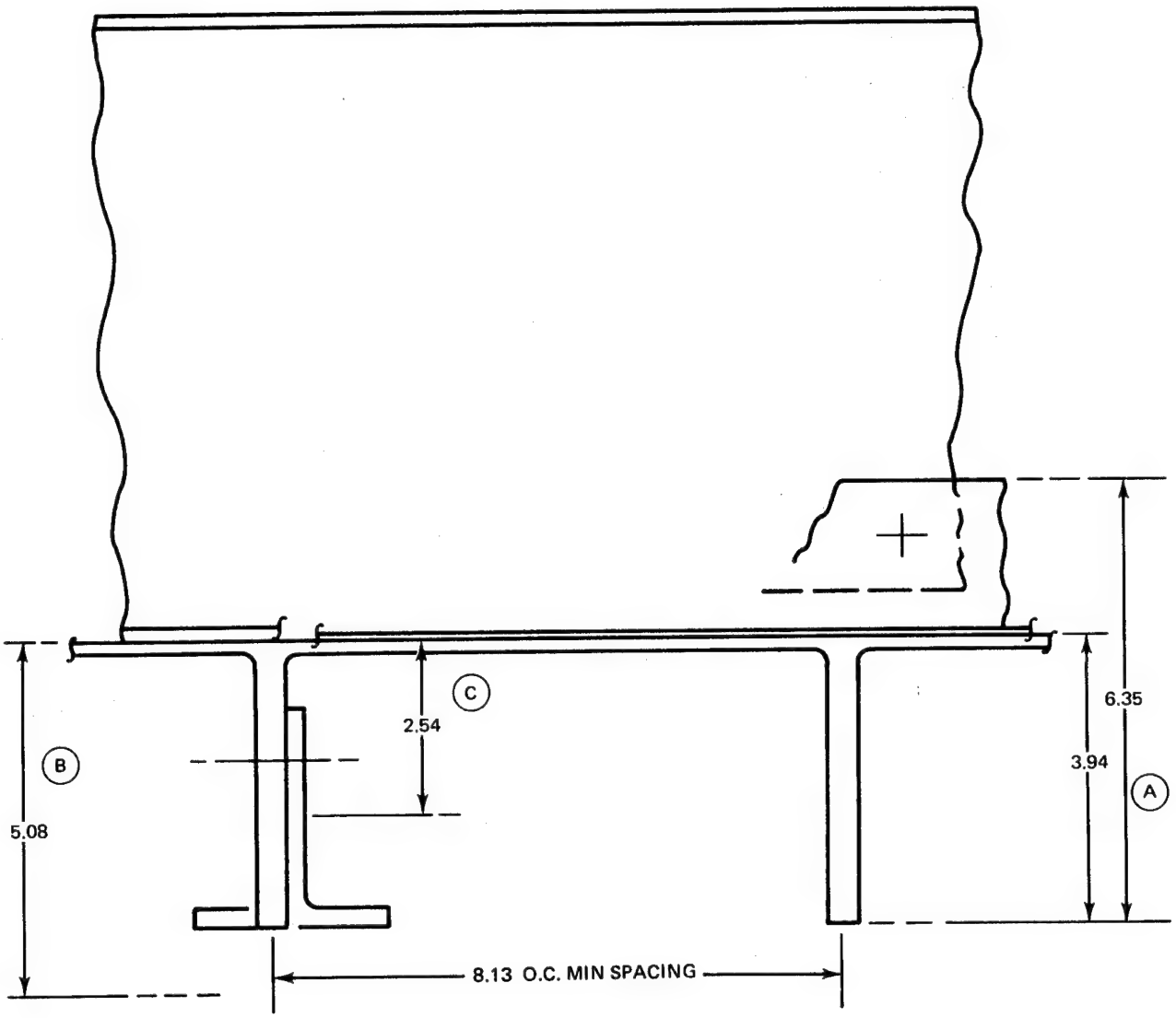

NOTE: ALL DIMENSIONS IN CENTIMETERS.

Fig. 54 Alternative Machining Methods For Concept 1, Orbiter LH_2 Tank

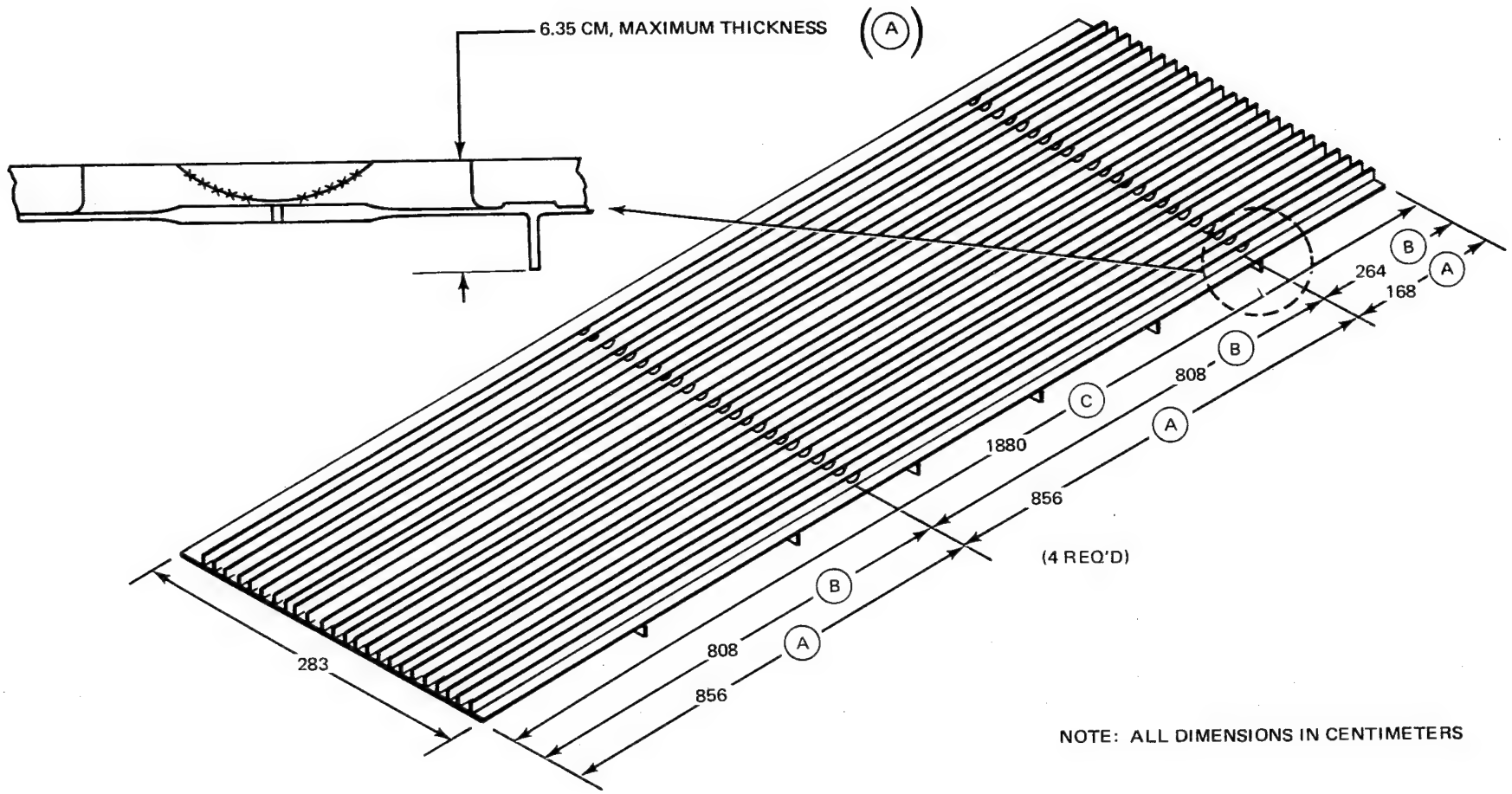

Fig. 55 Cylindrical Segment Machined as Flat Plate for Concept 1, Orbiter LH_2 Tank

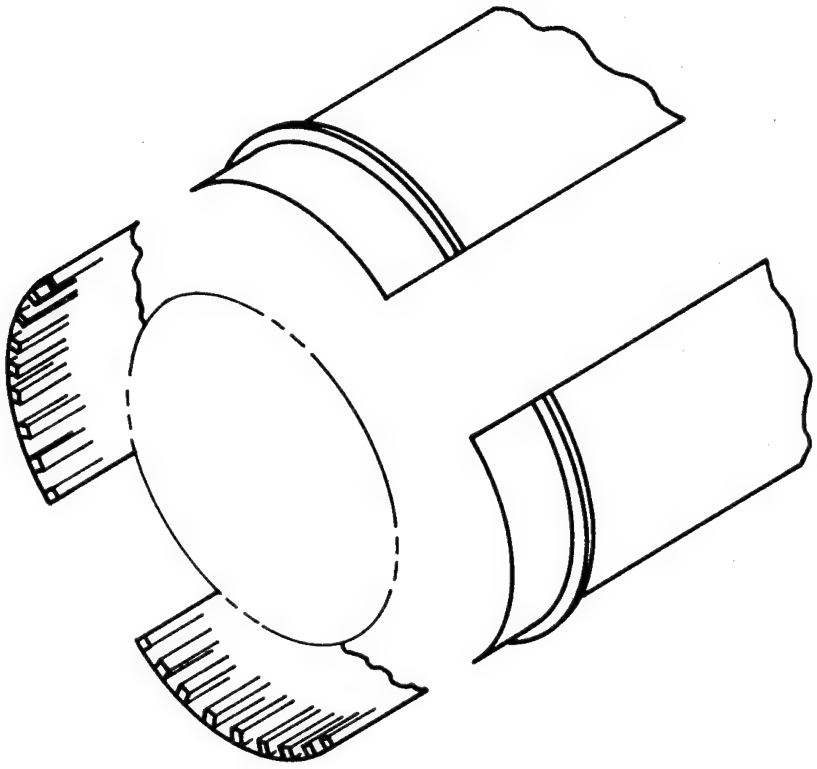

Fig. 56 Plates Rolled and Longitudinally Welded for Concept 1, Orbiter LH_2 Tank

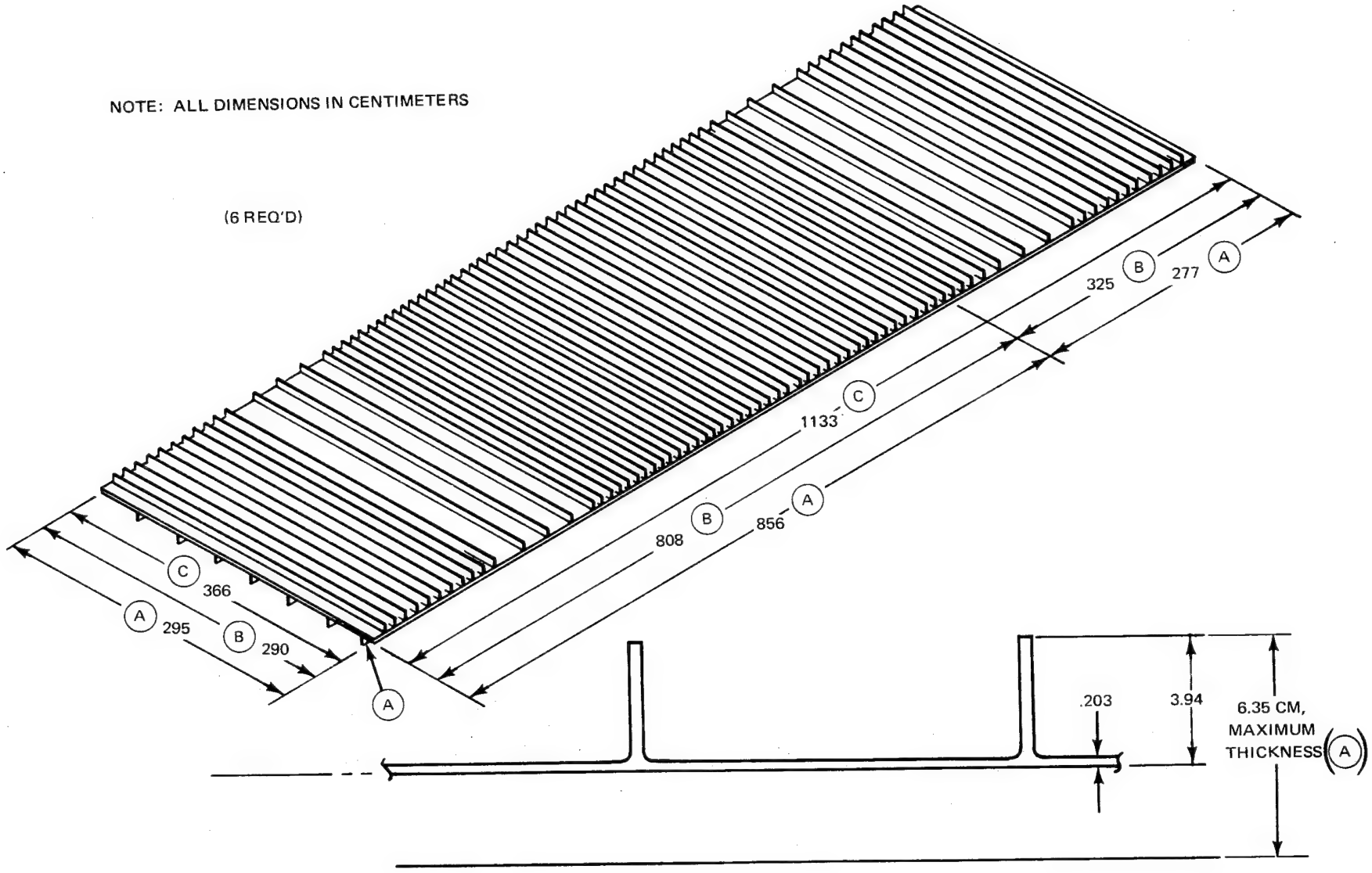

Fig. 57 Split Developed Cylinder Machined as Flat Plate for Concept 1, Orbiter LH_2 Tank

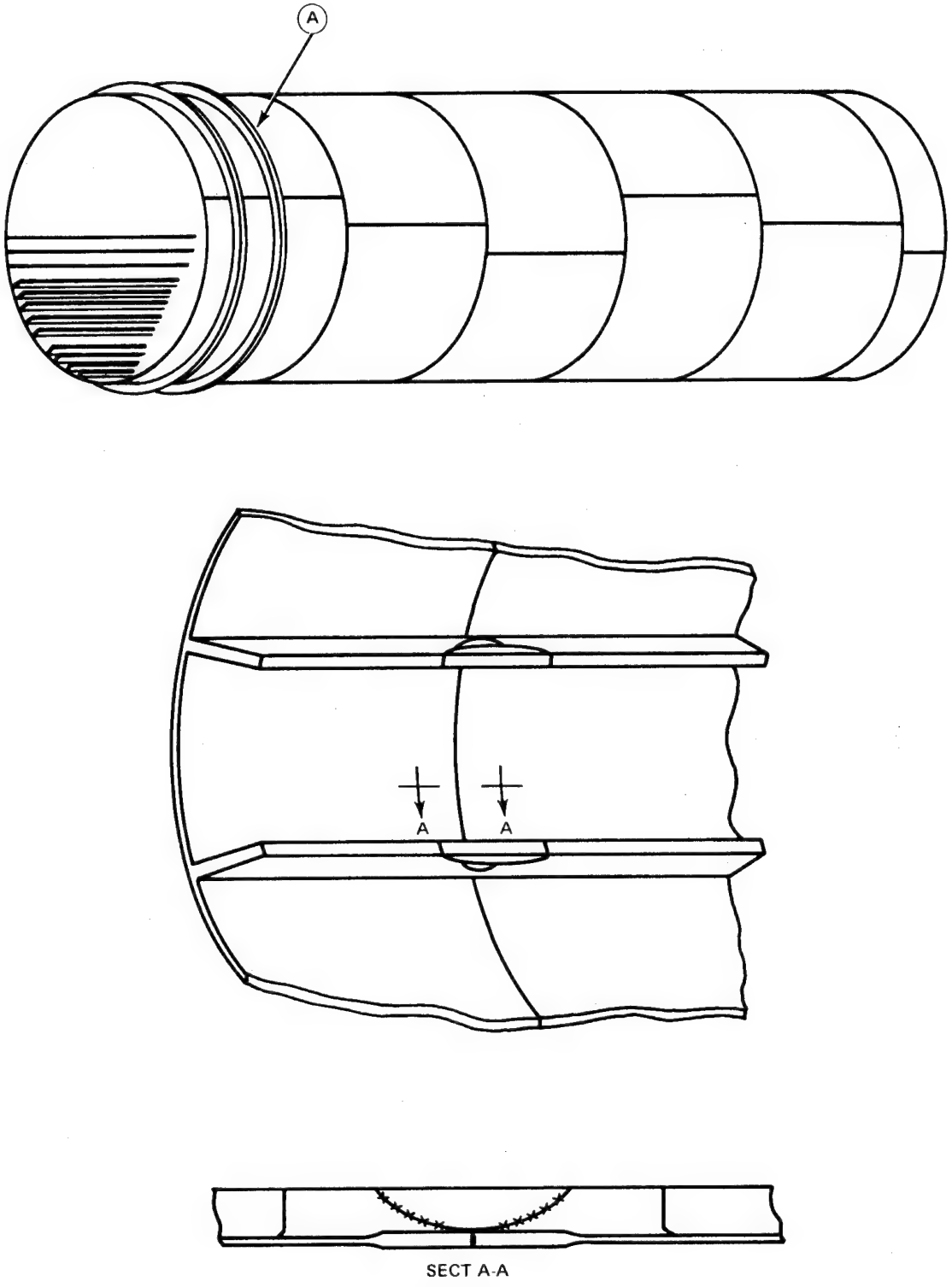

Fig. 58 Plates Rolled into Cylinders, Girth-Welded for Concept 1, Orbiter LH_2 Tank

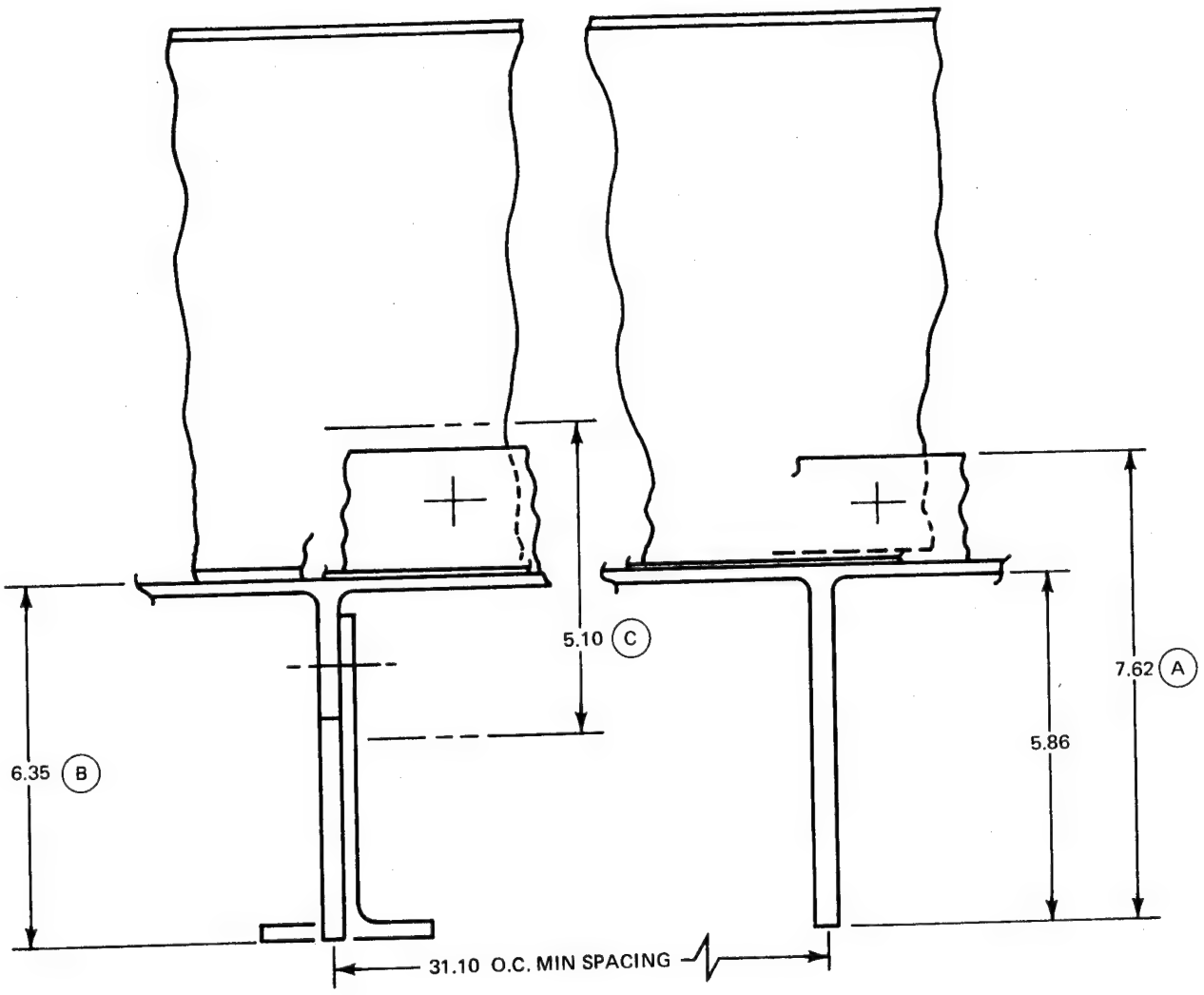

NOTE: ALL DIMENSIONS IN CENTIMETERS

Fig. 59 Alternative Machining Methods For Concept 1, Orbiter LO_2 Tank

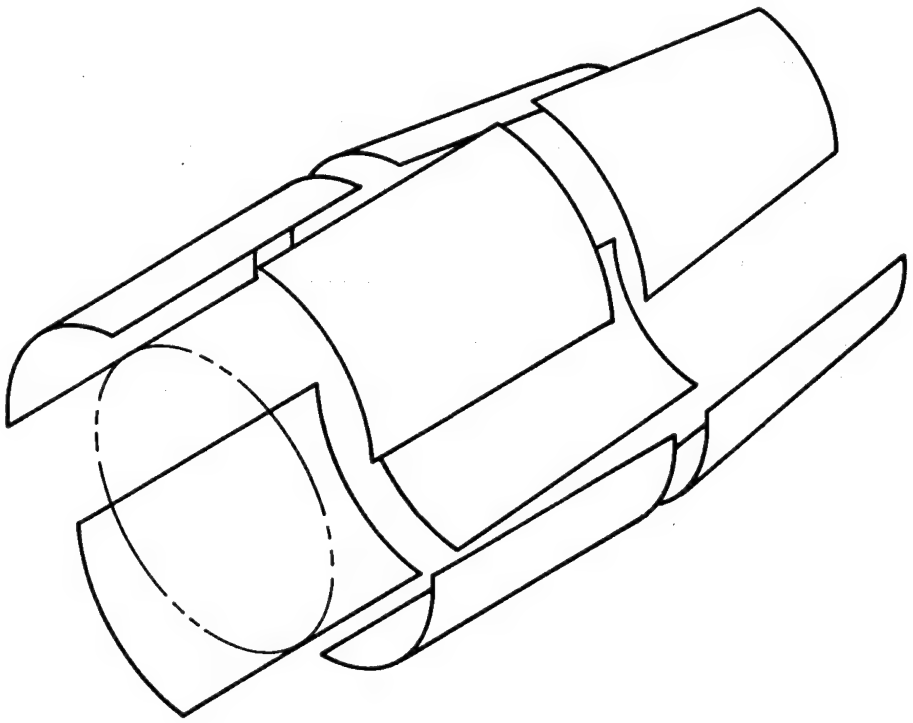

Fig. 60 Plates Rolled and Welded Longitudinally for Concept 1, Orbiter LO_2 Tank

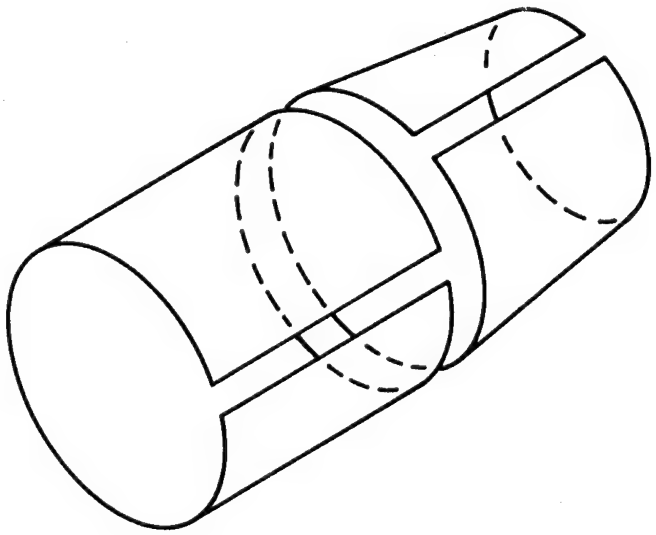

Fig. 61 Developable Surfaces Premachined in Flat for Concept 1, Orbiter LO_2 Tank

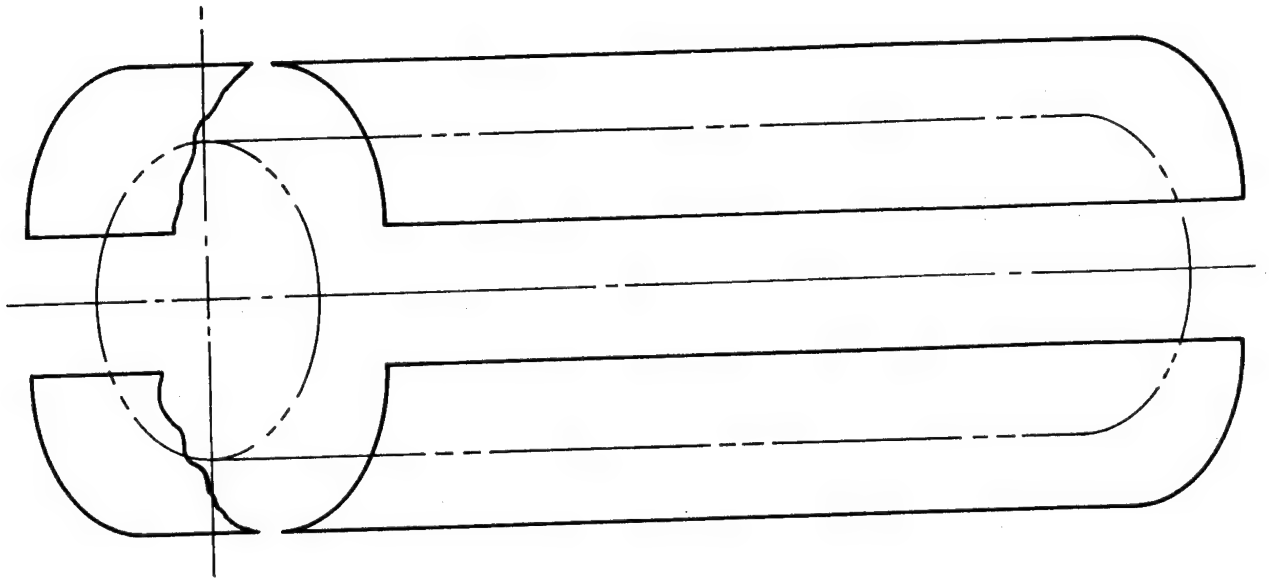

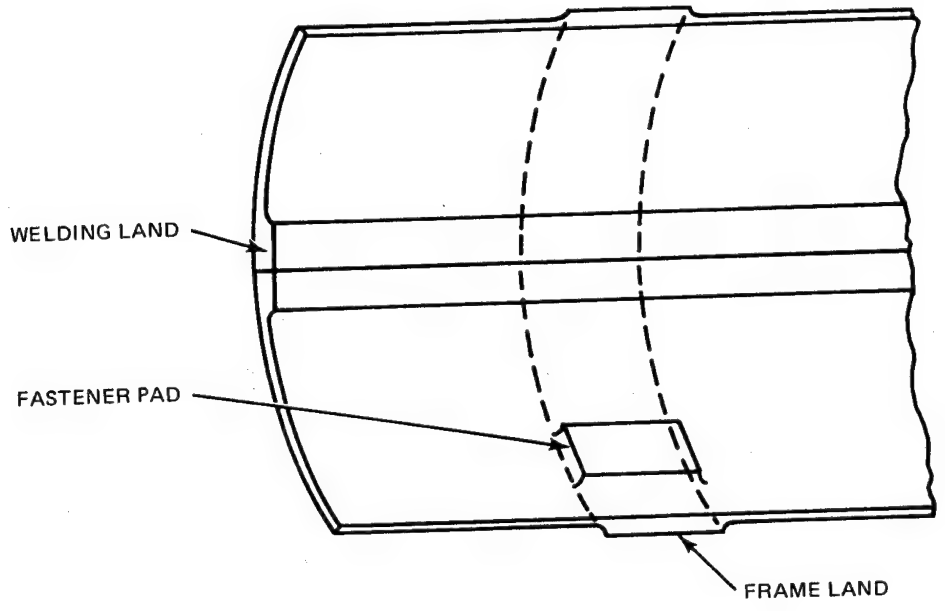

CHEM-MILLING DETAIL

Fig. 62 Plates Rolled and Welded Longitudinally for Concept 2, Orbiter LH_2 Tank

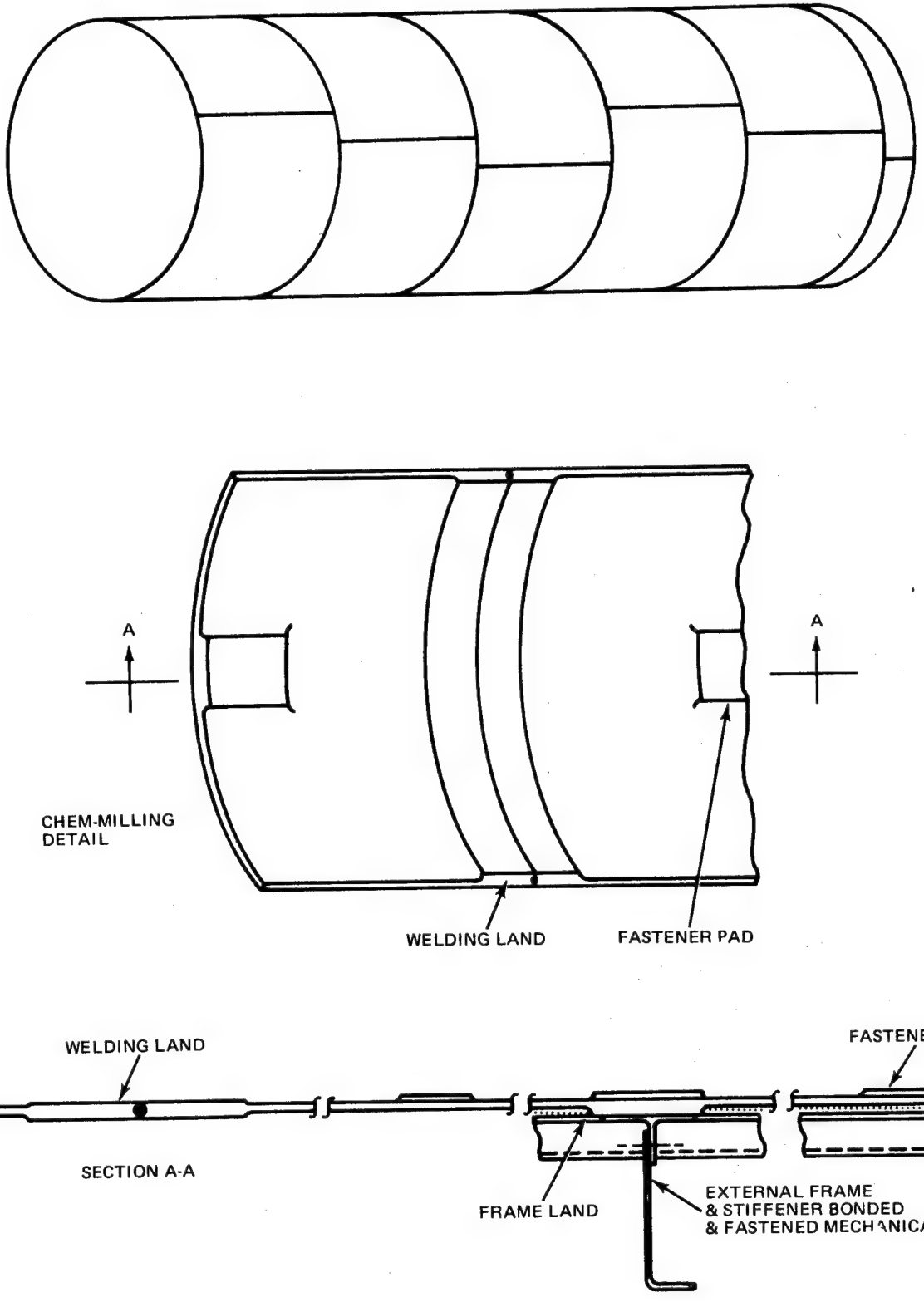

Fig. 63 Plates Rolled, Chem-Milled and Welded for Concept 2, Orbiter LH_2 Tank

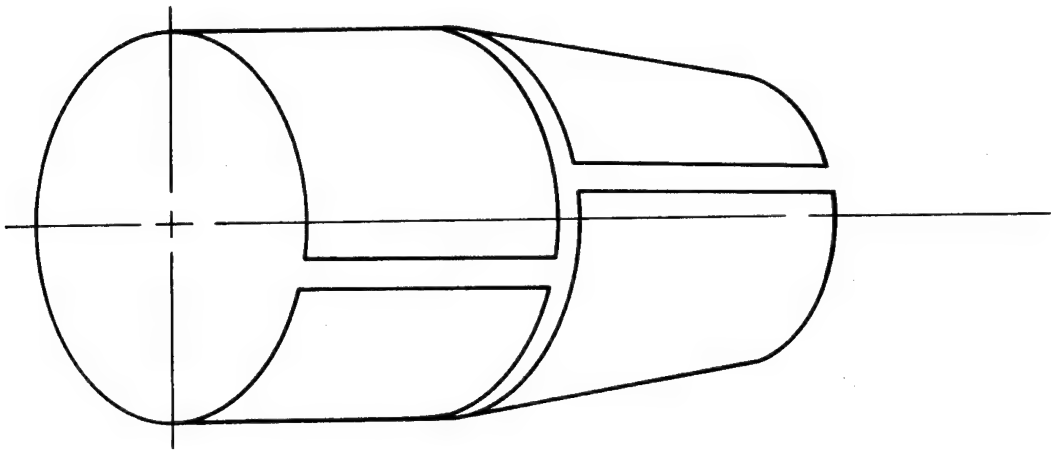

Fig. 64 Plates Rolled, Chem-Milled and Welded for Concept 2, Orbiter LO_2 Tank

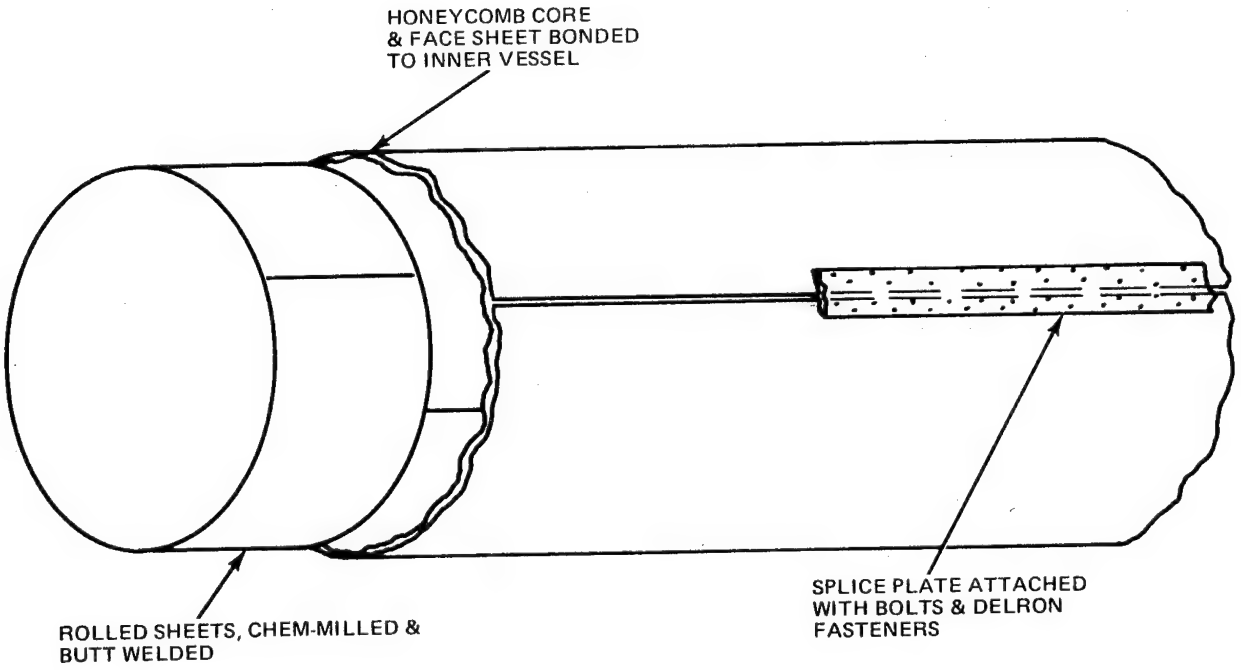

Fig. 65 Sandwich Construction, Method #1 for Concept 5, Orbiter LH_2 Tank

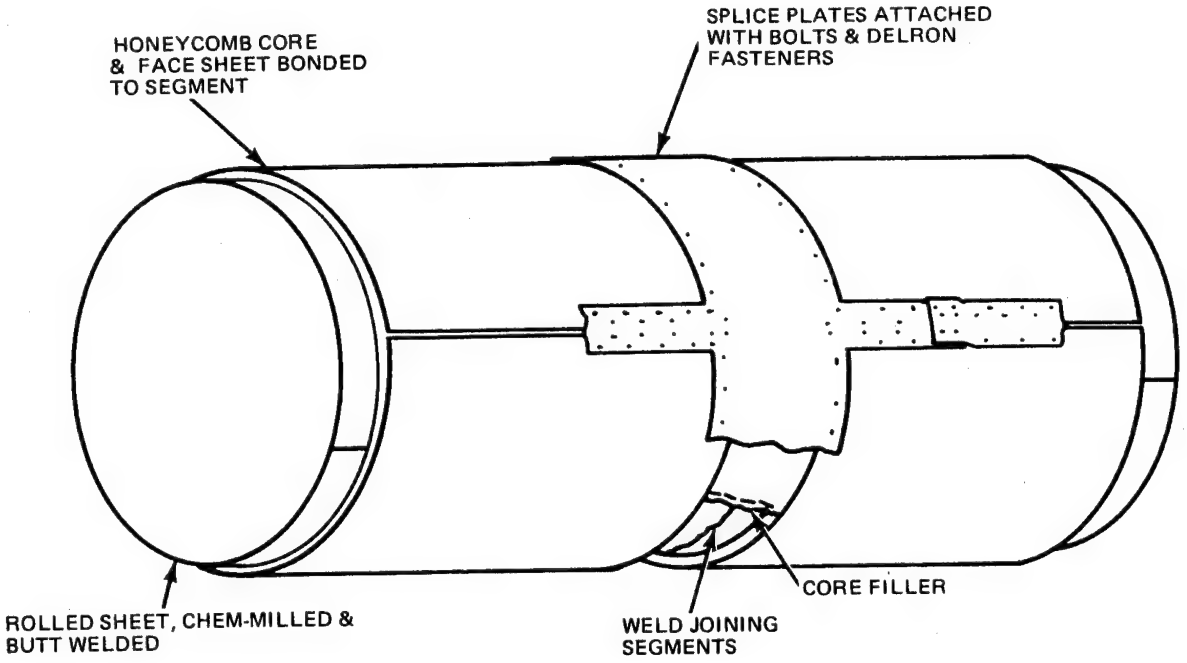

Fig. 66 Sandwich Construction, Method #2 for Concept 5, Orbiter LH_2 Tank

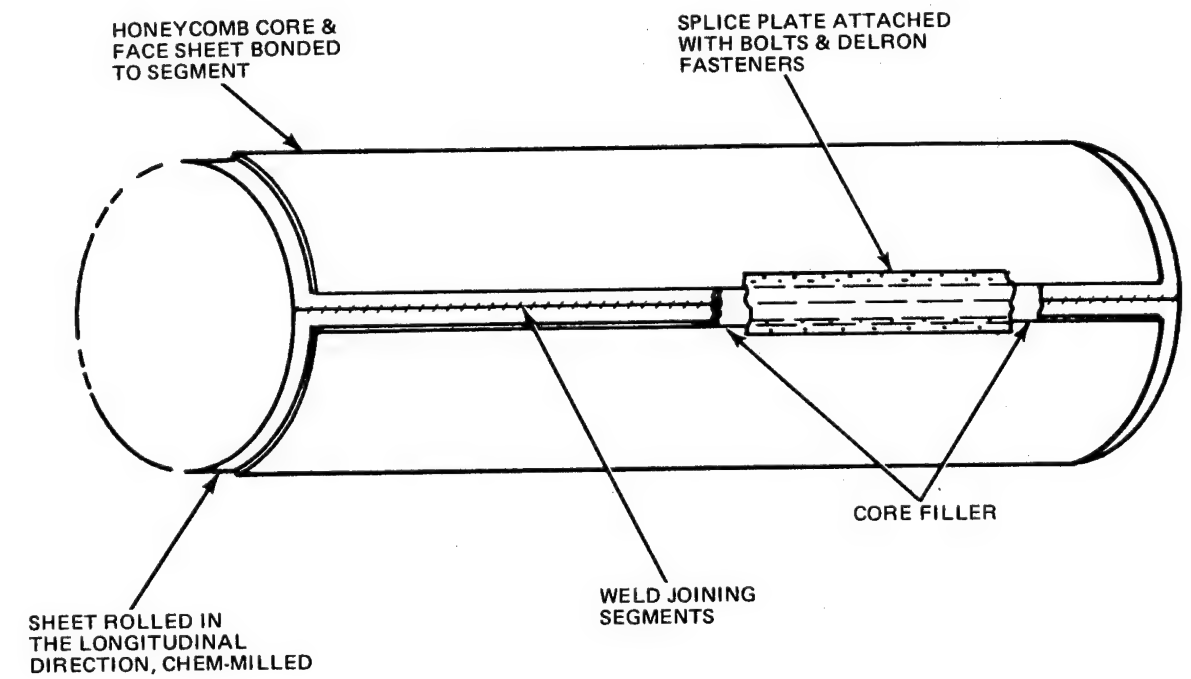

Fig. 67 Sandwich Construction, Method #3 for Concept 5, Orbiter LH_2 Tank

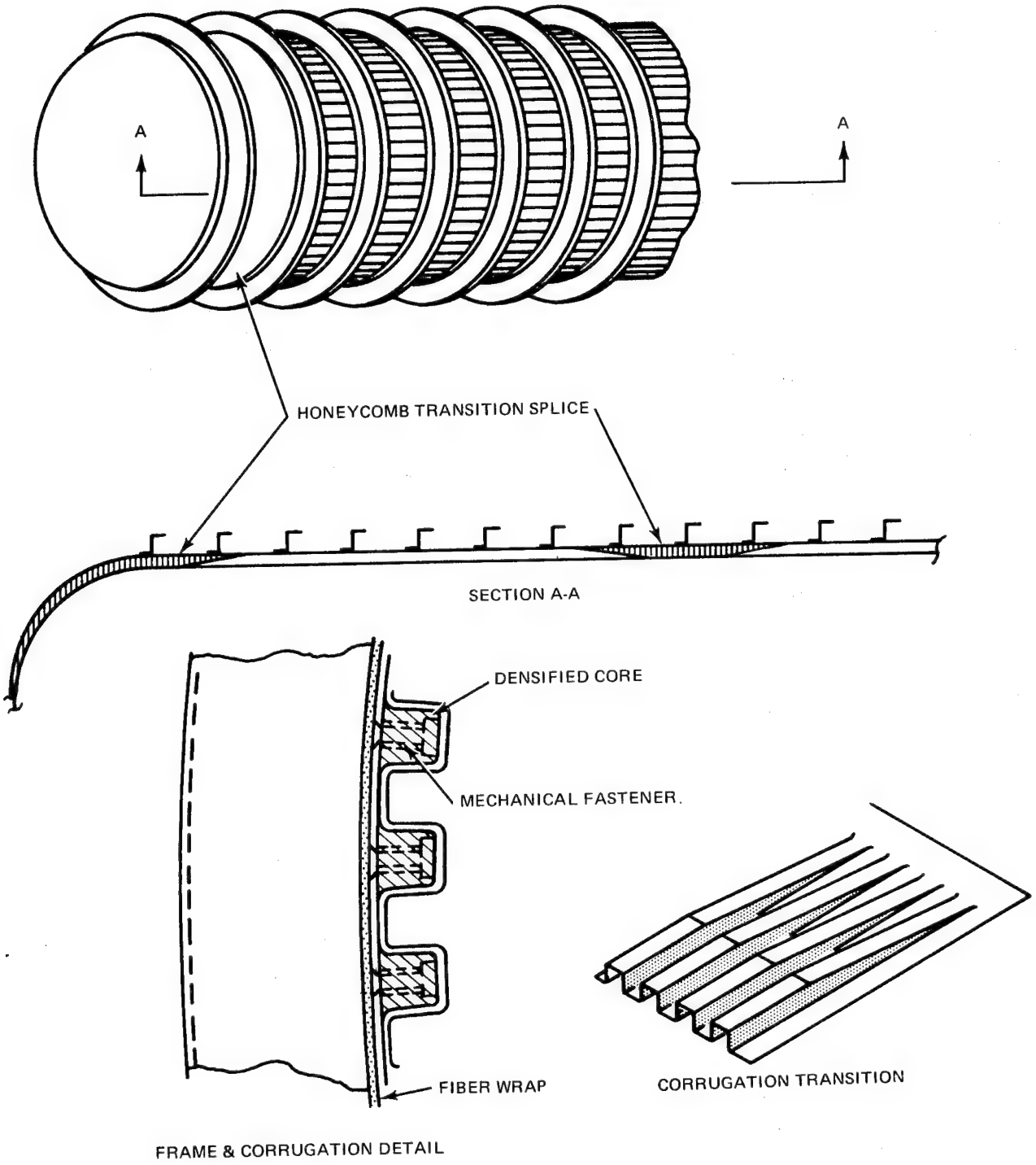

Fig. 68 Concept 6, Corrugated Sheet and Ring Frames

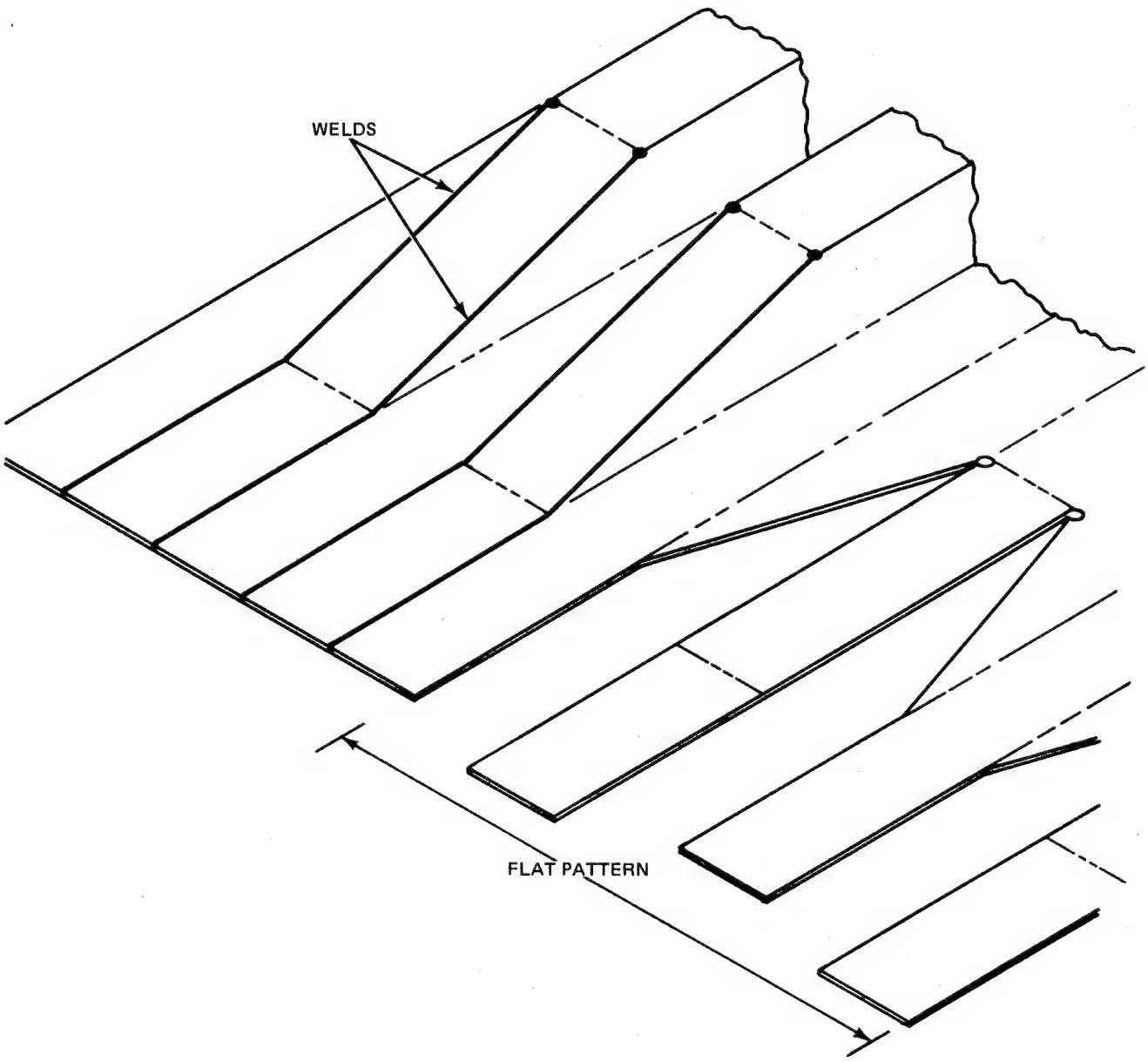

Fig. 69 Alternative Corrugation Transition

Table 37 – Orbiter LO_2 Tank, Limit Design Loading

Orbiter Station cm	Tank Radius cm	Case	Temp °K	System Pressure N/cm² Max.	System Pressure N/cm² Min.	N_θ^{**}, N/cm Max	N_ϕ, N/cm Bottom	N_ϕ, N/cm Top
1333	165	1	88	33.8	29.0	7190	2800	-
		2	88	33.8	29.0	5610	3420	-
		3	88	33.8	29.0	5610	-	3850
		4	319	13.8	10.3	566	-526	-
1650	180	1	88	33.8	29.0	9810	3070	-
		2	88	33.8	29.0	6130	3850	-
		3	88	33.8	29.0	6130	-	5260
		4	319	13.8	10.3	622	-1050	-

Case 1 End Boost
2 Max. + $q\alpha$
3 Max. - $q\alpha$
4 2 Pt Landing

* LO_2 Tank has internal insultation limiting wall temperature.

** Including Hydrostatic pressure.

Table 38 – Orbiter LH_2 Tank, Limit Design Loading

Orbiter Station cm	Tank Radius cm	Case	Temp °K	System Pressure N/cm² Max.	System Pressure N/cm² Min.	N_θ^{**}, N/cm Max.	N_ϕ, N/cm Bottom	N_ϕ, N/cm Top
2260	180	1	88	26.9	22.1	4910	-3050	2280
		4	319	13.8	10.3	613	-3330	3330
3000	180	1	88	26.9	22.1	5090	-5310	4030
		2	88	26.9	22.1	4790	-6190	7270
		3	88	26.9	22.1	4790	4210	-2980
		4	319	10.3	10.3	613	-5880	5790
3560	180	1	88	26.9	22.1	5350	-7500	5540
		2	88	26.9	22.1	4790	-8590	9360
		3	88	26.9	22.1	4790	4380	-3510
		4	319	13.8	10.3	613	-3160	3160

See Table 37 for notes.

Table 39 – Booster LO_2 Tank, Limit Design Loading

Booster Station cm	Tank Radius cm	Case	Temp °K	System Pressure N/cm² Max.	System Pressure N/cm² Min.	N_θ^{**}, N/cm Max.	N_ϕ, N/cm Bottom	N_ϕ, N/cm Top
7720	503	1	102	27.6	-	11380	7540	-2630
		2	111	17.3	-	8760	3510	-4910
		3	294	13.8	-	1753	-3860	3860
7870	503	1	102	27.6	-	12970	7670	-2770
		2	111	17.3	-	8760	3420	-5440
		3	294	13.8	-	1753		3510

Case 1 Wind load before launch
2 Off-nominal 3g initial boost
3 2 Pt landing spring back

* LO_2 tank has internal insulation limiting wall temperature.

** Including Hydrostatic pressure

Table 40 – Booster LH_2 Tank, Limit Design Loading

Booster Station cm	Tank Radius cm	Case	Temp °K	System Pressure N/cm² Max.	System Pressure N/cm² Min.	N_θ^{**}, N/cm Max.	N_ϕ, N/cm Bottom	N_ϕ, N/cm Top
4340	503	1	111	27.6	-	9110	4080	3860
		2	111	17.3	-	8760	4130	3510
		3	294	13.8	-	1753	-1930	1930
5330	503	1	111	27.6	-	9370	3750	3330
		2	111	17.3	-	8760	4280	3150
		3	294	13.8	-	1753	-4210	4210
6300	503	1	111	27.6	-	9630	3680	2840
		2	111	17.3	-	8760	4560	3140
		3	294	13.8	-	1753	-6660	6660

Case 1 Wind load before launch
2 Off-nominal 3g initial boost
3 2 Pt landing spring back

* LH_2 tank has internal insulation limiting wall temperature.

** Including Hydrostatic pressure

Table 41 – Concept 1 Structural Parameters: a) Orbiter LO_2 Tank

Orbiter Station cm	Overwrap Material	Overwrap Prestress, N/cm^2	b cm	t_{st} cm	d cm	t_w cm	t_ℓ cm	t_{eq} ** cm	Unit Weight kg/m^2
1333	PRD	69,000	30.75	.328	5.69	.0452	.144	.226	6.24
	PRD	103,400	30.75	.328	5.69	.0297	.138	.213	5.91
	S-Glass	51,700	46.75	.328	5.34	.0544	.119	.196	5.41
	S-Glass	69,000	46.75	.335	5.34	.0399	.121	.188	5.22
	Boron Alum	41,400	30.75	.328	5.69	.0483	.152	.257	7.08
	Boron Alum	55,200	46.75	.335	5.34	.0579	.124	.216	6.00
	Graphite	51,700	30.75	.328	5.69	.0549	.151	.241	6.69
	Graphite	69.000	30.75	.328	5.69	.0411	.145	.229	6.30
	Boron	41,400	30.75	.328	5.69	.0609	.138	.251	6.98
	Boron	62,100	46.75	.335	5.34	.0498	.122	.206	5.71
1650	PRD	69,000	20.80	.213	6.65	.0616	.201	.300	8.29
	PRD	103,400	20.80	.213	6.65	.0406	.190	.279	7.71
	S-Glass	51,700	31.10	.234	5.86	.0731	.167	.264	7.32
	S-Glass	69,000	31.10	.234	5.86	.0556	.164	.249	6.88
	Boron Alum	41.400	20.80	.213	6.65	.0736	.207	.346	9.56
	Boron Alum	55,200	20.80	.213	6.65	.0554	.200	.320	8.89
	Graphite	51,700	20.80	.213	6.65	.0739	.207	.318	8.78
	Graphite	69,000	20.80	.213	6.65	.0554	.200	.300	8.29
	Boron	41,400	20.80	.213	6.65	.0843	.188	.333	9.17
	Boron	62,100	31.10	.234	5.86	.0683	.168	.274	7.56

** Equivalent thickness of Aluminum

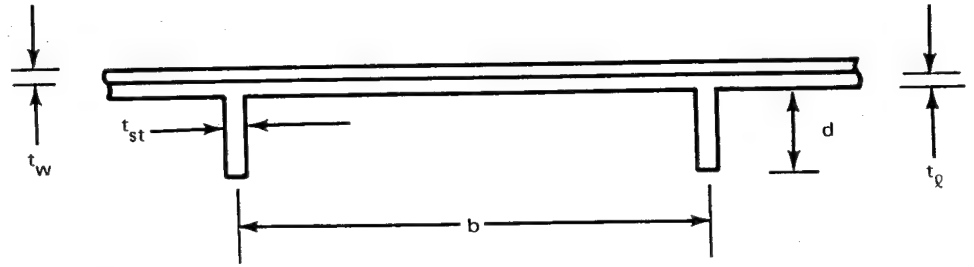

BASED ON 50.8cm RING SPACING FOR THE ORBITER, $I = 42.7cm^4$, $A = 4.24cm^2$, WITH 60.9cm SPACING FOR THE BOOSTER, $I = 606cm^4$, $A = 14.3cm^2$

Table 41 (Continued) b) Orbiter LH_2 Tank

Orbiter Station	Overwrap Material	Overwrap Prestress, N/cm^2	b cm	t_{st} cm	d cm	t_w cm	t_ℓ cm	t_{eq} cm	Unit Weight kg/m^2
2260	PRD	69,000	13.50	.429	3.71	.030	.108	.241	6.69
	PRD	103,400	13.03	.429	3.81	.027	.099	.236	6.54
	S-Glass	51,700	13.03	.429	3.81	.040	.099	.249	6.88
	S-Glass	69,000	13.03	.429	3.81	.026	.099	.241	6.69
	Boron Alum	41,400	13.03	.429	3.81	.066	.099	.287	7.91
	Boron Alum	55,200	13.03	.429	3.81	.045	.099	.264	7.32
	Graphite	51,700	13.03	.414	3.68	.048	.114	.258	7.17
	Graphite	69,000	13.03	.414	3.68	.032	.114	.249	6.88
	Boron	41,400	13.03	.429	3.81	.075	.099	.279	7.71
	Boron	62,100	13.03	.429	3.81	.040	.099	.253	6.88
3000	PRD	69,000	8.96	.429	3.78	.005	.170	.353	9.76
	PRD	103,400	↕	↕	↕	.002	↕	.352	9.72
	S-Glass	51,700	↕	↕	↕	.005	↕	.355	10.00
	S-Glass	69,000	↕	↕	↕	.005	↕	.355	9.76
	Boron Alum	41,400	↕	↕	↕	.010	↕	.360	10.14
	Boron Alum	55,200	↕	↕	↕	.007	↕	.356	9.86
	Graphite	51,700	↕	↕	↕	.012	↕	.356	9.86
	Graphite	69,000	↕	↕	↕	.007	↕	.355	9.86
	Boron	41,400	↕	↕	↕	.012	↕	.359	9.96
	Boron	62,100	8.96	.429	3.78	.007	.170	.356	9.86
3560	PRD	69,000	8.13	.447	3.94	All Metal Design	.203	.419	11.60
		103,400	↕	↕	↕		↕	↕	↕
	S-Glass	51,700	↕	↕	↕		↕	↕	↕
		69,000	↕	↕	↕		↕	↕	↕
	Boron Alum	41,400	↕	↕	↕		↕	↕	↕
		55,200	↕	↕	↕		↕	↕	↕
	Graphite	51,700	↕	↕	↕		↕	↕	↕
		69,000	↕	↕	↕		↕	↕	↕
	Boron	41,400	↕	↕	↕		↕	↕	↕
		62,100	8.13	.447	3.94		.203	.419	11.60

Table 41 (Continued) c) Booster LH_2 Tank

Booster Station cm	Overwrap Material	Overwrap Prestress, N/cm^2	b cm	t_{st} cm	d cm	t_w cm	t_ℓ cm	t_{eq} cm	Unit Weight kg/m^2
4340	PRD	69,000	20.17	.285	3.43	.0582	.188	.265	7.32
	PRD	103,400	20.17	.285	3.43	.0394	.175	.248	6.88
	S-Glass	51,700	16.32	.292	3.33	.0716	.145	.260	7.22
	S-Glass	69,000	16.32	.292	3.33	.0539	.149	.248	6.88
	Boron Alum	41,400	17.70	.302	3.48	.0811	.168	.305	8.44
	Boron Alum	55,200	16.32	.292	3.33	.0828	.142	.279	7.71
	Graphite	51,700	18.65	.285	3.43	.0741	.188	.277	7.66
	Graphite	69,000	20.16	.285	3.43	.0574	.178	.257	7.07
	Boron	41,400	17.70	.302	3.40	.1092	.152	.308	8.49
	Boron	62.100	17.70	.302	3.40	.0661	.152	.269	7.46
5330	PRD	69,000	6.43	.224	3.10	.0596	.193	.328	9.08
	PRD	103,400	6.61	.259	3.09	.0394	.178	.318	8.79
	S-Glass	51,700	11.42	.427	3.81	.0731	.150	.345	9.56
	S-Glass	69,000	11.42	.427	3.81	.0552	.152	.335	9.28
	Boron Alum	41,400	8.40	.328	3.32	.0866	.168	.378	10.50
	Boron Alum	55,200	11.42	.401	3.81	.0850	.146	.368	10.30
	Graphite	51,700	6.43	.224	3.10	.0741	.191	.340	9.43
	Graphite	69,000	6.43	.224	3.10	.0556	.186	.325	8.98
	Boron	41,400	11.42	.427	3.81	.1117	.154	.396	11.00
	Boron	62,100	11.42	.427	3.81	.0673	.156	.358	9.90
6300	PRD	69,000	6.12	.318	3.58	.0607	.198	.413	11.42
	PRD	103,400	7.39	.401	3.81	.0412	.183	.407	11.22
	S-Glass	51,700	7.72	.444	4.14	.0750	.156	.444	12.29
	S-Glass	69,000	7.72	.444	4.14	.0564	.156	.432	11.94
	Boron Alum	41,400	7.39	.401	3.81	.0848	.176	.464	12.83
	Boron Alum	55,200	7.39	.401	4.14	.0635	.176	.442	12.19
	Graphite	51,700	6.12	.318	3.58	.0775	.197	.427	11.80
	Graphite	69,000	6.12	.318	3.58	.0775	.193	.421	11.66
	Boron	41,400	7.72	.444	4.14	.1144	.159	.501	13.80
	Boron	62,100	7.72	.444	4.14	.0704	.159	.462	12.83

Table 41 (Continued) d) Booster LO_2 Tank

Booster Station cm	Overwrap Material	Overwrap Prestress, N/cm^2	b cm	t_{st} cm	d cm	t_w cm	t_ℓ cm	t_{eq} cm	Unit Weight kg/m^2
7720	PRD	69,000	15.98	.635	3.68	.0722	.234	.416	11.52
	PRD	103,400	15.74	.635	4.06	.0559	.209	.401	11.07
	S-Glass	51,700	12.71	.432	4.06	.0889	.186	.389	10.73
	S-Glass	69,000	12.71	.432	4.06	.0671	.186	.373	10.30
	Boron Alum	41,400	15.98	.635	3.68	.0912	.219	.452	12.48
	Boron Alum	55,200	12.71	.432	4.06	.0980	.183	.414	11.42
	Graphite	51,700	15.98	.635	3.68	.0922	.234	.431	12.09
	Graphite	69,000	15.98	.635	3.68	.0561	.221	.399	11.03
	Boron	41,400	12.71	.432	4.06	.1362	.188	.449	12.44
	Boron	62,100	12.71	.432	4.06	.0838	.188	.401	11.12
7870	PRD	69,000	10.32	.447	4.16	.0822	.266	.487	13.52
	PRD	103,400	8.94	.469	4.01	.0559	.244	.482	13.32
	S-Glass	51,700	8.61	.457	3.94	.1013	.211	.493	13.60
	S-Glass	69,000	8.61	.457	3.94	.0732	.216	.477	13.17
	Boron Alum	41,400	8.94	.469	4.01	.1148	.238	.561	15.51
	Boron Alum	55,200	8.38	.445	3.94	.1118	.208	.528	14.64
	Graphite	51,700	10.32	.447	4.16	.1052	.266	.506	14.00
	Graphite	69,000	10.32	.447	4.16	.0732	.264	.485	13.42
	Boron	41,400	8.61	.460	3.96	.1552	.213	.564	15.61
	Boron	62,100	8.61	.460	3.96	.0955	.213	.511	14.14

Table 42 – Concept 1, Orbiter Tanks, Wrap Stresses at P = 0 and T = 88°K

Overwrap Material	Tank	Orbiter Station cm	Overwrap Prestress N/cm^2	t_ℓ cm	t_w cm	f_ℓ N/cm^2	f_w N/cm^2
Boron	LO_2	1333	41,400	.137	.0614	6730	-14,480
	LO_2	1333	62,100	.122	.0497	6730	- 5,380
	LO_2	1650	41,400	.189	.0843	6730	-15,100
	LO_2	1650	62,100	.168	.0683	6730	- 5,380
	LH_2	2260[b] *	62,100	.292	.0990	6730	-58,600
	LH_2	2260[t] *	62,100	.083	.0340	6730	- 5,380
	LH_2	3000	62,100	.292	.0990	6730	- 5,860
	LH_2	3560	62,100	.292	.0990	6730	- 5,860
	LH_2	3560	62,100	.292	.0990	6730	- 5,860
Boron Alum	LO_2	1333	41,400	.150	.0482	6420	-19,600
	LO_2	1333	55,200	.122	.0579	4800	-10,480
	LO_2	1650	41,400	.207	.0665	8700	-13,270
	LO_2	1650	55,200	.170	.0794	4800	-10,480
Graphite	LO_2	1333	51,700	.150	.0548	1869	- 5,380
	LO_2	1650	51,700	.207	.0739	1860	- 5,380
	LH_2	All	51,700	.338	.1092	-	- 5,520

* The symbols b and t mean top and bottom points of cross-section at that station.

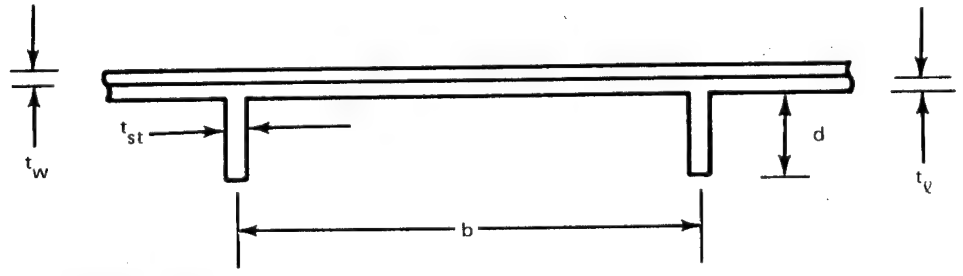

BASED ON 50.8cm RING SPACING FOR THE ORBITER, I = 42.7cm⁴, A = 4.24cm², WITH 60.9cm SPACING FOR THE BOOSTER, I = 606cm⁴, A = 14.3cm²

Table 43 – Concept 2 Structural Parameters a) Orbiter LO_2 Tank

Orbiter Station cm	Overwrap Material	Overwrap Prestress N/cm^2	b cm	t_a cm	t_{st} cm	t_f cm	b_a cm	b_{st} cm	b_f cm	t_w cm	t_ℓ cm	t_{eq} cm	Unit Weight kg/m^2
1333	PRD	69,000	44.20	.284	.137	.346	3.50	4.28	1.41	.0453	.143	.211	5.81
	PRD	103,400	44.20	.284	.137	.346	3.50	4.28	1.41	.0330	.143	.200	5.51
	S-Glass	51,700	44.80	.244	.109	.325	3.98	3.50	1.10	.0543	.119	.196	5.41
	S-Glass	69,000	44.80	.244	.109	.325	3.98	3.50	1.10	.0409	.119	.188	5.22
1650	PRD	69,000	39.50	.304	.188	.353	3.54	5.55	1.96	.0622	.201	.300	8.29
	PRD	103,400	39.50	.304	.188	.353	3.54	5.55	1.96	.0407	.201	.290	8.00
	S-Glass	51,700	41.40	.282	.157	.341	3.65	4.68	1.61	.0721	.168	.274	7.61
	S-Glass	69,000	41.40	.282	.157	.341	3.65	4.68	1.61	.0539	.168	.262	7.22
b) Orbiter LH_2 Tank													
2260	PRD	69,000	22.25	.345	.191	.353	3.62	4.53	1.69	.0406	.142	.279	7.71
	PRD	103,400	22.25	.345	.191	.353	3.62	4.53	1.69	.0203	.142	.269	7.46
	S-Glass	51,700	22.25	.345	.191	.353	3.62	4.53	1.69	.0279	.142	.279	7.71
	S-Glass	69,000	22.25	.345	.191	.353	3.62	4.53	1.69	.0203	.142	.274	7.61
3000	PRD	69,000	16.74	.338	.251	.351	3.22	5.41	2.22	All	.224	.406	11.27
	PRD	103,400	16.74	.338	.251	.351	3.22	5.41	2.22	Metal	.224	.406	11.27
	S-Glass	51,700	16.74	.338	.251	.351	3.22	5.41	2.22	Design	.224	.406	11.27
	S-Glass	69,000	16.74	.338	.251	.351	3.22	5.41	2.22	-	.224	.406	11.27
3560	PRD	69,000	13.37	.330	.236	.366	3.32	5.16	1.87	All	.285	.498	13.76
	PRD	103,400	13.37	.330	.236	.366	3.32	5.16	1.87	Metal	.285	.498	13.76
	S-Glass	51,700	13.37	.330	.236	.366	3.32	5.16	1.87	Design	.285	.498	13.76
	S-Glass	69,000	13.37	.330	.236	.366	3.32	5.16	1.87	-	.285	.498	13.76

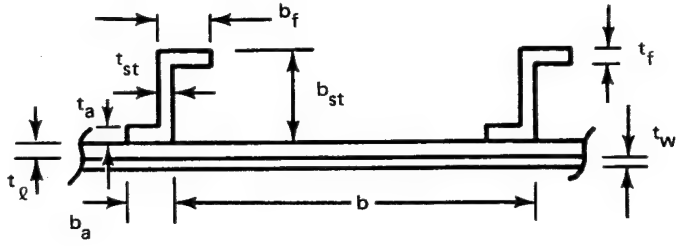

Table 43 (Continued) c) Booster LH_2 Tank

Booster Station cm	Overwrap Material	Overwrap Prestress N/cm^2	b cm	t_a cm	t_{st} cm	t_f cm	b_a cm	b_{st} cm	b_f cm	t_w cm	t_1 cm	t_{eq} cm	Unit Weight kg/m^2
4340	PRD	69,000	32.80	.312	.168	.338	2.98	4.82	1.68	.0549	.193	.287	7.96
	PRD	103,400	32.80	.312	.168	.338	2.98	4.82	1.68	.0406	.193	.279	7.71
	S-Glass	51,700	32.80	.312	.168	.338	2.98	4.82	1.68	.0436	.193	.292	8.10
	S-Glass	69,000	32.80	.312	.168	.338	2.98	4.82	1.68	.0406	.193	.290	8.01
5330	PRD	69,000	14.50	.328	.191	.330	3.15	4.49	1.76	.0620	.196	.386	10.69
	PRD	103,400	14.50	.328	.191	.330	3.15	4.49	1.76	.0441	.186	.368	10.20
	S-Glass	51,700	14.50	.328	.191	.330	3.15	4.49	1.76	.0714	.163	.373	10.29
	S-Glass	69,000	14.50	.328	.191	.330	3.15	4.49	1.76	.0526	.163	.361	10.00
6300	PRD	69,000	11.00	.322	.193	.322	3.11	4.44	1.61	.0330	.239	.462	12.73
	PRD	103,400	11.00	.322	.193	.322	3.11	4.44	1.61	.0330	.239	.462	12.73
	S-Glass	51,700	11.00	.322	.193	.322	3.11	4.44	1.61	.0330	.239	.467	13.18
	S-Glass	69,000	11.00	.322	.193	.322	3.11	4.44	1.61	.0330	.239	.467	13.18
d) Booster LO_2 Tank													
7720	PRD	69,000	17.07	.335	.219	.361	2.93	4.90	1.96	.0609	.249	.431	11.96
	PRD	103,400	18.23	.348	.234	.373	3.20	5.50	1.99	.0477	.241	.427	11.96
	S-Glass	51,700	18.50	.350	.239	.376	3.30	5.36	2.22	.0584	.234	.444	12.30
	S-Glass	69,000	18.50	.350	.239	.376	3.30	5.36	2.22	.0502	.234	.439	12.14
7870	PRD	69,000	17.07	.338	.216	.363	2.70	4.76	1.98	.0736	.279	.464	12.83
	PRD	103,400	18.78	.358	.244	.381	3.11	5.55	1.93	.0574	.277	.467	12.93
	S-Glass	51,700	17.97	.356	.236	.366	3.34	5.46	2.05	.0691	.262	.480	13.27
	S-Glass	69,000	17.97	.356	.236	.366	3.34	5.46	2.05	.0622	.262	.478	13.22

Table 44 Concept 3 Structural Parameters: a) Orbiter LO_2 Tank

Orbiter Station cm	Overwrap Material	Overwrap Prestress N/cm^2	b cm	t_{st} cm	d cm	t_w cm	t_ℓ cm	t_{eq} cm	Unit Weight kg/m^2
1333	PRD	69.000	30.75	.328	5.59	.0452	.144	.226	6.24
	PRD	103,400	30.75	.328	5.59	.0297	.139	.214	5.91
	S-Glass	51,700	46.75	.328	5.34	.0544	.120	.196	5.41
	S-Glass	69,000	46.75	.335	5.34	.0399	.120	.188	5.22
1650	PRD	69,000	20.77	.213	6.66	.0617	.201	.300	8.29
	PRD	103,400	20.77	.213	6.66	.0406	.189	.279	7.76
	S-Glass	51,700	31.13	.234	5.87	.0732	.167	.264	7.32
	S-Glass	69,000	31.13	.234	5.87	.0556	.164	.249	6.88
b) Orbiter LH_2 Tank									
2260	PRD	69,000	13.52	.429	3.71	.0300	.108	.241	6.69
	PRD	103,400	13.03	.429	3.81	.0281	.099	.236	6.54
	S-Glass	51,700	13.03	.429	3.81	.0396	.099	.249	6.88
	S-Glass	69,000	13.03	.429	3.81	.0258	.099	.241	6.69
3000	PRD	69,000	8.96	.429	3.78	.0052	.169	.353	9.75
	PRD	103,400	8.96	.429	3.78	.0021	.169	.352	9.71
	S-Glass	51,700	8.96	.429	3.78	.0052	.169	.357	9.80
	S-Glass	69,000	8.96	.429	3.78	.0048	.169	.357	9.80
3560	PRD	69,000	8.13	.446	3.94	All	.203	.419	11.61
	PRD	103,400	8.13	.446	3.94	Metal	.203	.419	11.61
	S-Glass	51,700	8.13	.446	3.94	Design	.203	.419	11.61
	S-Glass	69,000	8.13	.446	3.94		.203	.419	11.61

Table 44 (Continued) c) Booster LH_2 Tank

Booster Station cm	Overwrap Material	Overwrap Prestress N/cm^2	b cm	t_{st} cm	d cm	t_w cm	t_ℓ cm	t_{eq} cm	Unit Weight kg/m^2
4340	PRD	69,000	20.17	.284	3.43	.0582	.188	.265	7.32
	PRD	103,400	20.17	.284	3.43	.0394	.175	.248	6.88
	S-Glass	51,700	16.32	.292	3.33	.0716	.145	.260	7.22
	S-Glass	69,000	16.32	.292	3.33	.0539	.149	.248	6.88
5330	PRD	69,000	11.43	.426	3.81	.0668	.191	.366	10.10
	PRD	103,400	11.43	.426	3.81	.0394	.178	.338	9.32
	S-Glass	51,700	11.43	.426	3.81	.0607	.178	.363	10.05
	S-Glass	69,000	11.43	.426	3.81	.0483	.178	.356	9.85
6300	PRD	69,000	11.08	.432	4.06	.0668	.191	.470	12.97
	PRD	103,400	11.08	.432	4.06	.0478	.191	.460	12.74
	S-Glass	51,700	11.08	.432	4.06	.0529	.191	.475	13.13
	S-Glass	69,000	11.08	.432	4.06	.0478	.191	.472	12.84
d) Booster LO_2 Tank									
7720	PRD	69,000	16.00	.635	3.68	.0722	.234	.416	11.52
	PRD	103,400	15.76	.635	4.06	.0559	.211	.401	11.08
	S-Glass	51,700	12.71	.432	4.06	.0722	.211	.401	11.08
	S-Glass	69,000	12.71	.432	4.06	.0589	.211	.391	10.79
7870	PRD	69,000	10.32	.447	4.16	.0823	.266	.488	13.52
	PRD	103,400	8.94	.470	4.01	.0559	.244	.482	13.32
	S-Glass	51,700	8.61	.457	3.94	.1013	.211	.492	13.61
	S-Glass	69,000	8.61	.457	3.94	.0731	.216	.478	13.17

Table 45 — Concept 4 Structural Parameters

a) Orbiter LH_2 Tank

Station cm	b cm	t_a cm	t_{st} cm	t_f cm	b_a cm	b_{st} cm	b_f cm	t_b cm	t_ℓ cm	t_{eq} cm	Unit Weight kg/m^2
2260	29.85	.312	.231	.231	3.36	5.07	1.90	.0508	.208	.295	8.14
3000	16.75	.338	.251	.251	3.22	5.31	2.22	.0356	.223	.396	10.97
3560	13.38	.331	.236	.236	3.31	5.04	1.87	.0483	.284	.485	13.42
b) Booster LH_2 Tank											
4340	30.65	.297	.190	.190	3.55	5.48	1.93	.0559	.277	.356	9.84
5330	27.10	.328	.231	.231	3.34	5.41	1.99	.0483	.285	.386	10.68
6300	19.62	.346	.249	.249	3.08	5.53	2.43	.0406	.332	.485	13.42
c) Booster LO_2 Tank											
7720	26.60	.328	.246	.246	3.48	5.31	2.03	.0458	.351	.457	12.63
7870	27.50	.335	.249	.249	3.36	5.78	2.10	.0483	.391	.500	13.80

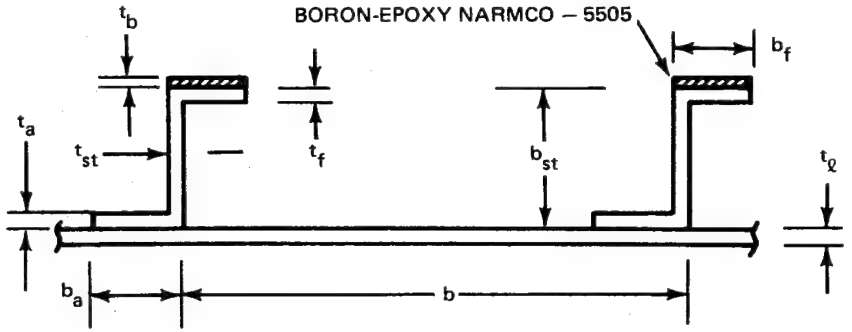

Table 46 – Concept 5 Structural Parameters, a) Orbiter LO_2 Tank

a) Orbiter LO_2 Tank

Station cm	Facing (1) Thickness cm	Core (2) Depth cm	General Instability Ncm, N/cm	Panel Instability Ncm, N/cm	Unit (3) Weight kg/m^2
1333	.221	0	980	1,180	6.10
1650	.310	0	1,760	2,120	8.58
b) Orbiter LH_2 Tank					
2260		0.955 (4)	5.380	6,780	6.05
3000	.125	1.078 (5)	10,600	14,300	8.58
3560	.160	1.078 (6)	14,110	18,460	10.48
c) Booster LH_2 Tank					
4340	.135	1.000 (7)	3,580	4,400	9.17
5330	.137	1.757 (5)	6,960	13,930	9.71
6300	.147	2.625 (8)	10,620	14,140	10.48
d) Booster LO_2 Tank					
7720	.165	1.904 (9)	10,000	11,170	11.42
7870	.188	1.860 (9)	11,070	12,470	12.63

(1) Equal Thickness 2219-T87 Aluminum Alloy Face Sheets.
(2) 2024-T81 Aluminum Alloy Honeycome Core.
(3) Includes Faces, Core, and Adhesive Bond.
(4) 30% 2.8 Density, 70% 5.0 Density.
(5) 50% 2.8 Density, 50% 5.0 Density.
(6) 60% 2.8 Density, 40% 5.0 Density.
(7) 33% 2.8 Density, 67% 5.0 Density.
(8) 83% 2.8 Density, 17% 3.5 Density.
(9) 42% 2.8 Density, 58% 5.0 Density.

Table 47 — Concept 6 Structural Parameters

a) Orbiter LO_2 Tank

Station cm	b cm	l cm	t cm	b_w cm	b_f cm	t_f cm	t_w cm	t_{wrap} cm	t_{eq} cm	Unit Weight kg/m^2
1333	.904	1.908	.102	5.64	2.37	.264	.211	.257	.444	12.50
1650	1.095	2.150	.114	6.58	2.77	.308	.246	.275	.531	14.88
b) Orbiter LH_2 Tank										
2260	1.397	2.610	.102	4.67	1.96	.219	.175	.212	.371	10.38
3000	2.040	3.120	.147	4.75	2.00	.224	.178	.215	.454	12.74
3560	3.070	4.070	.193	4.88	2.05	.229	.183	.221	.534	14.97
c) Booster LH_2 Tank										
4340	.937	1.948	.102	6.99	2.95	.328	.262	.314	.495	13.90
5330	.958	1.983	.104	7.06	2.97	.330	.264	.319	.506	14.20
6300	3.750	4.080	.188	7.14	3.00	.333	.267	.325	.597	16.73

Table 47 (Continued) — Concept 6 Structural Parameters

d) Booster LO_2 Tank

Station cm	b cm	ℓ cm	t cm	b_w cm	b_f cm	t_f cm	t_w cm	t_{wrap} cm	t_{eq} cm	Unit Weight kg/m^2
7720	1.517	2.640	.140	7.46	3.12	.350	.279	.339	.589	16.54
7870	1.540	2.710	.142	8.28	3.48	.389	.310	.378	.663	18.59

NOTE: Includes hydrostatic pressure.

Based on 25.4 cm ring spaceing for the orbiter and 30.5 cm ring spacing for the booster.

No flight loads were included in ring sizing.

Weight of local reinforcement of honeycomb and bond at ring-corugation intersection not included.

Local bending of ring flanges by corrugations not included.

Weight of corrugation to corugation or corrugation to end dome splices not included.

Rings overwrapped with S-Glass at 69,000 N/cm^2.

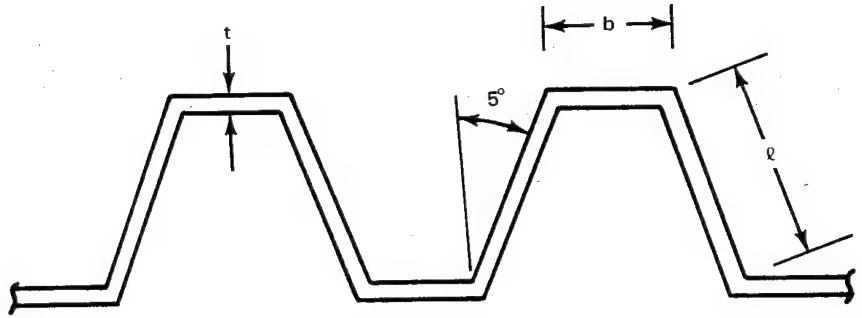

CORRUGATED WALL

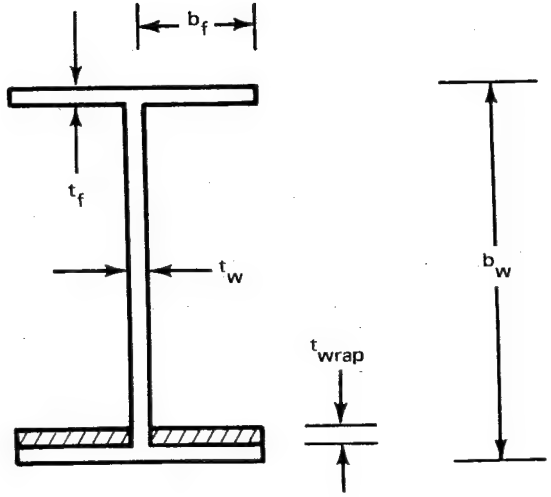

RING CROSS SECTION

Table 48 Uniaxial Filament-Wound Composite Material Properties for Use in Parametric Study of Filament Overwrapped Tanks

PROPERTY	BORON/ EPOXY	HTS GRAPHITE/ EPOXY
FILAMENT		
ULTIMATE STRENGTH, N/cm^2	276,000	241,000
ELASTIC MODULUS, N/cm^2	40×10^6	24×10^6
DENSITY, g/cm^3	2.60	1.80
COMPOSITE		
FILAMENT FRACTION IN COMPOSITE, VOL %	55	60
DENSITY, g/cm^3	1.99	1.49
LONGITUDINAL MODULUS, N/cm^2		
450°K	22.0×10^6	14.5×10^6
297°K	22.0×10^6	14.5×10^6
78°K	22.0×10^6	15.9×10^6
LONGITUDINAL TENSILE ULTIMATE STRENGTH, N/cm^2		
450° K	116,000	106,000
297° K	138,000	124,000
78° K	160,000	103,000
LONGITUDINAL TENSILE OPERATING STRESS(2), N/cm^2		
450° K	77,200	70,300
297° K	91,700	82,700
78° K	106,900	69,000
COEFFICIENT OF THERMAL EXPANSION, μ/° K		
297 to 78° K	2.39	0.20
297 to 450° K	4.5	0.20
78 to 450° K	—	0.20

NOTES:

(1) ASSUMED VALUE BASED ON 1.5 SAFETY FACTOR

(2) ALL OPERATING STRESSES ARE BASED ON ZERO-STRESS TO FULL-OPERATING-STRESS CYCLIC LOADING, WHICH IS CONSERVATIVE.

Table 49 – Concept Costs

a) Orbiter LH_2 Tank

Concept	Overwrap Material	Basic Tank		Overwrap		Total		Cost*
		Non-Recur $/m^2	Recur $/m^2	Non-Recur $/m^2	Recur $/m^2	Non-Recur $/m^2	Recur $/m^2	7 Tanks $/m^2
Baseline	-	8,580	1,000	-	-	8,580	1,000	15,580
1a	S-Glass	8,570	754	840	194	9,410	948	16,050
1a	PRD	8,570	754	840	216	9,410	970	16,200
1b&c	S-Glass	8,570	754	840	194	9,410	948	16,050
1b&c	PRD	8,570	754	840	216	9,410	970	16,200
2	S-Glass	4,210	603	775	194	4,985	797	10,560
2	PRD	4,210	603	775	205	4,985	808	10,640
3	G-Glass	8,500	754	840	205	9,340	959	16,050
3	PRD	8,500	754	840	226	9,340	980	16,200
4	-	5,590	797	-	-	5,590	797	11,170
b) Orbiter LO_2 Tank								
Baseline	-	12,000	1,370	-	-	12,000	1,370	21,590
1a&c	S-Glass	12,160	1,240	1,160	258	13,320	1,498	23,810
1a&c	PRD	12,160	1,240	1,160	291	13,320	1,531	24,040
1b	S-Glass	12,160	1,240	1,060	248	13,220	1,488	23,640
1b	PRD	12,160	1,240	1,060	280	13,220	1,520	23,860
2	S-Glass	11,580	570	1,030	258	12,610	828	18,410
2	PRD	11,580	570	1,030	291	12,610	861	18,640
3	S-Glass	11,470	1,640	1,150	269	12,620	1,909	25,980
3	PRD	11,470	1,640	1,150	302	12,620	1,942	26,210

* Non-Recur + 7x Recur

Table 50 — Summary of Unit Weights

Tank	Station, cm	Concept Unit Weights, kg/m^2						
		Baseline	#1	#2	#3	#4	#5	#6
Orbiter LO_2	1333	7.91	5.22*	5.22*	5.22*	-	6.10	12.50
Orbiter LO_2	1650	10.40	6.88*	7.22*	6.88*	-	8.58	14.88
Orbiter LH_2	2260	7.31	6.69**	7.60*	6.69**	8.14	6.05	10.38
Orbiter LH_2	3000	9.71	9.71**	11.27***	9.71**	10.97	8.58	12.74
Orbiter LH_2	3560	11.61	11.61***	13.76***	11.61***	13.42	10.48	14.97
Booster LH_2	4340	10.05	6.88*	7.95**	6.88*	9.84	9.17	13.90
Booster LH_2	5330	10.49	9.07**	10.00*	9.84*	10.68	9.71	14.20
Booster LH_2	6300	11.17	11.32**	12.74**	12.97**	13.42	10.48	16.73
Booster LO_2	7720	11.81	10.30*	11.96**	10.79*	12.63	11.42	16.54
Booster LO_2	7870	13.23	13.18*	12.83**	13.18*	13.80	12.63	18.59

* S-Glass overwrap at 69,000 N/cm^2

** PRD overwrap at 103,400 N/cm^2

*** All metal design

Table 51 – Summary of Costs and Weights

Concept / Tank	Cost/Weight, $/m^2 (7 Tanks)/kg/m^2						
	Baseline	#1	#2	#3	#4	#5	#6
Orbiter LO_2	21,590 / 9.15	23,860 / 6.05	18,530 / 6.22	26,100 / 6.05	- / -	- / 7.34	- / 13.69
Orbiter LH_2	15,540 / 9.54	16,125 / 9.34	10,610 / 10.88	16,125 / 9.34	10,570 / 10.84	- / 8.37	- / 12.69
Booster LH_2	- / 10.57	- / 9.09	- / 10.23	- / 9.89	- / 11.31	- / 9.79	- / 14.94
Booster LO_2	- / 12.52	- / 11.74	- / 12.39	- / 11.99	- / 13.21	- / 12.02	- / 17.56

Note: Weights are average of station weights.
Costs are average of station fabrication costs.

APPENDIX B

EXPERIMENTAL EVALUATIONS - ORIGINAL PROGRAM EFFORT

SUMMARY

Experimental work was undertaken to develop data supporting the tank design evaluation. Areas identified as needing evaluation, and experimental plans, are summarized below:

Filament-Winding Prestress Levels

Maximum reliably-achieved filament-winding prestress levels limit the weight saving by this technique. Data were developed for S-901 glass, PRD-49-III, Courtauld's HTS graphite, and boron filaments.

Bond Strength to Resist Buckling and Effect of Debond of Overwrap

For efficient overwrapped metal tank operation, high residual filament tension and moderate metal compression must be established during fabrication. It was presumed that metal shell buckling due to the constrictive wrap stresses would be precluded by adhesive bonding the metal shell to the overwrap. With the high shell diameter/thickness ratios of the Shuttle low-pressure tankage, the presence of minor imperfections could lead to buckling. Evaluations were conducted to confirm the capability of the bond to resist buckling, using subscale overwrapped cylinders with and without intentional debonds.

Stringer Attachment

The cost saving of using bonded-on instead of integral stiffeners is attractive. A demonstration was conducted showing that metal stringers can be attached to the outer surface of a composite reinforced shell by a combination of bonding and intermittent mechanical fastening, and that this assembly is structurally effective in resisting compressive loading.

DISCUSSION

Filament-Winding Prestress Levels

Maximum filament-winding prestress levels and tolerance levels were determined for the candidate filament reinforcements. The breaking stress as a function of winding speed was determined from tests in triplicate. The filament winding load was adjusted conventionally as follows. The low-tension filament left its braked spool, slipped around a fixed capstan, and was taken up at a much higher tension on the winding mandrel. By varying the braking torque at the spool, the filament tension measured by a load cell near the winding mandrel was adjusted to the desired value. The breaking strengths were measured at a series of about 7 winding speeds up to about 60 m/minute. The strengths were generally higher at lower winding speeds and for prepreg over in-process impregnated fibers.

The filamentary reinforcements evaluated were the following:

- S-901 glass /20-end roving
  - Preimpregnated with resin — Fig 70 shows fiber breaking strengths 100 to 169 kN/cm^2
  - Dry roving in-process impregnated with resin — Fig 71, for 20 ends, shows fiber breaking strengths 75 to 100 kN/cm^2; Fig 72, for 12 ends, shows fiber breaking strengths 58 to 100 kN/cm^2
- PRD - 49 - III 12-end yarn
  - Preimpregnated with resin — Fig 74 shows fiber breaking strengths 112 to 171 kN/cm^2
  - Dry yarn-in process impregnated with resin — Fig 73 shows fiber breaking strengths 110 to 148 kN/cm^2
- Courtauld's HTS graphite tow
  - Preimpregnated with resin — Fig 75 shows fiber breaking strengths 54 to 90 kN/cm^2
- Boron filament

  Preimpregnated, 3.2 mm-tape of .1 mm dia filaments — Fig 76 shows fiber breaking strengths 52 to 262 kN/cm^2

In conclusion, the recommended values for design, shown in Table 52, are above the minimum of the range of experimental test results, for each material. The justification for using these values and anticipating few failures during winding are twofold. First, it is presumed that the lowest observed values were associated with the extra handling inherent in a test program. Second, in production, less abusive fiber tensioning systems would permit safe higher tensions. It is seen in Table 52 that, at 60 m/minute max winding speed, the winding tension as a percent of (RT) single cycle design ultimate tensile strength ranges from 55% for S-901 glass and boron prepregs to 72% for PRD-49 prepreg and 38% for HTS graphite prepreg.

Bond Strength to Resist Buckling and Effect of Debond of Overwrap

Bond Strength to Resist Buckling - The Shuttle's low-pressure, cryogenic propellant tanks have walls of high diameter-to-thickness (D/t) ratio. When weight of the tankage is reduced by utilizing filament overwrapping of an inner high strength metal shell to carry part of the hoop load, the metal shell's thickness is further reduced. For efficient overwrapped metal tank operation, an initial prestress must be set up during fabrication, in which the filaments are in tension and the metal in compression. Insurance against metal shell buckling due to constrictive wrap compressive stresses is critical for cylinders of high D/t ratio.

Work reported in References 34 and 35 established a design approach and criteria for overwrapped metal tanks with load-bearing, non-buckling liners. Figures 77 and 78 give corresponding constrictive wrap buckling strengths for cylindrical metal tubes not bonded to the overwrap.

Shuttle propellant tanks, because of their low operating, proof, and burst pressures, have high D/t's for the membrane ranging from 1200 to 3000. The corresponding allowable constrictive wrap buckling strengths, based on the criteria of Figures 77 and 78, for these high D/t's are in the range of 70 to 700 N/cm^2. Such low compressive stress allowables are incompatible with the weight-saving prestress needed in the tank wall at cryogenic operating conditions. Bonding between the metal shell and overwrap can however reduce the tendency of the shell to buckle and is therefore mandatory for vessels of high D/t ratio.

The efficiency of bonding to prevent constrictive wrap buckling of non-structural liners has been demonstrated on several NASA programs (References 36 to 43). SCI had used adhesive bonding of the liner to the overwrap to keep thin low-strength aluminum liners with D/t of 1200 from buckling during pressure cycling over a 1 to 2% strain range (Reference 44). It should be noted that this work was conducted with thin (.025 cm) liners overwrapped with 0.192 cm of hoop wound glass composite, whereas the large propellant tanks of interest have a reversed thickness ratio. (On a typical case, the aluminum membrane might be .31 cm thick and the hoop winding, .10 cm thick. Another distinction is that the previous aluminum liner was weak and yielded on each application and on each release of operating pressure. For the large cryotankage, yielding is not permissible at operating or zero pressure conditions.

A thin 2219 aluminum shell, approximating the D/t ratio of the expected Space Shuttle full-sized tankage, was overwrapped with glass filament/epoxy resin composite material under high tension to induce a relatively high compressive residual prestress in the circumference of the aluminum shell. The primary purpose of this work was to verify that, because of the bonding of the composite to the shell, the aluminum could withstand the external radial pressure developed without buckling. The significance of this verification would be that lightweight tanks could be designed and fabricated using the bond to prevent buckling of the strong elastic metal shell of high D/t ratio.

The 30.5 cm.-dia. 2219-T62 aluminum shell of 0.025cm wall thickness was fabricated in accordance with the design shown in Figure 79 and circumferentially overwrapped in accordance with Figure 80 (-2 configuration). The .038cm.-thick overwrap was S-901 glass with a modified epoxy especially suited for cryogenic application. Prior to application of the overwrap, two pairs of strain gages were mounted on the aluminum cylinder to monitor the shell through fabrication and cryogenic testing. The location of the gages is shown in Figure 81.

The design objective was to provide enough composite material at a tension that would produce a compressive circumferential stress in the aluminum of about 19.0 kN/cm^2 at room temperature with no externally applied load, as shown in the design stress-strain relationships of Figure 82. Because of the high diameter-to-thickness ratio of the shell (D/t = 1200), it was necessary to provide internal support to the aluminum shell during the winding operation to avoid collapse. The support was obtained by filling the shell with oil and providing hydrostatic pressure. The shell internal pressure was held at 27.6 N/cm^2 during application of the first layer of overwrap and then increased to 57.9 N/cm^2 for application of the second layer. The pressure was maintained throughout the cure cycle of the composite. The wraps were applied at about 105N/20-end-roving (composite stress =25.9 kN/cm^2) and 100N/20-

end (composite stress = 24.4 kN/cm^2 for the first and second layers respectively. Analytically, at the end of winding, with internal pressure of 57.9 N/cm^2, this results in a uniform stress of 24.5 kN/cm^2 in the overwrap and approximately zero circumferential stress in the shell. Considering the slight variation of the actual winding pattern used vs the design value and the effects of the axial strength of the wrap (not considered in initial design), the attained aluminum compressive prestress at the completion of fabrication at zero internal pressure should have been 21.7 kN/cm^2.

Calculations were made to determine the stresses at various fabrication steps. Data from these calculations and measured values are contained in Tables 53 and 54. The net result of the measured values is the indication that the attained compressive prestress was significantly lower than the desired 19.0 kN/cm^2. The value achieved was probably between 6.7 and 12.2 kN/cm^2 compression. From the plot of buckling stress vs D/t shown in Figure 78, based on actual data from previous programs, the unbonded shell would have buckled at a compressive stress on the order of 655N/cm^2.

After fabrication, the tank was subjected to 12 thermal shock cycles from room temperature to 78^{o}K by submerging it in liquid nitrogen. No evidence of debonding or liner buckling was noted during the entire test.

It can be concluded that:

(1) A thin and strong metal cylinder with a well-bonded, tensioned filament overwrap can sustain high levels of circumferential compressive stress without buckling. The critical compressive stress level is significantly higher than the constrictive wrap buckling stress of a cylinder with unbonded overwrap.

(2) No debonding occurred between the overwrap and aluminum, demonstrating bond strength adequacy for filament-reinforced 2219 aluminum cylinder fabrication and cryogenic thermal shock exposure.

(3) Design calculations showed that even under the most severe temperature change, between 297^{o}K and 78^{o}K, the aluminum would remain in compression.

(4) No relaxation of the applied prestress occurred during the testing, as seen from the repeatability of the strain-gage data.

(5) The techniques used for prestress application to the glass filament overwrapped 2219 aluminum tank covered by this report were not adequate to provide the desired load because of variables not considered in the initial design analysis. The most important of these was the biaxial yield criterion in the metal. Hydraulic pressure introduced an undesired longitudinal tensile stress, which in combination with hoop compression caused yielding to occur during the cure cycle.

(6) Desired prestress levels can be obtained in overwrapped shells providing mechanical support (rather than hydrostatic support) is used as a mandrel.

(7) Strain gages located properly on the metal shell can be used to measure the effects of the overwrap through the various stages of fabrication and testing. These gages must be monitored at all stages of fabrication including cure if the data obtained is to be useful.

The following recommendations can be made:

(1) To reduce fabrication variables, a rigid mandrel should be used in place of the hydrostatic mandrel.

(2) Strain gages should be located in areas that are unaffected by the domes, welds, weld lands, or surface irregularities, in order to attain as near membrane conditions as possible.

(3) The strain gages should be monitored during all stages of fabrication, including cure.

(4) The resin should be treated in such a manner as to reduce migration during any portion of the fabrication procedure.

Effect of Local Debond of Overwrap

Because the metal strains in a stiffened pressure vessel are variable hoopwise as one crosses a stiffener, while the fiber strains try to remain constant, a mismatch in strains tends to occur. If mismatch does occur, debonding will precede it. To simulate the effect of such local debonding on the buckling resistance of a bonded constrictively wrapped liner, the following test was conducted. A glass-filament overwrapped 2219 aluminum cylinder with built-in "debonds" was designed, fabricated and tested. The tank configuration is the same as the tank described in the preceding section except that intentional delaminations were built-in along the length of the cylinder. The design is shown in Figure 80 (-1 configuration).

To create the debonds, .25 cm-wide Teflon strips of full cylinder length were placed at 2.5 cm intervals around the circumference except at the strain-gage locations. (See Fig 83.) The unit was then exercised repeatedly with internal pressure with and without overwrap. Initially, measured strain gage data deviated from predicted values. With continued cycling, data converged near to predictions, indicating that the cylinder was initially out of round and some "shaking-down" was required to prepare the unit for the planned evaluation. Dry filament overwrapping indicated that applied pretension was about 80% effective in inducing design prestress into the cylinder. This information was used in adjusting winding parameters for final test vessel fabrication.

The debonded cylinder was filament overwrapped with stresses reasonably close to design values. During cure, some changes occurred in axial strain gage readings. (No metal yielding was predicted from uniaxial stress considerations at the cure temperature). When internal pressure was relieved after curing, gages were linear to zero pressure, behaving as predicted.

No delamination, liner buckling or wrinkling, or change of test specimen appearance was noted when pressure was reduced to zero after curing. The unit was subjected to five thermal shock exposures by immersion in LN_2. No debonding or change in the test specimen appearance was observed.

The conclusion to be derived is that local debonding at stiffeners will not adversely affect the buckling resistance to constriction overwrap provided by bonding the fibers to the cylinder.

Stringer Attachment

One of the important cost saving design concepts, Concept 2, was the use of bonded-on stiffeners to replace integral ones. The adequacy of this bond, aided by end mechanical attachments to prevent "zippering" of the bond-line, had to be confirmed.

A test panel was constructed to test the concept and the fabrication details. A .160 cm-thick, 2024-T81 aluminum flat plate represented the tank wall. A unidirectional S-901 glass/epoxy layer .051 cm. thick, simulating the hoop overwrap, was placed in a direction normal to the applied compressive load. (An identical composite-layer was placed on the opposite metal face to avoid curling of the sheet during and after bonding.) Five equidistant 2024-T62 aluminum zee-stiffeners were bonded to the plate along their entire (cm) lengths and, in addition, bolted at their ends and mid-points. Shop-details of the panel design are shown in Fig 84. Shop strain gage locations are shown in Fig 85.

Highlights of the fabrication steps used are as follows:

Metal Components - The metal hardware components for the assembly were fabricated separately and then match drilled as an assembly prior to any other operations. As any piece of the hardware was required, it was chemically cleaned with paste cleaner and then primed to provide a suitable bonding surface.

Glass/Epoxy Composite - The glass/epoxy composite, which simulates the hoop wrap on the tank, was prepared by winding dry glass roving on a cylindrical mandrel, impregnating the glass with the resin system and then staging the resin system to an appropriate condition for handling. Single plies of the sizes required were then cut from this prepreg.

Component Fabrication - A scrim-supported adhesive film was applied to the prepared aluminum panel surfaces (front and back). The glass/epoxy prepreg plies were positioned. The aluminum bearing strips were laid in position. Using the pre-drilled holes for positioning, aluminum caul plates were bolted to both sides of the panel. This assembly was vacuum-bagged and cured. After appropriate preparation of the surface where the stringers were to be bonded, a new adhesive film was applied to the panel. The prepared Z-shaped stringers were bolted in place with a bearing bar (tooling) to provide pressure along the entire bonding surface. This assembly was then cured. After cure, the bearing bars were removed and the bolts replaced. Potting compound, aluminum-filled epoxy, 2.54 cm. deep, was added to the panel at the loading ends. The loading ends were then machined flat, square, and parallel. To ensure as uniform loading conditions as possible, the panel was mounted in the loading press and additional potting compound was cast at the base.

Testing was carried out in a universal testing machine. The ends of the test panel were potted to assure uniform application of compressive load. Load was applied in increments of 1360 kg. and strain gage readings were taken at each increment. Details of the test up are shown in Fig 86. Fig 87 and Table 55 give strain vs. applied load data.

Initial buckling was observed at a load of 11,340 kg, or a gross section stress of 13.1 kN/cm^2. An analysis, which did not include the effect of the glass layer, pre-

dicted elastic buckling of the sheet between stiffeners at a stress of 13.1 kN/cm^2 or essentially the test value. The ultimate stress prediction was approximately 23.2 kN/cm^2. This value is approximate since the analysis was performed using MIL HDBK 5A "A" material properties, which are minimum guaranteed properties, while the test panel may exhibit typical material properties (15% higher than the minimum). Failure occurred at an ultimate load of 21,800 kg. This corresponds to a gross section stress of 25.2kN/cm^2. Predicted failure was buckling of the free flange of the zee stiffener due to torsional instability. The failure mode of the test specimen was buckling of the unsupported flange and web at mid-span of the panel. No delamination occurred until ultimate load was reached, and then only locally at the point of the stiffener buckle (see Fig 88).

This test was considered fully successful in demonstrating the bonded attachment of the longitudinal stiffener and lends confidence to full-scale testing of a comparable concept for an actual vehicle.

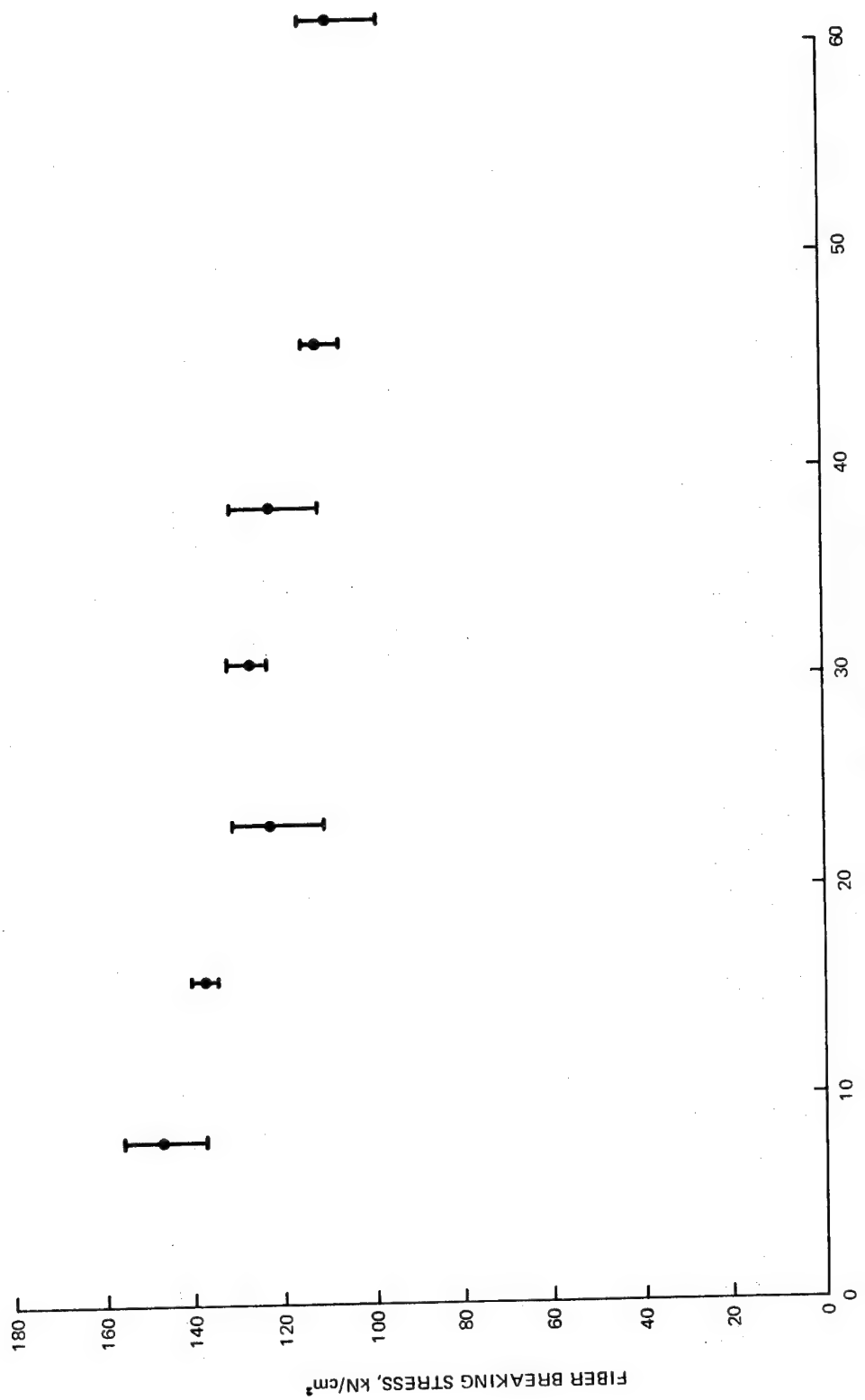

Fig. 70 Breaking Stress vs. Winding Speed for S-901 20-End Glass/Epoxy Preimpregnated Roving

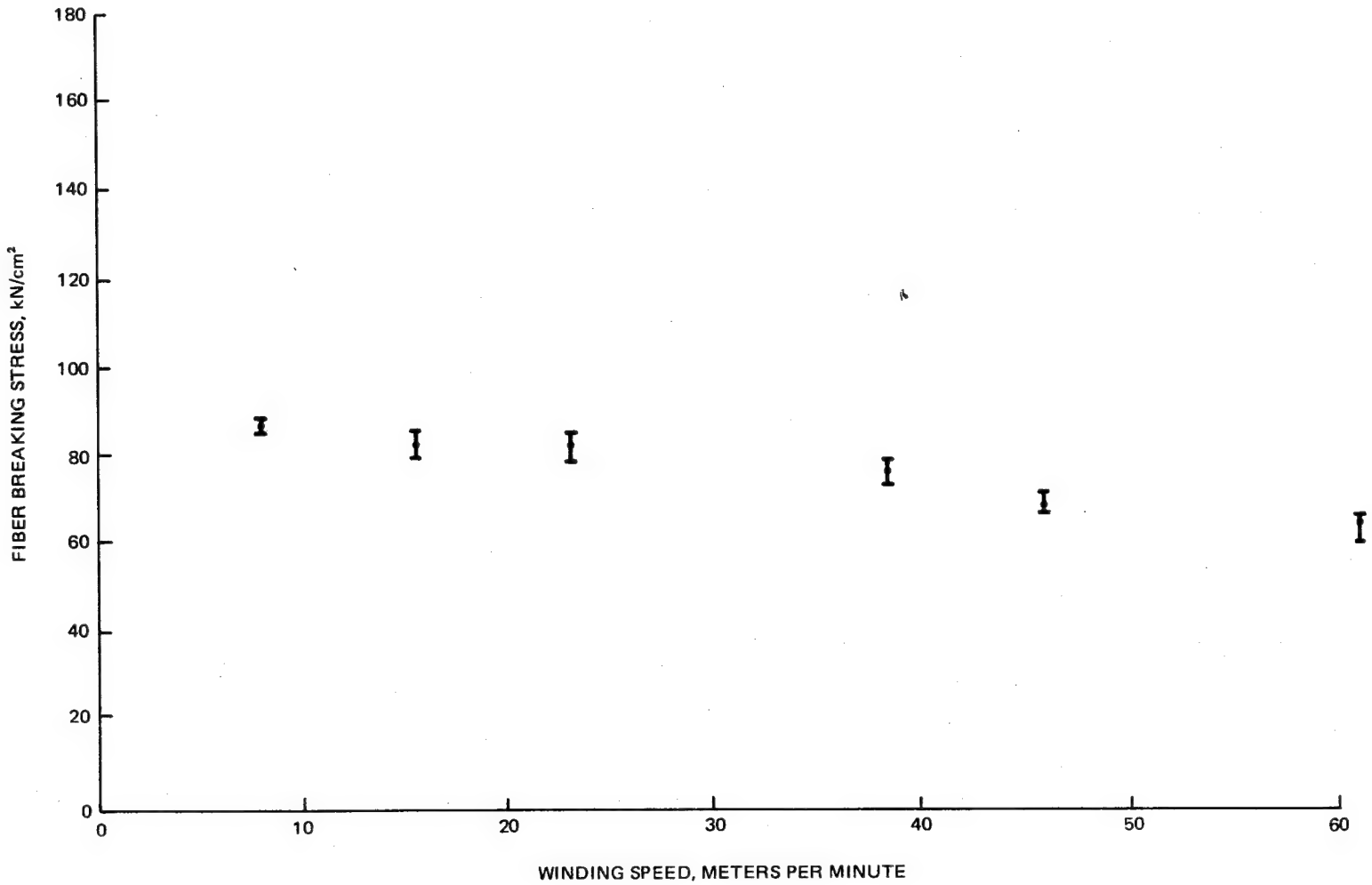

Fig. 71 Fiber Breaking Stress vs. Winding Speed for S-901 20-End Glass/Epoxy In-Process Impregnated Roving

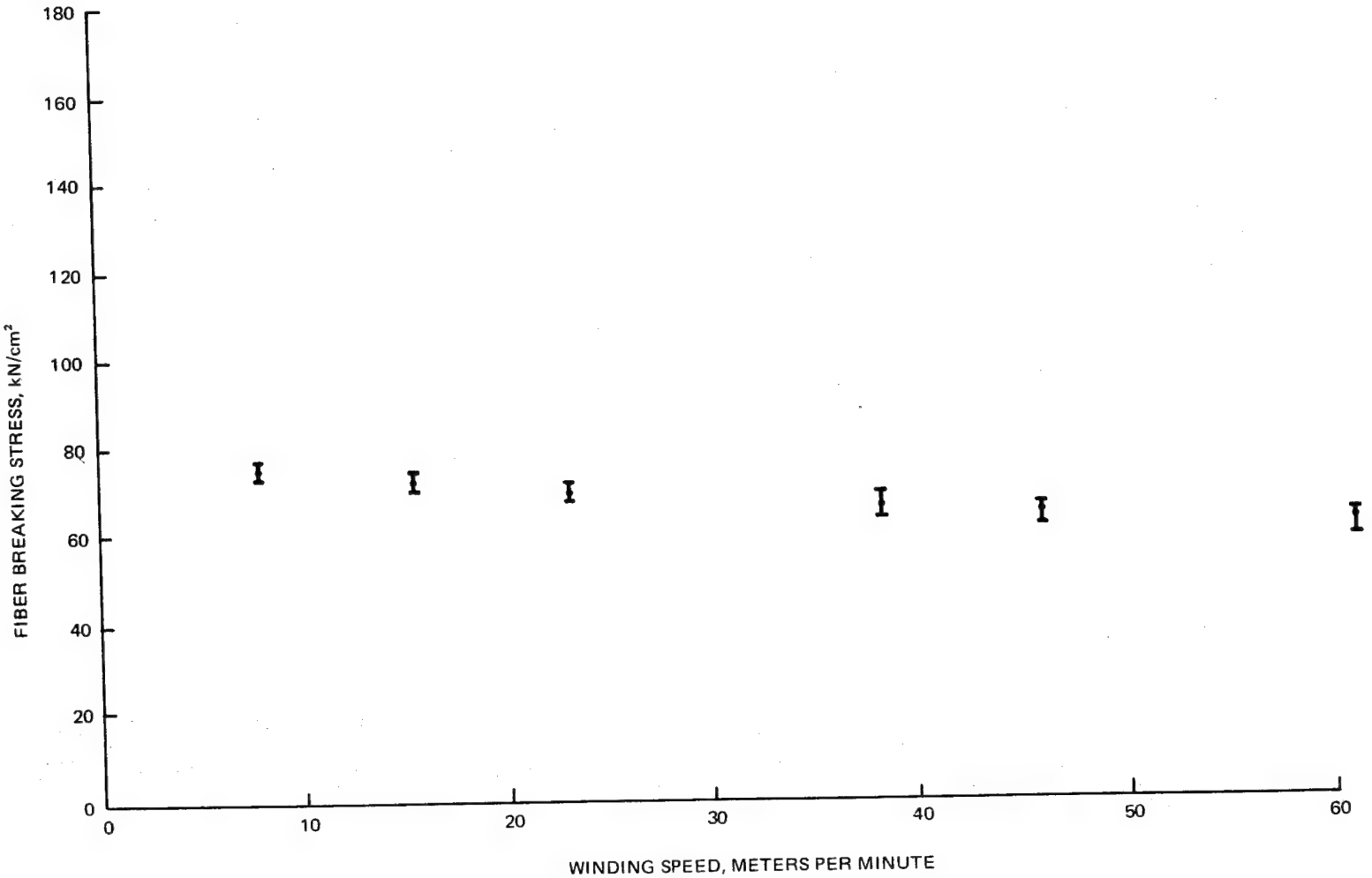

Fig. 72 Fiber Breaking Stress vs. Winding Speed for S-901 12-End Glass/Epoxy In-Process Impregnated Roving

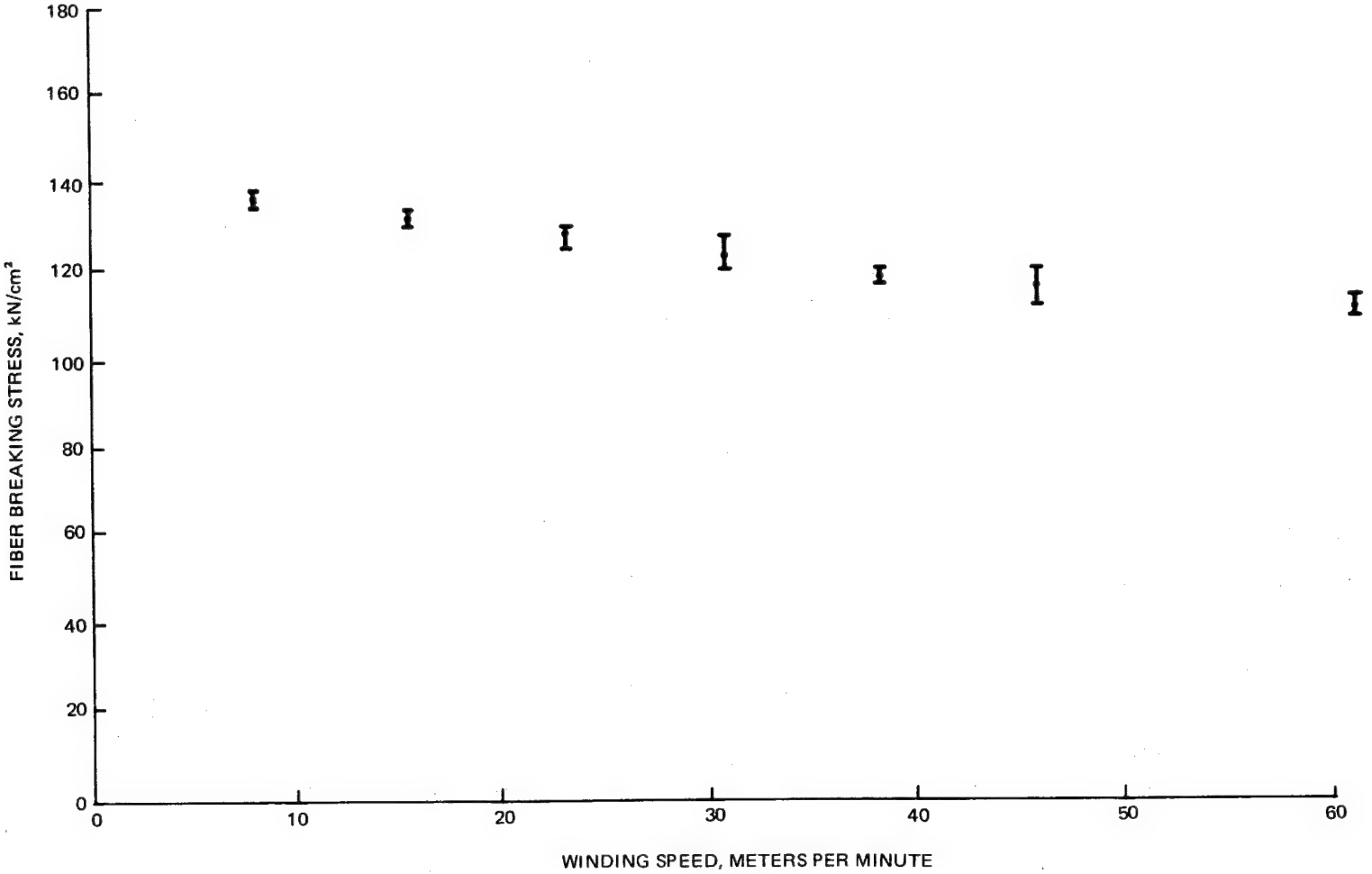

Fig. 73 Fiber Breaking Stress vs. Winding Speed for PRD-49-111/Epoxy In-Process Impregnated Roving

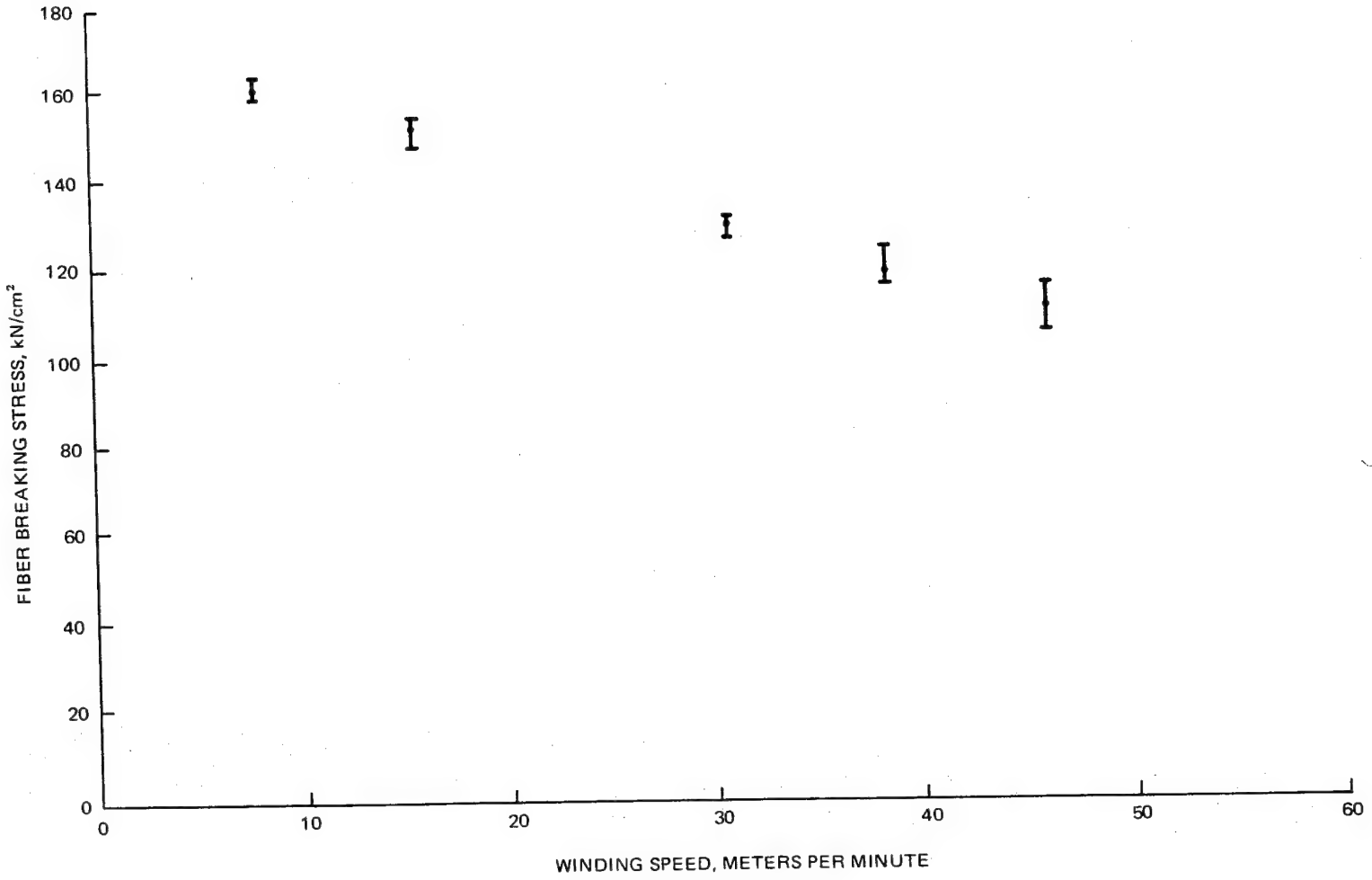

Fig. 74 Fiber Breaking Stress vs. Winding Speed for PRD-49-111/Epoxy Preimpregnated Roving

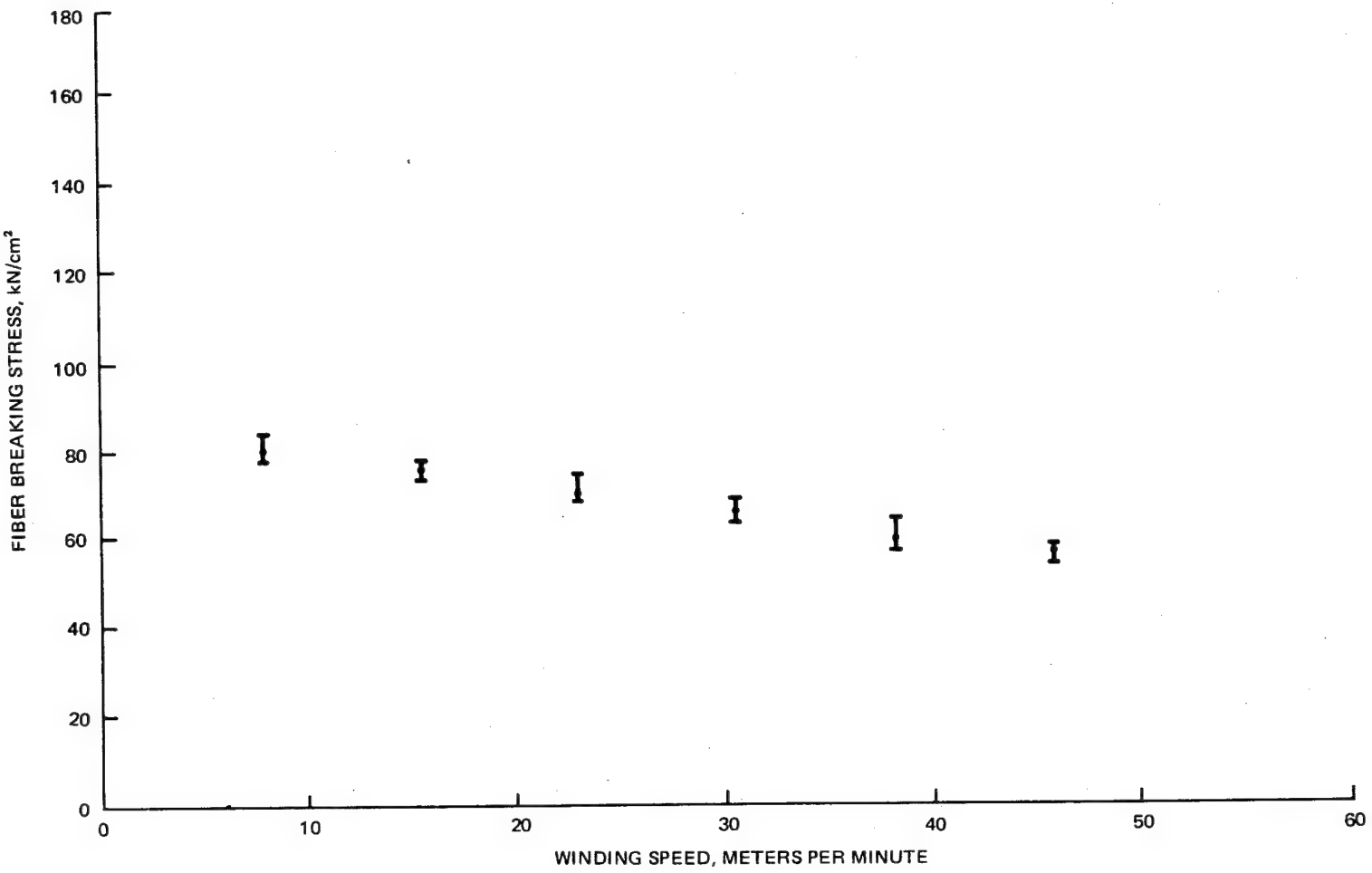

Fig. 75 Fiber Breaking Stress vs. Winding Speed for Courtauld's HTS Graphite Tow Preimpregnated Roving

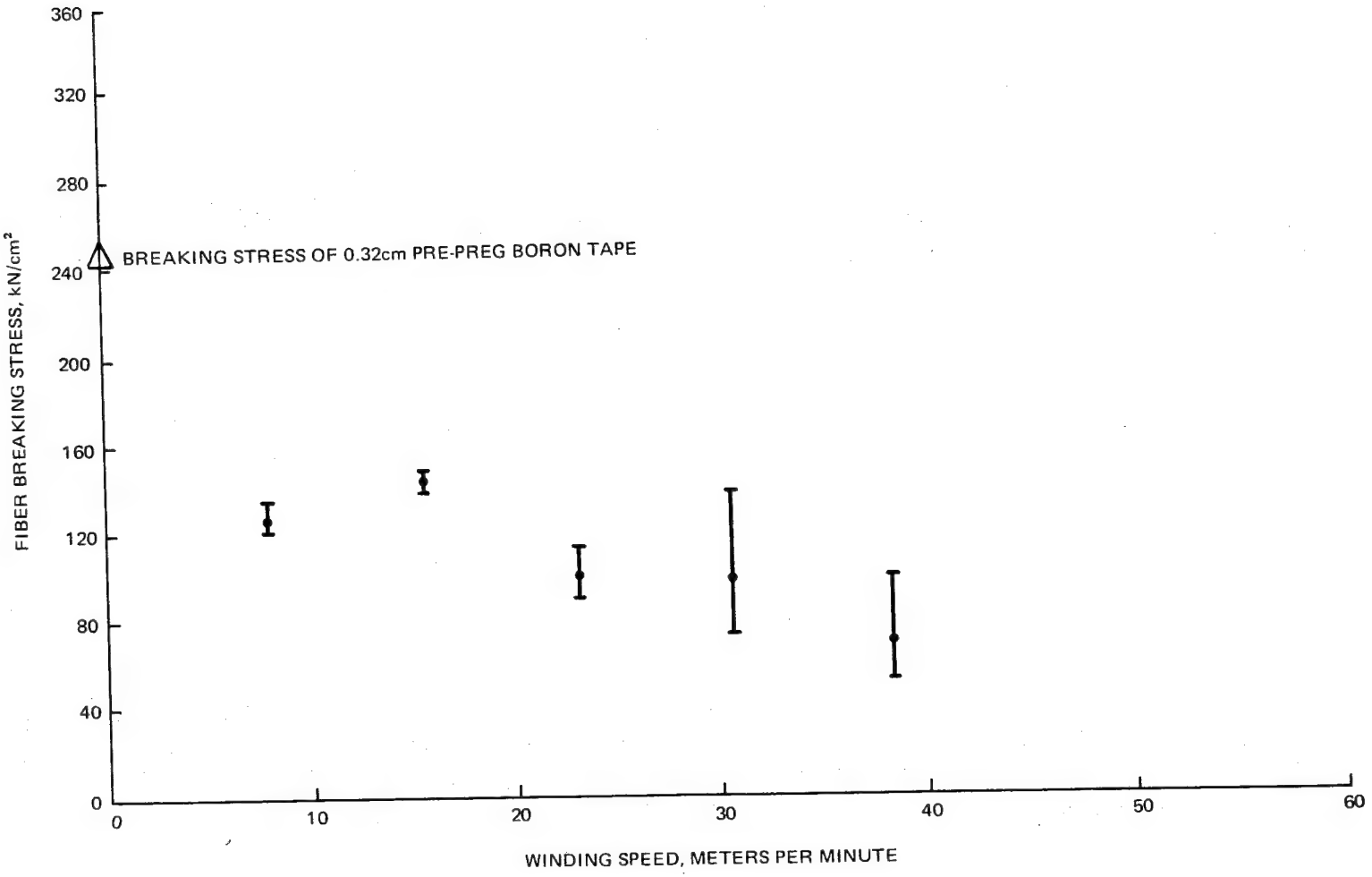

Fig. 76 Fiber Breaking Stress vs. Winding Speed for Boron Single Filament

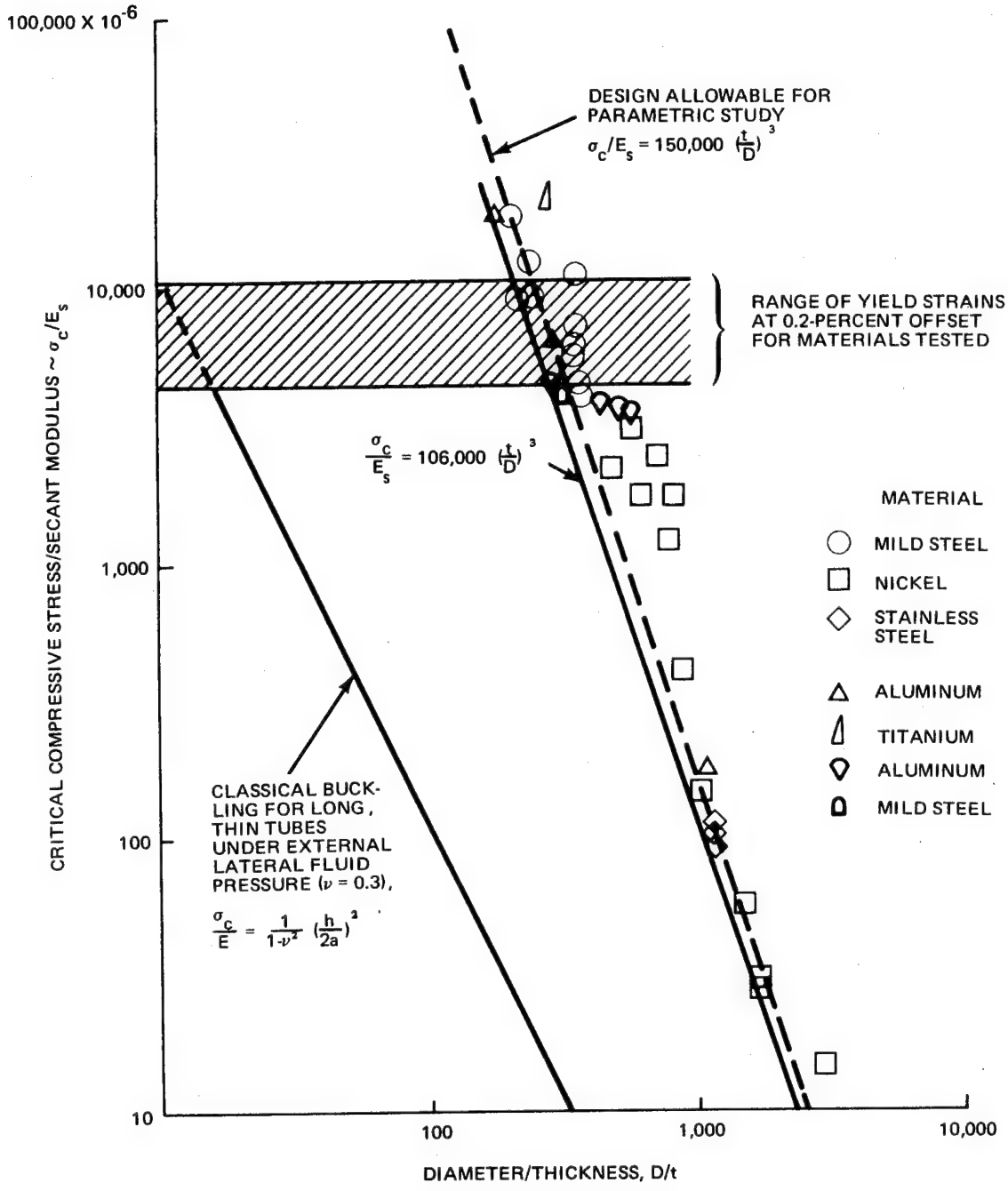

Fig. 77 Comparison of Constructive-Wrap Buckling Strengths for Cylindrical Tubes With Design Allowable Used in Parametric Study

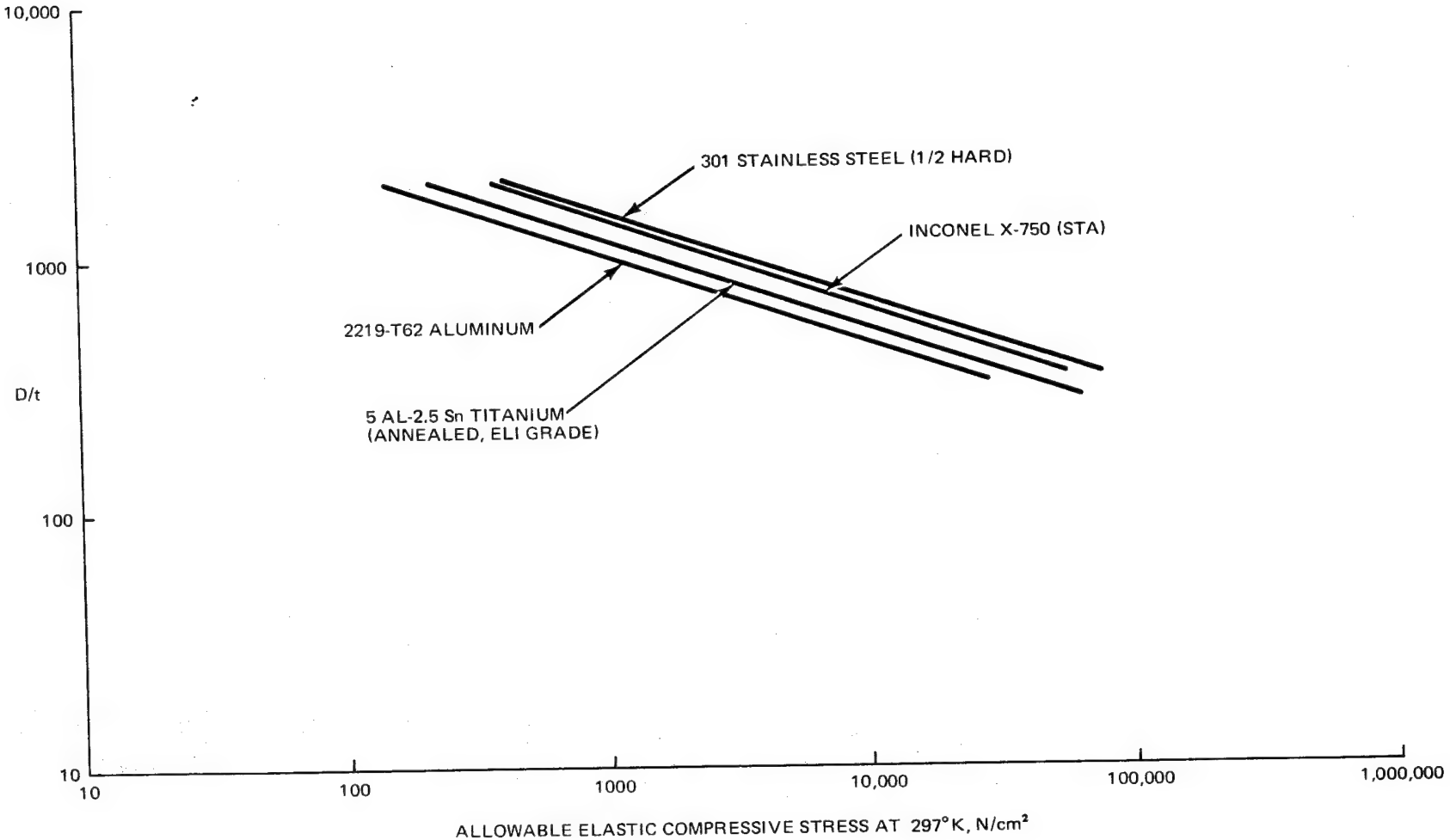

Fig. 78 D/t Ratio vs Allowable Elastic Compressive Stress at 297° K

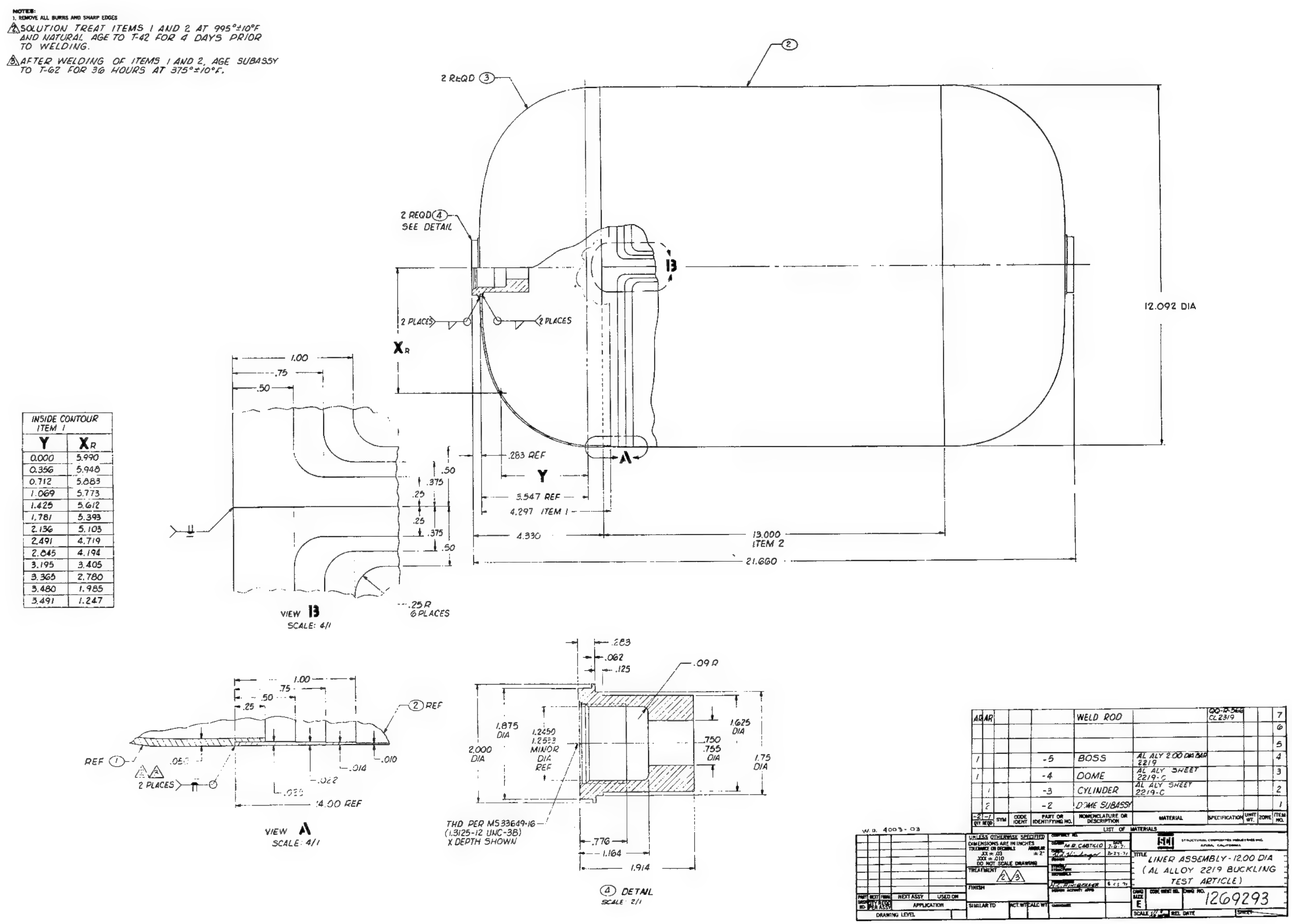

Fig. 79 — Vessel Shop Drawing — Liner Assembly

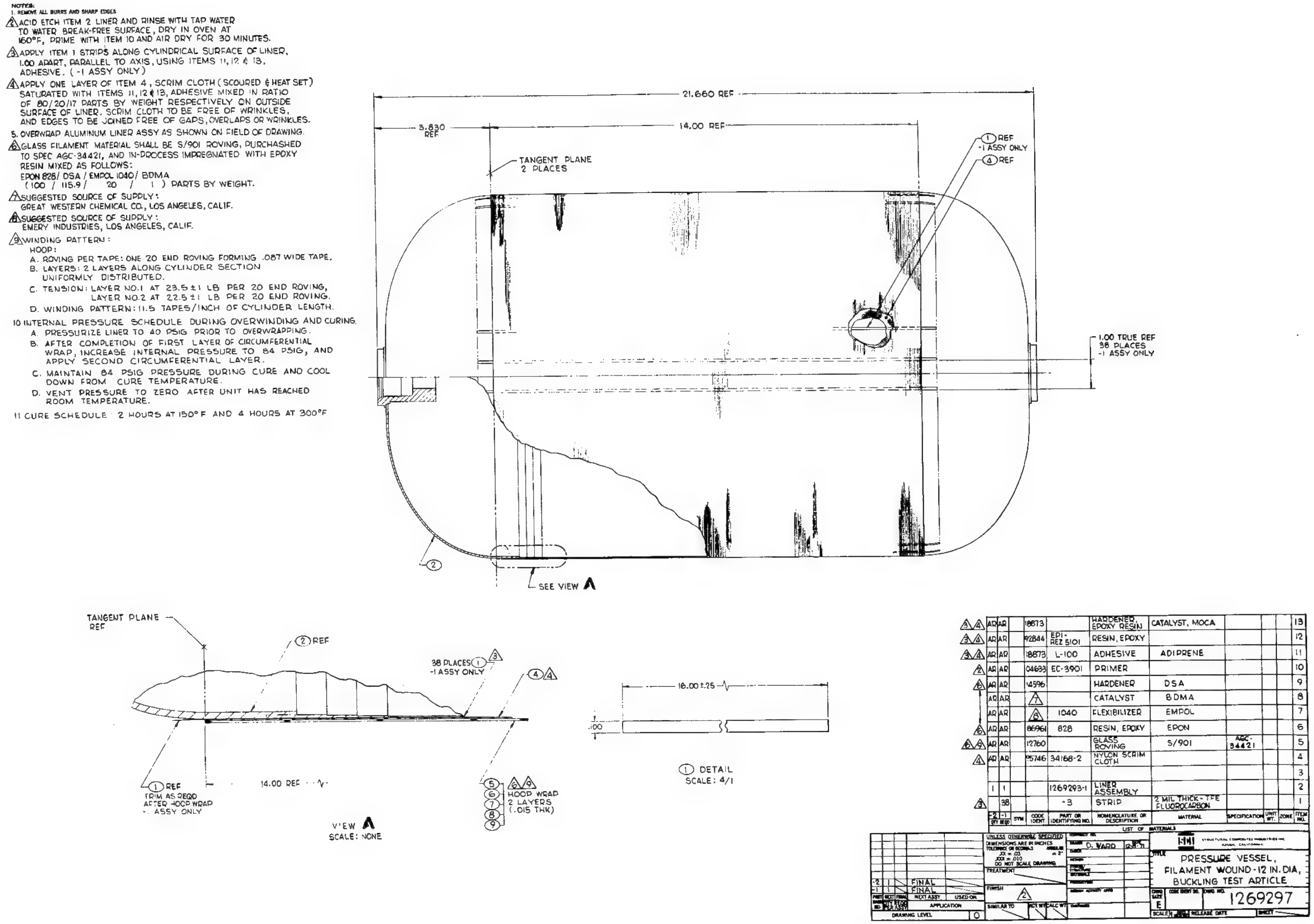

Fig. 80 Vessel Shop Drawing — Filament Winding

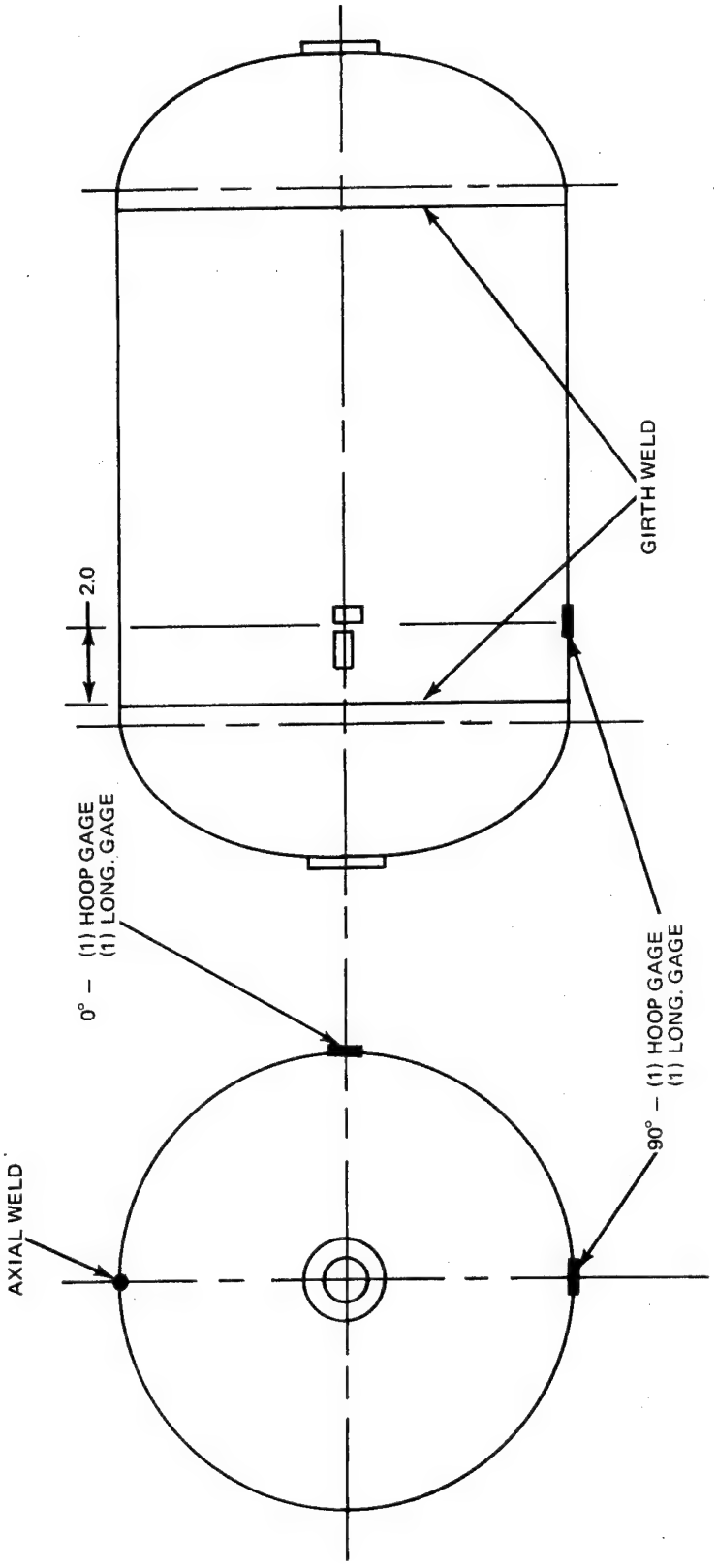

Fig. 81 Strain Gage Locations

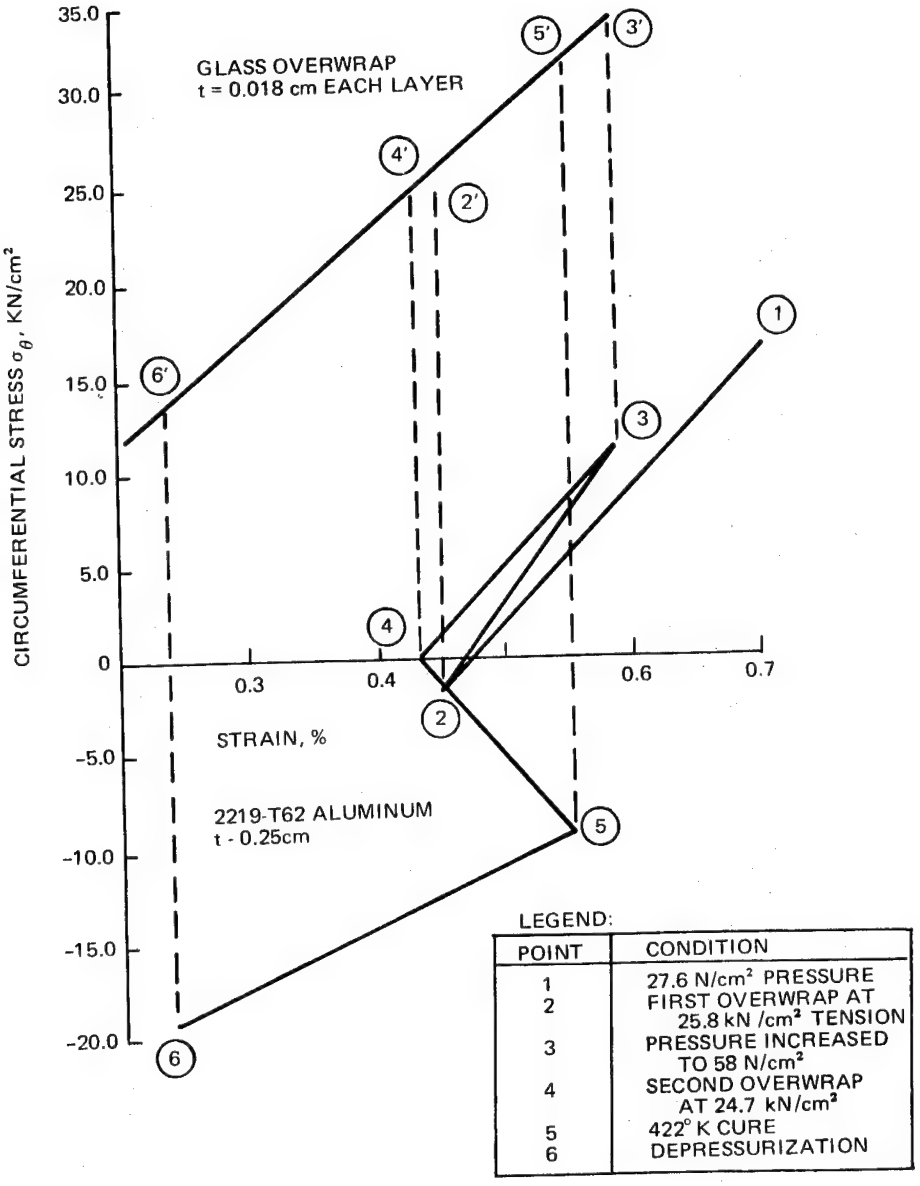

Fig. 82 Stress-Strain Diagram for 2219-T62 Aluminum Cylinder Circumferentially Reinforced with S-901 Glass Filament

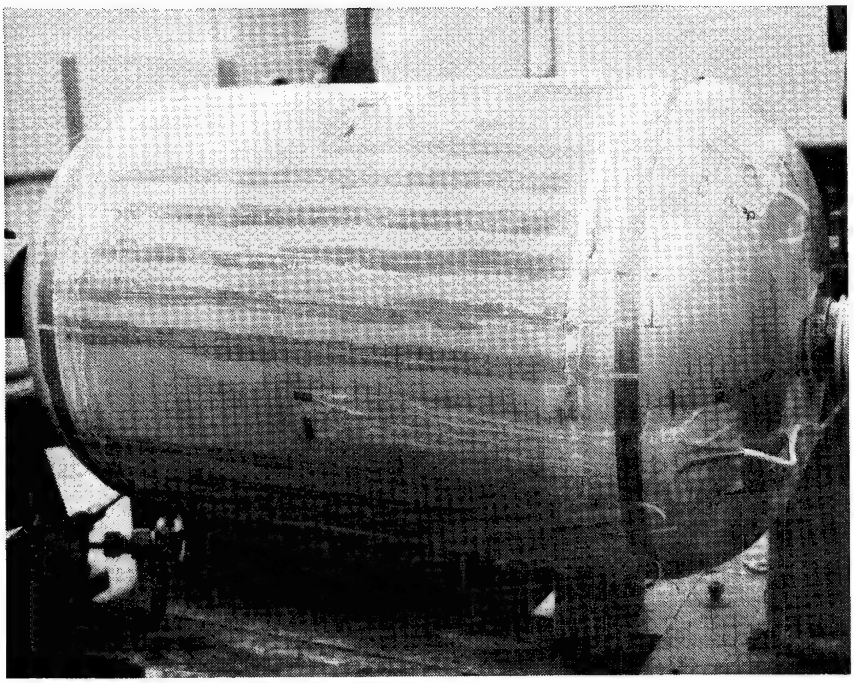

Fig. 83 Application of Teflon Strips and Strain Gages to 2219 Aluminum Shell Prior to Filament Overwrapping

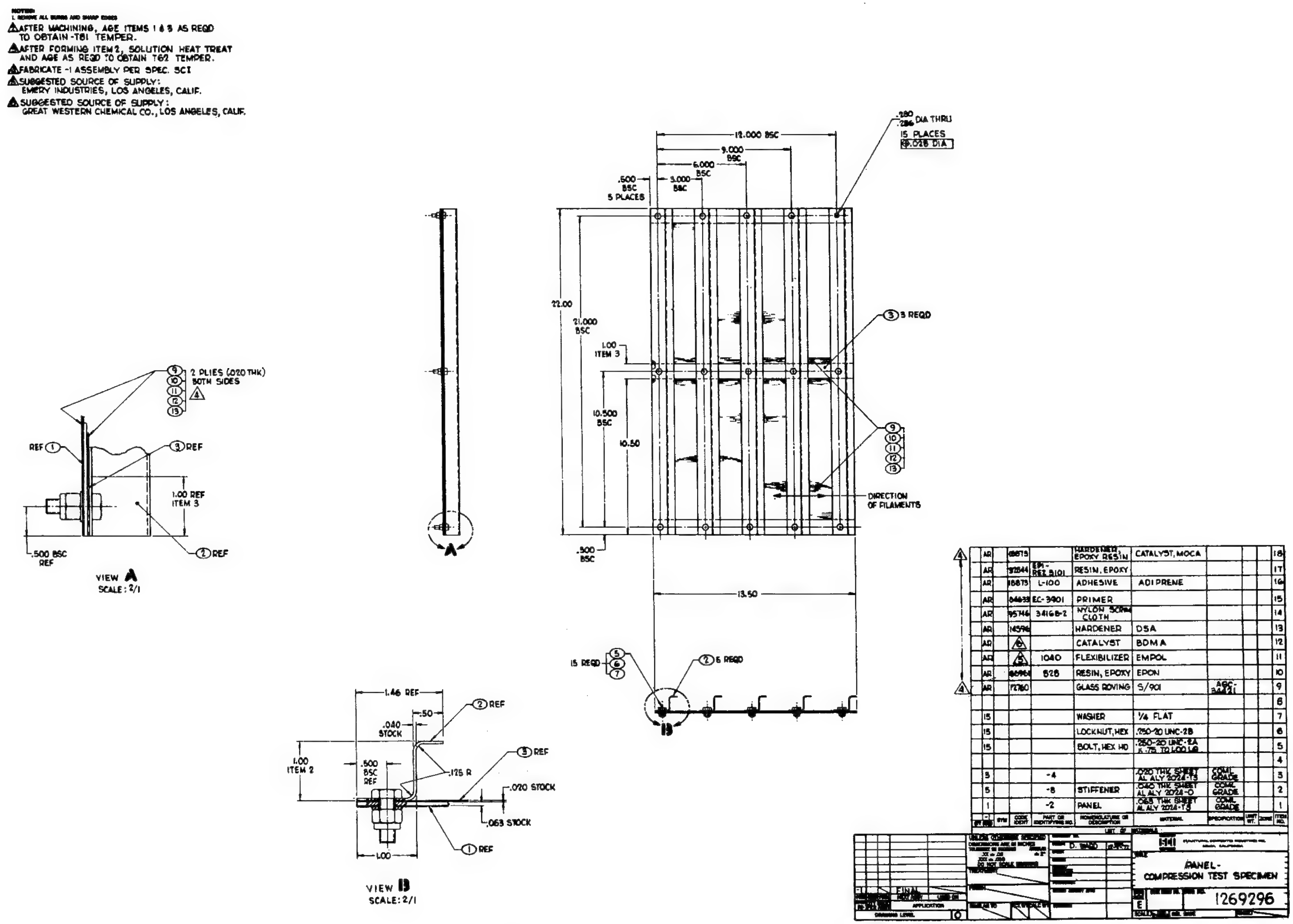

Fig. 84 Compression Panel Test Specimen

GAGE LOCATIONS:

(1), (2), (3), (4) – ON SIDE OF PANEL WITH NO STIFFENERS
(R.1), R.4) – ON SIDE OF PANEL WITH STIFFENERS
(R.2) – ON SUPPORTED STIFFENER FLANGE
(R.3) – ON UNSUPPORTED FLANGE OF STIFFENER

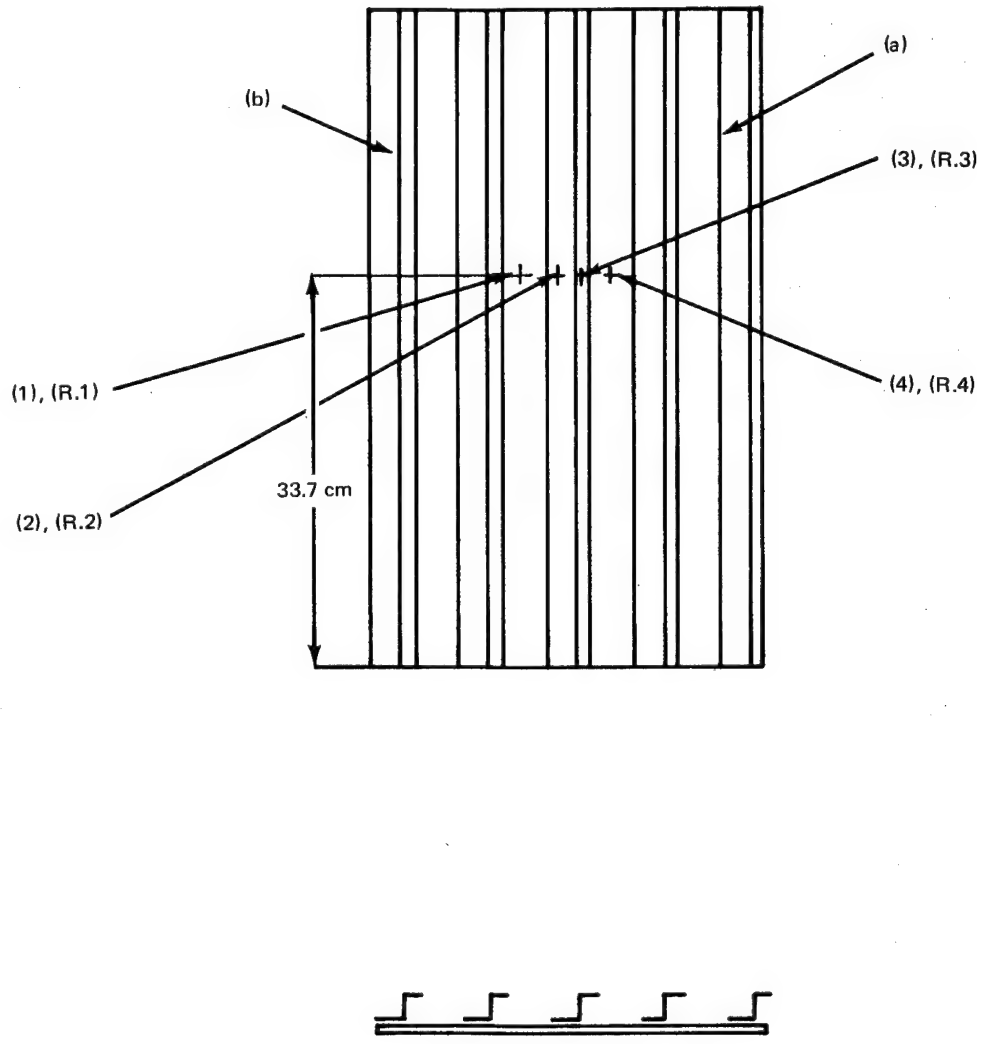

Fig. 85 Test Panel and Location of Strain Gages

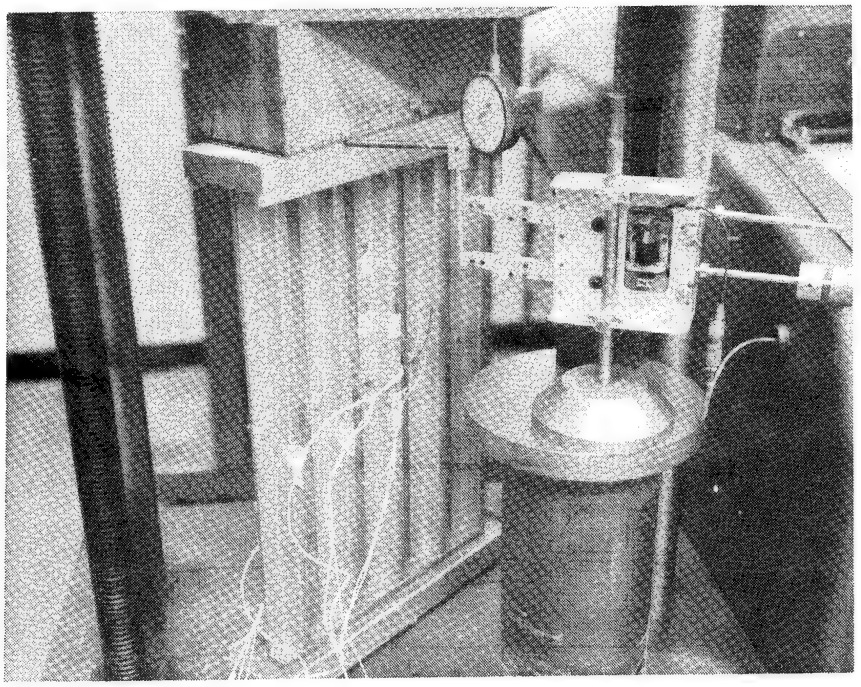

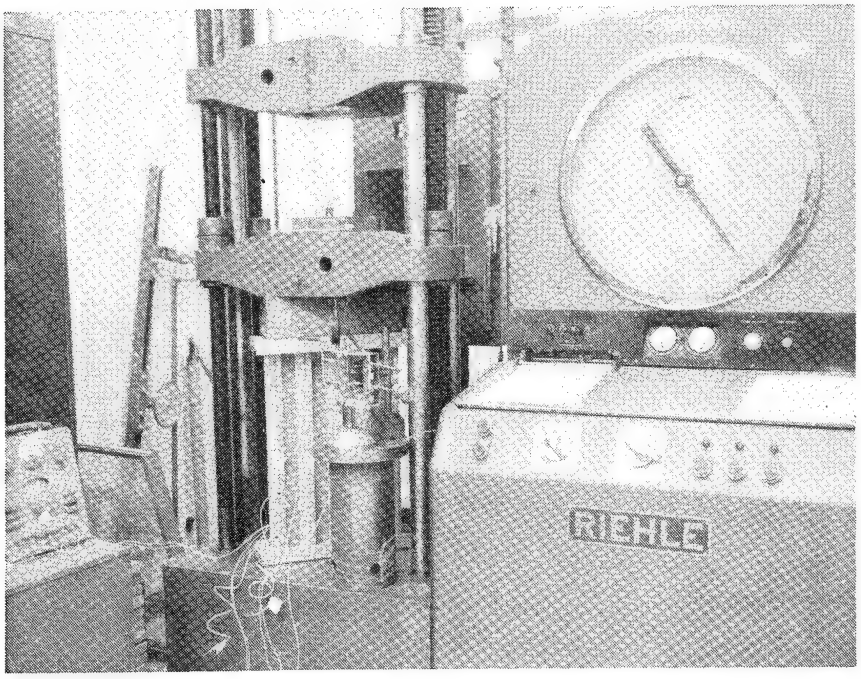

Fig. 86 Test Setup for Stringer-Stiffened Panel

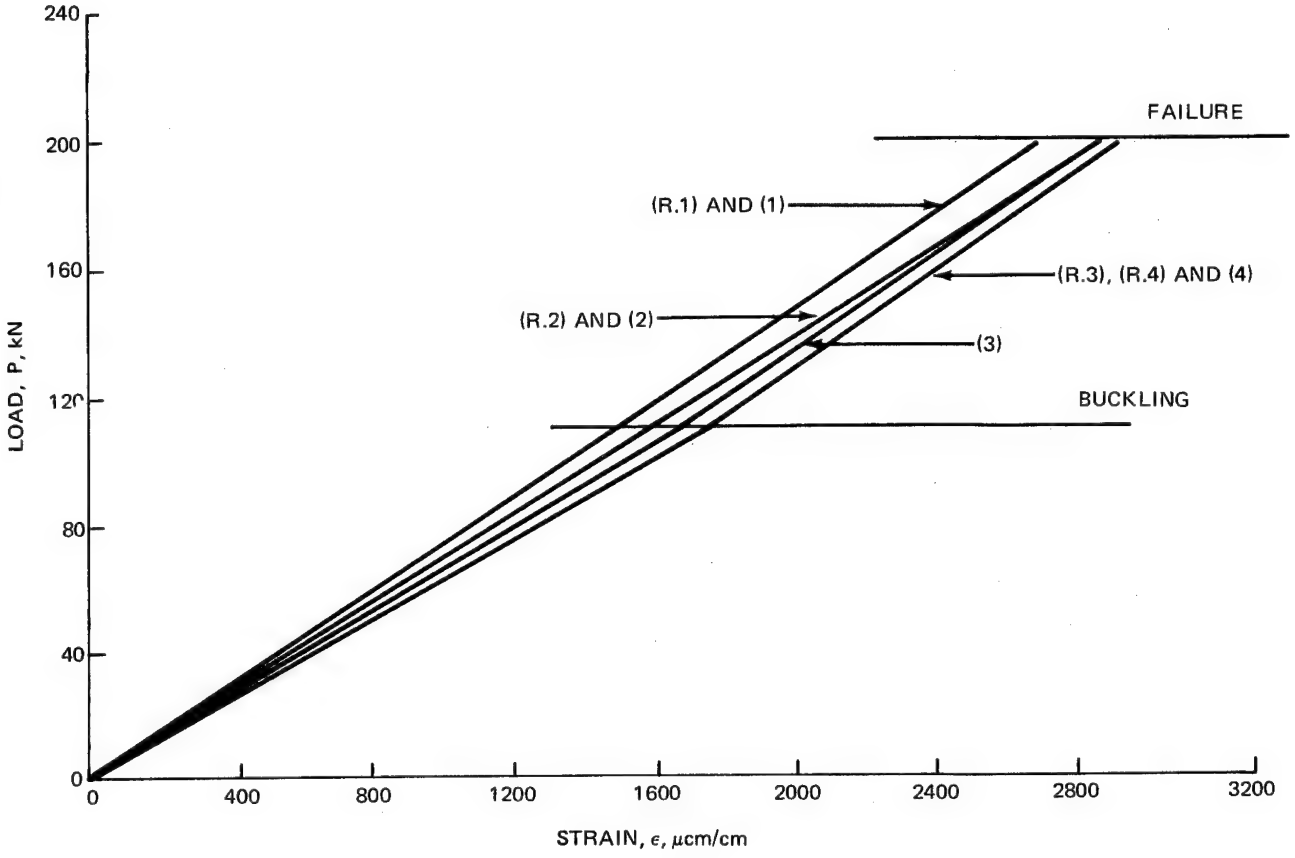

Fig. 87 Load – Strain Curves

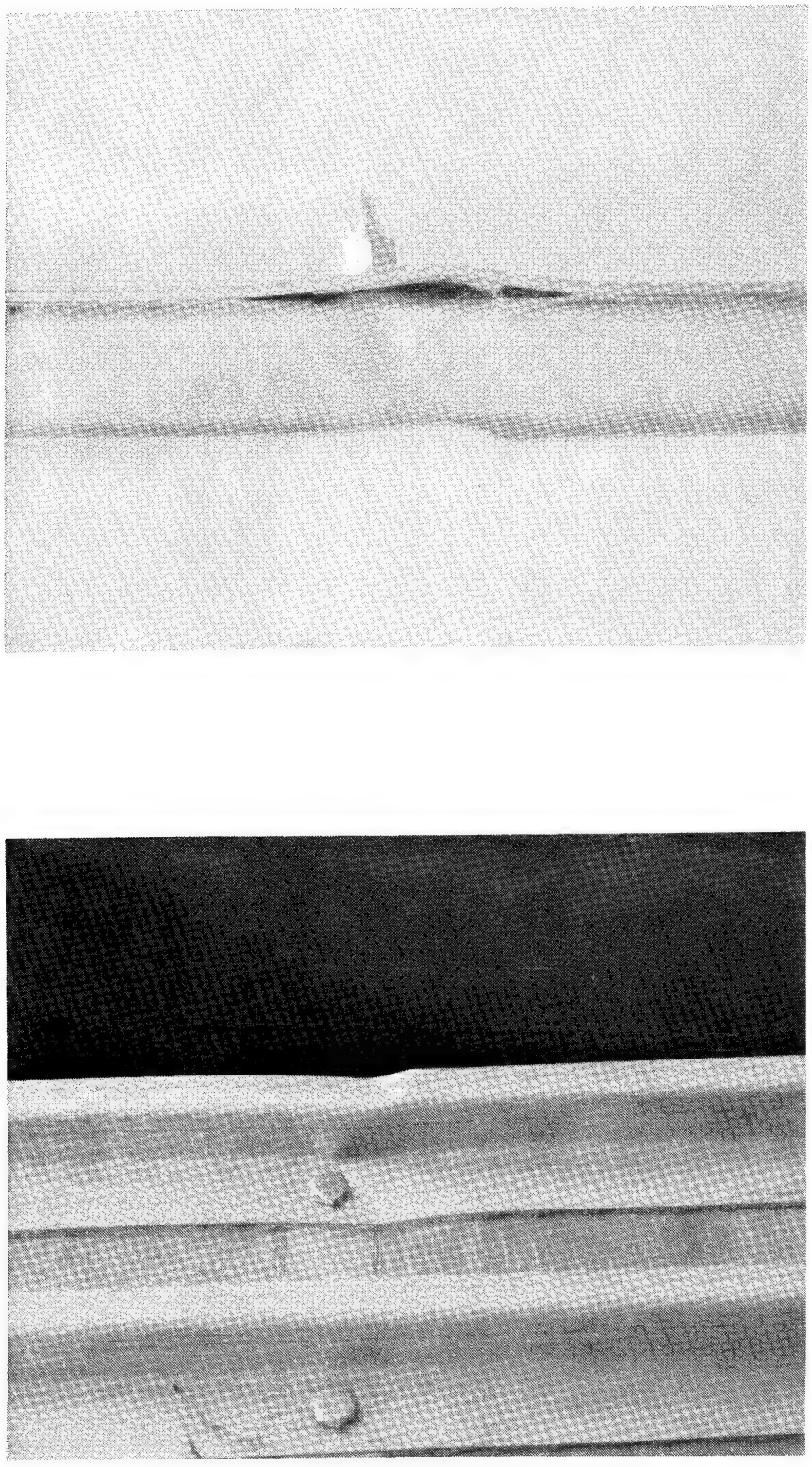

Fig. 88 Stringer-Stiffener Panel Primary Failure Location

Table 52 Maximum Recommended Winding Tension

	STRESS, kN/cm²			
	S-901 GLASS PREPREG	PRD-49 PREPREG	HTS GRAPHITE PREPREG	BORON
RANGE OF FILAMENT BREAKING VALUES	116/169	112/171	54/90	52/262
RANGE OF UNIDIRECTIONAL COMPOSITE BREAKING VALUES	78/113	72/110	32/54	28/144
MAXIMUM DESIGN VALUE, FILAMENT WINDING STRESS	124	138	69	124
MAXIMUM DESIGN VALUE, UNIDIRECTIONAL COMPOSITE WINDING STRESS	83	90	41	69

Table 53 Calculated and Measured Metal Stresses and Strains in 30.5 cm Diameter Glass/Epoxy Overwrapped Aluminum Shell

CONDITION		DESIGN				MEASURED							
PRESSURE N/cm²	WRAP NO	ϵ_H	ϵ_L	σ_H	σ_L	ϵ_H	ϵ_L	σ_H	σ_L	ϵ_H	ϵ_L	σ_H	σ_L
0	0	0	0	0	0	0	0	0	0	0	0	0	0
13.8	0	954	194	8.3	4.15	-200	-55	-1.8	-1.0	900	475	8.6	6.3
27.6	0	1908	388	16.5	8.25	1140	80	9.4	3.7	2210	825	19.4	12.3
27.6	1	-766	1271	-3.0	8.25	54	630	2.1	5.2	973	1365	11.6	13.7
57.9	1	539	1961	9.6	17.4	1278	1570	14.6	16.2	2430	2325	26.0	25.4
57.9	2	-1068	2491	-2.0	17.4	300	1923	7.6	16.4	1470	2685	19.2	25.8
57.9	IN CORE 422° K	-1031	1763	-3.7	11.7								
AFTER CURE													
57.9	2	-1031	1763	-3.7	11.7	100	1725	5.4	14.3	855	1480	10.9	14.3
41.4	2	-1551	1474	-8.8	7.9	-418	1372	0.3	10.0	-518	-353	-5.2	-4.3
27.6	2	-1984	1233	-13.1	4.8	-823	1070	-3.9	6.5	-55	848	1.9	6.8
13.8	2	-2417	992	-17.4	1.7	-1249	710	-8.5	2.4	-492	478	-2.8	2.6
0	2	-2850	751	-21.7	1.4	-1565	320	-12.2	-12.2	-1.6	-824	55	-6.8
0, 78° K	2	$\Delta\epsilon$ = 1 - 2046				$\Delta\epsilon$ = -2086 (ΔE) WAS AVERAGE FOR 8 CYCLES							

H = HOOP; L = LONGITUDINAL; ϵ = UNIT STRAIN X 10^6; σ = STRESS, kN/cm²

Table 54 Predicted and Derived Stresses in Glass/Epoxy Overwrap of Aluminum Shell

CONDITION	DIRECTION	STRESS IN OVERWRAP kN/cm²		
		DESIGN	0°	90°
27.58 N/cm²	H	25.9	19.2	6.6
1ST WRAP	L	0	0	0
57.92 N/cm²	H	33.4	26.8	
2ST WRAP	L	0	0	0
57.92 N/cm²	H	24.5	18.1	11.7
2ND WRAP	L	0	0	0
57.92 N/cm²	H	31.2	—	—
AT 422° K	L	0	—	—
57.92 N/cm²	H	25.6	19.5	15.9
AFTER CURE	L	3.8	2.1	2.0
0	H	14.5	8.1	4.5
	L	1.0	1.0	1.7
0 PSI 78°K	H	5.8	—	—
	L	-.3	—	—

Table 55 Load-Strain Readings in Z-Stiffened Panels

LOAD, P, KN	LINER STRAIN, μ cm/cm							
	1	2	3	4	R.1	R.2	R3	R.4
0	0	0	0	0	0	0	0	0
13.3	125	155	210	260	130	180	280	245
26.7	300	365	420	500	300	375	450	470
40.0	465	545	600	680	465	560	725	665
53.3	665	760	805	900	640	800	925	875
66.7	845	955	1015	1095	800	975	1095	1065
80.1	1040	1155	1210	1295	980	1190	1300	1265
93.4	1230	1355	1405	1495	1150	1385	1480	1440
107	1415	1560	1595	1685	1320	1595	1675	1660
120	1605	1765	1795	1875	1500	1785	1860	1840
133	1790	1955	1965	2050	1670	1985	2045	2020
147	1975	2155	2165	2240	1840	2165	2220	2205
160	2165	2350	2345	2425	2025	2375	2405	2395
173	2355	2550	2520	2625	2200	2570	2585	2590
187	2525	2740	2715	2820	2380	2765	2765	2765
200	2705	2925	2935	3055	2550	2950	2925	2915
214	FAILURE							

APPENDIX C

ONE-SIXTH SCALE TEST HARDWARE DRAWINGS

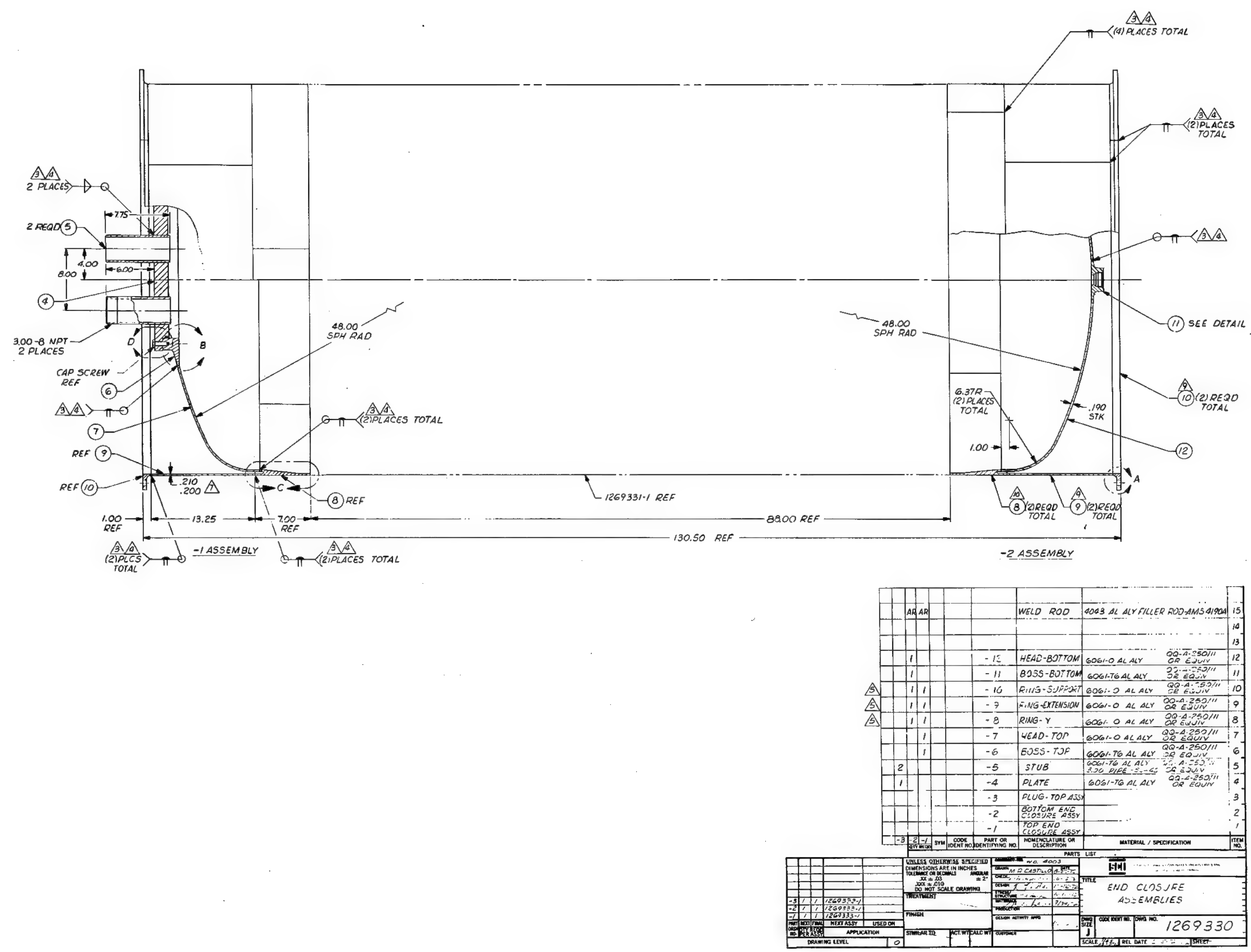

Fig. 89 Test Tank End Closure

NOTES: 1. REMOVE ALL BURRS AND SHARP EDGES

2. INTERPRET WELD SYMBOLS PER MIL-STD-20 AND AWS A2.0.

3. FUSION WELD PER MIL-W-8604, BY TUNGSTEN INERT GAS, MANUAL METHOD. USE ITEM 15 FILLER ROD AS REQUIRED.

4. DYE PENETRANT INSPECT WELD PER MIL-I-6866, TYPE II, METHOD A. NO CRACKS OR PROPAGATING DEFECTS ACCEPTABLE.

5. SOLUTION TREAT WELDED DETAIL TO CONDITION T42 PER MIL-H-6088 AS REQUIRED PRIOR TO FINAL SIZING AND MACHINING.

6. THIS DIMENSION MAY BE REDUCED TO 1.25 INCHES TO PERMIT REUSE OF END CLOSURE ASSEMBLIES.

7. THICKNESS MAY EXCEED THAT SHOWN AS LONG AS CENTROID DIAMETER IS LOCATED IN EXISTING THICKNESS.

8. WELD MISMATCH SHALL NOT EXCEED 20 PERCENT.

9. MAY BE FABRICATED FROM TWO PIECES.

10. MAY BE FABRICATED FROM THREE PIECES.

11. TAG WITH 1269330 AND APPLICABLE DASH NO.

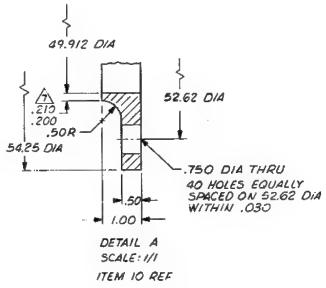

DETAIL A
SCALE: 1/1
ITEM 10 REF

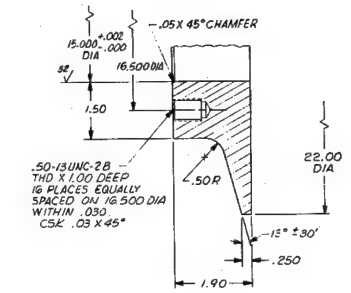

DETAIL B
SCALE: 1/1
ITEM 6 REF

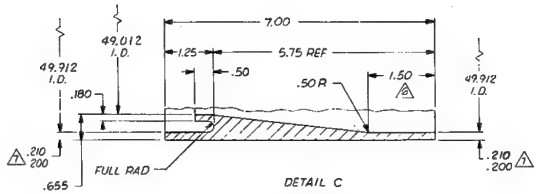

DETAIL C
SCALE: 1/1
ITEM 8 REF

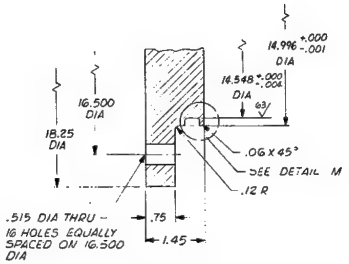

DETAIL D
SCALE: 1/1
ITEM 4 REF

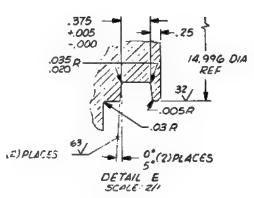

DETAIL E
SCALE: 2/1

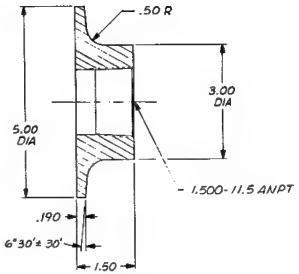

(11) DETAIL
SCALE: 1/1

Fig. 89 Test Tank End Closure (Continued)

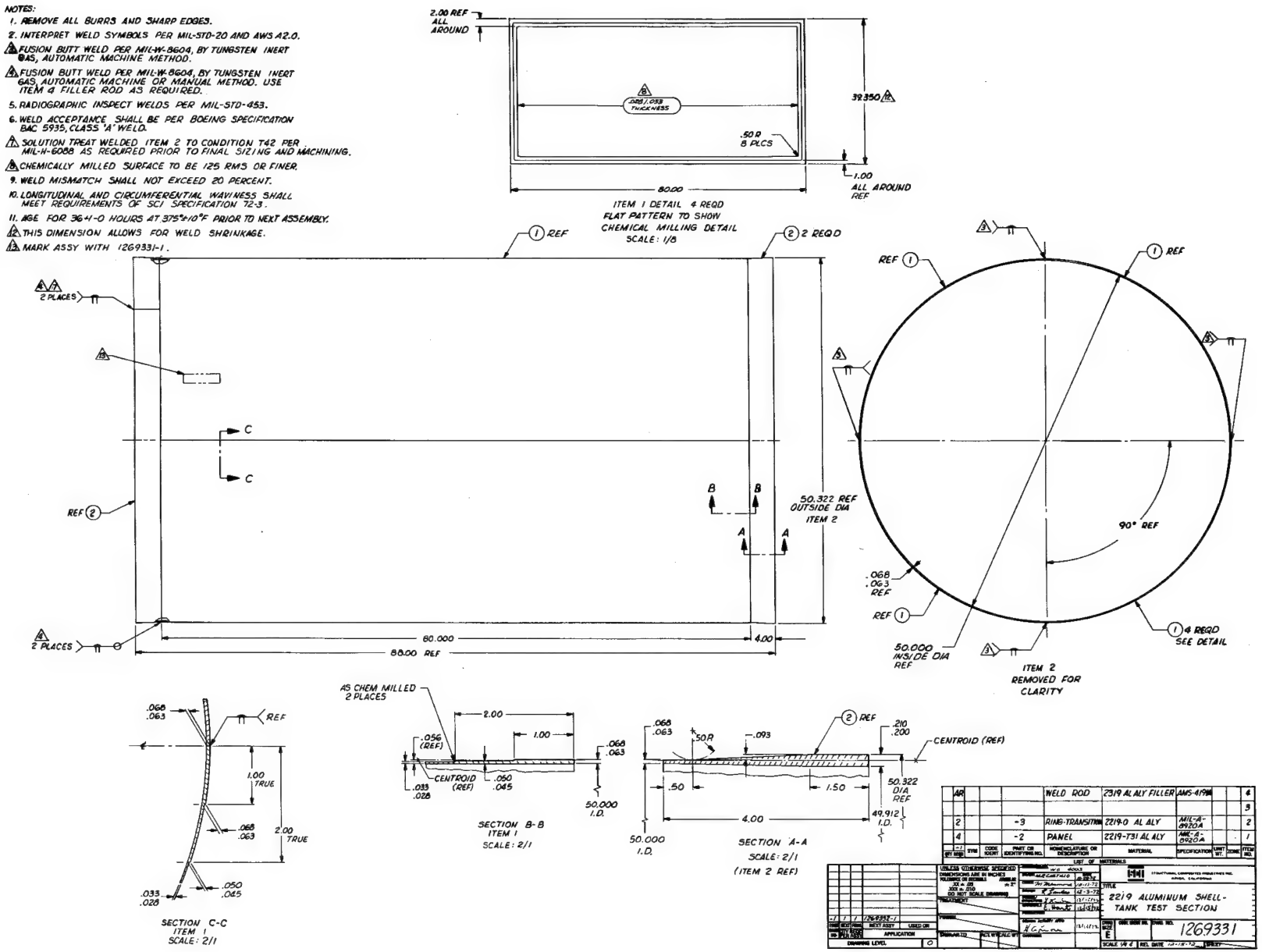

Fig. 90 Test Tank Aluminum Cylindrical Section

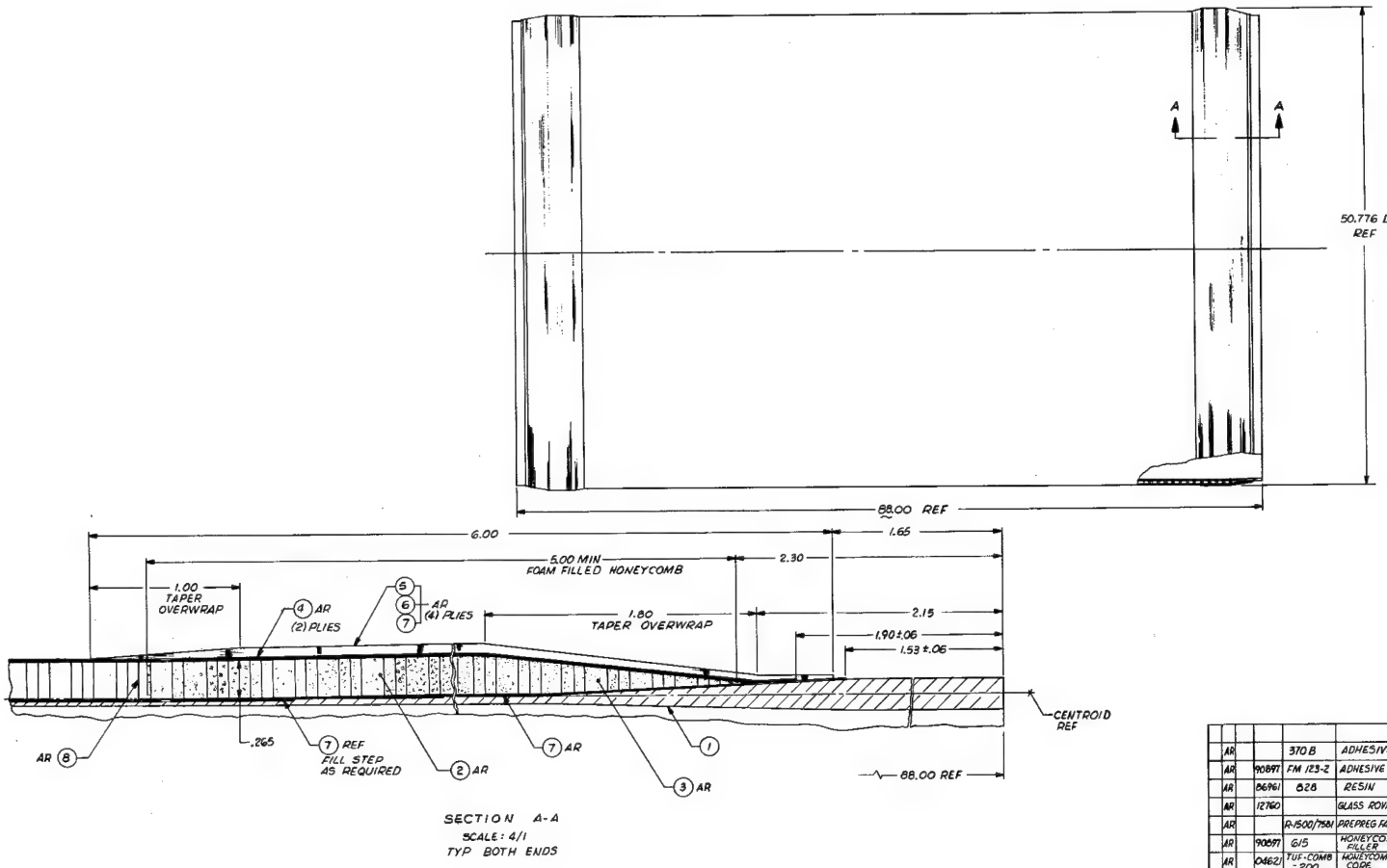

SECTION A-A
SCALE: 4/1
TYP BOTH ENDS

QTY REQ	SYM	CODE IDENT	PART OR IDENTIFYING NO.	NOMENCLATURE OR DESCRIPTION	MATERIAL	SPECIFICATION	UNIT WT.	ZONE	ITEM NO.
AR			310 B	ADHESIVE	RELIABOND, .10 WTHK	RELIABLE MFG CO.			8
AR		90897	FM 123-2	ADHESIVE	0.06 LB/FT²				7
AR		86961	828	RESIN	EPON				6
AR		12760		GLASS ROVING	S/901 , 20 END				5
AR			R-1500/7581	PREPREG FABRIC	RELIAPREG	RELIABLE MFG CO.			4
AR		90897	G15	HONEYCOMB, FILLER	CORFIL				3
AR		04621	TUF-COMB -200	HONEYCOMB, CORE	3/16 - 4.0 PCF (NOMINAL DENSITY)				2
1			1269331-1	2219 ALUMINUM SHELL					1

LIST OF MATERIALS

UNLESS OTHERWISE SPECIFIED DIMENSIONS ARE IN INCHES
TOLERANCES ON DECIMALS
.XX ± .01
.XXX ± .010
DO NOT SCALE DRAWING

W.O. 4002
M.R. CASTILLO 6-11-73
10-12-73
10-11-73
12-17-73

TREATMENT

1269332-1
PART NEXT ASSY USED ON
APPLICATION
DRAWING LEVEL C

SIMILAR TO

SCALE WT

STRUCTURAL COMPOSITES INDUSTRIES INC.
Azusa, California

TITLE
HONEYCOMB COMPOSITE REINFORCED 2219 ALUMINUM TANK-ASSEMBLY

DWG SIZE E
DWG NO. 1269332
SCALE 1 REL. DATE 12-6-73

Fig. 91 Honeycomb-Reinforced Cylindrical Section

NOTES:
1. REMOVE ALL BURRS AND SHARP EDGES
1. INTERPRET WELD SYMBOLS PER MIL-STD-20 AND AWS A2.0.
2. FUSION BUTT WELD PER MIL-W-8604, BY TUNGSTEN INERT GAS, MANUAL METHOD. USE ITEM 7 FILLER ROD AS REQUIRED.
3. RADIOGRAPHIC INSPECT WELDS PER MIL-STD-453.
4. WELD ACCEPTANCE SHALL BE PER BOEING SPECIFICATION BAC 5935, CLASS 'A' WELD.
5. WELD MISMATCH SHALL NOT EXCEED 20 PERCENT.
6. OVALITY OF FINAL ASSEMBLY SHALL BE WITHIN 2.00 T.I.R.
7 (triangle). PRIOR TO CRYOGENIC TESTING, THESE SURFACES SHALL BE BONDED TOGETHER WITH EPOXY RESIN MIXED AS FOLLOWS: EPON 828/PSA/EMPOL 1040/BDMA (100/116/20/1) PARTS BY WEIGHT.

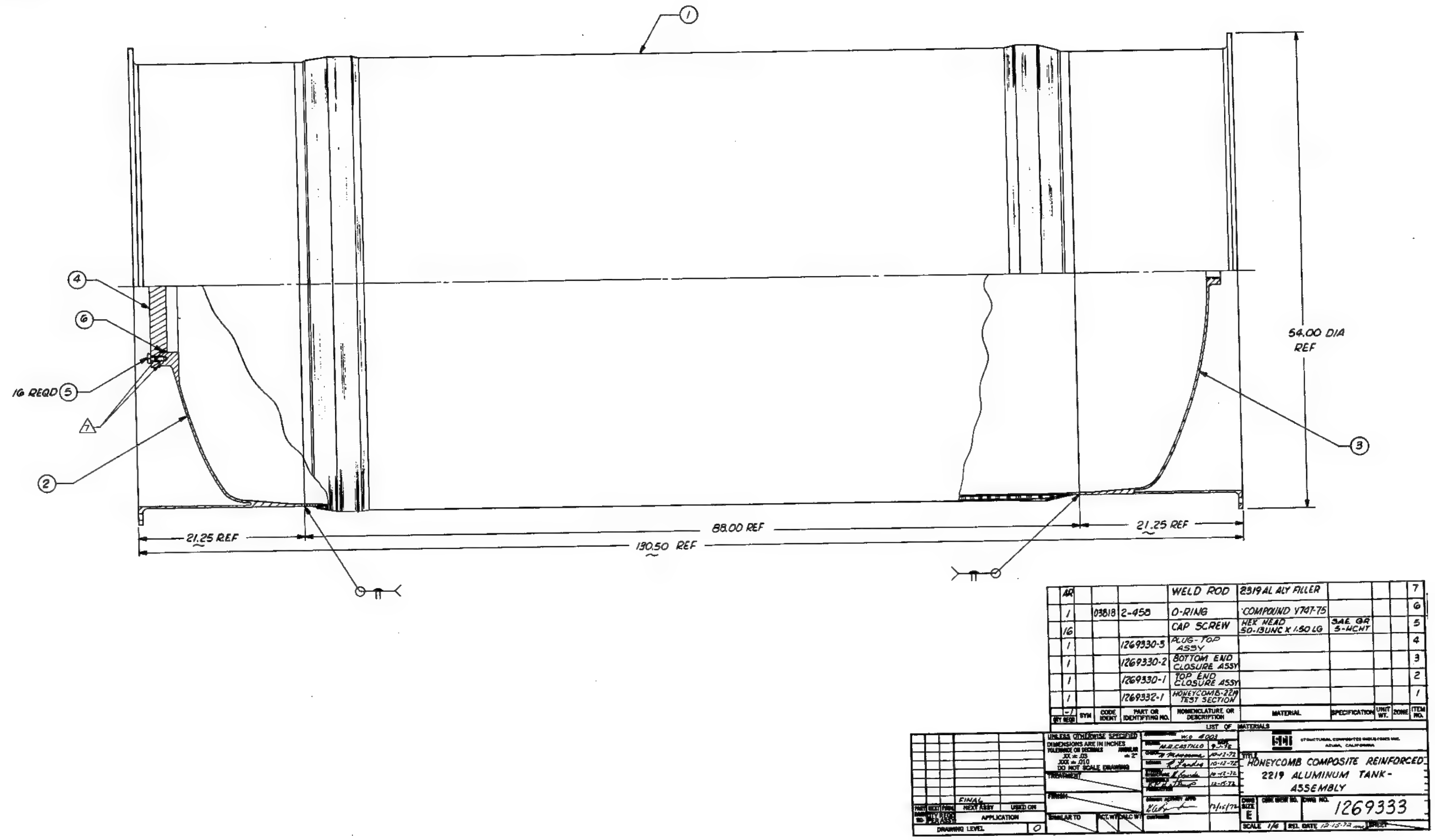

Fig. 92 Test Tank Assembly

REFERENCES

1. Morris, E., Darms, F., Landes, R., and Campbell, J., "Parametric Study of Glass-Filament-Reinforced Metal Pressure Vessels", NASA CR 54-855, Aerojet-General Corporation, April 1966.

2. Schwartzberg, F., et al, "Cryogenic Materials Data Handbook (Revised)", AFML-TDR-64-280 (Revised 1970), Martin -Marietta Corporation, July 1970.

3. Sessler, J., and Weiss, V,. "Materials Data Handbook - Aluminum Alloy 2219", NASA Contract NAS 8-11345, Syracuse University, March 1966.

4. Johns, R. H., and Kaufman, A, "Filament Overwrapped Metal Cylindrical Pressure Vessels", TMX-5271, NASA Lewis Research Center, 1966.

5. Mohlo, R., and Soffer, T. M., "Cryogenic Resins for Glass Filament - Wound Composites", NASA CR-72114, Aerojet-General Corporation, January 1967.

6. Morris, E. E., "Glass-Fiber-Reinforced Metallic Tanks for Cryogenic Service", NASA CR-72224, Aerojet-General Corporation, June 1967.

7. Lewis, A. and Bush, G., "Improved Cryogenic Resin/Glass - Filament - Wound Composites", NASA CR-72163, Aerojet-General Corporation, April 1967.

8. "Cryogenic Filament - Wound Tank Evaluation", Contract NAS 3-10289, Aerojet-General Corporation (work in progress).

9. SCI Structural Materials Handbook.

10. Hanson, M.P., "Static and Dynamic Fatigue Behavior of Glass Filament-Wound Pressure Vessels at Ambient and Cryogenic Temperatures", NASA TN-D-5807, May 1970.

11. Ranalli, E., "Analysis of an Integrally Stiffened Panel Subjected to Applied In-Plane Shear and Compression Loadings", Grumman Structural Analysis Report No. SAR-1, November 1966.

12. Rosenbaum, J., Kelsey, A., and Pardo, H., "Structural Synthesis of an Integrally Stiffened Panel Subjected to Compressive Load", Grumman Advanced Development Report No. ADR 02-21-65.1, March 1965.

13. Lourenso, O., and Ridgely, G., "Selection of Critical Element and Calculation of Minimum Margin of Safety for Zee Stiffened Panels", Grumman Aerospace Corporation, SAR71-2, November 1971.

14. Fletcher, R., and Powell, M., "A Rapidly Convergent Descent Method for Minimization", Computer Journal (British), Vol. 6, 1963, p. 163.

15. Fiacco, A. V., and McCormick, G. P., "The Sequential Unconstrained Minimization Technique for Nonlinear Programming, A Primal Dual Method", Management Science, Vol. 10, No. 4, January 1964. p. 601.

16. Reimer, C., and Iannone, P., "Computer Program for Overwrapped Cylindrical Tanks", Grumman Aerospace Corporation IOM 552-55M-72, June 1971.

17. Block, D. L., Card, M. F., and Mikulas, Jr., M. M., "Buckling of Eccentrically Stiffened Orthotropic Cylinders", NASA TND-2960, August 1965.

18. Dickson, J. N., and Brolliar, R. H., "General Instability of Ring-Stiffened Corrugated Cylinders under Axial Compression", NASA TN P-3089, January 1966.

19. Sullins, R. T., Smith, G. W., and Spier, E. E., "Manual for Structural Stability Analysis of Sandwich Plates and Shells", NASA CR-1457, December 1969.

20. Fulton, R. E., and Sykes, N. P., "Effects of Face-Sheet Stiffness on Buckling of Cylindrical Shells of Sandwich Construction", NASA TND-3454, February 1966.

21. Bruhn, E. F., "Analysis and Design of Flight Vehicle Structures", Section C 8.5; Tri-State Offset, 1965.

22. "Weight Savings Due to Use of Composite Materials - H3T Orbiter," GAC Memo B36-185MD-7, 26 April 1971.

23. Oken, S. and June, R. R., "Analytical and Experimental Investigation of Aircraft Metal Structures Reinforced with Filamentary Composites," Phase I, The Boeing Company, Contract NAS 1-8858.

24. Block, E. L., Card, M. F., and Mikulas, M. M. Jr., "Buckling of Eccentrically Stiffened Orthotropic Cylinders," NASA TN D-2960, August 1965.

25. Shanley, F. R., "Weight-Strength Analysis of Aircraft Structures," Dover Publications, New York, 1960.

26. Morris, E. E., and Alfring, R. J., "Cryogenic Boron-Filament-Wound Containment Vessels," NASA CR-72330, Aerojet-General Corporation, November 1967.

27. R. J. Alfring, E. E. Morris, and R. E. Landes, "Cycle-Testing of Boron-Filament-Wound Tanks," NASA CR 72899, August 1971.

28. "Structural Design Guide for Advanced Composite Applications-Second Edition," Contract F33615-69-C-1368, North American Rockwell Corporation, January 1971.

29. Morris, E.E., and Alfring, R. J., "Closed-End Cylindrical Graphite Filament-Wound Vessels," Aerojet Report 3779 to NOL under Contract N60921-16-C-0021, August 1969.

30. "Properties of Graphite Fiber Composites at Cryogenic Temperatures," NASA CR-72652, Naval Ordnance Laboratory, 13 May 1970.

31. "Graphite/Epoxy Tape Qualification", Report SCI-71-1 dated 12 March 1971, Structural Composites Industries under JPL Purchase Order FL-544105.

32. Hanson, M. P., "Tensile and Cyclic Fatigue Properties of Graphite Filament-Wound Pressure Vessels at Ambient and Cryogenic Temperatures," NASA TM-X-52539, April 1969.

33. "Cycle Testing of Graphite Filament-Wound Vessels," Contract NAS 3-13305, with Martin Marietta Corporation (work in progress).

34. Johns, R. H., and Kaufman, A., "Filament-Overwrapped Metallic Cylindrical Pressure Vessels," Journal of Spacecraft, July 1967.

35. Morris, E. E., Darms, R. E., Landes, R. E., and Campbell, J. W., "Parametric Study of Glass-Filament-Reinforced Metal Pressure Vessels", NASA CR 54-855, April 1966.

36. Sanger, M., and Molho, R., "Exploratory Evaluation of Filament-Wound Composites for Tankage of Rocket Oxidizers and Fuels", AFML-TR-65-381, October, 1965.

37. Sanger, M., Molho, R., and Morris, E., "Stainless Steel Lined Glass Filament-Wound Tanks for Propellant Storage", AFML-TR-66-264, December 1966.

38. Lewis, A., and Bush, G., "Improved Cryogenic Resin/Glass-Filament-Wound Composites", NASA CR 72163, April 1967.

39. Molho, R., and Soffer, L., "Cryogenic Resins for Glass Filament-Wound Composites", NASA CR-72114, January 1967.

40. Toth, J., et al., "Investigation of Structural Properties of Fiberglass Filament-Wound Pressure Vessels at Cryogenic Temperatures", NASA CR 54393, September, 1965.

41. Toth, J., et al., "Investigation of Smooth-Bonded Metal Liners for Glass Fiber Filament-Wound Pressure Vessels", NASA CR-72165, May 1967.

42. Hanson, M., "Glass, Boron, and Graphite Filament-Wound Composites and Liners for Cryogenic Pressure Vessels", NASA TM-X-52350, April 1967.

43. Hanson, M., "Static and Dynamic Fatigue Behavior of Glass Filament-Wound Pressure Vessels at Ambient and Cryogenic Temperatures", NASA TN D-5807, May 1970.

44. "Cryogenic Filament-Wound Tank Evaluation", NASA CR 72948, Contract NAS 3-10289, Structural Composites Industries, July 1971.

DISTRIBUTION LIST

Recipient	No. of Copies
NASA-Lewis Research Center 21000 Brookpark Rd. Cleveland, OH 44135	
Attn: J. E. Dilley, MS 500-313	1
J. R. Faddoul, MS 49-3	6
R. H. Kemp, MS 49-3	1
J. C. Freche, MS 49-1	1
G. T. Smith, MS 49-3	1
T. D. Gulko, MS 49-3	1
J. R. Barber, MS 500-205	1
Library, MS 60-3	1
AFSC Liaison Office, MS 501-3	3
Technical Utilization, MS 3-19	1
R. H. Johns, MS 49-3	1
R. F. Lark, MS 49-3	1
G. M. Ault, MS 3-13	1
National Aeronautics and Space Administration Washington, DC 20546	
Attn: MTG/J. G. Malament	1
MHE/N. G. Peil	1
KT/Technology Utilization Office	1
RW/G. C. Deutsch	1
Library	1
NASA-Ames Research Center Moffett Field, CA 94035	
Attn: Library	1
NASA-George C. Marshall Space Flight Center Marshall Space Flight Center, AL 35811	
Attn: S&E-ASTN-ES/E. Engler	1
S&E-ASTN-MX/E. Cataldo	1
S&E-PE-M/W. A. Wilson	1
Library	1
NASA-Goddard Space Flight Center Greenbelt, MD 20771	
Attn: Library	1

Recipient	No. of Copies
NASA-John F. Kennedy Space Center Kennedy Space Center, FL 32899 Attn: Library	1
NASA-Langley Research Center Hampton, VA 23365	
Attn: R. W. Leonard, MS 188	1
M. F. Card, MS 245	1
Library	1
NASA-Manned Spacecraft Center Houston, TX 77058	
Attn: ES-5/R. E. Johnson	1
SMD/R. E. Vale	1
Library	1
Jet Propulsion Laboratory 4800 Oak Grove Dr. Pasadena, Ca 91103	
Attn: W. M. Rowe	1
Library	1
NASA-Scientific and Technical Information Facility Box 33 College Park, MD 20740 Attn: NASA Representative	2
Aeronautical Systems Division Air Force Systems Command Wright-Patterson Air Force Base Dayton, OH 45433	
Attn: ASD/ENF/C. F. Tiffany	1
Library	1
Air Force Aero Propulsion Laboratory Research and Technology Division Air Force Systems Command United States Air Force Wright-Patterson AFB, OH 45433 Attn: ARRP/Library	1

Recipient	No. of Copies
Air Force Materials Laboratory Wright-Patterson Air Force Base Dayton, OH 45433	
Attn: MAN/H. S. Swartz	1
MAC/E. Jaffe	1
MATC/S. Litvak	1
Air Force Missile Test Center Patrick Air Force Base, FL	
Attn: Library	1
Air Force Office of Scientific Research Washington, DC 20333	
Attn: Library	1
Air Force Rocket Propulsion Laboratory (RPM) Edwards, CA 93523	
Attn: Library	1
Air Force Systems Command Andrews Air Force Base Washington, DC 20332	
Attn: Library	1
Arnold Engineering Development Center Air Force Systems Command Tullahoma, TN 37389	
Attn: Library	1
Bureau of Naval Weapons Department of the Navy Washington, DC	
Attn: Library	1
Commander U.S. Naval Missile Center Point Mugu, CA 93041	
Attn: Technical Library	1
Commander U.S. Naval Weapons Center China Lake, CA 93557	
Attn: Library	1

Recipient	No. of Copies
Commanding Officer Naval Research Branch Office 1030 E. Green St. Pasadena, CA 91101 Attn: Library	1
U.S. Army Missile Command Redstone Scientific Information Center Redstone Arsenal, AL 35808 Attn: Document Section	1
Commanding Officer U.S. Army Research Office (Durham) Box CM, Duke Station Durham, NC 27706 Attn: Library	1
Director Code 6T80 U.S. Naval Research Laboratory Washington, DC 20390 Attn: Library	1
Office of Research Analyses (OAR) Holloman Air Force Base, NM 88330 Attn: RRRD/Library	1
Naval Ship R&D Center Annapolis Laboratory Annapolis, MD 21402 Attn: Mr. C. Hershner, Code 2742	1
Picatinny Arsenal Dover, NJ 07801 Attn: Library	1
Plastics Technical Evaluation Center Picatinny Arsenal Dover, NJ 07801	1
Space and Missile Systems Organization Air Force Unit Post Office Los Angeles, CA 90045 Attn: Technical Data Center	1

Recipient	No. of Copies
U.S. Air Force Washington, DC Attn: Library	1
U.S. Air Force Wright-Patterson Air Force Base Dayton, OH 45433 Attn: AFFDL/W. H. Goesch AFML/T. J. Reinhart, Jr. AFML/J. Whitney	 1 1 1
U.S. Naval Ordnance Laboratory White Oak Silver Spring, MD 20910 Attn: R. Simon, Nonmetallic Mat'ls. Div. Library	 1 1
Aerojet Nuclear Systems Co. P. O. Box 13070 Sacramento, Ca 95813 Attn: Libarary	 1
Propulsion Division Aerojet-General Corp. P. O. Box 15847 Sacramento, CA 95803 Attn: Technical Library, 2484-2015A	 1
Space Division Aerojet-General Corp. 9200 East Flair Dr. El Monte, CA 91734 Attn: Library	 1
Aeronautronic Division of Philco Ford Corp. Ford Rd. Newport Beach, CA 92663 Attn: Technical Information Dept.	 1
Aerospace Corp. P. O. Box 95085 Los Angeles, CA 90045 Attn: Document Library	 1

Recipient	No. of Copies
Air Products and Chemical Co. Allentown, PA 18105 Attn: P. J. DeRea	1
Allegheny Ballistics Laboratory Hercules, Inc. P. O. Box 210 Cumberland, MD 21052 Attn: W. T. Freeman Library	1 1
Atlantic Research Corp. Shirley Highway and Edsall Rd. Alexandria, VA 22314 Attn: Security Office for Library	1
ARO, Inc. Arnold Engineering Development Center Arnold Air Force Station, TN 37389	1
Battelle Memorial Institute 505 King Ave. Columbus, OH 43201 Attn: Defense Metals Information Center Report Library, Room 6A L. E. Hulbert	1 1 1
Beech Aircraft Corp. Wichita, KS 67201 Attn: Library	1
Bell Aerosystems Box 1 Buffalo, NY 14205 Attn: T. Reinhardt Library	1 1
B. F. Goodrich Co. Aerospace and Defense Products 500 South Main St. Akron, OH 43311 Attn: Library	1

Recipient	No. of Copies
The Boeing Co. Aerospace Group P. O. Box 3999 Seattle, WA 98124	
Attn: J. T. Hoggat	1
Library	1
Brunswick Corp. Defense Products Division P. O. Box 4594 43000 Industrial Ave. Lincol, NE 68504	
Attn: W. Morse	1
General Dynamics/Convair P. O. Box 1128 San Diego, CA 92112	
Attn: H. F. Rodgers, MS 549-00	1
Library	1
Goodyear Aerospace Corp. 1210 Massilon Rd. Akron, OH 44306	
Attn: Library	1
Hamilton Standard Corp. Windsor Locks, CT 06096	
Attn: Library	1
IIT Research Institute Technology Center Chicago, IL 60616	
Attn: R. H. Cornish, Mech and Materials Div.	1
Lawrence Livermore Laboratory Box 808 Livermore, CA 94550	
Attn: T. T. Chiao	1
Lockheed-California Co. Burbank, CA 91503	
Attn: Library	1

Recipient	No. of Copies
Lockheed-Georgia Co. Advanced Composites Information Center Dept. 74-14, Zone 402 Marietta, GA 30060	1
Lockheed Missiles and Space Co. P. O. Box 504 Sunnyvale, CA 95087 Attn: Library	1
LTV Corp. P. O. Box 5003 Dallas, TX 75222 Attn: Library	1
Marine Engineering Laboratory NSRDC ANNADIV Annapolis, MD 21402 Attn: 560/K. H. Keller	1
Martin Marietta Corp. P. O. Box 179 Denver, CO 80201	
Attn: F. Swartzberg	1
C. A. Hall	1
A. Feldman (Dr.)	1
Library	1
Materials Sciences Corporation 1777 Walton Road Blue Bell, PA 19422 Attn: Nancy Sabia	1
McDonnell-Douglas Corp. 5301 Bolsa Ave. Huntington Beach, CA 92647	
Attn: R. F. Zemer, Dept. A3-250	1
H. Babel	1
Library	1
McDonnell-Douglas Corp. P. O. Box 516 St. Louis, MO 63166	
Attn: R. Hepper, Dept. E400	1
B. Whiteson, Dept. E457	1
Library	1

Recipient	No. of Copies
North American Rockwell 12214 Lakewood Blvd. Downey, CA 90241	
Attn: R. Field, Mail Code AD75	1
L. J. Korb, Mail Code AD-88	1
Library	1
Rocketdyne Division North American Rockwell 6633 Canoga Ave. Canoga Park, CA 91304	
Attn: E. L. Hawkinson, D/566 AC10	1
Library	1
Oak Ridge National Laboratory Oak Ridge, TN 37830	
Attn: T. W. Pickel	1
Owens-Corning Fiberglas Technical Center Granville, OH 43023	
Attn: A. B. Isham	1
Rohr Corp. Dept. 145 Chula Vista, CA 91312	1
Sandia Laboratories Albuquerque, NM 87115	
Attn: H. M. Stoller, Dept. 5310	1
Structural Composites Industries 6344 N. Irwindale Ave. Azusa, CA 91702	
Attn: E. E. Morris	1
Thiokol Chemical Corp. Wasatch Div. P. O. Box 524 Brigham City, UT 84302	
Attn: Library Section	1

Recipient	No. of Copies
TRW Systems 1 Space Park Redondo Beach, CA 90200 Attn: Technical Libr. Doc. Acquisitions	1
United Aircraft Corp. 400 Main St. East Hartford, CT 06108	1
United Aircraft Corp. United Technology Center P. O. Box 358 Sunnyvale, CA 94088 Attn: Librarian	1
U.S. Rubber Co. Mishawaka, IN 46544	1
Whittaker Corp. 3640 Aero Court San Diego, CA 92123 Attn: V. Chase	1
University of Nebraska Dept. of Engineering Mechanics Lincoln, NE 68503 Attn: R. Foral	1
University of Oklahoma School of Aerospace Mechanical and Nuclear Engineering 865 Asp Ave., Rm. 200 Norman, OK 73069 Attn: C. W. Bert	1
National Technical Information Service Springfield, VA 22151	20